| Title | Evaluating controls of acoustic noise propagation across the continental margin |
| --- | --- |
| Author(s) | Daly, Eoghan |
| Publication Date | 2021-08-23 |
| Publisher | NUI Galway |
| Item record | http://hdl.handle.net/10379/16906 |

# Evaluating Controls of Acoustic Noise Propagation Across the Continental Margin

## Eoghan Daly

*A thesis submitted for the degree of Doctor of Philosophy to the
National University of Ireland, Galway*

Supervisor: **Dr. Martin White**

**Earth & Ocean Sciences
The Ryan Institute
School of Natural Sciences
National University of Ireland, Galway**

**April 2021**

# Table of Contents

# Glossary of Abbreviations

S.I. (Système International d'Unités) abbreviations for units and standard notations for physical measurements, formulae, chemical elements and chemical abbreviations are used in this work. Other abbreviations are listed below.
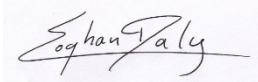
| | |
|---|---|
| **ADC** | Analogue to Digital Converter |
| **ADDs** | Acoustic Deterrent Devices |
| **BNLs** | Bottom Nepheloid Layers |
| **c** | Sound speed |
| **CTD** | Conductivity, Temperature and Depth |
| **dB** | Decibels |
| **$D_L$** | Vertical displacement |
| **E** | Energy (in Joules; J) |
| **EEZ** | Exclusive Economic Zone |
| **ENAW** | Eastern North Atlantic Water |
| **ENLs** | Enhanced bottom Nepheloid Layers |
| **FFT** | Fast Fourier Transform |
| **FIR** | Finite Impulse Response |
| **GAMs** | Generalized Additive Models |
| **I** | Acoustic intensity |
| **IIR** | Infinite Impulse Response |
| **INLs** | Intermediate Nepheloid Layers |
| **IWs** | Internal Waves |
| **$K_1$** | Diurnal tidal constituent |
| **$L_O$** | Ozmidov length scale |
| **$L_T$** | Thorpe displacement (rms) |
| **$M_2$** | Semidiurnal tidal constituent |
| **MFAS** | Mid Frequency Active Sonar |
| **MPAs** | Marine Protected Areas |
| **MSFD** | Marine Strategy Framework Directive |
| **MSPD** | Maritime Spatial Planning Directive |

| | |
|---|---|
| **N** | Buoyancy frequency |
| **N** | Spreading coefficient |
| **NMPF** | National Marine Planning Directive |
| **OC** | Organic Carbon |
| **Pwr** | Acoustic Power (in Watts; W) |
| **P** | Sound Pressure (µPa) |
| **PAM** | Passive Acoustic Monitoring |
| **PANiC** | Propagation of Acoustic Noise in Canyon |
| **PB** | Porcupine Basin |
| **PE** | Parabolic Equation |
| **PSD** | Power Spectral Density |
| **PTS** | Permanent Threshold Shift |
| **RL** | Received Level |
| **RMS, rms** | Root Mean Square |
| **SACs** | Special Areas of Conservation |
| **SEL** | Sound Exposure Level |
| **SL** | Source Level |
| **SNR** | Signal to Noise Ratio |
| **SPL** | Sound Pressure Level |
| **SPM** | Suspended Particulate Matter |
| **TL** | Transmission Loss |
| **TTS** | Temporary Threshold Shift |
| **UTC** | Coordinated Universal Time |
| **VMS** | Vessel Monitoring Systems |
| **zero-peak, 0-peak** | Zero to Peak Pressure |
| $\varepsilon$ | Energy dissipation |
| $\rho c$ | Acoustic impedance |
| $\rho$ | Density |
| **µPa** | Micro-Pascals |
| $\lambda$ | Wavelength |

## Declaration:

I, Eoghan Daly, certify that this thesis is all my own work and that findings presented within are correct, to the best of my knowledge. I have not obtained a degree with this university or elsewhere on the basis of any of the work herein. Contributions by co-authors on articles presented here are clearly outlined on the cover page of each published chapter.

Signed: *Eoghan Daly*

Date: 30/04/2021

## Funding:

# Acknowledgements

First and foremost to my supervisor Martin White. You have guided me seamlessly over the last six years through final year undergraduate project, an internship and the PhD. The confidence and belief you have shown in me and your casual approach (except when it comes to pushing out science, ideas or concepts) has enabled me to find my feet as an independent researcher. I am forever grateful and hope our working relationship and your sterling mentorship can continue into the future.

To the staff at EOS, each and every one of you have inspired me with your passion and knowledge for geoscience and your ability to teach it to me. Special thanks to my GRC of Eve, John and Peter. To all my post-grad buddies, past and present, long-term and visiting, you are all class and the friendship, support and craic has been unreal and I will miss that office dearly. Sheena, you are an absolute star; the technical assistance, tactical advice and moral support have been second to none. Sinéad and Annette, thank you both for kindly getting me up to speed in the world of research.

iCRAG has supported us as PhDs and post-docs above and beyond their remit and I will remain a believer in their vision. A massive thank you to Murray, Jenn, Fergus, the two Aoifes and all the team for everything over the last four years. To Chris, Florian, Louise, Clare, Mick and all at DIAS Geophysics, a huge thankyou for all the tech support and collaboration over the last few years, not to mention the use of the iMARL gear.

To Prof. Colin Brown. Thank you for all your guidance, support and advice over the course of my project and your help with the computations. It was very reassuring to have your expertise at the end of an email. A depth of gratitude is owed to RV Ops and Paul Gaughan at the MI and to John Barry, Kieran Adlum and the crew at P&O for providing a stellar service in offshore research surveying and data acquisition. Thank you to Sebastian Krastal at Kiel Uni. for the use of your seismic airgun. To Chris Loadman from Turbulent Research, Prof. Eddie Jones (NUIG) and to Sam Forbes and the team at RS-Aqua, thank you all for the signal processing support, without which the project would not have succeeded. To Oliver O'Cadhla, Rory Dunphy, Gareth Parry, Clare and Louise at PAD, and to the guys at Jasco Applied

# Abstract

The ocean's ability to transmit underwater sound efficiently over long distances enables anthropogenic noise as a cause of pollution in the global ocean. Ever increasing noise from sources such as sonar, seismic surveys, shipping and piledriving, hold the potential to adversely impact on the surrounding marine environment or 'acoustic habitat' to varying degrees. This project quantifies and characterises sound transmission across the continental margin and gauges physical controls on propagation. This allows for assessment and understanding of the processes and potential for noise pollution to impact on marine fauna around sensitive margin ecosystems. A desk study of an industrial seismic survey in the Porcupine Basin was conducted, while acoustic model capacity (2D) and feasibility (3D) have been explored. An offshore experiment was implemented on the eastern margin of the basin to evaluate, compare and contrast propagation along and across a small submarine canyon and adjacent slope. An array of five short-term fixed acoustic and hydrographic moorings were deployed over the study area from depths of 900 - 250 m and a controlled seismic sound source was deployed in a transect around the survey site. All measured data were processed, analysed and examined in the context of assessing physical processes, controls and damage thresholds or disturbance to marine life. Results from these studies and subsequent acoustic modelling identified range from source, slope angle, topography and water column structure as moderators of human noise propagation. Canyon geomorphology was found to enhance noise internally and across margin in both directions, by up to 21 dB re:1μPa zero-to-peak and 12 dB re:1μPa$^2$s SEL. Seismic airguns, and for the first time bottom trawling, have been confirmed as noise polluters in the Irish offshore, exhibiting levels of concern to marine wildlife. Findings reported herein, inferring that noise could cause damage or disturbance to resident or transient marine mammals along the Irish margin, especially around ecologically diverse canyon hotspots, underline the requirement for regulatory management within Ireland under various European directives, with obligations to monitor ocean noise and enforce mitigation strategies to tackle this pollution source. Key findings and future work planned from this project are intended to align with governance and monitoring initiatives regionally and within the Irish offshore sector. The motivation being to highlight and address anthropogenic noise as a detrimental stressor on a marine environment already under considerable and growing pressure from a multitude of human impacts, including microplastics, ocean acidification and global climate change.

# Chapter 1: Introduction

*"The Ocean is a mighty harmonist…"*

William Wordsworth, 1828. *On the power of sound*, st. XII.

## 1.1. Background Context and Motivations

The ocean is a realm both dense and dark when compared to our everyday world and it has always been a source of wonderment and mystery. Light, as with all electromagnetic waves, does not travel well underwater. Sound, on the other hand, transmits most efficiently and with great speed through the ocean, as some of our scientific forebearers, like Aristotle (384 – 322 BCE) and Leonardo de Vinci (1452 – 1519) eluded to in the early days. Daniel Colladon and Charles Sturm conducted the first and impressively accurate measurement of sound speed (within ~2%) on Lake Geneva in 1826 and since then our understanding of the processes and usefulness of ocean sound has continued to expand. Ocean acoustics provides a primary tool for marine mammals and humans alike, to use for communication, hunting, navigation and for understanding this watery realm. Sound can travel huge distances underwater, across entire ocean basins if ducted within the deep sound channel at the lower end of the sonic frequency band (~10 – 200 Hz). Eminent oceanographer Walter Munk (1917 – 2019) and his colleague Carl Wunsch utilised this property for investigating variability in ocean temperature (Munk and Wunsch, 1979), coining the phrase 'ocean acoustic tomography'. Munk further went on to detect sound signals at ocean basin scales (5 – 10 x$10^3$ km) during the 'Heard Island Feasibility Test', while using acoustic thermometry to measure large-scale temperature change (Munk et al., 1994).

Anthropogenic noise (anthrophony) is an almost ubiquitous ocean-wide feature, superimposed on natural (geophony) and biological (biophony) sounds, which tend to be more intermittent in their influence on background sound levels. This is one of the reasons that anthrophony has been recognised and classed as a pollutant under the Marine Strategy Framework Directive (MSFD) (Descriptor 11: Introduction of

energy, including underwater noise; Tasker et al., 2010). Anthropogenic noise manifests from a wide-ranging collection of sources, including military sonar, offshore seismic surveys, shipping and marine development (see Fig. 1.1), with a varied array of distances, frequency bands and levels of impact on the surrounding marine environment. The general trend has been for human noise to increase in the ocean, yet still, through correct mitigation strategies and regulatory measures this development can be halted or even reversed (e.g. Duarte et al., 2021). An example of that potential was witnessed (and studied) in 2020, during a drop in merchant and leisure shipping activity due to the global SARS-CoV-2 pandemic (Thomson
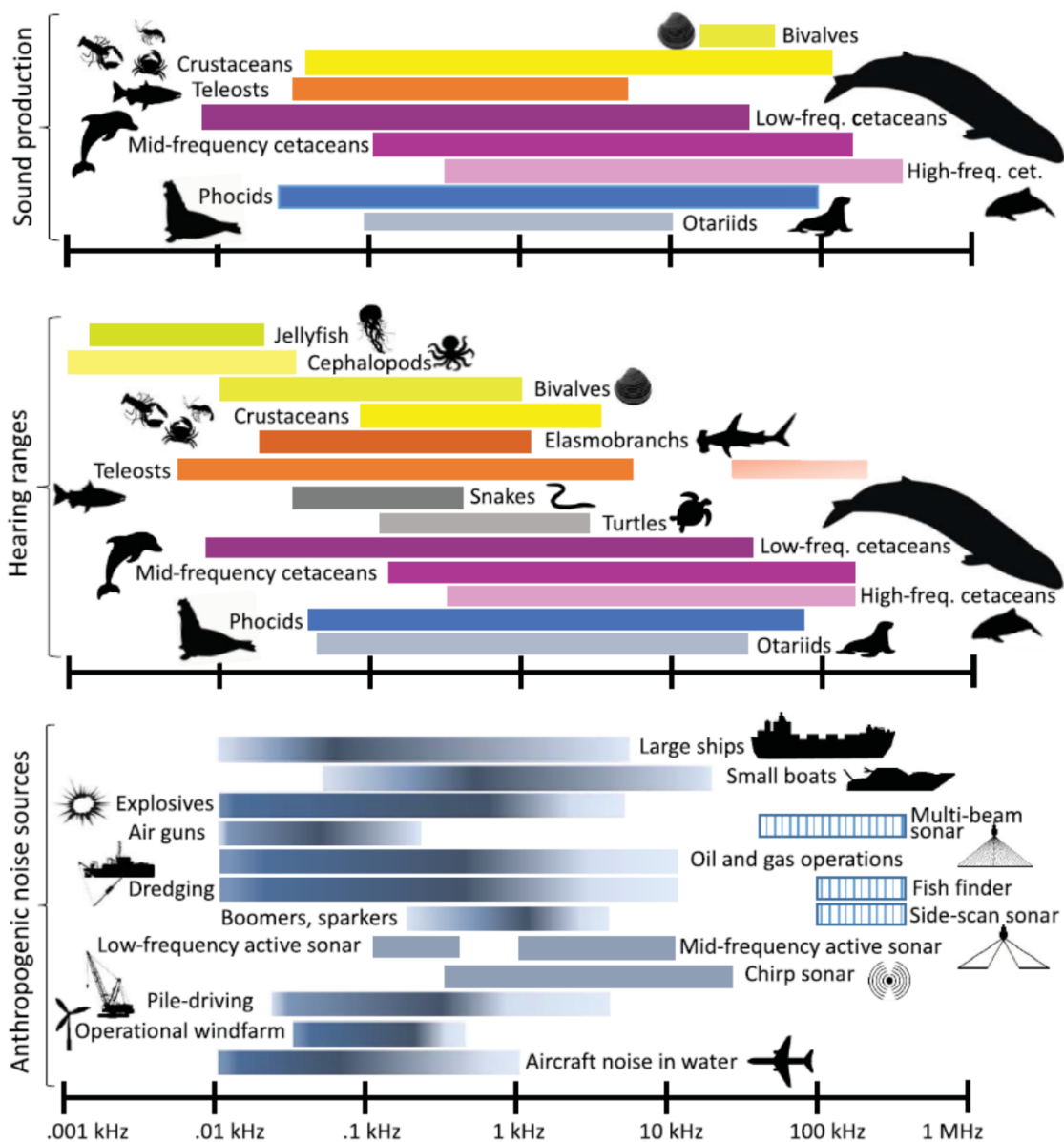


**Fig. 1.1.** Frequency bands of indicative anthropogenic noise sources and of hearing and sound production of key marine taxa. Taken from the comprehensive and recently published review by Duarte et al., (2021).

and Barclay, 2020), where the ocean and seas found themselves unusually quiet during a brief reprieve from the 'din' of human endeavour.

Many marine fauna, most notably (but not exclusively) marine mammals, use sound as their leading sensory apparatus and are thus rendered susceptible to disturbance, damage, injury and in extreme cases mortality from intrusive levels of anthropogenic noise pollution (e.g. Slabbekoorn et al., 2010; Southall et al., 2019). The continental margin along the Irish Exclusive Economic Zone (EEZ) is the commonest setting to find most of its 24 species of resident or transient marine mammals, including the enigmatic and deep diving beaked whales and the largest mammal to ever inhabit the planet, the blue whale (Baleanoptera musculus) (O'Cadhla et al., 2004; Berrow et al., 2018).

The continental margin, including along the northeast North Atlantic, is an oceanic setting characterised by boundary conditions in oceanographic processes, geomorphology, underlying geology and depth changes, where tidal energies are dissipated and transformed from deep ocean to shelf seas. Submarine canyons incise these continental slopes and shelf edges over geological time. An example is the vast and dendritic Whittard Canyon system along the Celtic Shelf slope (Amaro et al., 2016), which hosts a myriad of marine fauna, up through the trophic levels, based around benthic, cold water coral and sponge ecosystems below and enhanced primary production above. Likewise, the Porcupine Basin (hereafter denoted PB) hosts canyons, channels and carbonate mounds that interact with oceanographic processes such as the European slope current, bottom boundary currents and tidally driven Internal Waves (hereafter IWs) (White, 2003, 2007). Sound propagation, including anthropogenic noise, is moderated by each of these controlling factors as it transmits through the water column in all directions across the continental margin.

One of the chief motivations throughout the study was to gauge the impact of anthropogenic activity on the marine environment and acoustic habitat of the continental margin, specifically on the dangers of ocean noise pollution to marine mammals in Irish waters.. This project was also driven in part by Ireland's necessity to measure and monitor human noise in the ocean, spanning many criteria under various frameworks (e.g. the Habitats Directive, MSFD, Marine Spatial Planning

Directive (MSPD) and the National Marine Planning Directive (NMPF)) in addressing ocean noise pollution.

The basic hypothesis that this thesis intends to address is as follows:

> *What are the physical controls on anthropogenic noise propagation across the continental margin and to what degree do each increase the potential to harm marine fauna?*

Specifically, does the enhanced topography around submarine canyons increase noise exposure relative to either distance from source or variation caused by internal water column dynamics? To what extent does the continental margin setting exacerbate noise pollution from offshore seismic surveys and bottom trawling; and within a regional frame, how do these acoustic habitats impacted along the margin compare to those adjacent in the deep ocean and on the shallower shelf? Can seafloor geological layers be constrained as a control on sound propagation, given the available data and modelling capacity?

## 1.2. Research Objectives

The primary aim of this project was to measure, analyse and assess noise levels and what controls those levels in the vicinity of the continental margin, in the context of harm thresholds and disturbance to marine life and to provide this evidence of assessment in line with governance and monitoring initiatives.

The objectives, some of which only became apparent through opportunity during survey (i.e. a trawling event) are listed below:

- Characterise a regional soundfield in the PB
- Identify physical controls on propagation and proportional effects of each
- Investigate canyon propagation, including the occurrence of sound 'channelling' and 'focussing', compared to a typical slope setting
- Define bottom trawling as a noise pollutant

- Relate findings to potential harm and disturbance to marine mammals and align with noise management, mitigation strategies and policy (regionally and locally), under existing regulatory frameworks

- Develop processing/analysis methods as a computational acoustics toolbox

- Build modelling capacity for future monitoring of the Irish offshore

## 1.3. Outline of Thesis

Chapter 2 provides a comprehensive literature review, on a cross section of relevant topics, such as the physics of sound propagation, noise pollution, oceanography, marine biology (sources, local presence and impacts) and noise management strategies and initiatives.

Chapter 3 details the methodology used in deploying, recovering, processing, analysing, modelling and disseminating marine acoustic and associated hydrographic data. Some of the methods developed are novel, for instance semi-automated seismic airgun shot identification and also the deployment and application of the 'ORCA' hydrophone recorders, used for the first time in Ireland during this project.

Chapter 4: *Seismic Survey Sound Propagation: A Porcupine Basin Noise-field* (Daly et al., 2020), describes and specifies a regional soundfield in the PB and provides quantitative detail on variation over contrasting range, slope angle and seasons. This chapter was a progression from previous work carried out by Crawford, (2016) and additionally afforded a knowledge ramp from the start of project to the provision of main findings. Sinéad Crawford Jordan contributed to the work carried out during the publication of Chapter 4, by sharing data and Matlab code but more crucially, by generously imparting knowledge and training in marine acoustic analysis and modelling.

Chapter 5 comprises the central findings from the survey and controlled noise experiment (termed PANiC; Propagation of Acoustic Noise in Canyon) along the eastern flank of the PB, contrasting the geomorphologies of a submarine canyon

and typical slope. Findings resulted from an in-depth analysis of noise propagation through various sound metrics, along strategically selected sound pathways and from analysis of background ambient noise. Results of hydrographic sampling and estimation of water column dynamics augment the central findings by providing a supporting dataset that has been statistically correlated with acoustics results and qualitatively assessed in terms of propagation controls.

Chapter 6: *Bottom Trawling Noise: Are Fishing Vessel Polluting to Deeper Acoustic Habitats?* (Daly and White, 2021), analyses and displays results following an event during the PANiC survey where a bottom trawler came within close range to one of the acoustic moorings. This opportunistic study offered findings most relevant to anthropogenic noise along the continental margin by providing another noise source type with the potential for ecological harm.

Chapter 7 reviews each of the three main results chapters as a synthesis of key findings in the context of impact and significance. Additionally, future work resulting from this PhD project is suggested and the manuscript is concluded.

Appendix A contains a collection of figure plots and tables, supplementary to the main findings presented in Chapter 5, that complete the series of results for all propagation pathways analysed, key examples of which have been included within the main chapter.

Appendix B comprises supplementary material from Chapter 6.

Appendix C: *Bottom Trawling at Whittard Canyon: Evidence for Seabed Modification, Trawl Plumes and Food Source Heterogeneity* (Daly et al., 2018), links the acoustic impacts reported in Chapter 6 with a wider set of physical and ecological impacts resulting from bottom trawling, further highlighting this human activity as detrimental to the marine environment. This corresponding work was mostly carried out previous to the commencement of the PhD programme but was finished and published during the early stages of the PhD project.

Appendix D is a short glossary of work completed as outreach and public engagement throughout the PhD project, aimed at highlighting and raising public awareness on ocean science, noise pollution and human impacts on the marine environment.

# Chapter 2: Literature Review

The fundamental controls of sound propagation around the continental margin, along with a description of the study area, including local geoacoustic parameters, occurrence of marine mammals and human footprint are covered in the initial sections of this chapter. This provides a backdrop for a focused review on source levels and the negative impacts of anthropogenic noise on marine fauna. The chapter is concluded with an examination of regulatory frameworks, mitigation strategies, protected areas and global ocean change in the context of future marine ecology and human influence.

## 2.1. Ocean Sounds and Noise Controls

### 2.1.1. Basic principles of ocean acoustics

Sound propagates through a medium as a mechanical disturbance or wave that oscillates its particles and in the case of water (or air) it compresses and rarefies the particles longitudinally as a pressure wave (Urick, 1983; Medwin and Clay, 1997; Erbe, 2011). The initially compressed particles and the consequent increase in density from its equilibrium value are subjected to a restoring force quantified by the bulk modulus parameter (e.g., Ainslie, 2010). The fundamental quantity used to study underwater acoustic propagation is sound pressure. Although particle velocity is an equally important physical manifestation of a passing sound wave, in that instantaneous intensity is a product of particle velocity and sound pressure (Carey, 1995), it will not be scrutinised here in relation to sound measurement. In rock and consolidated sediments the acoustic energy will also travel transversely as a shear wave, (but more slowly than a pressure wave).

Acoustic intensity (I) is the energy (E) [Joules; J], that flows with propagation direction per unit Area (A) [m$^2$] per unit time (T) [s] and is equal to the squared pressure ($P^2$) [Pascal; Pa] divided by specific acoustic impedance ($\rho c$): I = E / AT = $P^2$ / $\rho c$ , where $\rho$ is density [kg m$^{-3}$] and c is sound speed [m s$^{-1}$]. Acoustic Power

(Pwr) [Watts; W] is the quantity of acoustic energy radiated over a given time: Pwr = E / T = IA, [W; J/s; kg m$^2$ s$^{-3}$] (Erbe, 2011). Frequency of sound (f) is the rate (per second; Hertz, Hz) that the pressure wave oscillates at; sound speed (c) is the speed of the propagation through a given medium and the wavelength ($\lambda$) [m] of the pressure wave is a function of both: $\lambda$ = c / f (Kinsler et al., 1999).

Sound level metrics and parameters used to measure and analyse both impulsive and continuous noise sources and received levels are found throughout the literature (e.g., Urick, 1983; Medwin and Clay), for example in good practice guides (Carey, 2006, 1995; Robinson et al., 2014) and through published standards (International Organization for Standardization, 2019, 2017); detailed descriptions can be found in Chapter 3.4.1.

### 2.1.2. Sound propagation and loss

The ocean can be viewed as a waveguide, being bound at the surface by the air-water interface and below by the seafloor, while to a vastly greater degree unbound in the horizontal (Urick, 1983; Jensen et al., 2011; Wilcock et al., 2014). This is especially true when at far enough range from source to have small grazing angles (i.e. large angle of incidence). Sound can be ducted through the water column, for instance, constrained to a surface duct or to the deep sound channel (also known as the SOund Fixing And Ranging channel; SOFAR), depending on sound speed, which in turn is a function of temperature, salinity and depth (or hydrostatic pressure) (Urick, 1983; Jensen et al., 2011; Etter, 2018). Sound waves will refract towards water depths with a lower sound speed or a sound speed minimum, which can be at the surface (e.g., in a fully mixed water column or higher latitudes) or at the deep sound channel ~1000 m depth (lower-mid latitudes), while at even greater depths pressure will force an increasing sound speed with depth and consequently upward refraction (e.g., Jensen et al., 2011; Etter, 2018). The deep sound channel is the mechanism that allows for basin wide propagation of lower frequency noise (Mercer et al., 2009) (Fig. 2.1 adapted from Wilcock et al., 2014, Figure 1). The seafloor interface of the ocean waveguide is the most problematic for estimating acoustics, especially around the rugged topography of the continental margin where geological layers can have variable thicknesses and geoacoustic parameters
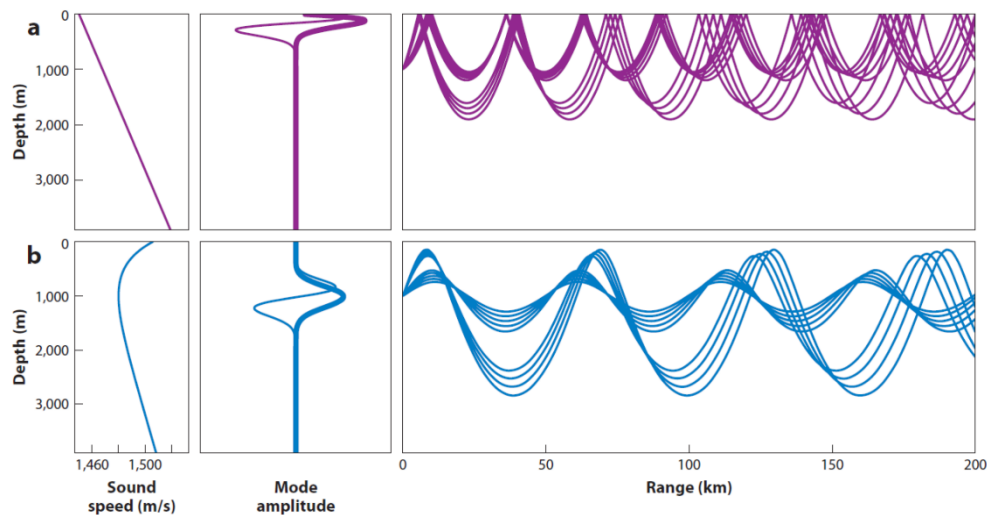
**Fig. 2.1.** Ray paths of (a) shallow, i.e. Polar and (b) deep, i.e. lower latitude, sound channels. Left panels are idealised sound speed profiles; middle panel shows 1st (bold) and 2nd modes at 50 Hz and; right panels are ray traces. Note: Deep sound channel rays do not interact with the surface boundary. Adapted from Wilcock et al., (2014, p. 3).

(Wilcock et al., 2014). These lossy settings can complicate how sound energy is absorbed, reflected or scattered, in particular for lower frequency sound that will penetrate to greater depths below the seafloor (Wilcock et al., 2014).

Sound propagation loss (or transmission loss) in the ocean is due to a combination of attenuation loss and spreading loss. Attenuation loss includes that due to absorption, scattering, diffraction and leaking from ducts (Urick, 1983; Etter, 2018). Loss due to boundary scattering is dependent on surface (or bottom) roughness, while volume scattering from suspended particles decreases with depth; both mechanisms of which are dependent on frequency (Ainslie, 2010; Jensen et al., 2011). Spreading loss increases per unit area of wavefront as the sound energy spreads away from the source point in a spherical shape until it is constrained by top and bottom boundaries where it transforms to cylindrical spreading (see details in Chapter 3.4.3).

There are many specific examples of propagation theory, measurement and prediction in the literature, under various environmental conditions. An example of this is how a sloping seafloor will moderate how bottom-surface reflections behave (Tindle and Deane, 1985), where sound generated in shallow water can manifest as a component of ambient noise in the deep sound channel worthy of consideration

(Wagstaff, 1981; Ross, 1993). Likewise, sound rays propagating over a shoaling seafloor will experience increased bounces with range and thus faster attenuation (McCauley et al., 2000a, b).

Although not technically an environmental control, azimuthal angle from a directional sound source is another consideration for assessing sound propagation. Azimuthal differences in source levels are frequency dependent as seen from an impulsive seismic airgun array (MacGillivray, 2006; Erbe, 2011) or from a continuous shipping source (Arveson and Vendittis, 2000).

*2.1.3. Reflective geological layers*

A sound wave can be approximated as a plane wave locally. Depending on grazing angle and the fluid (sedimentary) or elastic (hard substrate) properties of the seafloor, a component of the incident wave will transmit to deeper subseafloor and a component will be reflected back to the water column (Ainslie, 2010; Jensen et al., 2011). The nature of reflection and transmission in a fluid and/or elastic seabed is frequency dependent, with higher frequencies (> 5 kHz) being attenuated in the upper 10s of metres of seabed and infrasonic frequencies (< 20 Hz) remaining dependent on properties in the basement rock half space (a mathematical model where only one boundary exists, i.e. the top of the crust, assumed homogeneous, and all others are infinitely far away), often kilometres below the surface sedimentary layers (Ainslie, 2010; Jensen et al., 2011). The amount of bottom loss at a given frequency, across a seafloor that varies in layer thickness and acoustic properties is a major factor that renders geoacoustic modelling of real ocean settings such a complex task, with many approximations and generalisations required (Li et al., 2004; Jensen et al., 2011).

Another phenomenon resulting from stratigraphic geological layers is the arrival of a head wave, where compressional wave speeds between an overlying (e.g., sedimentary) and underlying (e.g., bedrock) layer are faster than in water and given a critical range of grazing angles will propagate along the subseafloor boundary re-emitting into the water column and arriving at a receiver in advance of the direct water wave (e.g., Figure 12 in Duncan et al., 2013).

*2.1.4. Internal water column dynamics*

Internal water column density structure with associated fronts and internal waves (IWs) will moderate sound propagation through refraction. Fronts, which are both temporally and spatially variable due to environmental factors, such as tide or seasonal stratification, in turn force a variable sound speed profile in the water column and associated propagation conditions. Lynch et al., (2003) found that the position of local oceanic fronts altered the acoustic field spatially and temporally, with upwards refraction from warmer bottom waters reducing bottom interaction. However they found that scattering from internal wave packets undermines the predictability of propagation variation on models using sound speeds that consider the front but not the IWs. Differences of up to 20 dB were found between a seasonal (summer) front and a winter mixed column for anthropogenic noise in the Celtic Sea shelf (Shapiro et al., 2014). Tidal forcing of temperature change in shelf seas, especially over a changing topography will moderate the acoustic field both at high frequency bands (Carbone and Hodgkiss, 2000) and lower frequencies (Finette et al., 2007). Both studies find additional moderation during the presence of IWs.

Tidally initiated IW perturbations arising in a seasonally stratified water column, often appearing as high amplitude short period solitary wave packets (solitons) along the pycnocline, can alter the propagation of sound passing through them. Duda, (2004) notes a mode coupling mechanism, where exchange of energy between modes, caused by a dynamic sound speed field due to solitons (but not longer wavelength internal waves), can vary propagation levels by as much as 20 dB when the source is at depth (100 m) and to a lesser degree (8 dB at 20 m) when shallower. Zhou et al., (1991) discovered an associated resonance effect at frequencies in line with soliton and wave packet wavelengths, as sound propagates through them. Frequency dependent sound propagation through an isotropic (IW) and/or anisotropic (soliton) sound speed field causes a complicated variation in transmission loss. This loss is as a function of azimuth (angle of propagation relative to IW wave crest) and mechanisms, for instance adiabatic loss (effectively attenuation) or mode coupling (energy transfer) (e.g., Badiey et al., 2002, 2011; Oba and Finette, 2002).

*2.1.5. Wave equations and acoustic modelling*

Sound propagation can be accurately characterised by a three-dimensional, time-dependent full wave equation which itself is a derivation of the equations of state, continuity and motion (e.g., Kinsler et al., 1999). When used for mathematical modelling of marine acoustics this full wave equation is often simplified to a second order, linear, partial differential equation and using some generalisations is regularly reduced further to a harmonic function, the Helmholtz Equation (e.g., Ainslie, 2010; Jensen et al., 2011; Etter, 2018). Variations of these equations and derivations are adapted for each of the model types used to model acoustic propagation or signal loss.

Ocean acoustic modelling ranges in complexity, computational overhead and applicability to a given requirement, depth, grid size or frequency band. Each of these are a function of the model type, which will increase in comprehensiveness from simple spreading laws through to ray theory, Parabolic Equation (PE), normal mode and wave number integration (e.g., Korakas and Hovem, 2013; Etter, 2012, 2018); see Fig. 2.2 for model applicability. Other modelling methods, including the Finite Difference Method (FDM) and Finite Element Method (FEM), which utilise 'direct discretisation' of the principle equations are finding increasing research application, while pushing the bounds of modern computational capacity (Jensen, et al. 2011; Spiga, 2015). FDM is particularly useful for a range of applications involving elastic seafloor or rough surfaces (e.g., Stephen, 1988). This project utilised the Parabolic Equation (PE) (Chin-Bing et al., 1993; MacGillivray and Chapman, 2012) model RAMGeo, on the AcTUP platform (Duncan and Maggi, 2006), chosen for its range dependence (i.e. RAM: Range-dependent Acoustic Model; Collins, 1993) across a fluid seabed and depth capabilities at low and intermediate frequencies. RAMGeo is confined to (multiple) single frequency outputs and being a 2D model is also restricted to 2D variation in parameters of the propagating medium. Perhaps more importantly, RAMGeo is limited by not accounting for propagation through elastic media (i.e. shear waves in the subseafloor), considering the steep topography and hard substrate found around canyons.

| Model type | Applications | | | | | | | |
| --- | --- | --- | --- | --- | --- | --- | --- | --- |
| | Shallow water | | | | Deep water | | | |
| | Low frequency | | High frequency | | Low frequency | | High frequency | |
| | RI | RD | RI | RD | RI | RD | RI | RD |
| Ray theory | ○ | ○ | ◐ | ● | ◐ | ◐ | ● | ● |
| Normal mode | ● | ◐ | ● | ◐ | ● | ◐ | ◐ | ○ |
| Multipath expansion | ○ | ○ | ◐ | ◐ | ◐ | ◐ | ● | ◐ |
| Fast field | ● | ◐ | ● | ◐ | ● | ◐ | ◐ | ◐ |
| Parabolic equation | ◐ | ● | ○ | ○ | ◐ | ● | ◐ | ◐ |

Low frequency (<500 Hz)          RI: Range-independent environment
High frequency (>500 Hz)         RD: Range-dependent environment

● Modeling approach is both applicable (physically) and practical (computationally)

◐ Limitations in accuracy or in speed of execution

○ Neither applicable nor practical

**Fig. 2.2.** Model applicability chart. Produced by Etter, (2018), originally adapted from Jensen, (1982).

## 2.2. The Northeast North Atlantic Continental Margin

### 2.2.1. Geographical setting and underlying geology

The northeast North Atlantic margin holds an assortment of geomorphologies, such as seamounts, submarine canyons, gullies, fans and channels, as the ocean rises from the Porcupine Abyssal Plain to the Porcupine Seabight, the Rockall Trough and the Hatton Rockall Basin, and rising again to the banks of Porcupine, Rockall and Hatton (Shannon, 1991; Sacchetti et al., 2012). The eastern flank of the Porcupine Seabight or Porcupine Basin (PB) contains the Gollum Channel system which deepens to the centre of the basin, a minor canyon (which this project focusses on) and some carbonate mound provinces to the northeast and north (Huvenne et al., 2003; White and Dorschel, 2010).

The PB is an extensional deep sedimentary basin holding sediments up to 10 km thick aging from the Mesozoic to Cenozoic, overlaying a failed rift system and thinning continental crust (Shannon, 1991).

There is a paucity of upper subseafloor data, either on sediment type and thickness or geoacoustic parameters for the PB, which complicates any range dependent modelling efforts. Surface sediments surrounding the top half of the PB down to the 500m depth contour are classified by the EMODnet-Geology Project as 'mud to sandy mud' (Stevenson, 2012). The only openly accessible borehole data is that of an IODP expedition in 2005 to the Belgica Mound Province. Taking an approximate average of sediment types across boreholes shows clay down to 50 mbsf (metres below sea floor) and mixed layers of varying thickness down to 270 mbsf (excluding challenger mound boreholes which were predominantly coral rubble and wackestone), with a possible mid-pliocene boundary between 50 and 140 mbsf (Expedition Scientists, 2005).

*2.2.2. Hydrography and internal dynamics*

The main upper watermass found in this region, as it advects from a more southerly source is Eastern North Atlantic Water (ENAW) (Harvey, 1982; Ellett et al., 1986, 1983; Holliday et al., 2000), which through winter mixing is relatively homogeneous down to 700 – 800 m. The ENAW can become modified throughout its northwards advection by Sub-Arctic Intermediate Water (SAIW) and Western North Atlantic Water (WNAW), depending on their variable influence. Directly below ENAW a wedge of Mediterranean Overflow Water (MOW) can be found, with characteristically low oxygen values, at latitudes as high as 53°N or higher, although the extent of this wedge varies temporally (Arhan and King, 1995; Van Aken, 2000; Ullgren and White, 2010). MOW occupies the entire PB between ~800 – 1000 m (White, 2006). Deeper waters of the region are the cool and fresh Labrador Sea Water (LSW) (Talley and McCartney, 1982), with a characteristically high oxygen concentration in this area between 1500 and 2000 m depth (McGrath et al., 2012). Below that North East Atlantic Deep Water (NEADW) and Lower Deep Water (LDW) (van Aken and Becker, 1996; van Aken, 2000) which holds high silicate levels through dilution of Antarctic Bottom Water (AABW).

The variable nature and mixing effects of mesoscale activity will influence the presence and proportion of watermasses in the regional upper ocean (Sherwin et al., 2012, 2015), through increased turbulence as eddies spin off the North Atlantic Current (NAC). Ocean circulation surrounding and within the PB is complex. As general advection approaches the PB, transports to the east turn northward in line

with the NAC and transports to the south veer southwards in an anticyclonic re-circulation around the area of ENAW formation (Pollard et al., 1996; e.g., Figure 2). Anticyclonic eddies have been observed in the centre of the PB, using drogued Argo drifters (Pingree, 1993) and satellite SST and ocean colour (Miller, 2009), further demonstrating the variance and unpredictability in hydrographic conditions.

The European continental slope current that originates off the Iberian margin, is mostly continuous as it progresses northwest and flows poleward into the Rockall Trough, becoming stronger more northwards and in winter (Huthnance, 1986, 1984; Hill and Mitchelson-Jacob, 1993; White and Bowyer, 1997; Souza et al., 2001), with springtime reversals and yearly residual flows of ~2 cm s$^{-2}$ around the Goban Spur (Pingree et al., 1999). A filament of the continental slope current around the Goban Spur diverts northeast into the PB, at least occasionally if not more often, as was observed in the PB along the Irish shelf at 51.5°N at depths ~300 m and above, through temperature and salinity profiles (Mohn et al., 2002; White, 2006).

Over the shelf break, tidally generated, long wavelength internal wave oscillations of the seasonally stratified thermocline (or pycnocline) and their shorter wavelength, non-linear, internal solitary wave packets propagate both over the shelf and out to deeper waters. IWs vertically mix up nutrient rich waters to surface layers, especially during spring tides, that sustain blooms of primary producers well into the neap tides (Sharples et al., 2007, 2009), with species assemblages differing to those adjacent over the shelf and over deeper water. IWs with wavelengths of 30 – 35 km and amplitudes of 40 – 60 m and 60 – 100 m shoreward and seaward respectively, will maintain (when present) solitons of 1 – 2 km wavelengths and similar amplitudes, constrained within the troughs of the internal tidal wave (i.e. equal phase speeds). These solitons are not only generated at the shelf break but over deep water, where bottom reflected tidal rays or 'beams', originating at critical slope angles, perturb the seasonal pycnocline, as observed from 'sun glint' satellite in the Bay of Biscay (e.g., Pingree and New, 1989; Azevedo et al., 2002; New and Da Silva, 2002; Vlasenko and Stashchuk, 2015). Semidiurnal ($M_2$) tides are found to be responsible for internal tidal energy, including formation of partly standing internal waves at a large dendritic canyon system at Whittard Canyon, nearby to the south of our survey site (Hall et al., 2017; Aslam et al., 2018). Additionally, there is evidence for a diurnal tidal constituent ($K_1$) driving along slope currents just north of our canyon survey area (White, 2003, 2006; White and Dorschel, 2010) suggesting our site might also

be influenced by these $K_1$ tides or be within a boundary zone between these dominant tidal constituents.

### 2.2.3. Regional biology

In total there have been 24 species of cetacean (whale, dolphin and porpoise) detected across deep, shelf and coastal Irish waters, using a range of methods, including sightings, strandings and acoustic monitoring (Berrow, 2001; O'Brien et al., 2009; Berrow et al., 2010). All cetaceans, either migratory or resident (with the exception of inshore harbour porpoises) have a higher density of occurrence along the continental margin compared to adjacent waters, especially odontocete species which are consistently found over areas of maximum slope (Berrow et al., 2018; Barile et al., 2021). Fin whale song was the most frequently detected by Charif and Clark, (2009), who found their prevalence highest in December and January, with no large-scale migratory patterns, while they vocalised more so at night and to the north, along the south-eastern bounds of the Rockall Trough (Berrow et al., 2018; Barile et al., 2021). Fin whales were located in the PB through acoustic monitoring and sightings between 1999 – 2001 (O'Cadhla et al., 2004) and were detected and found to dominate the 18 – 26 Hz band at a location quite close (~58 km; east PB) to our study area, increasing in call density from mid-July onwards (McCauley, 2015) and gathering in autumn (Baines et al., 2017). Blue whales were acoustically detected in all areas of the Irish continental margin, throughout the year, between 1996 – 2005, peaking in Nov/Dec (Charif and Clark, 2009), however they were only detected in summer/autumn of 2015-2016 through Passive and Static Acoustic Monitoring (PAM and SAM) (Berrow et al., 2018). No blue whales were detected within the PB in 2014 – 2015, either to the north or east (McCauley, 2015).

PAM, though limited in range of detection, has the advantage of portability during a marine mammal survey. Sperm whale clicks were the most frequently detected using PAM along the continental margin in this region of the northeast North Atlantic (Berrow et al., 2018), as these animals migrated to the north from spring to autumn, with the most of this population thought to be solitary males (Berrow, 2001). Additionally, they were found in the PB in spring and summer (O'Cadhla et al., 2004), and as with fin whales, they gathered in autumn (Baines et al., 2017).

Beaked whales (family Ziphiidae), an enigmatic creature the biology of which is still relatively unknown, specialise in deep diving for their preferred pray and are thought to favour submarine canyons and trenches (Macleod, 2000; Berrow, 2001; Barlow and Gisiner, 2006). Considering Cuvier's beaked whales had been found to be most common in the wider region, later studies using PAM found Sowerby's beaked whales to be the most common, with higher numbers favouring the northern extent of the Irish continental margin, while the Cuvier's remained further south (Berrow et al., 2018). McCauley, (2015) found that 12 – 13% of cetacean event sound samples were due to beaked whales at his east PB acoustic station.

Long finned pilot whales and white sided dolphins are found mostly along the shelf edge (Berrow, 2001) with sightings mostly in spring (O'Cadhla et al., 2004). Humpbacks are one of the least frequent cetaceans along this part of the margin, as they seasonally migrate (Jan-Mar) to more southerly breeding grounds (Charif et al., 2001; Charif and Clark, 2009), rarely picked up acoustically (Berrow et al., 2018) and only in the summer months. Neither Humpback nor Minke whales were observed or acoustically detected in the PB (O'Cadhla et al., 2004; McCauley, 2015).

The impact of noise on the acoustic environment is not limited to marine mammals, with fish and invertebrates likewise prone to adverse impacts (Slabbekoorn et al., 2010). By far the most studied fish and invertebrate species along the Irish margin are target species for the fishing industry, such as demersal whitefish (e.g. Cod, Haddock, Hake) and prawn (Nephrops). Biophysical interaction occurs between oceanographic processes across the slope/shelf edge, for instance vertical nutrient mixing due to internal dynamics and biological processes, from base level proliferation through to food sourcing and spawning strategies for many target species present (e.g., Gerritsen et al., 2013; Gerritsen and Lordan, 2014; Marine Institute, 2019).

### 2.2.4. Marine industry

The impact of human activity on the marine environment has been increasing each decade since industrialisation began. Halpern et al., (2008) identified the waters around Ireland and the British Isles as one of the top four areas of predicted

cumulative input from all marine anthropogenic activity globally, with our study area being classified as 'High impact' and the adjacent shelf as 'Very high impact'.

The PB, as with the surrounding sedimentary basins, have had ongoing interest from the hydrocarbon industry, with exploration peaking at times of higher oil and gas prices. There were 187 wells drilled in the Irish offshore, 55 of which were in waters > 200 m, involving 30 companies up to 2005 (ISPSG, 2005). 30 of these wells were in the PB (Croker and Shannon, 1987; Shannon and Naylor, 1998; Naylor and Murphy, 2002) with very limited information or data on these wells being released or published. Industrial seismic survey activity has been summarised in the Irish
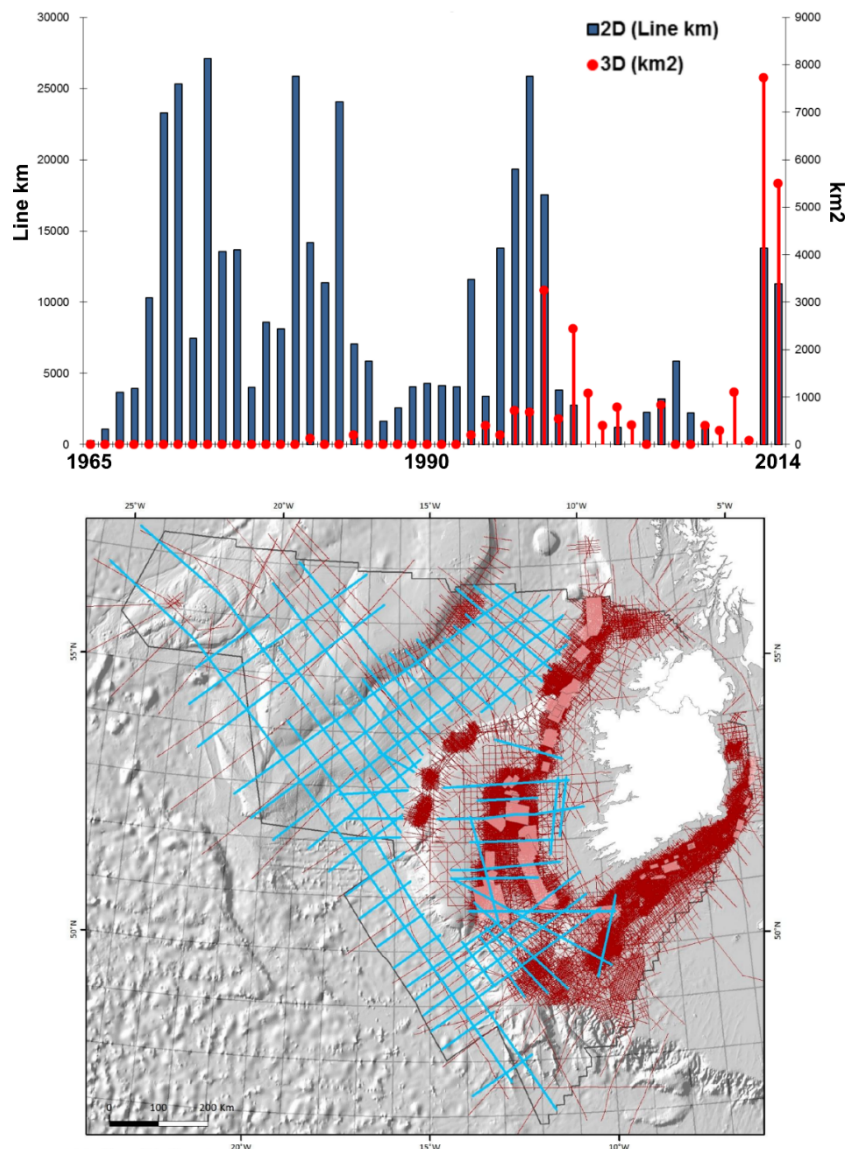


**Fig. 2.3.** Seismic survey effort per year (top) and coverage map (bottom) with the DCENR/Eni regional seismic survey 2013 – 2014 in light blue. Reprinted from Hanrahan and Morgan, (2015, pp. 21 - 24).

offshore including the PB (Croker and Shannon, 1995; Shannon et al., 2001), along with national government sponsored seismic and borehole programmes (ISPSG, 2005). However, finding an up-to-date quantification of seismic survey effort for the PB in the literature has been unsuccessful. A yearly seismic effort plot and coverage map (Fig. 2.3) have been extracted and adapted here from an industry/governmental conference presentation (Hanrahan and Morgan, 2015). The government sponsored DCENR/Eni regional seismic survey 2013 – 2014 (16,800 km of long offset seismic, gravity and magnetic data) is shown in blue (Fig. 2.3 b). Globally the increase in shipping is responsible for an addition of up to 3 dB per decade to the ocean's ambient noise (Andrew et al., 2002; Erbe et al., 2019). Locally there are no major shipping routes through the PB but just to the south, shipping density starts to increase considerably, as seen from a density map for 2019 in Fig. 2.4 (EU Atlas of the Seas). Of note in this figure is the prevalence of trawling along the margin where fishing has been limited to depths above 800 m in EU waters since December 2016 (EU, 2016/2336, 2016). Local target species include demersal whitefish (e.g., cod, haddock, monk), pelagic species (herring, mackerel) and shellfish (most notably the prawn *Nephrops norvegicus*) (Gerritsen et al., 2013;
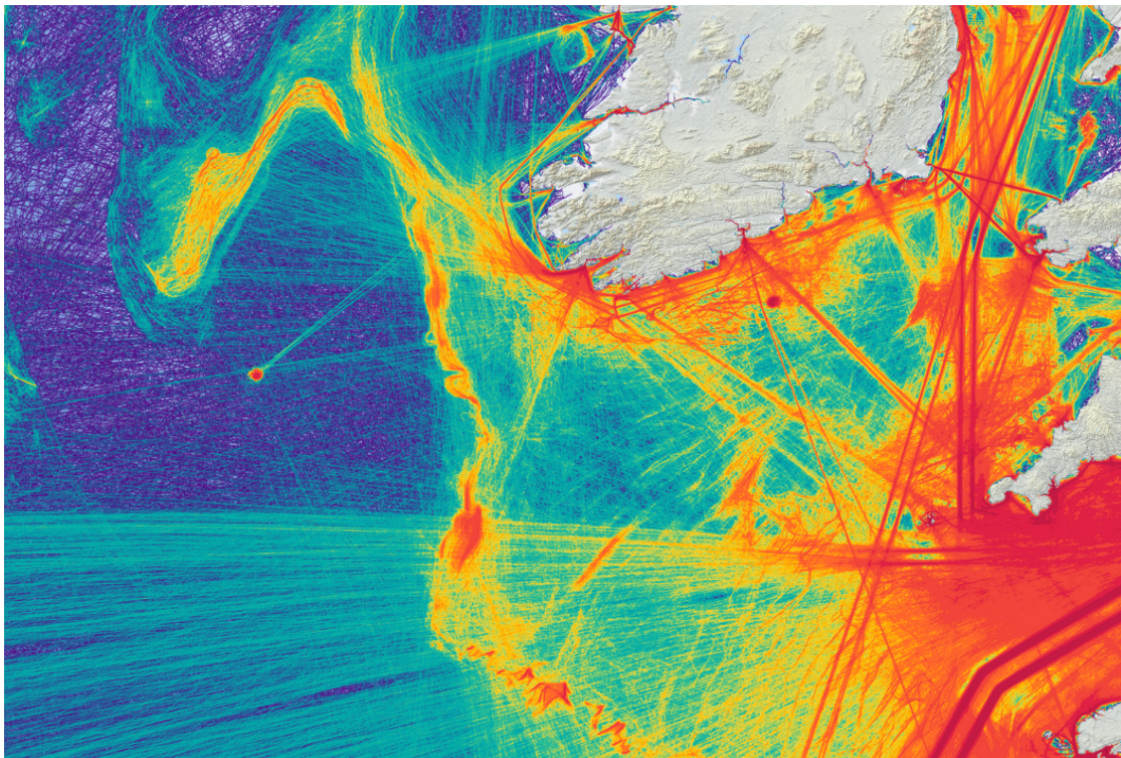


**Fig. 2.4.** Shipping density map of all vessel types from AIS data in 2019 (EU Atlas of the Seas; https://ec.europa.eu/maritimeaffairs/atlas/maritime_atlas).

Gerritsen and Lordan, 2014; Marine Institute, 2019). Bottom trawl fishing in particular has long lasting impacts on the surrounding marine environment, at least an order of magnitude greater than all other human impacts combined (Eastwood et al., 2007; Halpern et al., 2008; Benn et al., 2010).

Piledriving for windfarm development is another impactful activity (Bailey et al., 2010) not yet realised but shortly on-stream for the west coast of Ireland, however, most likely these installations will occur at more inshore sites closer to landfall.

## 2.3. Natural and Ambient Ocean Sounds

Sources of sound in the ocean originate from various inputs ranging from natural physical phenomena to biological and anthropogenic. Some of these sources can be impulsive or transient in nature within a given range before becoming continuous at greater range as they become part of the general background noise. The National Research Council (of America) provide a detailed overview of the various sounds found in the ocean, both natural and anthropogenic, however they highlight the need for further research, for example from natural sea-surface sound sources (National Research Council, 2000, 2003, 2005). Wenz Curves, depicting natural noise sources (wind and wave action) and shipping in the ocean were published nearly six decades ago (Wenz, 1962), yet are still widely used and cited today and have been extended at lower frequencies for sea-states (Cato, 2008) and adapted to include various other sources (for cited examples see Figure 4.2 from Carey and Evans, 2011). Included herein  is a labelled adaption from Jasco's handbook (Erbe, 2011) (Fig. 2.5).

### 2.3.1. Natural physical sources

Excluding shipping noise, the dominant sources of noise across all frequency bands in the ocean averaged over long periods are from natural processes (National Research Council, 2003). Of all the natural inputs of sound, wind driven surface gravity waves dominate through different processes at different frequency bands. Noise from wave action correlates more strongly with wind speed than surface wave height or sea-state (Etter, 2018 and references within). The infrasonic (i.e. < 20 Hz)
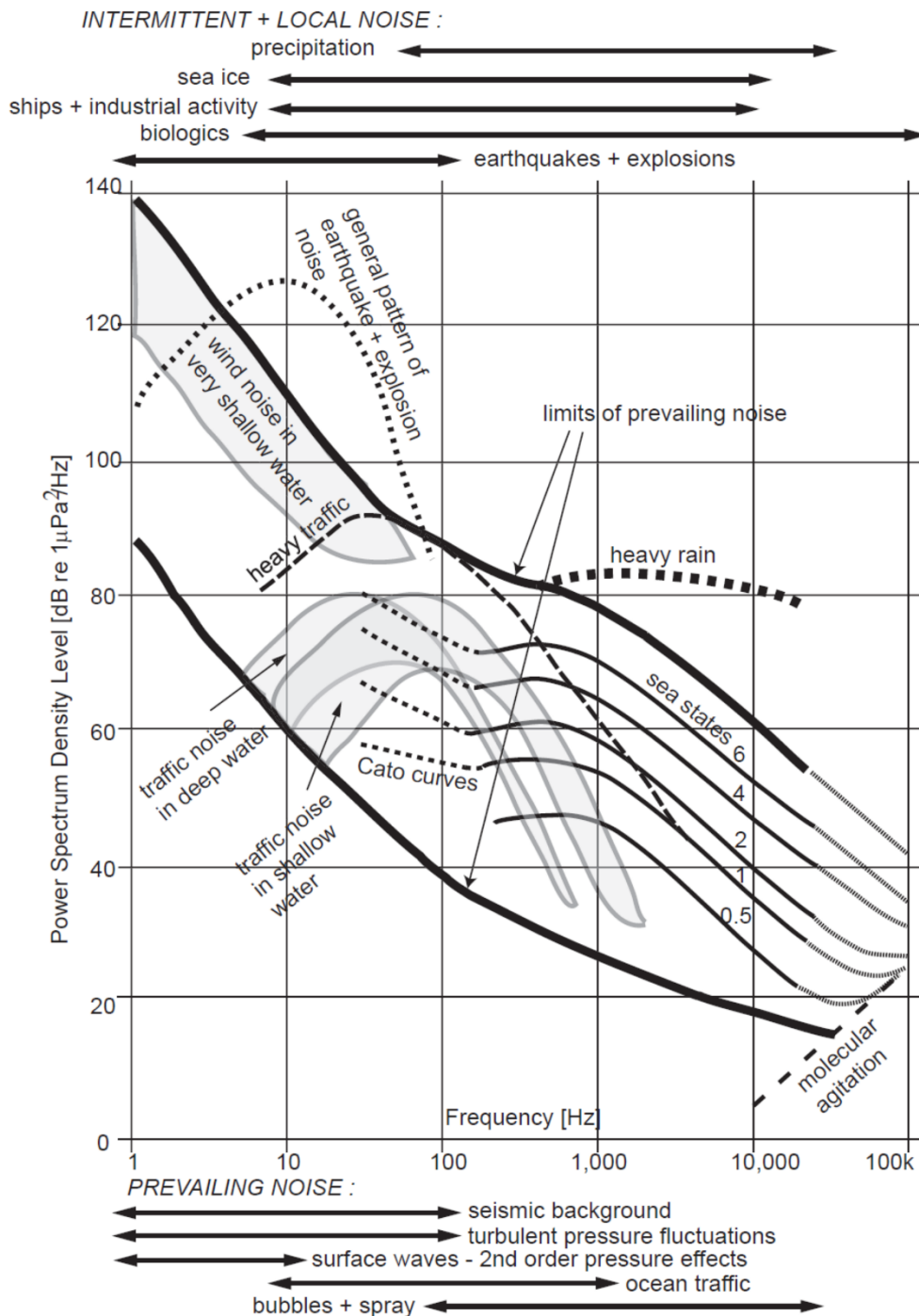
**Fig. 2.5.** Wenz curves (Wenz, 1962) adapted from Erbe, (2011, p. 9).

components of wave noise are termed microseisms and result from surface gravity waves (or even ultragravity waves) interacting from opposing (or nearly opposing) directions, during or shortly after a storm event (National Research Council, 2003; Carey and Evans, 2011; Wilcock et al., 2014). Bubbles entrained in the water column due to wave action create a ringing sound as they oscillate, that provides a component of wind driven natural noise above very low frequencies (Wilcock et al.,

2014). Using a highly impressive method of observing ocean noise, Zhao et al., (2014) dropped drifting hydrophones from an aircraft into the path of three oncoming hurricanes to investigate wind/wave generated sound. They found a non-linear relationship between wind speed and noise that was frequency dependent between the competing phenomena of breaking wave noise and bubble attenuation, concluding that noise from large (hurricane) breaking waves mostly attenuated locally but intermittently penetrated to depths and that bubble curtain attenuation only acted to depths of 2 m even with the greatest of waves (Zhao et al., 2014). Breaking waves on the shore of Monterey Bay provided an anisotropic (shoreward) and omnidirectional rise in ambient noise (20 – 700 Hz) dependent on wave size, with potential to propagate to deeper continental shelf waters (Wilson Jr et al., 1985).

Other, more intermittent, ephemeral and/or regional natural sources also occur, for instance rain (peaking ~15 kHz) is louder when falling vertically (when rain is light) than when incident to sea surface, but less wind dependent when heavy, where it simply adds to the wind driven increase in noise (Ma et al., 2005). Ice provides various sources of noise (e.g., cracking, fracturing), can have a seasonal component and can also occur from icebergs reverberating when they collide with each other or the seafloor (Wilcock et al., 2014 and references within). Earthquake generated 'T-waves' ducted in the deep sound channel, most commonly from a sloping topography (i.e. continental margin) provide one of the primary sources of long-range propagation from discrete seismic events (Okal, 2008).

### 2.3.2. Biological sources

Marine mammals provide the largest, most diverse and broadband input of sound energy to the ocean and although there are a number of marine mammal groups, such as cetaceans, sirenians and carnivores (which include pinnipeds, otters and polar bears) this thesis will primarily focus on the sub-order Cetacea, for its relevance along continental margin settings. Due to the fact that ocean water is three orders of magnitude denser than air, coupled with the fact that it is devoid of light below 100 m in anything but the clearest of waters, makes the ocean realm an ideal medium for audition to prevail as a sensory tool used by mammals and other marine fauna. A plethora of studies and reviews have been carried out on marine mammals' use of sonar and vocalisation for the purposes of navigating, hunting and

communicating, with ongoing research into many aspects of these topics (Wartzok and Ketten, 1999; National Research Council, 2003; Richardson et al., 2013). An example of this is basin wide communication or sensing topography through low frequency transmission (National Research Council, 2003 and references within). Cetaceans are not only diverse in habitat and morphology but also in output frequency bands and hearing sensitivity discussed later in this chapter in relation to harm from humans. Fish and invertebrates also make a considerable contribution to the ambient sound field in the ocean.

Mysticetes (Baleen whales) use baleen plates or sheets to sieve their pray (e.g., small fish, krill, plankton) from the sea water. The largest mammal ever known to inhabit the planet, the blue whale (*Baleanoptera musculus*), falls into this group. Baleen whales communicate, and thus contribute to the ambient soundscape, using low frequency (mostly below 1 kHz) songs, moans or calls, for example blue whales use phrases which consist of up to three units of output > 10 s long each (e.g., Thode et al., 2000; Širović et al., 2007; Wilcock et al., 2014). They use these low frequency, high intensity calls for communication most importantly for mating and feeding, the character of which can vary globally between geographical groups and can be detected at distances of hundreds of kilometres using various methods of acoustic localisation and source level estimation (Thode et al., 2000; Širović et al., 2007; McDonald et al., 2009). Source levels vary from study to study. As a single study example, blue and fin whales were found to have a source of 189 dB re: 1 µPa @ 1 m with blue whales peaking at 25 – 29 Hz and fin at 15 – 28 Hz (Širović et al., 2007).

Odontocetes (Toothed whales and dolphins) hunt fish, squid and other sea creatures. In general they are smaller than mysticetes and more social, in that they live in small or large family groups or pods. Odontocetes emit sound as clicks or click-trains at higher frequency bands than mysticetes. They use rapid sonic echolocation pulses or clicks to build an image of target pray using a biosonar signal generator and a melon (forehead) containing 'acoustic fat' to radiate their clicks in narrow acoustic beams equivalent to a narrow 'field of view' used by many land predators to see their pray (Cranford et al., 1996; Madsen and Wahlberg, 2007; Jensen et al., 2018; Tønnesen et al., 2020). While this mechanism is common across species, morphology and frequency; click characteristics andrange of detection are species or family specific, with larger animals detecting to greater

ranges (Cranford et al., 1996; Madsen et al., 2005; DeRuiter et al., 2010; Tønnesen et al., 2020). For instance, the sperm whale (the largest of the toothed whales) can display directivity (azimuthal) differences of 27 – 35 dB and source levels of between 223 – 236 dB re: 1 µPa @ 1 m (Møhl et al., 2000, 2003).

Fish likewise provide a biological source input of sound to the ocean, through various mechanisms (e.g., through contraction of sonic muscles or rubbing together of bony structures) and for various reasons (communication, alarm, mating) (Kihslinger and Klimley, 2002; Kasumyan, 2008; Slabbekoorn et al., 2010), although in general to a lesser amplitude and more locally than cetaceans. Snapping shrimp rapidly close their claw to generate a sudden impulsive signal for debilitating pray. They have a massive noise to body size ratio and can emit a peak-to-peak pressure of up to 189 dB re: 1 µPa over a very broad-spectrum output (Au and Banks, 1998; Versluis et al., 2000).

### 2.3.3. Background ocean noise

Background or ambient sound in the ocean is an accumulation of multiple sound sources, both natural and anthropogenic, almost always sourced at the surface both locally and further afield. Variation in ambient noise at any given location is wide and dependent on many environmental factors, for instance with depth at equivalent sea conditions, noise is louder in shallower shelf seas. Ambient noise is frequency dependent, where natural sources will dominate up to 10 Hz (wave action or microseisms) and again from ~300 Hz upwards (wave, wind and rain, including distant storms) with frequencies in between predominantly caused by anthropogenic sources (e.g., local and distant shipping, seismic surveys and piling) but will also include bioacoustics sources (low frequency marine mammals) (Ross, 1993; Curtis et al., 1999; Hildebrand, 2009; Jensen et al., 2011).

An effect of note in relation to trawling along the shelf break (Chapter 6), is that of shelf edge enhancement, where noise generated around the shelf edge is entrained into the deep sound channel. This occurs through reflection from a downward sloping seafloor, thus adding to ambient noise at far greater ranges (Wagstaff, 1981; Ross, 1993) as discussed further in Chapter 7. In addition to ambient noise trends increasing decadally (e.g., 3 dB decade$^{-1}$; Hildebrand, 2009) due to anthropogenic forcing from increased development and shipping (Andrew et al., 2002; McDonald

et al., 2006; Hildebrand, 2009; Chapman and Price, 2011), the increase in whale numbers globally since whaling embargoes were introduced, is also adding to background noise (Cato and McCauley, 2002).

## 2.4. Direct Damage to Marine Fauna and Environmental Consequences

There has been extensive research carried out on the adverse effects of human noise including death, damage and behavioural response, as listed in a systematic literature assessment by Harding, et al., (2021), which includes 651 entries, while comprehensive reviews have been carried out on different aspects of this research, such as auditory weighting functions (Houser et al., 2017). This section reviews physical damage to marine mammals, impacts on fish and wider environmental consequences in the context of marine acoustic habitats, while the following section emphasises behavioural disturbance as a key impact in relation to human noise sources.

### 2.4.1. Marine mammal injury thresholds

A hearing threshold shift is a harmful physiological change to an animals hearing mechanism, where their sensitivity to detecting low amplitude sound is decreased as a function of frequency, either for a period of recovery (Temporary Threshold Shift; TTS) or permanently (Permanent Threshold Shift; PTS). This damage relating to mammals, fish and invertebrates can be caused by exposure to bursts of very loud impulsive noise or to prolonged exposure to more constant sources loud enough to cause damage. Both are similar to that experienced by humans on land, an illustration being a loud rock concert or working for years in an industry using loud power tools. One of the primary sources of research that compiled a wide collection of empirical data for quantifying PTS and TTS over the years has been Southall et al., (2007), who divided marine mammals into the hearing groups: low, mid and high frequency cetaceans; pinnipeds in water; and pinnipeds in air. Each group have an estimated auditory bandwidth and a frequency weighting which reflects the group's hearing sensitivity and susceptibility to harm. More recently this working group has updated their noise exposure criteria (Southall et al., 2019) by utilising the work of others (e.g., Finneran et al., 2011, 2002; Finneran, 2016, 2015;

Tougaard et al., 2015) that include newer auditory weighting functions that can be applied to a received sound signal, as was carried out in Chapter 6 (Daly and White, 2021). The works above and much of the extended work that they rely on and reference, correctly comes with cautionary advice and caveats, for instance where the actual hearing sensitivity for these wild animals, especially the low frequency cetaceans are not known but estimated from data on other mammals including humans (Southall et al., 2019). When differences between individual baleen whales and uncertainties in frequency weighting functions are taken into account, the task of predicting TTS for these cetaceans from airgun noise becomes even more complicated, increasing the potential range of harm by 400 – 600 m for a set of modelled animals (Gedamke et al., 2011).

On the topic of airgun seismics, ringed and spotted seals were found to be unaffected by a single airgun at sound exposure levels as high as 181 dB re: 1 µPa$^2$s and peaks of 207 dB re: 1 µPa, albeit under controlled conditions (Reichmuth et al., 2016). In comparison, harbour porpoises are not so resilient, having one of the lowest thresholds of all tested cetacean species at Sound Exposure Levels (SELs) of 164 dB re: 1 µPa$^2$s and peaks of 200 dB re: 1 µPa (Lucke et al., 2009).

A source of even greater potential harm to cetaceans in the wild is that of naval and military activity, especially the use of Mid-Frequency Active Sonar (MFAS) (in general ~3 – 10 kHz). MFAS was found to be responsible for death and mass strandings of various cetacean species (Parsons, 2017; Miller, 2009), with particular concern for beaked whales, despite the lack of, and classified nature of source data available (Cox et al., 2006; DeRuiter et al., 2013; Bernaldo de Quirós et al., 2019).

### 2.4.2. Impact on fish and invertebrates

As with marine mammals previously, the impacts on fish are becoming well understood and reviewed from a collection of human sources that range in impact from death and damage to behavioural response and communication masking (Popper et al., 2003; Popper and Hastings, 2009; Slabbekoorn et al., 2010; Popper and Hawkins, 2019). Depending on their hearing mechanism, which varies across species, fish can suffer damage from particle motion more so than sound pressure exposure (Hastings, 2004; Hawkins and Popper, 2017), which creates issues in

using traditional measuring methods (hydrophones) and metrics (sound exposure) to measure, assess and monitor the environmental impact on fish.

Seismic airguns have been found to cause long-term severe damage to fishes hearing apparatus (McCauley et al., 2003). Shipping too can impact on fish habitat by vastly reducing communication space (Putland et al., 2018) or for instance raise stress levels and reduce predator evasion (Simpson et al., 2016).

Even though research is in its early stages, squid and other cephalopods may have developed auditory capacity to detect prey and avoid predation and are consequently at risk of anthropogenic noise pollution (Mooney et al., 2012). Jellyfish (cnidarians) likewise are susceptible to acoustic damage from anthropogenic noise even though they do not rely on hearing (Solé et al., 2016), highlighting the need for regulation of noise to protect a broader cohort of marine life.

### 2.4.3. Acoustic habitats

Recent work has highlighted the notion of an acoustic habitat or an acoustic environment, providing a useful tool to assess the 'acoustic health' of a soundscape within a given marine environment, taking into account the collection of marine fauna and anthropogenic noise stressors present (Tyack, 2008; Merchant et al., 2015; Duarte et al., 2021). An overall assessment of a local or regional soundscape, using broad studies encompassing the various sources and species affected can then be used to monitor changes in the condition of an acoustic habitat in line with regulatory frameworks and mitigation efforts (Merchant et al., 2016, 2020) as discussed further in Section 2.6.

## 2.5. Anthropogenic Noise Sources and Behavioural Impacts on Marine Mammals

Human activity has increasingly added noise energy to the ocean especially since the industrial revolution and the prevalence of merchant shipping. Anthropogenic noise or 'anthrophony' takes the form of many source types, both impulsive and continuous (e.g., Hildebrand, 2009; Merchant et al., 2016; Erbe et al., 2019) , and

with increased shipping and offshore development (e.g., windfarms), requires more rigorous regulation and mitigation strategies (Tasker et al., 2010). Anthrophony, in all its forms, has impacted on the natural marine environment, manifesting as a set of stressors to many marine lifeforms over various spatial and temporal scales and across wide frequency bands, depending on source type and receiver (i.e. animal) sensitivity (Duarte et al., 2021).

One of the most impactful stressors, behavioural disturbance in marine mammals, where an animal or group of animals are interrupted from normal activities due to anthropogenic noise, can be species specific and depends on the noise source (National Research Council, 2000, 2003, 2005; Cato et al., 2004; Erbe, 2013; Richardson et al., 2013). It can take various forms, from startling to defensive diving, avoidance, communication masking, separation of mother and young and by altering migratory routes or foraging methods (Nowacek et al., 2007; Ellison et al., 2012; Richardson et al., 2013; Erbe et al., 2016).

The following aims to cover a select range of subtopics on behavioural effect while highlighting certain areas most relevant to this thesis. Each source type is examined by first looking at source noise generation and output followed by its impact on marine mammal behavioural response, being the most relevant environmental stressor and one of the main motivating factors for carrying out this work.

### 2.5.1. Seismic surveys, shipping and bottom trawling

2.5.1.1. Source noise

One of the loudest pulsed noises found in the ocean is that of offshore geophysical surveys using seismic airgun arrays for exploration of hydrocarbons, which can be somewhat widespread globally, dependent on viability dictated by oil prices. This form of noise is most pertinent to this PhD project, having been investigated in Chapter 4 (Daly et al., 2020) and used as a controlled source experiment in Chapter 5. A full description of how an airgun operates can be found in methods (Chapter 3.2.1). Primary and residual pulses along with interference spectra are displayed in Fig. 2.6 a & b. Strength of an airgun array is proportional to airgun air pressure, amount of guns in the array (Fig. 2.6 c) and to the cube root of each airgun volume, while airgun depth (not directly proportional to strength) is convenient for tuning primary-to-bubble ratio (Dragoset, 2000). Airgun and array source signatures and
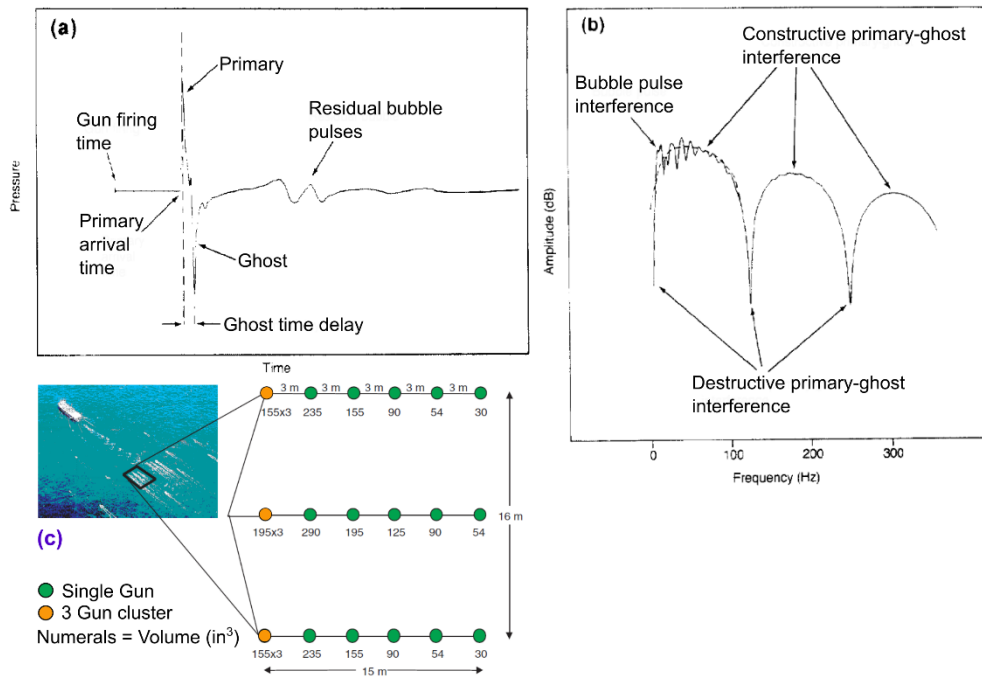
**Fig. 2.6.** Airgun signature (a) and spectra (b) with labelled characteristics adapted from Dragoset, (1990, p. 2). (c) is a typical airgun array setup adapted from Dragoset, (2000, p. 2).

spectra are most readily available from manufacturers using industrial modelling software (e.g., www.gundalf.com) but have been studied in greater detail for single guns (Duncan and McCauley, 2000; Crocker and Fratantonio, 2016) and gun arrays (Nedwell et al., 1999; McCauley et al., 2000a; Duncan, 2009). Peak frequencies are well below 500 Hz but will still show elevated spectra > 2000 Hz and Source Levels (SLs) can be anything between 221 dB re: 1 µPa RMS @ 1 m (e.g., for the Mini-GI gun used in this project; Crocker and Fratantonio, 2016) up to 262 dB re: 1 µPa @ 1 m for a 2 x 14-gun array, although Nedwell et al., (1999) admit that this higher end (modelled) value is exceptionally and suspiciously high.

Shipping, predominantly through propeller cavitation and engine vibration, is by far the most globally and regionally pervasive source of anthropogenic noise (Erbe et al., 2019), with a lot of modern research concentrated on ship noise in the context of environmental damage and regulation (Erbe et al., 2012; Merchant et al., 2012). There are many specific studies into source levels of cargo ships (Scrimger and Heitmeyer, 1991; Arveson and Vendittis, 2000; Wang et al., 2012). Shipping source levels used for comparison in Chapter 6 (Daly and White, 2021), along with other studies from the literature, demonstrate a wide variety of source level estimates and peak frequency bands. Smaller more inshore/coastal sources also contribute to the

ambient soundscape for example, jet skis (Erbe, 2013b) or rigid inflatable boats (RIBs) (Erbe et al., 2016), although not nearly to the extent of shipping.

Bottom trawl fishing can be seen as a subset of ship noise, with the addition of noise from the fishing gear being dragged along the seafloor (as demonstrated in Chapter 6; Daly and White, 2021) and although there are some previous studies carried out on trawler noise, the majority focussed on noise in relation to target catch (e.g., Buerkle, 1977, 1973; Ona and Toresen, 1988; Ona and Godø, 1990). Other research has looked in more detail at source levels of fishing vessels but only from radiated noise while the vessel is underway (Peña et al., 2011; Peterson et al., 2011; Peng et al., 2018a, b) but not actively bottom trawling. Trawling was statistically investigated in relation to ambient noise in the Arabian Sea and found to dominate in the absence of a sea breeze (Kannan et al., 2015). One study was found that investigated the difference in noise from a fishing vessel dependent on if it was actively fishing or not, exhibiting spectral levels between 80 – 1000 Hz to be considerably higher (5 – 10 dB) while trawling (Hovem et al., 2015). Despite 10 dB representing a 10-fold increase (in power or SEL) the authors stated it was "…not very much higher…"

2.5.1.2. Human impact

Seismic surveys are well known to disturb marine fauna, with larger arrays being more disruptive (e.g., McCauley et al., 2000; Gordon et al., 2003; Thompson et al., 2010) but disruption can be reduced by increasing the firing interval which will in turn reduce the cumulative effect and contract the zone of impact (Breitzke and Bohlen, 2010). Mobile fauna such as mammals utilise species specific avoidance tactics (Stone and Tasker, 2006). Studies on baleen whales, including humpback (e.g., Cato et al., 2013; Dunlop et al., 2015, 2017) and blue (Di Iorio and Clark, 2009), have shown avoidance of seismics surveys at approximately 4 km range, a slowing down of migratory progression (McCauley et al., 2000b; Dunlop et al., 2015, 2017) and changes to communication patterns (Di Iorio and Clark, 2009). By contrast, young male humpbacks can be attracted to airgun arrays, possibly mistaking them for another whale breaching (McCauley et al., 2000b). All the above studies are limited by methods, models and sample size, each of which are improving with time (Cato et al., 2013).

Toothed whales, having a higher frequency repertoire for vocalisation than baleen whales, are less susceptible to the lower frequency peak noise from airgun shots, for instance by 35% less of a decrease in sightings due to the presence of a survey (Kavanagh et al., 2019). However, odontocetes remain susceptible and show behavioural disturbance due to the unintentional higher frequency component of airguns up to 3 kHz and beyond (Madsen et al., 2002, 2006). Even though research is sparse on beaked whales due to difficulties in sighting and acoustic monitoring, they too are at risk from seismic surveys, with controlled exposure experiments being proposed as the best method to gauge their behavioural response (Barlow and Gisiner, 2006). Beaked whales are pertinent to this project due to their presence in our study area (McCauley, 2015) and their deep diving behaviour and potential favouring of canyon habitats.

As well as direct collisions, shipping can harm marine mammals by emitting persistent sound that increases ambient levels to considerable distance and masks an animal's ability to communicate or echolocate (e.g., Southall, 2005; Erbe et al., 2019 and references within). Low frequency (20 – 200 Hz) noise from large cargo vessels has been found to raise stress levels and alter foraging behaviour for large mysticetes (Rolland et al., 2012; Blair et al., 2016), while shipping can also directly cause behavioural effects on high frequency species (Wisniewska et al., 2018). Smaller, higher frequency emitting whale watching vessels are found to force sperm whales to change course more frequently (Richter et al., 2006). Reduced foraging ability and habitat degradation are found in smaller cetaceans and seals in shallower inshore waters from both large vessels and smaller craft, including at locations adjacent to Special Areas of Conservation (SACs) (Merchant et al., 2014; Chen et al., 2017; New et al., 2020).

### 2.5.2. Other anthropogenic sources and impacts

2.5.2.1 Source noise

Piledriving for offshore development (mostly wind farms) is confined to shallower shelf/coastal waters, where SL, being proportional to diameter of pile (among other parameters, e.g., depth) will vary, for example 226 dB re: 1 µPa @ 1 m from a 1.8 m pile peaking at 100 Hz (Bailey et al., 2010), or 168 dB re: 1 µPa RMS @ 1 m (at 3 kHz) (Luís et al., 2008). Military and naval operations are also responsible for high levels of sound energy input to the ocean, that said they are notoriously difficult to

study due to their covert nature and classified datasets. MFAS used for vessel and submarine detection (e.g., emitted across a band 4.5 – 5.5 kHz in Bernaldo de Quirós et al., 2019) is perhaps responsible for the greatest cetacean mortality per single event. Hydroacoustic Monitoring programmes are in place to detect nuclear explosions in the ocean (e.g., the CTBT (Lawrence, 2004; ctbto.org); and mine clearing exercises regularly take place involving the neutralising of unexploded ordnance (Bagocius, 2013).

The hydrocarbon industry employs many methods of exploration, prospecting, extracting and processing offshore oil and gas (Jiménez-Arranz et al., 2018), with continuous noise input not just limited to drilling (Erbe and McPherson, 2017) or production (e.g., Erbe et al., 2013) but substantially from the thrusters of the large vessels used to keep them in place and from smaller offshore support vessels. Observed and modelled levels of source noise for entire operations, including thrusters and industrial activity have been found for mobile drilling rigs of 150 – 195 dB re: 1 µPa RMS @ 1 m (Parnum et al., 2013;  Erbe and McPherson, 2017; MacDonnell, 2017) and for an offshore production vessel of 188 dB re: 1 µPa @ 1 m (Erbe et al., 2013). It must be noted that SLs will not only vary depending on rig size, amount of thrusters and type of activity undertaken, but on method and metrics used to calculate the broadband level (e.g., frequency bands) and are not always directly comparable.

Other continuous sound sources smaller in scale but growing in number are also found in the world's seas and oceans. Acoustic Deterrent Devices (ADDs) designed to harass and deter pinnipeds away from fish farms emit 'sweeping tonal broadcasts' of 3 – 40 kHz at levels up to 185 dB re: 1 µPa RMS @ 1 m (Lepper et al., 2014; Findlay et al., 2018), that said, these relatively high frequencies in relatively shallow water will have environmental impacts more local in nature. Erbe et al., (2018) report an increase to coastal ambient underwater noise of up to 36 dB while investigating noise from passenger airplanes transferred to the water column and caution that, as many airports are coastally based this noise needs environmental consideration.

2.5.2.2. Human impact

Occurring mostly in shallower waters, piledriving will affect the most common species found in these habitats, for instance dolphins and seals. Bottlenose

dolphins showed behavioural response as far away as 50 km to a piledriving site but were not found to suffer physiological harm until approximately 100 m from source (Bailey et al., 2010) and were found to have a zone of behavioural disturbance where levels were 14 dB above background (Luís et al., 2008), while Carstensen et al., (2006) found harbour porpoises left an area under construction for extended periods after noise events. ADDs are found to disturb not only their target seal species, but resident cetaceans as well (Lepper et al., 2014; Findlay et al., 2018).

## 2.6. Managing Anthropogenic Noise Pollution

The MSFD is the main statutory framework that governs underwater noise for all EU states (European Commission, 2008) under Descriptor 11 (D11): Energy including underwater noise, or more specifically "Introduction of energy, including underwater noise, is at levels that do not adversely affect the marine environment". Under D11, Anthropogenic noise in the ocean is classed as a pollutant (Tasker et al., 2010). Good Environmental Status (GES) criteria and indicators (e.g., Criterion 11.1: distribution in time and place of loud low and mid frequency impulsive sounds or Criterion 11.2: Continuous low frequency sound) are used by member states to monitor noise pollution in their jurisdiction (Van der Graaf et al., 2012; Dekeling et al., 2014a, 2014b). More broadly, GES indicators (for D11) can be used across member states to guide policy and monitoring strategies, for example, the provision of a Noise Register to establish base-levels and trends in impulsive noise across EU EEZs. Erbe, (2013) highlights the many challenges involved in coordinating an international response to underwater noise regulation. Different nations/groups use different criteria, methods of monitoring and threshold levels for injury and disturbance to marine fauna under guidelines which are often updating as the science and understanding of behavioural response develops (Erbe, 2013).

Through regulatory frameworks, any maritime development or activity with potential for harm will require an Environmental Impact Assessment (EIA) prior to commencing a project. Primarily regarding marine mammals, zones of harm must be calculated, and mitigation strategies proposed as part of any EIA, following accepted guidelines (Merchant et al., 2012; Faulkner et al., 2018) (for an infographic

example of an EIA workflow see Fig. 2.7 adapted from Faulkner et al., 2018; Figure 1). Due to these relatively recent requirements, regulatory understanding and the methods employed by environmental consultancy companies are not always up to date, coupled with multiple physical and biological factors and a somewhat un-standardised field of science, provides many problems in modelling (Farcas et al., 2016), measuring (Duncan and McCauley, 2008) and assessing environmental impact.
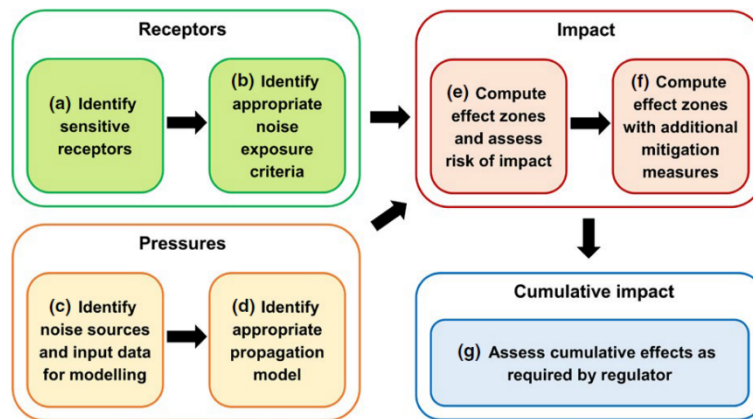


**Fig. 2.7.** Environmental Impact Assessment (EIA) workflow diagram taken from Faulkner et al., 2018, p. 2532.

Decreasing the harm from human noise, through mitigation strategies that include noise reduction measures and zones of safety (i.e. exclusion zones) are key regulatory tools in the protection of vulnerable marine fauna. A 'carrot and stick' approach is proposed by Merchant, (2019) for reducing noise from three main industries responsible (shipping, piledriving and offshore seismics) through stricter regulatory control and incentive-based measures. Guidelines are published to minimise the risk of noise exposure (most commonly from seismic surveys) through mitigation methods such as lower volume arrays directed more exclusively in the vertical, safety exclusion zones (internationally common at 500 m), soft-start (or ramp-up) procedures and onsite monitoring using marine mammal observation and passive acoustics. Different nations and regulatory bodies implement different guidelines, highlighting the need for a common consensus and standardisation of noise reduction strategies (Compton et al., 2008; Nowacek et al., 2013; Wright and Cosentino, 2015). In Ireland anthropogenic noise mitigation guidelines were issued and are maintained by the National Parks and Wildlife Service (DAHG, 2014). The

International Quiet Oceans Experiment (IQOE) is a collaboration of international experts in the field, coordinated by the Scientific Committee on Ocean Research (SCOR), that aims to consolidate strategies of mitigation across nations and regulatory bodies (Boyd et al., 2011; Ainslie et al., 2019). The most recent initiative under IQOA is an Open Portal to Underwater Soundscapes (OPUS) (Thomisch et al., 2021), that will facilitate the upload of standardised data to a centre for shared use and the provision of a cumulative sound map. Regionally there are monitoring initiatives including OSPAR, which aims to build an impulsive noise register for the northeast Atlantic (OSPAR, 2017; Merchant et al., 2020). JONAS (Joint framework of Ocean Noise in the Atlantic Seas), of which Ireland is a contributor and STRIVE, which was an Irish Environmental Protection Agency (EPA) noise monitoring programme between 2007 – 2013 (Beck et al., 2013; Sutton et al., 2013) are the most locally relevant. For a comprehensive subset of monitoring programmes see Ainslie et al., (2019): Table 1.

An important tool in the quest to limit the impacts of human activities on the marine environment, including that of acoustic pollution, is the use of area-based protection, such as SACs or Marine Protected Areas (MPAs). One suggestion is to focus on areas of special ecological concern that are already in quiet locations of the ocean, to build protection around them through exclusion zones before human noise energy increases in these areas, thus limiting the societal cost of further regulation (Williams et al., 2015). Another tactic is to simply add more MPAs in areas of important marine habitats. Such plans are underway in Irish waters, to increase the network of MPAs, in both shallow and deep water, through expert scientific and legislative consultation (Marine Protected Area Advisory Group, 2020), in order to adhere to Ireland's commitments on the OSPAR convention, the MSFD, the UN Convention on Biological Diversity and on UN Sustainable development Goals (e.g., SDG number 14, Life under water).

An unexpected reprieve from the pervasive addition of anthropogenic noise pollution was experienced by marine ecosystems, as observed during the COVID-19 pandemic, which forced an economic slowdown in global shipping (Thomson and Barclay, 2020). Unfortunately, it will only prove a temporary break from this aspect of human interference with the oceans. Ocean acidification, forced by extra ocean uptake of anthropogenic $CO_2$, not only negatively impacts many marine species in its own right but also further enhances noise in the ocean due to less

chemical absorption of sound caused by increased pH levels (Hester et al., 2008). Other factors, for instance the increase in plastic pollution (Wieczorek et al., 2018) or climate change and long-term ocean warming trends, further compound the combined effects of anthropogenic forcing on the health of the natural marine environment.

# Chapter 3: Methods

This chapter details some of the conventional methods used to measure sound levels along with some novel approaches taken specifically for this project. Some detail is provided on testing and validation procedures that do not appear within the main outputs of the project. Oceanographic instruments and methods of analysis are covered, as are computational methodologies and structures.

## 3.1 Main Study Area and Survey Design

The northeast North Atlantic hosts a varied range of topographic features, as the ocean floor rises from abyssal depths to meet the western European continental shelf, including features such as the shallow banks of Hatton, Rockall and the Porcupine. South of the Porcupine Bank and southwest of the Irish coast, the Porcupine Basin (PB; otherwise known as the Porcupine Seabight) is a semi-enclosed sedimentary basin opening out at its base (~2500 – 3000 m), from the southwest, into the Porcupine Abyssal Plain. The geology of this extensional, deep sedimentary basin includes Mesozoic and Cenozoic sediments up to 10 km thick, underlain with thinning continental crust (Shannon, 1991; Van Rooij et al., 2007). Features of the Porcupine Basin include the Gollum Channel, which is a branching channel system that converges from the eastern side of the basin to a centralised channel at the basin centre (Fig. 3.1). Directly north of the north most branch of the Gollum Channel is a minor, east-west orientated submarine canyon incised to the shelf edge, just below the 200 m contour and opening onto the basin floor below 1500 m. Directly south of this canyon, between it and the Gollum Channels, the topography is more similar to a typical (gently inclined and un-incised) slope setting.

It is due to the geomorphological contrast of these two settings that the area was chosen for study of sound propagation. A research experiment using a controlled airgun  source and an array of fixed acoustic moorings was commissioned and executed in June 2018 on-board the R.V. Celtic Voyager, titled 'Propagation of

Acoustic Noise in Canyons (PANiC)', which provided a full set of results for Chapters 5 and 6.
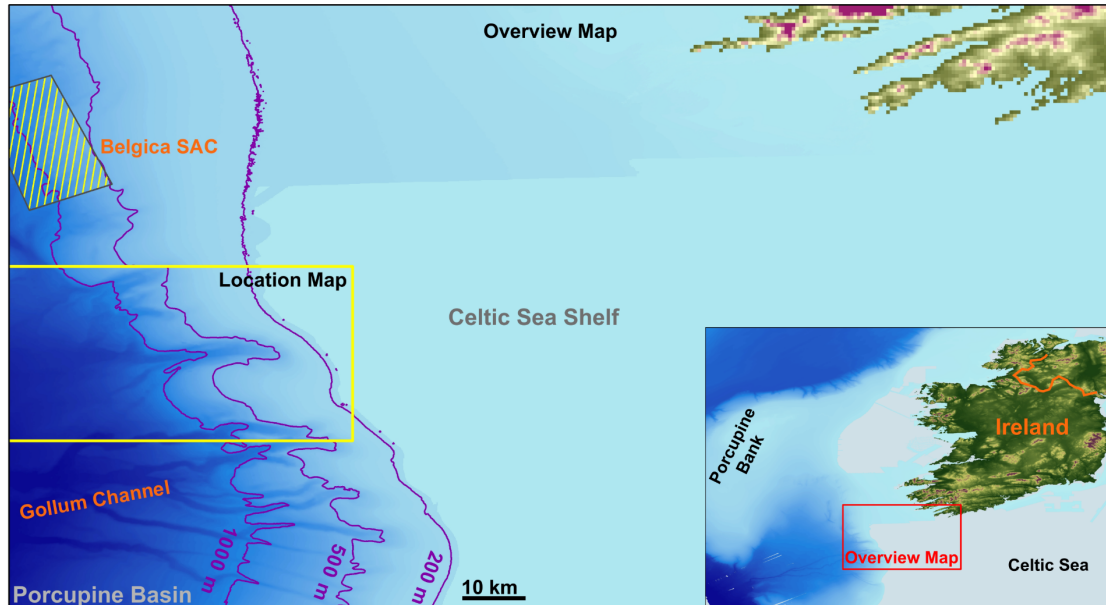


**Fig. 3.1.** Overview map of the area including an inset of the greater region. Boundary of the location map Fig. 3.2. is marked with a yellow box.

Within the PANiC survey area, two locations were selected, at suitable depths, to place acoustic moorings along the canyon axis and two range comparable locations were chosen across the slope, parallel with canyon axis, to match the canyon moorings. A fifth mooring was placed on the shelf edge at the canyon head. These mooring positions are denoted as M1 – M5 throughout the project and are labelled in Fig. 3.2. As well as fixed acoustic moorings, a drifting buoy was employed to gain additional data, in a way that was portable during the survey. Unfortunately, a loose piece of chandlery precluded the drifter's acoustic data from any comparative analysis.

A sound source airgun transect was plotted that part encircles the fixed moorings traversing both parallel and orthogonal to canyon (and slope) axes (yellow line in Fig. 3.2). The primary objective was to mimic a full scale industrial seismic survey, which would likely shoot along transects parallel to the margin keeping depth as constant as possible (i.e. the north-south section here). The objective was also to provide here a varied selection of depths at source, receiver depths and ranges,

thus the addition of the two east-west sections. Locations of specific interest were identified as end points of pathways that travelled straight through two mooring positions forming a grid like pattern, seen as numbered airgun shot points prefixed with the label A and propagation pathways displayed as pink lines in Fig. 3.2. This grid shape was also designed with 3D modelling in mind, where having these evenly spaced points across varying depths would feed observed values into any 3D model build for calibration and verification purposes. In order to provide enough data points yet limit the input of noise energy to the surrounding environment, shot timing for the airgun was chosen at 60 s intervals along the transect, switching to 30 s intervals while passing through the points of interest A1 – A13. This, along with the small volume capacity of the airgun itself, limits the anthropogenic impact of the survey compared to an industrial operation (that could fire an array, of say 32 airguns or more, every 10 seconds), yet provides a sufficient noise source for measuring received sound levels.
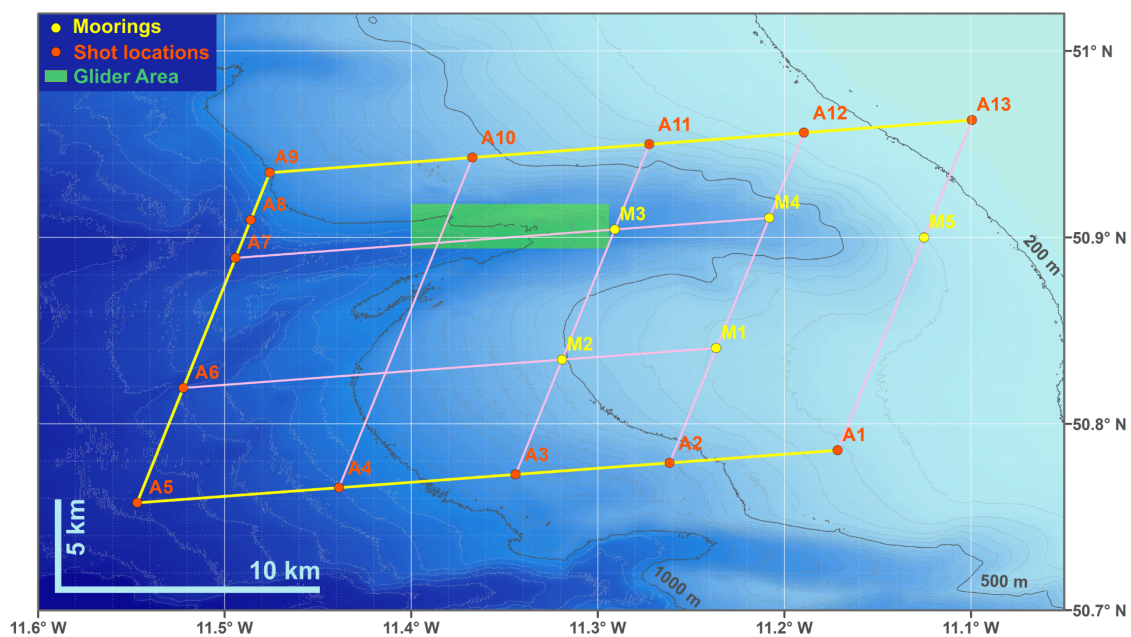


**Fig. 3.2.** Location map showing mooring positions prefixed with an M (yellow points), airgun transect (yellow line), Airgun locations prefixed with an A (orange points), propagation pathways (pink lines) and glider survey area (green polygon). Note that for this map projection (WGS84) distance scalebars are not equivalent northward and eastward.

As part of the process of conducting an offshore seismic airgun survey for research, various paperwork had to be in place. Ship time on the Celtic Voyager had to be applied for to the Irish Marine Institute and won through a competitive cruise proposal application. Permission had to be sought from the Petroleum Affairs Division (PAD) at the Department of Communications, Climate action and Environment (DCCAE) to conduct an offshore seismics survey. Guidance was sought from the National Parks and Wildlife Service (NPWS), with regard to mitigation of airgun noise impacts, and a resulting Risk Assessment was submitted. On guidance from the NPWS, a marine mammal observer (a member of the Irish Whale and Dolphin Group, IWDG) joined the cruise and observed for marine mammals during daylight hours of airgun operation. No sightings took place while the guns were firing. Also, ramp-up or 'soft-start' procedures were incorporated as a mitigation strategy following NPWS guidance (DAHG, 2014). A marine notice was issued to the Irish Coastguard for transmission to seafarers, warning of our mooring locations. Additionally, a notice was issued to the fishing industry of our intentions to convene a seismics survey at its location. A final cruise report was completed and supplied to the Marine Institute.

## 3.2 Hardware, Mooring Design and Deployment

### 3.2.1. Airgun operation

The airgun used was a Sercel MiniGI gun with a 20 cubic inch ($in^3$) generator chamber and a 20 $in^3$ injector chamber combining to make the gun a 40 $in^3$ capacity airgun. The principle behind having two separate firing chambers is that when their firing is offset by some milliseconds, the second expulsion of air from the injector chamber moderates the implosion of the primary bubble created by the first expulsion from the generator chamber and flattens the bubble oscillation to produce a sharp initial impulse but very little residual pulses, resulting in a 'cleaner' shot and higher resolution return signal. On advice from the owner of the airgun (Fig. 3.4a) (Prof. Dr. Sabastian Krastel from the University of Kiel, who kindly lent us the device), our timing offset was set to 0.25 ms throughout the PANiC survey.

In order to operate the airgun, a large air compressor and air collectors had to be brought on-board (Fig. 3.4b, c), which had to be compressed to 130 – 135 bar of pressure. Due to the inherent danger of working around such high pressure, full training was undertaken (provided by Sebastian Krastel), a Standard Operating Procedure (SOP) was produced, and extra safety measures were put in place, for example, cordons around the pressurised gear and discussing safety concerns with the ship's crew.

### 3.2.2. Recording of underwater acoustics

The hydrophones used to measure the instantaneous changes in sound pressure were GeoSpectrum M14-600 phones, considered as industry standard, marine grade deep water hydrophones. They are a medium frequency omni-directional phone rated to 6000 m with a pre-amplified output gain, in this case set to 35 dB by the manufacturer on order, with an output signal of voltage (Fig. 3.4d). The output signal was highpass filtered > 2 Hz (on special request from its usual > 5 Hz highpass) and had no lowpass filter imposed.

Each hydrophone had its own recorder, an RS-ORCA, provided by the supplier RS-Aqua (Fig. 3.4e). The ORCAs are a broadband underwater acoustic recorder, processor and real-time data acquisition system, with five channels available and with adjustable sampling rate and duty cycling capabilities. All ORCAs during the PANiC deployment were set to 48 kHz, with no duty cycling. Each ORCA has a titanium casing rated to 3000 m, an internal battery pack of 72 replaceable lithium batteries, a 500 Gb Solid State Drive (SSD) for storage and dedicated 'Trak' software for setup, testing and data download. In total, 10 sets of hydrophones and



**Fig. 3.4.** Acoustic source and receiver equipment. (a) airgun and harness, (b) air compressor readout dials, (c) air collectors and dials, (d) GeoSpectrum M14-600 hydrophone (e) RS-ORCA acoustic recorder.

recorders were provided by the iMARL suite of instruments hosted by DIAS Geophysics in Dublin; eight of which were utilised for the PANiC experiment.

### 3.2.3 Hydrography and positional data

SeaBird MicroCAT SBE-37 temperature and conductivity sensors were mounted on moorings M2 and M3 and on the drifting buoy, with the deeper instruments on M2 and M3 including a pressure sensor. Readings were measured every minute and saved to file (Fig. 3.5a).

The vessel mounted Conductivity Temperature Depth (CTD) package consisted of a rosette of 12, 10 L Niskin bottles and a SeaBird SBE-911 CTD sensor, the workhorse of oceanographic instrumentation (Fig. 3.5b). Included on the payload was a turbidity meter, fluorometer and oxygen sensor. The main CTD unit, which measured raw temperature, conductivity and pressure, sampled as voltages at 24 Hz, through post-processing output its data to bins of either 1 dbar of pressure or 1 m depth. The primary variables of pressure, temperature and conductivity provided the derived variables of salinity, potential temperature, density and sound speed (ms$^{-1}$, Chen Malaro equation), and along with the other sensors the additional variables of turbidity (uncalibrated), fluorescence and dissolved oxygen.

The glider, named 'Lochra na Mhara' translating to 'Warrior of the Sea' (Fig. 3.5c), hosted by the Marine Institute, was a Slocum 1$^{st}$ generation sea-glider, with a
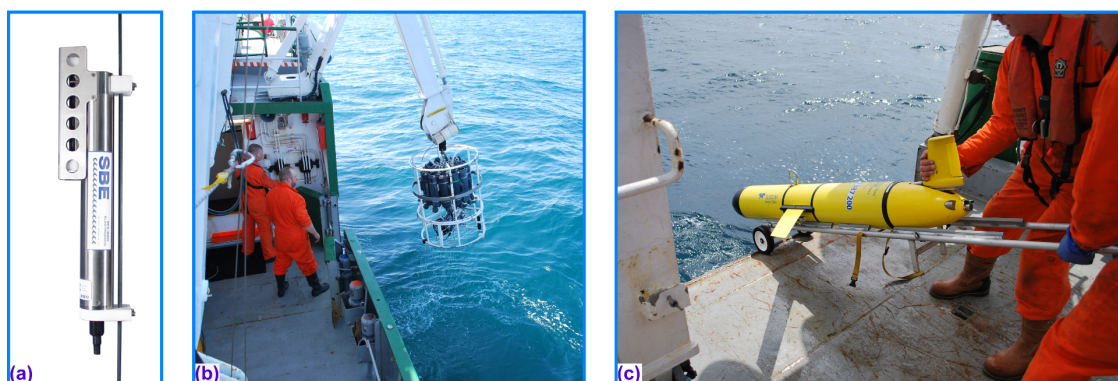


**Fig. 3.5.** Hydrographic instruments. (a) MicroCAT, (b) CTD rosette, (c) Sea-glider

payload of instruments that included temperature, conductivity, pressure, turbidity, fluorescence and dissolved oxygen. The glider required a pilot on-board the research cruise and was constrained to dive to 800 m (almost full depth capacity) within a designated area (marked as a green rectangle in Fig. 3.2), with this survey being its first successful deep-water deployment. There were issues that prevented the provision of the PANiC glider data over the course of the following two years. Eventually, the author had to assist the Marine Institute in setting itself up as a Data Assembly Centre (DAC) for the 'Everyone's Gliding Observatories – EGO' glider data management package. This involved implementing an EGO toolbox on Matlab, collating all required ancillary and calibration files, providing a step-by-step SOP for other users, and packaging the processed data for upload to the Global DAC (GDAC), the EU marine service, Coriolis. The effort resulted in the retrieval of the fully calibrated and processed dataset for the PANiC survey. Using a Matlab script, temperature, pressure and salinity have been used to derive a variable of sound speed from the glider data, for further analysis in Chapter 5.

On-board the Celtic Voyager the Shipboard Computer Systems (SCS) saved to file various positional and environmental parameters from the research vessel, every 10 s throughout the duration of the cruise. Outputs included latitude, longitude, time, heading, water depth, surface temperature, surface salinity, sea-state, wind speed and wind direction (amongst others). SCS data, once processed by the Marine Institute, was used here to more accurately constrain positions of mooring deployment and airgun locations compared to the traditional method of paper log sheets (of which we also used, to great convenience).

### 3.2.4 Mooring design

The moorings for the PANiC survey were designed with a number of considerations taken into account, such as number of available instruments, planned instrument depths, recovery strategy and noise limitations. Another consideration was storage space and vessel operability. Once all moorings and anchor weights had been stowed on the Celtic Voyager, along with the air compressor and air collectors, the working deck was at full capacity, with little room remaining for deployment operations.

It was decided that the deepest mooring locations over the canyon and slope, would each host two hydrophone recorders, one as close to the seabed as possible (~4.5 m above bottom), while the second recorder was placed at 100 m depth to ensure a depth below the seasonal thermocline. This 100 m depth was common with the single recorders on all other moorings and the drifter (Fig. 3.6a). These two deeper moorings (M2 and M3) also had the only MicroCATs with pressure sensors included. The moorings were fabricated in sections for storage and deployment purposes and were finally connected during deployment (Fig. 3.6b). They were deployed weight first (a chain clump) and lowered steadily from the vessel's net-drum, which could only fit one mooring line at a time. Instruments were attached to pre-marked positions on the mooring line, as it was lowered, using metal backing plates or 'strong-backs' as a protective interface between line and equipment. All moorings were full depth from bottom to surface. The main buoyancy for the mooring line was in the form of subsurface floats (CRP80s) with an upwards force at approximately double that of the downwards weight of all the instruments and chandlery attached to the line, while the anchor weight was set to approximately four times the total upwards force (i.e. buoyancy less the weight on the rope) (for details see Fig. 3.6c). A surface spar-buoy and beacon locator and also a leading line and small dan-buoy were used for recovery purposes. Although each mooring had an acoustic release placed directly above the chain weight, these were purely for back-up in case of line fouling or loss of surface buoys. The main purpose of having surface buoys was for visibility, to prevent getting snagged by any passing bottom trawlers, but also for ease of recovery.

In order to limit self-noise or 'strum' caused as water advects across a taut mooring line, noise buffers or 'flaps' were attached to the line above and below each hydrophone recorder. These makeshift flaps were made out of tarpaulin, and although it is not fully understood how they work (perhaps by creating turbulence in the passing water), anecdotal evidence and advice was received from an experienced technical manager working with the R.V. operations team, which led to the flap's inclusion. Every piece of chandlery was also lashed together with twine to prevent the metal 'clinking' as another self-noise source.

A drifting buoy was designed and built, in addition to the fixed moorings, and held a payload of one recorder and two MicroCATs. The purpose of the drifter was to be portable and easily deployable in different locations. Although the drifter was
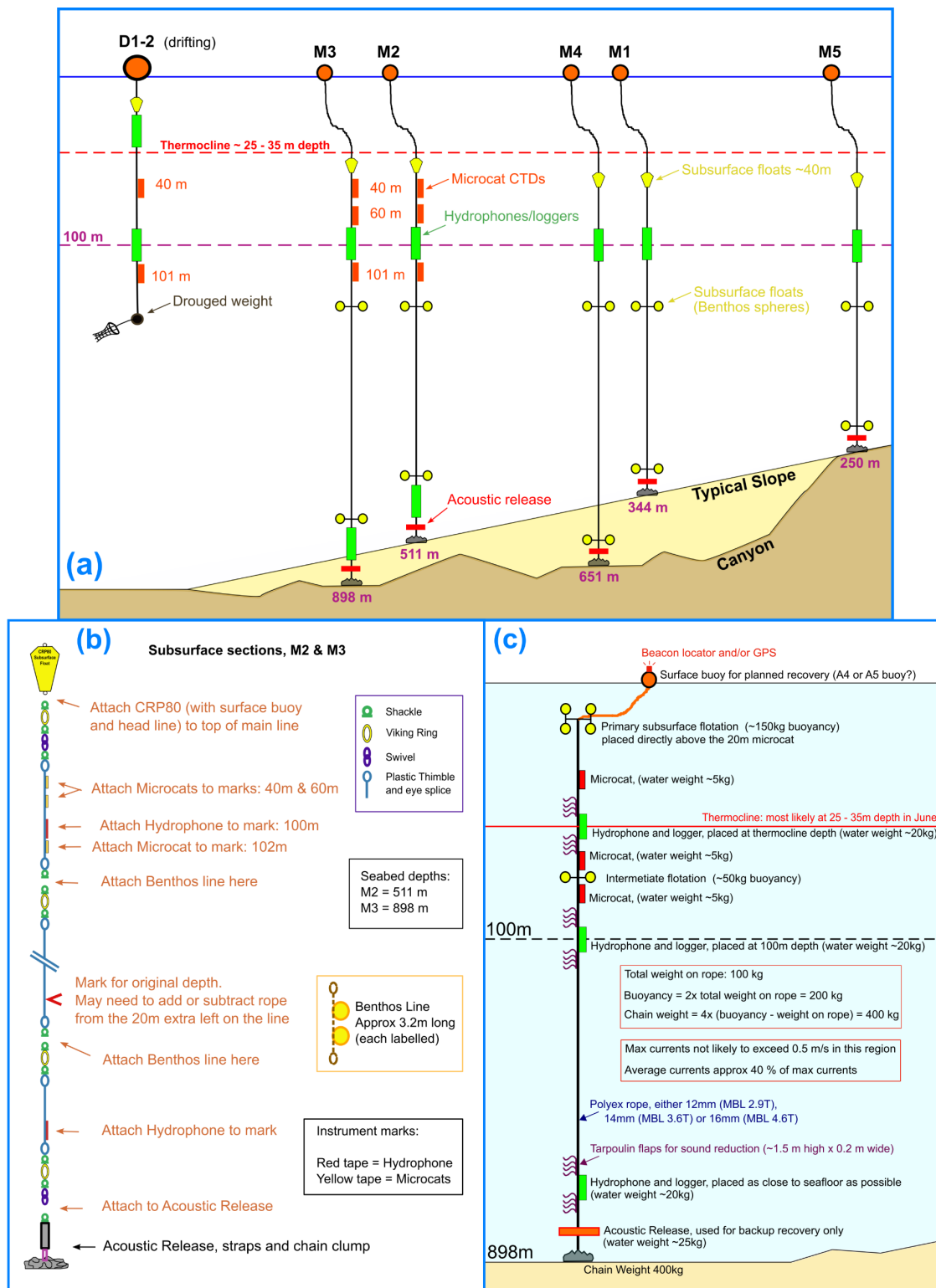
**Fig. 3.6.** Mooring design. (a) Schematic of mooring placement within canyon and slope settings, including depths of instrument placement, (b) Diagram used for deck work of the separate sections (up until subsurface float) for the deeper moorings M2 and M3, including chandlery, (c) placements of instruments, buoyancy floats and acoustic buffers, including approximate weights and floatations.

successfully deployed in two separate locations, each with dedicated airgun transects conducted, the data proved less than useful due to a consistent self-noise (probably 'clinking' from chandlery) and had to be rejected.

An unforeseen issue encountered with the mooring design was that the rope used (14 mm Polyex) stretched somewhat during the deployment causing the instruments to be shallower in the water column than originally planned. After post-deployment measurement, the stretch was estimated at 1 – 4% of original length, depending on overall length and weight on mooring (also, in-situ MicroCAT pressures indicated 1.1 and 2.9% stretch for M2 and M3 respectively). Deploying the moorings weight first and letting that weight hang during the lowering process caused the stretch. The choice of Polyex rope was a compromise between using chain or wire (more expensive and much heavier) and using Dyneema rope (extremely strong and light but extremely cost prohibitive).

Moorings deployed as part of the Irish Sea research survey (Chapter 6), were manufactured using cut-outs and chandlery from the PANiC moorings and followed a very similar design, except for being much shorter/shallower for the Irish Sea shelf.

## 3.3. Data Processing and Filtering

### 3.3.1 Conversion to units of pressure

The ORCA hydrophone recorders record raw voltage output from the hydrophones at a pre-set 48 kHz to .WAV files of size 1 Gb each, which translates to file recording lengths of approximately 3 hrs 6 mins when recording one channel only. The .WAV file output from the ORCAs are a pre-processed, digitised, discrete time-series, generated from the hydrophone which itself measures analogue, instantaneous sound pressure fluctuations.

To achieve this pre-processing, the ORCA passes the signal through an analogue to digital converter (ADC), which measures the ratio of an analogue input value to a reference value and expresses it in the form of a digital value. The ADC in this case is a TEXAS Instruments ADS-8861, serial interface, true differential input,

SAR- ADC. When evaluating the output quality of an ADC there are a number of performance parameters to consider: a) Resolution is measured as a sampling depth in number of bits (N-bits), in this case a 16 bit converter, b) Speed is measured as a sampling rate in conversions per second, in this case 1 MHz (or 1-MSPS), c) Accuracy of an ADC is judged by its monotonicity and linearativity, both reported as a set of graphs in engineering units within the ADC's manual. As part of a looped circuit the ADC employs a Successive Approximation Register (SAR), which uses a binary search to determine the result of each conversion. Here it finds the closest binary value across the full scale range (FSR) of hydrophone voltage output and assigns a digital output value. This digital output value has a sampling depth resolution between $2^{N=16}$ = 65536 possible output values, where the least significant bit (LSB) is the smallest change the ADC can resolve, given its full scale range entered to the circuit loop as (an external) voltage reference ($V_{ref}$) where:

$$1\,LSB = \frac{FSR}{2^N} = \frac{V_{ref}}{2^N} \tag{E2.1}$$

The above information was gleaned from a range of online resources, from the ADC manual and from available literature (e.g., Erbe, 2011; Rodríguez-Pérez et al., 2011). Although the ADC conversion occurred internally within the ORCA, the discrete digitised output was still in raw (or pre-processed) format and the parameters of $V_{ref}$ and N-bits had to be manually entered into a Matlab routine. This followed a DC correction to remove DC offset as part of the process to convert the signal to pressure units (shown in the box diagram, Fig. 3.7).

The next step in converting to units of pressure (in micro-pascals, µPa) is to apply calibration coefficients specific to each calibrated hydrophone. These calibration coefficients were provided by the suppliers as a range of frequency dependant sensitivity values in engineering units per hydrophone. Contact was made with an
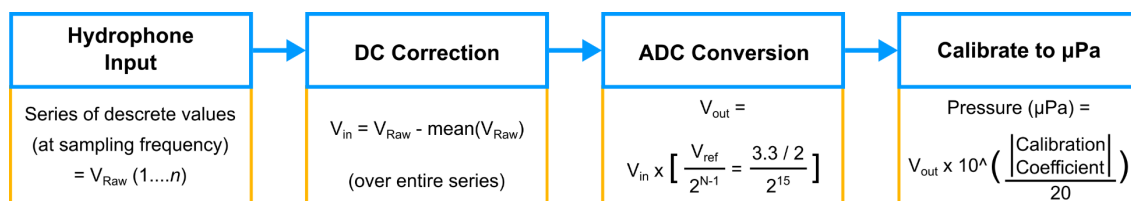


**Fig. 3.7.** Data processing box diagram, showing the progression from raw .WAV files to a calibrated pressure-time series.

acoustics engineer, Chris Loadman with Turbulent Research, who very helpfully explained and advised on the setup, calibration and conversion of raw ORCA acoustic data. Those personal communications confirmed that the setup used (e.g., +35 dB preamp gain and 0 dB front-end gain) was ideal for its deep-water application. It was then decided to use a single value calibration coefficient per hydrophone, averaged across our frequencies of interest (< 10 kHz) from the provided frequency dependent sensitivity values. These values are flat up to 1 kHz and relatively flat up to 10 kHz as seen in Fig. 3.8, which also displays the single value calibration coefficients used. Later it was confirmed that the hydrophones were calibrated using an in-water multipoint frequency sensitivity test, with a projector and reference hydrophone. Using single value calibration coefficients was relatively straight forward to implement through the Matlab routine to achieve a pressure-time series (see last box of Fig. 3.7).
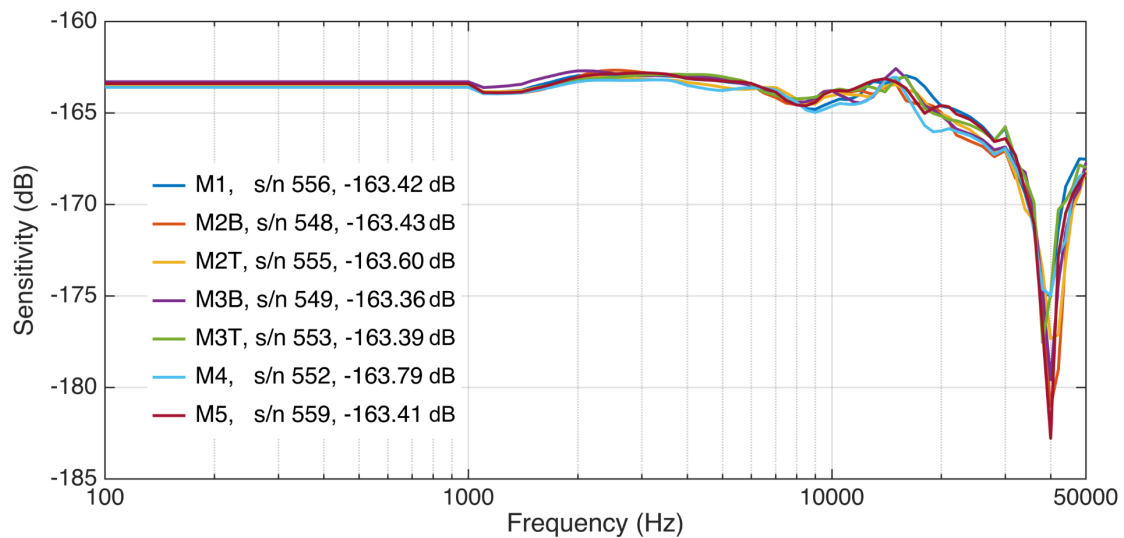


**Fig. 3.8.** Calibration coefficients provided by suppliers, displayed as a sensitivity value in dB. Legend entries for each individual hydrophone include mooring label, hydrophone serial number and frequency averaged single value sensitivity used for processing.

### 3.3.2. Signal filtering

Due to the presence of low frequency ambient noise (and potential self-noise), especially at the deepest mooring M3, the signals had to be filtered. This was in order to achieve a Signal to Noise Ratio (SNR) sufficient enough to integrate over values of pressure squared, that had ambient noise removed ($P^2_{s+n} - P^2_n$, where s

= signal, and n = noise), as was necessary for analysis of pulsed signals described in the next section. Methods of filtering marine acoustic signals is not standardised and within the literature it is most often not detailed what type of filters were used. Due to this, filtering experiments were undertaken here involving testing, comparison, trial and error. This followed personal communications from Chris Loadman (Turbulent Research) and Eddie Jones (Prof. in Electrical and Electronic Engineering at NUIG) and following a course in digital signal processing (Coursera).

The first type of filter ruled out for use was a simple (first order) DC Block filter which did produce very high SNRs but proved to be sub-optimal due to its coarse magnitude response. Although a Finite Impulse Response (FIR) filter would lend most naturally to a discrete time-series, an Infinite Impulse Response (IIR) filter was ultimately chosen for its relatively light overheads compared to a computationally expensive FIR in achieving a similar magnitude response. Example comparisons of each filter response are displayed in Fig. 3.9, including the specific IIR filter that was implemented across the entire dataset analysed (Fig. 3.9a), along with filter parameters inset on the plots of each filter. During the analysis, the chosen IIR filter was passed across each data segment using the Matlab function 'filtfilt', which passes the filter forward across the data and then passes it again in reverse in order to preserve phase and in this case temporally preserve the filtered signal (i.e. no phase shift). As part of a structured set of customised Matlab codes and functions, the IIR filter was high-passed across all of the data at 10 Hz for analysis of zero-peak values and 20 Hz for 90% energy levels (both metrics described in next section). Separately a band-pass filter (100 – 1000 Hz) was also implemented and
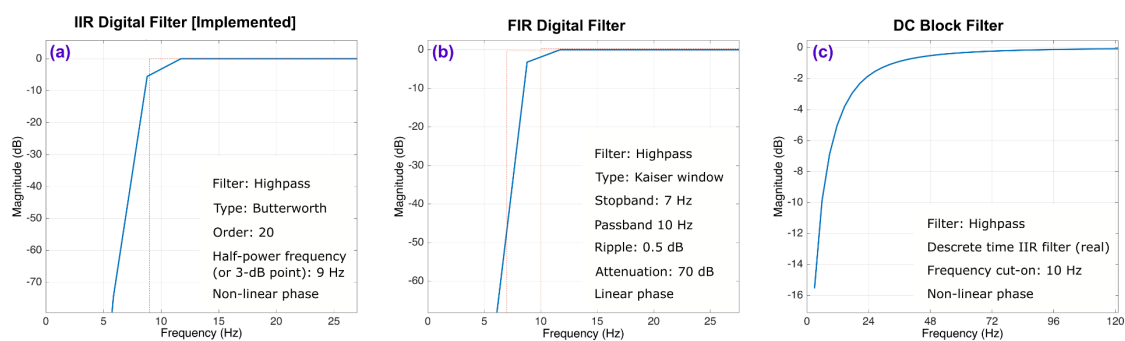


**Fig. 3.9.** Filter outputs as magnitude (dB) per frequency for (a) the IIR filter that was used throughout all analysis, (b) and (c) FIR and DC Block filters respectively, that were both rejected for use.

used for 90% energy levels. There was an exceptional case where the pathway M3B-A6 required a highpass of 20 Hz in order for the main signal to become centered around the zero line for zero-peak analysis and here it was considered prudent to keep the 10 Hz filters for all other pathways and leave this one as an outlier. For spectral analysis, the unfiltered, highpass (> 20 Hz) and bandpass filtered datasets were all included throughout.

## 3.4. Analysis and Interpretation

### 3.4.1. Output sound metrics

Various sound metrics are derived from raw and/or filtered pressure-time series data that are mostly standardised (e.g., Robinson, 2014) but range in parameters and type, depending on application (e.g., pulsed Vs continuous). The following metrics are used throughout the subsequent chapters, details of which have been amalgamated here from various literature on noise measurement and reporting (e.g., Madsen, 2005; Erbe, 2011; Merchant et al., 2012; Robinson et al., 2014), some details of which also appear briefly in the methods sections of Chapters 4 and 6 (Daly et al., 2020; Daly and White, 2021). A particularly useful and clearly laid out report for understanding and implementing sound and noise measurements throughout this project was that of (McCauley et al., 2000). The International Organization for Standardization (ISO) standards (e.g., ISO, 2017, 2019) have not been utilised for this project nor their equivalent American National Standards Institute (ANSI) versions. Following is a description of the main output sound metrics used throughout this thesis:

The Decibel:

Because sound levels can span many orders of magnitude, the standardised logarithmic decibel scale is introduced to simplify reporting. The decibel (dB) is a (base 10) logarithmic ratio of the magnitude of a given quantity to a reference value:

$$Level\ of\ A\ (in\ dB) = 10 \log_{10} \left[ \frac{A}{A_0} \right] \tag{E3.2}$$

where A is any given value and $A_0$ is its reference value. The reference value for underwater sound is 1, for example a reference sound pressure value of 1 µPa, or a reference spectral power value of 1 $\mu Pa^2 Hz^{-1}$. This differs from the reference value of 20 for sound in air. There is a simple and convenient logarithmic relationship between the value of a quantity and its squared counterpart:

$$20 \log_{10} \left[ \frac{A}{A_0} \right] = 10 \log_{10} \left[ \frac{A^2}{A_0^2} \right] \tag{E3.3}$$

Sound Pressure Level:

Sound Pressure Level (SPL), given in units of pressure ($P$), most commonly for marine acoustics in units of micropascals (µPa), can be an instantaneous, discrete or an averaged level, reported in dB as:

$$SPL = 20 \log_{10} \left( \frac{P}{P_{ref}} \right) \ [dB] \tag{E3.4}$$

with $P_{ref}$ as the reference value of 1 µPa. The most common way to average SPL is the root mean square method ($SPL_{rms}$) formally stated as:

$$SPL_{rms} = 20 \log_{10} \left( \frac{\left\{ \frac{1}{T} \int_{t_0}^{t_e} P_{(t)}^2 \, dt \right\}^{\frac{1}{2}}}{P_{ref}} \right) \quad [dB \ re: 1 \ \mu Pa] \tag{E3.5}$$

where the time window T is finish time ($t_e$) less start time ($t_0$), $P^2$ is instantaneous (or discrete value) squared pressure and $P_{ref}$ = 1 µPa is the reference value. Convenient for coding routines it can be informally stated as:

$$SPL_{rms} = 20 \log_{10} \left( \frac{(\bar{P}^2)^{\frac{1}{2}}}{P_{ref}} \right) = 10 \log_{10} \left( \frac{\bar{P}^2}{P_{ref}^2} \right) \quad [dB \ re: 1 \ \mu Pa] \tag{E3.6}$$

here $\bar{P}^2$ is the mean value of squared pressure over a given set of samples, of which sample numbers, or more importantly sample duration, must always be clearly reported (Robinson et al., 2014). $SPL_{rms}$ is especially useful for evaluating continuous/ambient sound (e.g., bottom trawling noise in Chapter 6).

Sound Exposure Level:

The energy of an acoustic signal is defined as the time integral of power (Pwr) over a given duration:

$$E = \int_{t_0}^{t_e} \text{Pwr} \, dt \qquad\qquad\qquad \text{(E3.7)}$$

And when expressed as energy (E) per unit area (A), or 'energy flux', it is the time integral of Intensity (I):

$$\frac{E}{A} = \int_{t_0}^{t_e} I \, dt \qquad\qquad\qquad \text{(E3.8)}$$

Intensity (I) for a plane wave is the squared pressure of a measured signal divided by the specific acoustic impedance ($\rho c$) as follows:

$$I = \frac{P^2}{\rho c} \qquad\qquad\qquad \text{(E3.9)}$$

where $\rho$ = density and c = sound speed. If the specific acoustic impedance ($\rho c$) of the water column is considered constant (a reasonable assumption, as it deviates very little in the ocean), the above equation can be reduced to an equation of 'equivalent energy' or a pseudo-measurement of energy directly proportional to measured energy, and when converted to decibels is known as a Sound Exposure Level (SEL):

$$SEL = 10 \log_{10} \left( \frac{\int_{t_0}^{t_e} P^2(t) dt}{P_{ref}^2} \right) \quad [dB \, re \colon 1 \, \mu Pa^2 s] \qquad\qquad \text{(E3.10)}$$

For analysis purposes, in the time domain, when investigating pulsed airgun shot signals, SEL was computed per shot (before averaging over a number of shots per location) by excluding a single valued background noise level (mean square pressure) from each element throughout the calculation:

$$SEL = 10 \log_{10} \left( \frac{\frac{1}{fs} \sum_i^n (P_i^2 - \bar{P}_{ns}^2)}{P_{ref}^2} \right) \quad [dB\ re: 1\ \mu Pa^2 s] \qquad \text{(E3.11)}$$

where fs is sampling frequency, $P_i^2$ is the $i^{th}$ element of the squared pressure-time series, n is the final sample point in the series and $\bar{P}_{ns}^2$ is the mean squared noise level for that shot or that series of shots per location.

Received airgun shot levels which had a long range from source or were otherwise weak proved problematic, in that the SNR was too poor for the above method of background noise exclusion to work. This manifested as a downward trajectory of the cumulative (noise excluded) sound exposure curve into negative space, rendering it impossible to calculate a single value SEL level per signal segment. For the PANiC survey data, extensive signal testing experiments identified an approximate threshold level, where the total SEL directly across a shot (using a duration as short as possible) had to be at least 2.5 – 3 dB higher than a background level taken between shots, for the calculation to work. Various durations and timings relative to the shot were trialled for inclusion as a background level and the method decided on and implemented was to take separately two 1 s snippets from the start and from the end of a 30 s shot sample and use the lowest mean square noise level from the four snippets. It was due to the presence of low frequency noise that many source receiver pathways contained poor SNR and because of this all data was filtered, as described earlier in section 3.3.2 before the above method of noise exclusion was carried out on all filtered signals. In the case of airgun noise analysis in Chapter 5, in the interest of consistency, only a single filter regime was reported throughout, regardless of clarity/SNR of a given pathway or the fact that a range of filtered and raw data had been processed.

90% Energy SEL values, being the exposure level between the occurrence of 5% and 95% of the total energy, are a common and conventional metric used in marine acoustics. Here 90% energy start times ($t_{5\%}$) and end times ($t_{95\%}$) were extracted from an energy percentage curve derived from a cumulative total energy (sound exposure) curve. In turn, these sample times were used to integrate across to find a single value 90% energy SEL value, and timings were also retained for further use in extracting segments for spectral analysis, later in the process.

Various shot timings were trialled for selection of the start and finish of a shot signal. A Matlab code was written to extract, display and manually input start and finish times of a shot signal and save to file for every individual shot pathway, taking 10 shots per location to bring through analysis. Although this somewhat automated process of having to manually input shot timing was the most efficient attempt, having to pick the start and finish time of each individual shot proved very labour intensive. This method did have the benefit of being able to identify shots with poor SNR (through the use of displaying heavily filtered signals around the band of interest), in a way that a fully automated airgun shot identifier could not handle. An example of this method was developed and used on a full size industrial seismic survey in the Porcupine Basin and is described in Chapter 4 (Daly et al., 2020), although the process was greatly refined for the Chapter 5 PANiC experiment using newly developed code. When extracting 90% energy levels and timings for PANiC, three sets of input shot times were concurrently used, all using the manually picked shot start time, with the first set using a manually picked finish time and the two remaining sets separately using fixed durations of 1 and 2 s.

Power Spectral Density

Spectral analysis for this project, uses the Welch method of applying a Fast Fourier Transform (FFT) on an input waveform, to extract the frequency component (at 1 Hz resolution) of a given signal (Welch, 1967). The output is a Power Spectral Density (PSD), which in turn can be converted to dB referenced to a value of 1 $\mu Pa^2 Hz^{-1}$. Matlab provides the 'pwelch' function for estimating the PSD of a discrete-time signal using Welch's averaged, modified periodogram method, where various windowing functions can be chosen, depending on application and user requirement for resolution versus side-lobe attenuation. Although a search was conducted here, consensus was not found on windowing functions and in many cases from the literature, no details of how the spectral analysis was carried out were reported. For impulsive airgun noise, Chapters 4 and 5 have used a rectangular window, with window lengths equal to the length of one shot and passed across (i.e. averaged over) a signal comprising a sequence of (usually 10) shots, with no overlaps. This method was applied in all impulsive noise spectral analysis, following advice/personal communications from Sinéad Crawford Jordan arising from her project previous to this (Crawford, 2016). Start times for the shot signals spectrally analysed for the PANiC survey were taken as 90% energy start times

and, as with the SEL analysis above, three sets of shot durations were analysed for PSD, with the first set having a duration between 90% energy start/finish times and the second and third sets separately using 1 s and 2 s durations.

For continuous bottom trawling noise, Chapter 6 has used a Hamming window function, with window lengths of 1 s across signal segments of 60 s long and no overlaps. This choice is somewhat arbitrary, although rectangular windows are not recommended for continuous noise. Examples from the literature include using a Hanning window (similar to Hamming), with no overlap, for investigating shipping noise (McKenna et al., 2012) and using a Hamming window with 50% overlap for a Mobile Offshore Drilling Unit (MODU) prospecting for hydrocarbons (MacDonnell, 2017).

On this project all PSD estimates via Welch's method were carried out with the number of FFT points set to be equal to sampling frequency (48 kHz), resulting in an output of one sided, single frequencies from 0 – 24 kHz (50% reduction in highest output frequency is due to the Nyquist Theorem). From a PSD estimate at 1 Hz resolution, a banded SEL can be calculated by integrating across PSD values within any given frequency band. In practical terms this is the sum of values within that band multiplied by duration (in seconds) before conversion to decibels. A broadband SEL was calculated across all frequencies. 1 Hz spectra were also banded across the lower decade bands (10 – 100, 100 – 1k, 1k – 10k Hz) and for a band across the remaining frequencies (10 – 24 kHz) for integration to SEL levels.

One third (1/3) octave centered bands were also extracted from PSD estimates for all acoustic data reported in this project (as is convenient for such work) to use in conjunction with modelled transmission loss values described later. In order to achieve a more accurate banding of each 1/3 octave range (most important for the lower frequencies), the 1 Hz interval PSD outputs were linearly interpolated x10 to achieve a 0.1 Hz resolution before extracting 1/3 octave band SEL values.

Rise Times

Rise times were calculated within a Matlab routine for zero-peak and 90% energy levels. For zero-peak, the rise time was the number of samples (converted to seconds) measured from the first sample below zero (immediately previous to peak)

to the peak sample, when the peak was positive, and from the first sample above zero when peak was negative. Rise time for 90% energy levels was the number of samples between 5% and 95% on the cumulative percentage energy curve, converted to seconds.

### 3.4.2 Computational structures and scripts

All computations were carried out through Matlab using dedicated scripts newly developed for this project. Spreadsheet software was also used to store and organise metadata. This project follows in part from an MSc project (Crawford, 2016), which shared its Matlab codes with this one. Those MSc codes were used to guide and check the newly developed suite of scripts for this programme. As part of the overall analysis, which included many hundreds of .m script and function files, there were a number of scripts written to check, validate and compare the primary coding used for analysis. These secondary scripts are not described any further here but are included with the material archived as part of the programme.

Each results chapter has had its own set of Matlab scripts, functions and structures developed to meet its specific application. There is a natural progression apparent in the written scripts and functions, where greater practice and experience gained has resulted in a more ordered and efficient set of codes. As Matlab code development was undertaken single-handedly, without provided training or guidance, no apologies are made for inefficient or poorly structured code, especially during the early stages of the project. Chapter 5 contained the newest, most efficient set of Matlab files, the structure of which can be seen in Fig. 3.10, which shows in brief detail the named scripts and accompanying functions used to take raw input data (along with metadata) through analysis, to a point where its output data can be plotted and archived.

### 3.4.3. Modelling, source estimation and auditory weighting

Modelling was carried out for investigating sound Transmission Loss (TL), which can in turn be used for estimating Source Levels (SL) or for examining how modelled sound propagation varies over given pathways. TL is simply the drop in level of sound from source to receiver, TL = SL – RL, where RL is received level. Thus, using a modelled TL along with either SL or RL will estimate the remaining

**Acoustic Data Input:**

Raw .WAV data files
1Gb & 3hrs long
each

**Metadata Input:**

Location, time, date, depth
ship's position
range etc.

**Extract and preprocess shot data**

Extract 10 shots per location given an exact
point in time. Convert to µPa as a set of 10
columns, one per 30s shot sample.
[ExtractWavs.m]

**Filtering**

Make and save
various filters for
use in scripts
[MakeFilters.m]

**Find shot timings**

For displaying through different
filters to pick and manually enter
and save shot start and end times
[FindStartEndTimes.m]

**Check Timings**

Visually display each
shot to confirm
timing is correct
[CheckTimes.m]

**Primary analysis of input data to outputs of various sound metrics**

Main script for analysis per hydrophone mooring recorder from all inputs of processed shot sets, timings and
metadata. Structured output of various sound metrics, calling a set of specific functions for each [AnalyseMxx.m]

**SPL Peaks**

Peak-peak (Pp),
Zero-Peak (Zp),
for raw and
filtered data, per
shot and per
location, plus rise
times per shot
and per location

[CalcPeaks.m]

**Energy/SEL**

Highpass and
bandpass filtered
90% energy per
shot and location,
for three time
windows: 90% E,,
1s and 2s, also
rise times and
header files
[CalcEnergys.m]

**MSP & SNR**

Mean square pressure
(MSP): in dB including
for highpassed and
andpassed data

Signal to Noise Ratio
(SNR): in dB and also
as a ratio, for original,
highpassed and
bandpassed data

[MSPSNR.m]

**PSDs & 1/3 Octave**

Banded SEL and 1/3
octave SEL, both for
3 time windows: 90%
Energy, 1s & 2s. Also
output columns for
frequencies used
and headers

Output and saved
separately is an array
of PSD values per
location

[PSDout.m]

**Ambient Noise**

MSP (and dB) noise from unfiltered,
highpass and bandpass data [Noise.m]

**Shot Timings**

Output of manually picked timings, used per
shot, including start, finish times & duration

**Output**

Structured .MAT
file outputs saved per
mooring recorder from AnalyseMxx.m

**Metadata**

Summary table, columns: single value metrics,
rows: pathways per recorder. Range, depth at
gun, depth at phone, phone depth, date and
time at centre of each location and headers, etc.

**Hydrograpyh**

Suite of scripts for
analysing and outputting
water column data from
various instruments

**Backup & Archive**

Save all data and work
to backup drives.
Catalogue and
archive everything

**Bathymetry**

Extract bathymetry using
ArcGIS for each pathway
and save as .MAT file
per hydrophone recorder

**Legend**

⬗⬖ Inputs/outputs
☐ Matlab Scripts
☐ Matlab Function
→ Main Data
→ Metadata

**Output Displays**

Various scripts used for outputting all data as figure plots and tables.
Also use Excel for tables and Inkscape for touching up graphics.
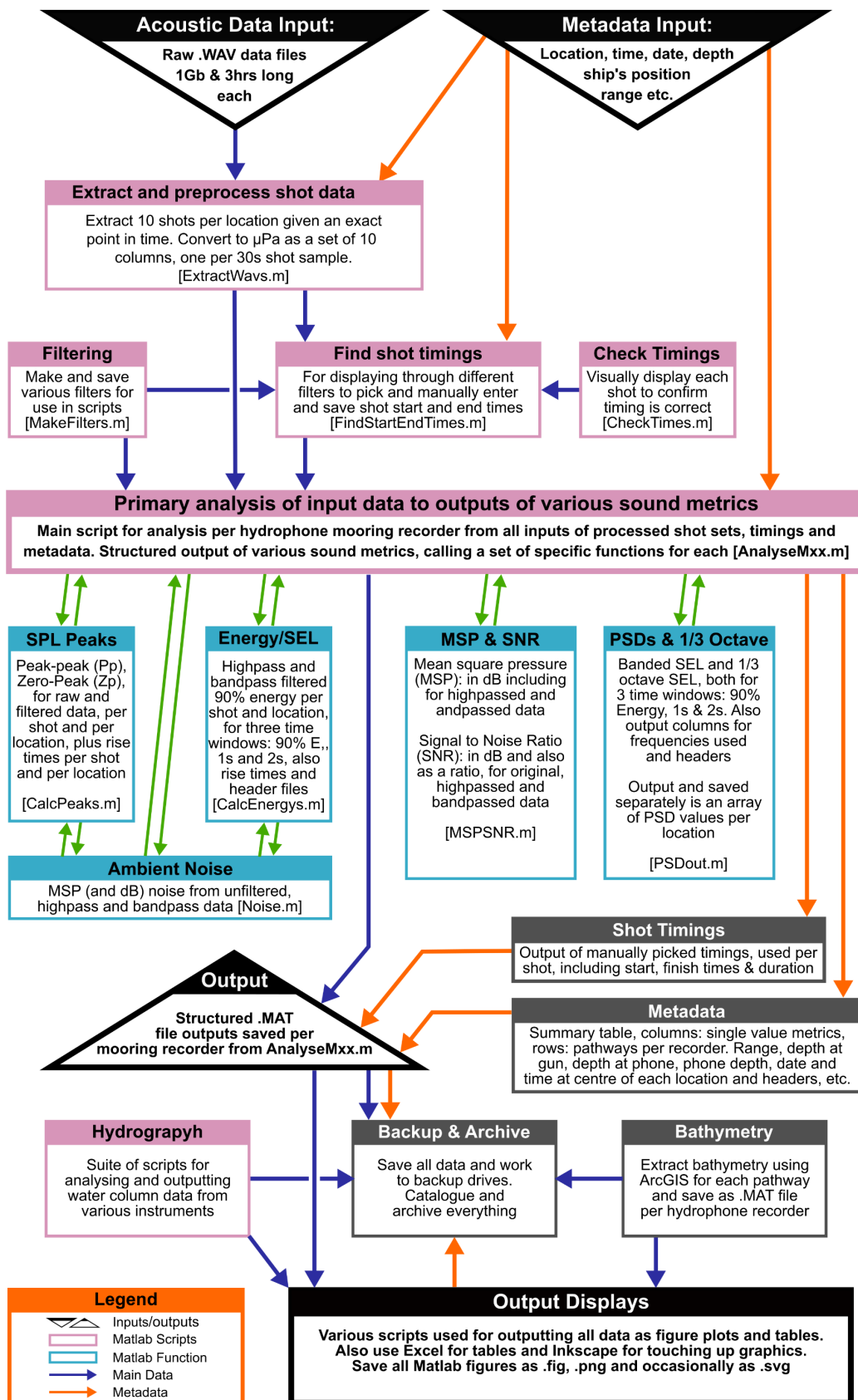Save all Matlab figures as .fig, .png and occasionally as .svg

**Fig. 3.10.** Box diagram of input data, computational structures, codes, functions and outputs.

unknown variable. Because TL is modelled and constrained by the limits and errors of the specific model chosen, its use to predict an SL, for example, from a measured RL, can only be seen as an estimate rather than a measurement.

The simple spreading law model, being one of the most basic methods of assessing TL, assumes a lossless medium (i.e. no attenuation) and estimates over a given range r, using a spreading coefficient N:

$$TL = N \log_{10} r$$

with N = 20 for spherical spreading (in the near-field unbounded by surface or seabed boundaries) and N = 10 for cylindrical spreading in the far-field. When calculated using real values, N can be higher than 20, as is the case with its use in Chapter 4. Also in Chapter 4, when calculating observed TL, azimuthal difference in SL (difference due to angle from airgun array direction of travel) was considered throughout.

A Parabolic Equation (PE) model was chosen for all acoustic modelling applications used herein, due to its suitability for low to mid frequencies in deeper water, over large distances (Medwin and Clay, 1997; Jensen et al., 2011). The optimum model identified and utilised was RAMGeo from the AcTUP suite of acoustic models (Duncan and Maggi, 2006). As detailed in Chapter 4 (Daly et al., 2020) RAMGeo approximates seabed layers parallel with bathymetry in a modified fashion from the Range dependent Acoustic Model (RAM) (Collins, 1995), from which it is derived. RAM only approximates in the horizontal. RAMGeo is fully range dependent over a fluid seabed and this ability to account for changes over range is a major advantage. The biggest disadvantage of RAMGeo is its inability to account for shear wave propagation through an elastic seabed. Various input parameters can be tweaked to suit an application within RAMGeo, for example, adjusting subseafloor parameters, such as substrate density, P-wave velocity and P-wave attenuation. This was carried out by Crawford (2016) in order to calibrate a model to observed values for the Porcupine Basin, and these adjusted subseafloor parameters have been kindly shared for use with the modelling work here.

Source level estimates calculated from the sum of RLs and modelled TLs were examined over a set of pathways from a bottom trawling source in Chapter 6. By

adjusting the input source depth within the RAMGeo models, the difference in SLs emanating from either a surface trawling vessel or from trawling gear along the seabed could be compared. This novel approach to source level estimation at contrasting water depths, while providing interesting results, is not without its considerable limitations (e.g., real noise will emanate from both source depths), discussed in detail in Chapter 6.

In an effort to reflect marine mammal hearing sensitivity within RLs (and resulting SLs), auditory weighting functions for three of the main hearing groups were applied following Southall et al., (2019), using a weighting equation and parameters from Finneran, (2016). These weighting functions produced a discrete set of negative values (at 1 Hz resolution) which get added to received levels at each frequency to account for where each hearing group are more or less effected by the sound they are exposed to. These weighting functions are displayed as auditory weighting curves over frequencies of interest to Chapter 6 in Fig. 3.11.
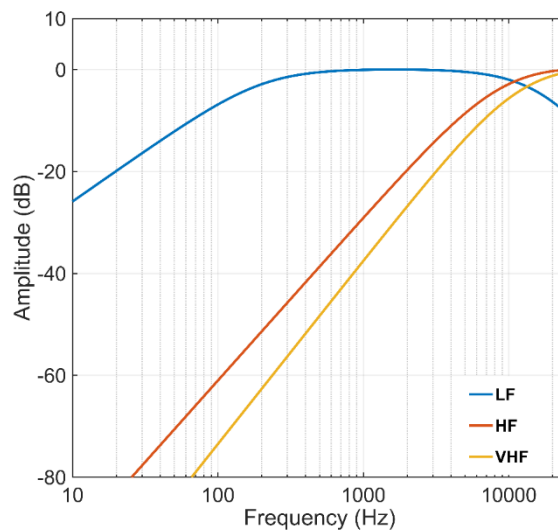


**Fig. 3.11.** Auditory weighting functions for Low Frequency (LF), High Frequency (HF) and Very High Frequency (VHF) marine mammal hearing groups, adapted from Southall et al., (2019).

*3.4.4. Hydrography and water column dynamics*

Following the processing of CTD, MicroCAT and glider data (section 3.2.3.) a set of Matlab scripts was employed to display the data in various ways, including water column profiles, sections and Temperature-Salinity (TS) plots. For the comparative winter profiles used in Chapter 5, modelled data was extracted from the open-source World Ocean Atlas model (WOA18), for monthly statistical mean temperature (from 2005 to 2017) at the nearest available location (1/4° grid) (Locarnini et al., 2018). To identify values of glider data that fell closest to indicative temperature values, a computational routine was developed that identified those individual rows of data per dive and ascent. This method introduced a margin of error where values were not exactly at indicative temperatures, which depended on the rate of change in the vertical, but in general did not amount to anything larger than (0.03 °C).

Regarding water column dynamics, the buoyancy frequency N (or Brunt-Vaisala frequency) is the oscillation frequency a parcel of water would have if vertically displaced within a stratified water column. More practically, N can be seen as a measure of how stable a fluid is to vertical displacement and within oceanography is defined in terms of potential density ($\rho$) as:

$$N^2 = \frac{-g}{\rho_{(z)}} \frac{d\rho}{dz} \hspace{4cm} \text{(E3.12)}$$

where g = gravity and z = depth. In turn, N was used here to calculate modal structure and phase speeds of internal waves using the open source Matlab function 'dynmodes.m' (Klinck, 1999). The equations used by dynmodes.m to compute modal structure and phase speed are not displayed here but are similar in nature to those used by Münnich et al., (1992) for an enclosed (lacustrine) internal seiche.

# Chapter 4:

# Seismic Survey Sound Propagation: A Porcupine Basin Noise-field

Eoghan Daly[1,2], Sinéad Crawford Jordan[1], Martin White[1,2].

[1]Earth and Ocean Sciences, Ryan Institute, National University of Ireland, Galway
[2]Irish Centre for Research in Applied Geosciences (iCRAG)

**Contributions:** E. Daly: Conceptualisation, Data curation, Formal analysis, Investigation, Methodology, Visualisation, Writing (original draft). S.C. Jordan: Data provision, Methodology, Knowledge transfer. M. White:  Conceptualisation, Methodology, Project administration, Mentorship, Reviewing and editing.

## Abstract

Anthropogenic noise in the oceans water column, including from offshore seismic surveys, is ever increasing, bringing greater ecological pressure on the marine environment and with that a need to measure, understand and mitigate against these sources of noise pollution. Here, a previous study on an offshore seismic survey along the Irish continental margin is utilised to gain further insight into sound propagation in this sensitive area for marine mammals. Propagation pathways, along with seasonal variability and modelled slope conditions are investigated to constrain sound levels relative to those that can cause harm. Results are discussed in the context of noise pollution in the Porcupine Basin, for example, geoacoustic and environmental parameters, including slope angle, topography, seasonality and the water column. Acoustic model functionality is assessed. Noise exposure criteria and behavioural disturbance to marine mammals are considered alongside regulatory frameworks, with the future aim of increasing Ireland's capacity to limit the effects of ocean noise pollution.

## 4.1. Introduction

No less than in air, underwater sound has a myriad of source types, frequencies and output amplitudes, each of which impact, to some degree, on the surrounding marine environment. It has long been known that sound propagates efficiently in the ocean and to great distances, especially from low frequency sources (e.g., Munk and Wunsch 1979; Munk et al., 1994), the basic physical theories of which are well established. Sound propagation from source is dependent on frequency and governed by physical processes such as absorption, scattering, reflection and refraction. It is also controlled by environmental (or geoacoustic) parameters including water depth, topography, water column properties, surface roughness and layered subseafloor properties (Urick 1983; Medwin and Clay 1997; Jensen et al., 2011). Sound sources can vary in nature from physical to biological or anthropogenic (Hildebrand 2009; Erbe 2011) and were originally quantified by Wenz (1962) using the widely recognised 'Wenz Curves'. Natural physical sources occur over varied timescales, at various intervals, from occasional earthquakes to common meteorological events, such as wind driven storms (Burgess and Kewley 1983; Zhao et al., 2014). Over millennia, marine mammals have adapted their sound production and hearing capabilities for hunting, communication and navigation (e.g., Cranford et al., 1996; Madsen et al., 2005; Jensen et al., 2018), making them the predominant bio-acoustic sound source in the ocean.

Anthropogenic noise in the ocean is classed as a pollutant (Tasker et al., 2010) that increasingly requires regulation, monitoring and further research. There are many types of anthropogenic ocean noise sources identified worldwide, each with a different level of environmental impact. Source types of noise include global ships passage (Chen et al., 2017; Wang et al., 2012), pile driving during offshore construction (Carstensen et al., 2006; Luís et al., 2008; Bailey et al., 2010), high powered sonar (especially in the defence sector) (Parsons 2017; Bernaldo de Quirós et al., 2019), underwater explosions (Lawrence 2004; Bagocius 2013), drilling for hydrocarbons (Erbe and McPherson 2017) and seismic airguns, each of which impact, to some degree, negatively on marine fauna (Merchant et al., 2016). Offshore hydrocarbon exploration, through the use of seismic airguns is known to be one of the largest contributors to underwater ocean noise (Richardson et al., 2013; McCauley et al., 2000a; Nieukirk et al., 2004). This geophysical technique utilises bubble oscillations from large seismic airgun arrays directing acoustic

energy downwards towards the seabed and measuring returning sub-seafloor layer reflections, but with the side effect of horizontal sound propagation through the water column (Duncan and McCauley 2000).

The northeast North Atlantic continental margin hosts varied geomorphological slope types and oceanographic processes (Fig. 4.1). It forms a transition between the oceanic crust under deep water and continental crust under shallow shelf seas (Sacchetti et al., 2013). The Porcupine Basin (PB) is an extensional, deep sedimentary basin holding Mesozoic and Cenozoic sediments up to 10km thick, underlain with thinning continental crust (Shannon 1991; Van Rooij et al., 2007).

Hydrography of the region consists of a surface mixed layer, with Eastern North Atlantic Water (Harvey 1982) present down to approximately 800 m, overlying a wedge of Mediterranean Overflow Water between 800 – 1200 m (White 2006). Lower deep water resides below this, typically Labrador Sea Water and North Atlantic Deep Water (Pollard et al., 1996). Hydrography is dynamic along the northwest European continental margin, where deeper water undergoes mesoscale variability and boundary currents can dominate shallower water (Pollard and Pu 1985; Vermeulen 1997; Mitchell and Huthnance 2008). It is also a region of significant tidal energy conversion to baroclinic internal wave energy (White and
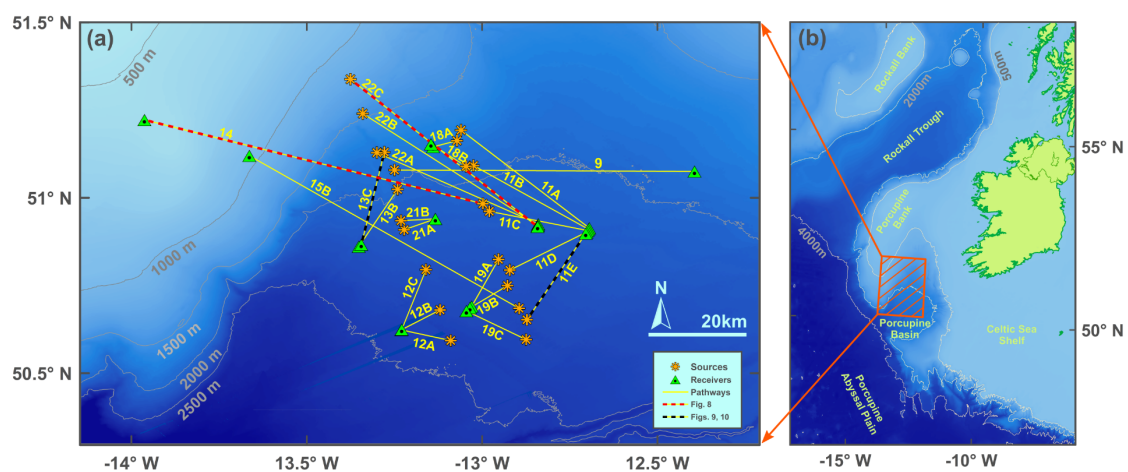


**Fig. 4.1**. Survey area bathymetry map. (a) displays source (orange asterisks), receiver (green triangles) and labelled (yellow) propagation pathways. Red dashed pathways 14 and 22C are used in Fig. 4.8, while black dashed pathways 13C and 11E are used in Figs. 4.9 and 4.10. (b) Overview map of the Irish offshore and continental margin of the northeast North Atlantic.

Dorschel 2010; Aslam et al., 2018). Enhanced dynamics lead to a variable sound speed profile and alter the conditions for sound to propagate.

For decades, the PB has experienced episodes of interest from the hydrocarbon exploration industry (Shannon and Naylor 1998; O'Cadhla et al., 2004), with interest peaking during times of favourable oil prices and licencing conditions. Crawford (2016) monitored one such 3D seismic survey in 2014, using drifting acoustic recorders to acquire data at varying distance from source.

The continental margin along the northeast North Atlantic, including the PB, is also found to be a distinct habitat for migrating and resident marine mammals (Berrow et al., 2018) with the large abundance and diversity (Berrow 2001; O'Cadhla et al.,, 2004; O'Brien et al.,, 2009; Berrow et al., 2010) related in part to the physical oceanographic processes present and associated biophysical interactions with lower trophic levels. A major motivation for studying anthropogenic noise across the continental margin is that noise effects on the marine environment are not fully understood, especially when impacting on marine mammals. Loud impulsive anthropogenic noise from various sources including military sonar, explosions and seismic surveys (Lawrence 2004; Chen et al., 2017; Erbe and McPherson 2017; Parsons 2017; Bernaldo de Quirós et al., 2019), is known to damage marine mammals (termed Temporary and Permanent Threshold Shifts: PTS & TTS) and sometimes lead to mortality (Southall et al., 2007; Tougaard et al., 2015; Southall et al., 2019). Other less extreme impacts, such as avoidance, altered migration patterns and communication masking (Southall et al., 2007; Erbe 2013a; Stone and Tasker 2006; Lucke et al., 2009; Southall et al., 2019) add to the necessity for regulation of noise pollution in the global oceans (Erbe 2013b), for example in Europe under the MSFD (Tasker et al., 2010). Regional scale measurement and monitoring of anthropogenic noise are integral parts of any existing or upcoming regulatory frameworks (e.g., Sutton et al., 2013).

Here, pre-existing data is utilised to develop new analysis methods and to extend a regional set of results and interpretations for the PB sound field, south west of Ireland, while under exposure to pulsed noise generated by a seismic survey source (Fig. 4.1a). We expand the analysis of Crawford et al., 2016 to assess noise propagation variability at further ranges and under additional propagation controls using their regional model parameter data. The role of the continental margin in

noise propagation characterisation is also briefly assessed and potential research questions highlighted.


## 4.2. Materials and Methods


### 4.2.1. Data acquisition

During the summer of 2014, the MV Polarcus Amani carried out a 7270 km$^2$ 3D seismic survey in the northwestern region of the PB (Fig. 4.1) using an array of 33 seismic airguns, with a combined volume totalling 3480 in$^3$ towed at seven meters depth (Crawford 2016). Acoustic noise data was gathered simultaneously with, and in close proximity to that seismic survey (Crawford et al., 2016). Hydrophone recorders measured sound pressure in the water column, from which is produced a calibrated pressure-time series (e.g., Fig. 4.2b). Recorders were deployed on a drifting buoy at distances 5 – 60 km from the survey vessel. Airgun array specifications, timestamped position, speed, and directional data were provided by the operators Polarcus MC Ltd. The recorders used were Wildlife Song-Meters, with a low noise hydrophone (bandwidth 2 – 48,000 Hz; sensitivity -164.4 dB re: 1 v/µPa) mounted on the drogued drifter at 150 m below sea surface. Although 25 separate source to receiver pathways were identified, Crawford et al., (2016) has published analysis and transmission loss values for six of these (Fig. 4.1: 11E, 12B, 12C, 18A, 22A and 22C). Here we consider all ranges defined by the 25 source-receivers pathways characterizing the survey.


### 4.2.2. Acoustic signal processing and analysis

Sound metrics utilised here include zero to peak pressure levels (0-peak), Sound Exposure Levels (SEL), Power Spectral Density (PSD) and Transmission Loss (TL). Motivated by the potential impact of seismic surveys on marine mammals, the two metrics mostly focussed on were 0-peak and single pulse SELs. 0-peak is the measure of the initial received pulse maximum (±) pressure amplitude in micro-Pascals (µPa) (Fig. 4.2c) and is a criterion used to assess effects on marine fauna reported in Decibels as follows:

$$0\text{-}peak = 20 \log_{10}\left[\frac{P_{peak}}{P_{ref}}\right] \quad (dB\ re\text{:}\ 1\ \mu Pa\ ), \tag{4.1}$$

where $P_{ref}$ is the reference pressure value of 1 µPa (for underwater acoustics), in convention with marine acoustic best practice (Robinson et al., 2014) and used in text hereafter. After conversion from volts to Pascals, 0-peak values were calculated for each individual shot and averaged over all shots in a given envelope. SEL is a pseudo-measurement of the energy contained in a signal over a given time (e.g., here a single seismic airgun pulse). Once specific acoustic impedance is assumed constant, the equivalent energy or sound exposure (E) can be defined as the time integral of squared pressure ($P^2$):

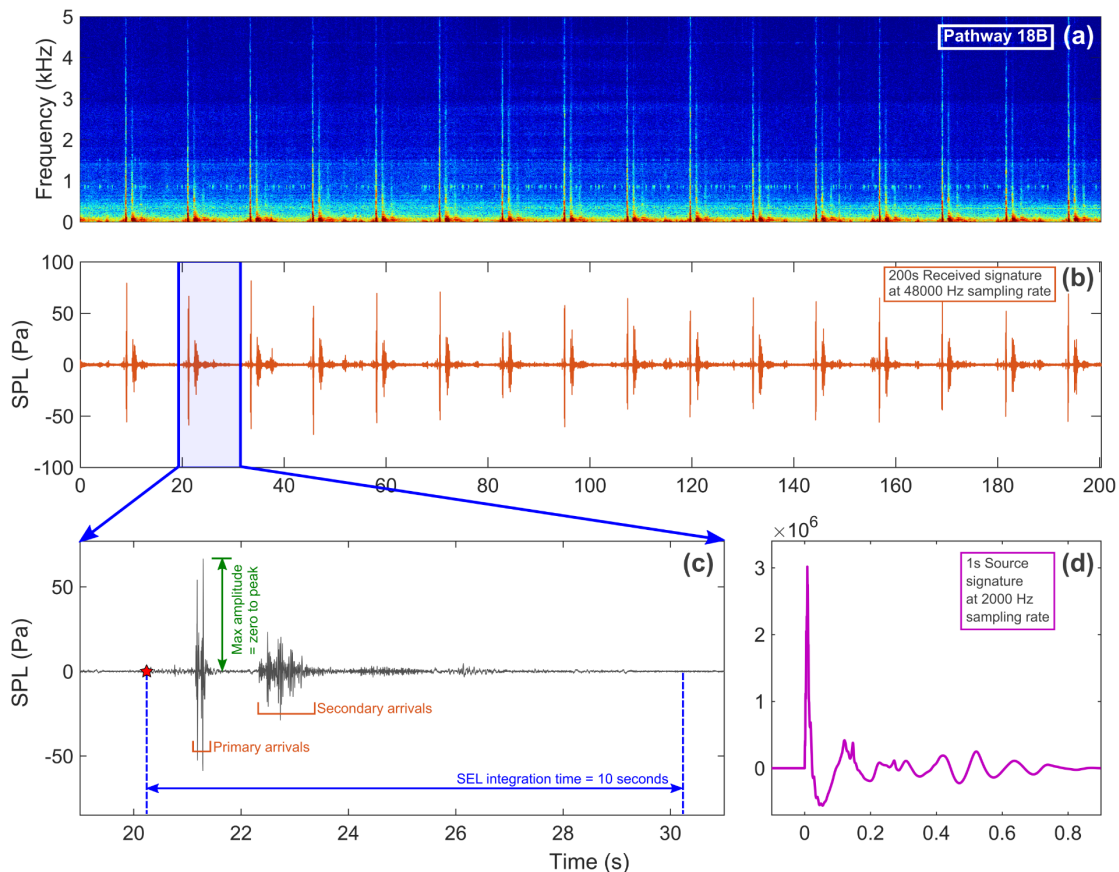$$E = \int_{t1}^{t2} P^2(t)dt \tag{4.2}$$



**Fig. 4.2**. Airgun array shot signals from example pathway 18B. (a) Spectrogram of frequency over 200s time interval. (b) Waveform or 'signature' of shot arrivals measured by the recorder over the same 200 s at a receiver range of 10km from source. (c) Single shot schematic of how 0-peak (green arrow), manually identified start point (red star) and integration period (blue arrow) are identified and calculated. (d) Modelled source signature of 1s duration, which is azimuth dependent. Note the difference in y-axis scale between (c) and (d).

integrated over a stated time period (e.g., shot duration, here being: $t_2 - t_1 = 10$ s; Fig. 4.2c). SEL is then sound exposure reported in decibels relative to a reference level:

$$SEL = 10\log_{10}\left[\frac{E}{Eref}\right] \quad (dB\ re: 1\ \mu Pa^2 s), \qquad (4.3)$$

The Power Spectral Density is a Fast Fourier Transform (FFT) of a pressure-time series and is reported in dB re: 1 $\mu Pa^2$/Hz over a stated frequency band, herein using the Welsh rectangular window (Welch 1967) method to estimate a PSD for each shot. The PSDs were then integrated over 1/3 octave frequency bands for both source and received pressure time-series before calculating Transmission Loss (TL). 1/3 octave analysis was constrained to bands between 7.98 and 501.19 Hz centre frequencies, being an overall bandpass which represents the vast bulk of seismic airgun energy, especially at far field ranges to source (note: the word 'range' in this paper exclusively refers to distance from source to receiver in kilometres).

Airgun shot SELs calculated in the time domain, incorporating all frequencies, have been termed here $SEL_{pulse}$, and are integrated across the entire envelope of shots per pathway  (e.g., eight shots x 10 s = 80 s envelope length; as detailed below) then divided by the number of shots in that envelope. In the frequency domain, over 1/3 octave bands, termed $SEL_{1/3}$, shots have been averaged during the transform process and will have slightly lower values (< 1 dB) to $SEL_{pulse}$ due to band limiting. All received shots were assigned a 10 s duration throughout (Fig. 4.2c) and PSDs integrated over that duration. Transmission Loss (TL) is the difference between Source Levels (SL) and received Levels (RL) ($SEL_{pulse}$ or $SEL_{1/3}$) reported in dB:

$$TL = SL - RL \qquad (4.4)$$

and being a ratio (logarithmically), is the only unit not to require stated reference values (Robinson et al., 2014).

For analysis, a 200 second window was chosen to have sufficient time to provide enough shots for averaging yet be short enough (~450 m at seismic vessel speed of 4.5 knots) to represent an individual source/receiver pathway. 200 s windows were centred around a known source/receiver pathway, then eight of the most optimum shots were selected for analysis. The resulting collated and processed

pressure time-series envelopes are representative of any given pathway, regardless of range or clarity of signal. For pathways with a short range or clear signal, sorting of shots was unnecessary, and shots were kept sequential across the centre point. For fainter, more distant signals, manual selection was required to prevent inclusion of a previous shot's energy, especially from the more poorly defined shots that commonly ran into each other (i.e. signal duration longer than shot interval). This method allowed for picking the start time of any shot arrival with an accuracy of 0.01 s. From all 200 s windows, eight of the shots with a defined start point (with or without headwave present) were chosen for being closest to the middle of the window and for being side by side whenever possible; this was achievable for 23 of the 25 available pathways. The above method differs from Crawford et al., (2016), in that here shot identification is not fully automated. The advantage of this new method is the ability to analyse almost all pathways, especially at greater range, compared to automation which would only work for the more clearly defined signals and could not discern shot overlap. Source levels, following methods in Crawford (2016), were derived from a modelled waveform at a sampled frequency of 2000 Hz and calculated over a 1 s duration (Fig. 4.2d).

Variations in ambient or background noise were orders of magnitude smaller in amplitude than the airgun signals and were not considered for analysis as part of this survey.

### 4.2.3. 2D Numerical modelling

Following previous works (e.g., Medwin and Clay 1997; Jensen et al., 2011) a Parabolic Equation (PE) model was chosen based on its suitability over large distances, in deep water, for low to mid frequencies (< 5 kHz). Here, following Crawford (2016), the best suited model was identified as RAMGeo from the AcTUP suite of acoustic models (Duncan and Maggi 2006). RAMGeo has been used in this study to investigate various real and synthetic sloping conditions, seasonal variations and differences in depth of receiver. For these purposes new parameters have been derived and introduced to the models, such as synthetic bathymetry data and seasonal sound speed profiles from legacy CTD data. RAMGeo is a modified version of the Range-dependent Acoustic Model (RAM)(Collins 1995), in that it approximates seabed layers parallel to bathymetry rather than purely horizontal as RAM does. It is suited to low to mid frequency propagation modelling, is fully range

dependent and runs on AcTUP through a graphical user interface. The major advantage of RAMGeo is its range dependency over a fluid seabed. A disadvantage is that RAMGeo does not account for any shear wave propagation through an elastic seabed; a process that may occur in any consolidated or non-fluid layers found in the Porcupine Basin. One of the main challenges to calibrating and executing an ocean acoustic model is constraining input parameters; an important set of which is sub-seafloor geology (controlling substrate density, P-wave velocity and P-wave attenuation). Using RAMGeo, the parameters for sub-seafloor layers must remain constant with bathymetry, thus requiring tweaking to match observed values. Following from work carried out by Crawford (2016), a sub-seafloor model tailored for the PB (Model E; Table 4.1) was used in the subsequent model studies into slope and seasonality, due to its closest match with observed values. In general, the modelling workflow implemented here followed that of the previous modelling framework (Crawford et al., 2016: Figure 2.6), with the addition of modelled seasonality and idealised sloping conditions.

Table 4.1.–Geoacoustic parameters of sediment type for modelling

| Seabed layer sediment types | Depth below top of layer (m) | Compressional Wave Velocity (m/s) | Density (kg/m3) | Compressional Wave Attenuation (dB/λ) |
|---|---|---|---|---|
| Clay | 0 | 1549 | 1488 | 0.1 |
|  | 25 | 1581 |  |  |
|  | 50 | 1612 |  |  |
| Clay-Silt-Sand | 0 | 1642 | 1596 | 0.2 |
|  | 100 | 1759 |  |  |
|  | 200 | 1863 |  |  |
| Clastic Sediment | 0 | 1950 | 2100 | 0.4 |

Note: Adapted from Crawford (2016), Model E

## 4.3. Results

### 4.3.1. Sound level observations in the Porcupine Basin

All measured levels show a frequency response with sound energy dominating between 10 and 300 Hz. Although the noise propagation field contains relatively benign topography, measured sound levels vary across pathways of equal range (Fig. 4.3). Source levels of $SEL_{pulse}$ from the 33-gun array vary slightly with azimuth

between 227.98 and 228.62 dB (re: 1 $\mu Pa^2s$);   (red star in Fig. 4.3a). Received values generally decrease with greater range from source, as would be expected due to absorption and basic spreading laws. Both 0-peak (re: 1 $\mu Pa$) and $SEL_{pulse}$ (re: 1 $\mu Pa^2s$) values reduced from ~160 and ~144 dB at 5 km respectively, to values of ~135 and ~125 dB at 74 km (Fig. 4.3a). Within the general trend of decreasing received levels with distance from source there is variation across pathways of equal range, for example, an ~ 8 dB difference in 0-peak values was found at 30 km. This difference is most likely due to a combination of factors, such as slope angle, sub-seafloor composition and hydrography. Fig. 4.3b displays the same received $SEL_{pulse}$ values averaged over common ranges, in order to compare with simple spreading law curves where:

$$TL = N \cdot Log_{10}(R) \tag{5}$$

with R being range from source in metres and N being a 'spreading coefficient' with values of N = 20 representing spherical spreading (green curve in Fig. 4.3b) and N
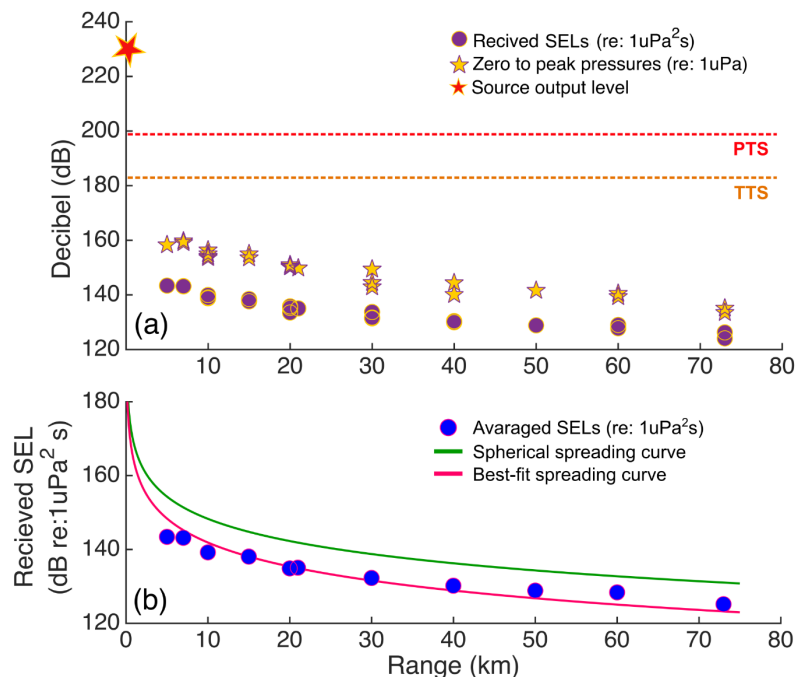


**Fig. 4.3**. Measured sound levels (a): Observed $SEL_{pulse}$ values (purple circles) and 0-peak pressures (yellow stars) for all pathways analysed. Approximate source output level (in $SEL_{pulse}$ re: 1 $\mu Pa^2s$ @1m) is indicated with a red star. SEL threshold shifts in labelled red and orange dashed lines are discussed in section 4.4.1. (b): blue circles are averaged $SEL_{pulse}$ values. Curved lines are spreading curves; green represents spherical spreading; pink is best fit to $SEL_{pulse}$ (see equation 5).

= 10 being cylindrical spreading (Jensen et al.,, 2011). By altering N to an average of observed values of TL/log$_{10}$(R), here N = 21.6, a best fit spreading curve is generated and represented by the pink curve in Fig. 4.3b.

The variation in range and bathymetry across example pathways can be seen in Fig. 4.4. Here time domain TL values (source minus received SEL$_{pulse}$) increase with
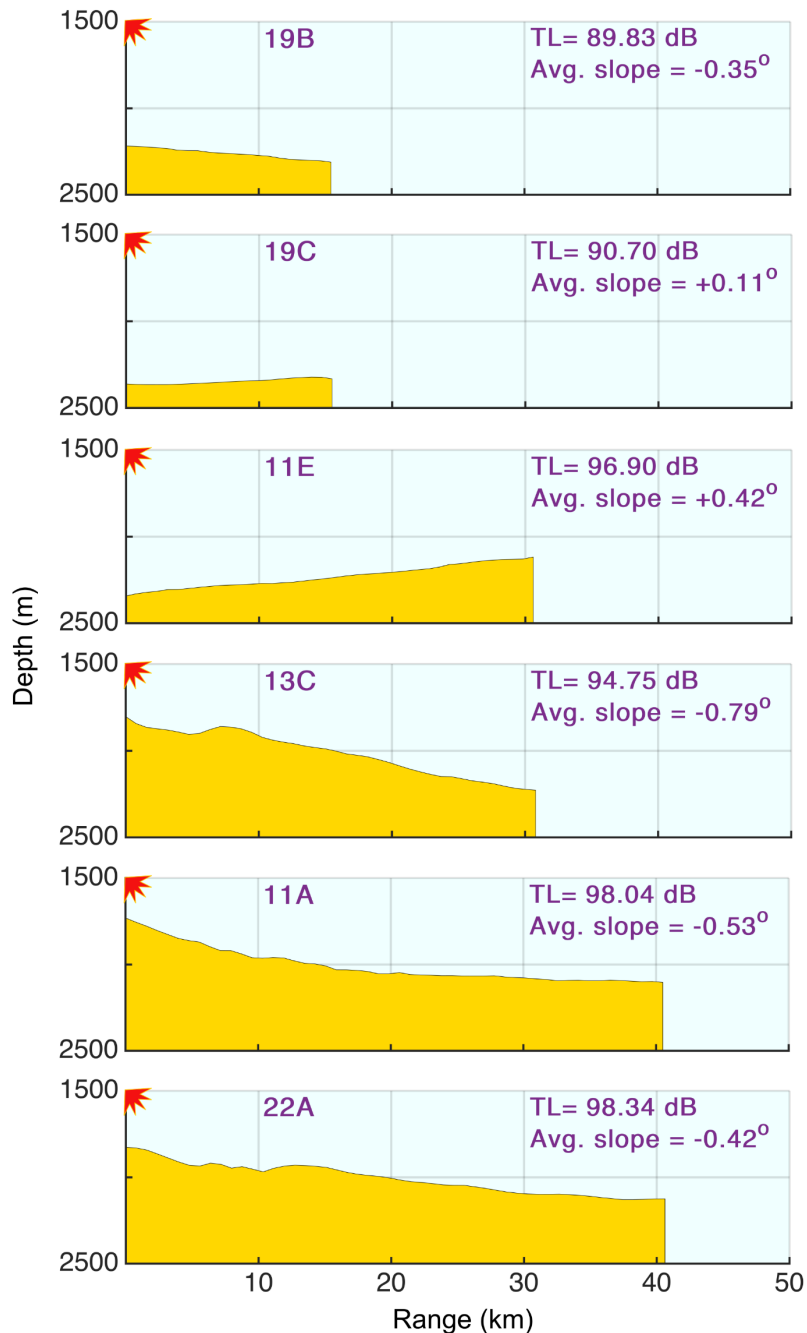


**Fig. 4.4.** Topography and range of example pathways (as shown in Fig. 4.1) with inserted values of observed time domain TL in decibels and average slope over pathway (in degrees). Sources are at 7 m depth on left hand side (zero range). Vertical exaggeration = 13.

increased range. Assessing all TL values has identified pathways 11E (average slope of 0.42° from source to receiver) and 13C (average slope: -0.79°) as having the greatest difference in $SEL_{pulse}$ (2.2 dB re: 1 $\mu Pa^2s$) transmission losses for any pathways of equal range, principally due to their difference in average slope angle (1.21°).

In order to compare PSD curves across ranges, Fig. 4.5 highlights pathways with an indicative range (i.e. 5, 15, 30, 40, 50, 60 km). Power (energy per duration of the eight shots averaged per pathway envelope) can be seen to rapidly increase with frequency initially and peak between 25 and 75 Hz for all pathways, with those of shorter range being generally higher than longer pathways. All pathways show a decreasing trend in power levels with increased frequency up to 501 Hz although this trend is not uniform across range or frequency. The shortest pathway in Fig. 4.5 displays a secondary rise in power levels between 200 and 300 Hz. Observed TL values (source minus received $SEL_{1/3}$) were calculated at all 1/3 octave bands between 7.94 and 501.19 Hz. Fig. 4.6a is a contour plot of these $TL_{1/3}$ values for given pathways at all ranges. For display purposes, for a single range with multiple common pathways, only the deepest pathway was selected. Zones of lower $TL_{1/3}$ seen as the lighter coloured areas represent higher received levels indicating enhanced noise propagation compared to darker areas. Fig. 4.6b displays broadband (8 – 501 Hz) transmission loss ($TL_{broad}$) across all pathways, where as expected, values increase with distance from source due to diminishing received levels.
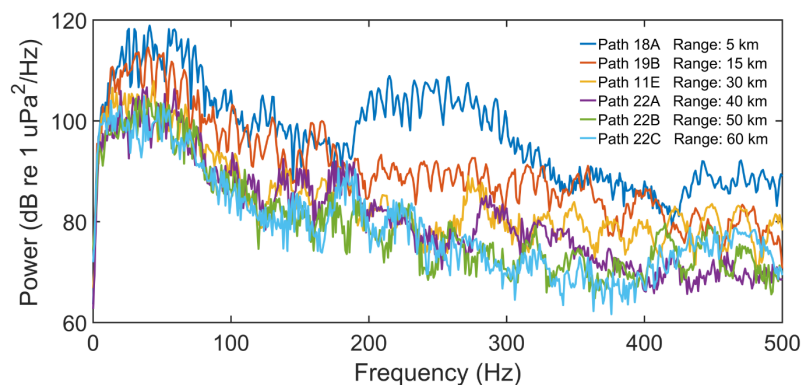


**Fig. 4.5.** Power spectral density (PSD) plot for six pathways, each with an example range. Data here is interpolated 1:10 from 1Hz interval power per frequency values.
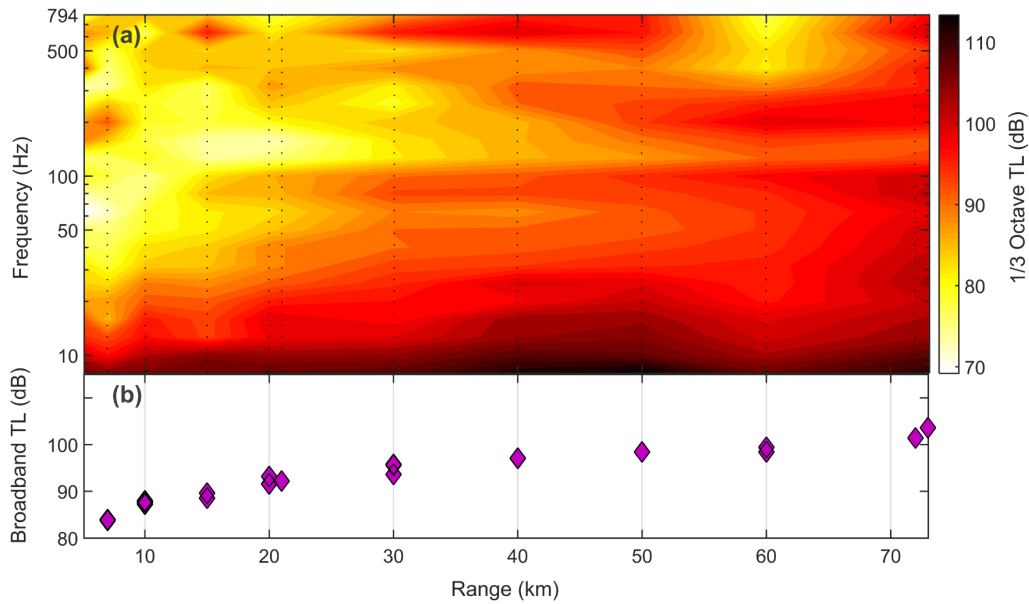
**Fig. 4.6.** (a): Contour plot of observed 1/3 octave TL values as a function of range for 10 indicative pathways (shortest to longest): 18A, 21A, 12A, 19C, 12C, 11E, 22A, 22B, 9, 15B. (b): Broadband (8 – 501Hz) transmission loss (TL$_{broad}$) values across all pathways.

### 4.3.2. Numerical model outputs

4.3.2.1. Modelling validation

As a basic method for model validation and to gauge the strength of the models presented here, Fig. 4.7 plots all the modelled 1/3 octave TL values against observed values at each path from a sub-set of ten pathways chosen for their sloping character. There are inherent margins of error in using this method, for example the modelled values are for an exact frequency (each at the 1/3 octave
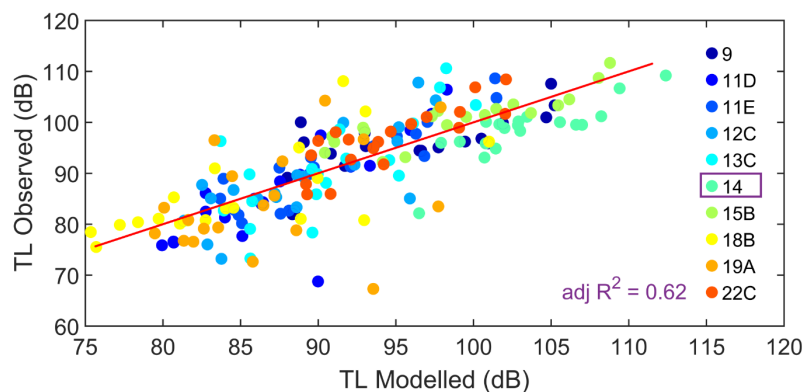


**Fig. 4.7.** Observed versus Modelled 1/3 octave TL values for a subset of pathways. $R^2$ value here is indicative rather than definitive.

centre frequency), whereas the observed values are a cumulative calculation between the lower and upper bounds of each 1/3 octave frequency band. The linear regression coefficient of determination ($R^2$) value included in Fig. 4.7 is purely indicative and not a direct measure of comparison.

## 4.3.2.2. Seabed slope effects

One of the main objectives of the model analysis used was to contrast up versus down-slope pathways in the context of continental margin control of pulsed noise propagation. As an example of this Fig. 4.8 displays differences in up/down slope propagation (lower values or lighter shades of TL) between pathway 14 and 22C over a common 500 Hz, with pathway 14 chopped to a common range with 22C. Pathways 14 and 22C were chosen for having the largest difference in average slope (up/down), however they do differ in range, which precludes direct comparisons of sound levels.   Attenuation is greater over the shoaling bathymetry of pathway 14, having an increasing number of surface/bottom reflections with range from source and consequent increases in grazing angles (angle from seabed to ray-path) causing greater attenuation when compared to the deepening pathway of 22C, even at such small changes (2.11°) in average slope angle. Developing this further, at 500Hz sound energy along pathway 14 covers most of the water column,
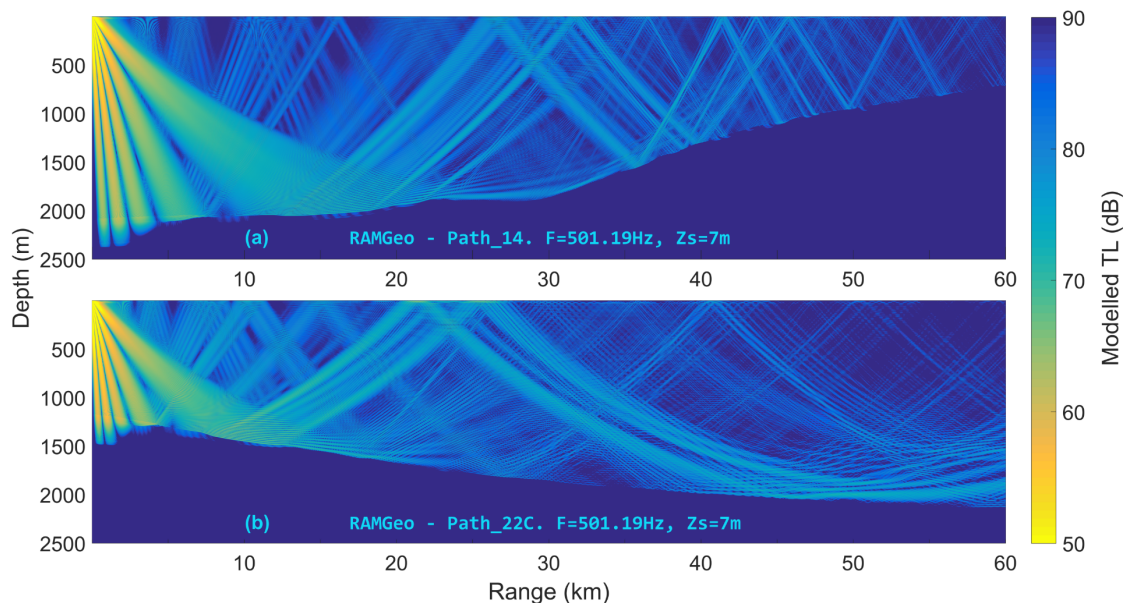


**Fig. 4.8.** RAMGeo Model outputs for source to receiver transmission loss at 500 Hz from a source 7m deep for (a): pathway 14 (average slope +1.2°) and (b): pathway 22C (-0.91°).

whereas along 22C it is mainly located close to the seafloor. Amount, shape and intensity of these reflections will also vary across differing frequencies.

To assess the influence of seabed slope, evidenced by TL differences (see Fig. 4.4), pathways 11E and 13C, having equal range and opposing slopes, were investigated further. Pathways of idealised bathymetry were constructed using exaggerated slopes (i.e. constant 5° slopes up and down), while retaining common range and depths at mid-range. These idealised slope pathways show a marked difference in $SEL_{1/3}$ compared to the real pathways of a more gradual topography. In Fig. 4.9a, modelled values for the real pathways 11E and 13C show a marginal difference in $TL_{1/3}$, whereas the modelled idealised upslope pathway in Fig. 4.9b clearly shows a higher TL than the downslope pathway, for example with values 10 dB higher from 158Hz upwards in 1/3 octave centre frequencies. Fig. 4.9b demonstrates how a shoaling seafloor creates more surface/bottom reflections over distance compared with a deepening slope (an effect also seen in the model outputs of Fig. 4.8), thus increasing TL and providing a lower sound level with inclination for a given range.
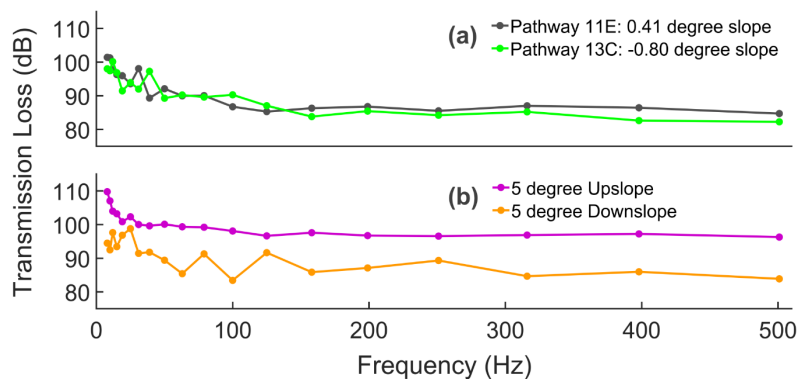


**Fig. 4.9.** Modelled 1/3 octave TL values. (a): Real pathways 11E (grey) and 13C (green) (b): Idealised pathways of a constant 5° upslope (pink) and 5° downslope (orange). All pathways have a range of 30 km.

### 4.3.2.3. Seasonal changes

Seasonal influence on sound propagation, both above and below the seasonal thermocline, is examined by focusing on the comparisons of modelled TL values from the gently upwards sloping pathway 11E (Fig. 4.10). With the hydrophone

receiver depth placed above the seasonal thermocline there was very little difference between summer and winter across all frequencies (excepting an anomalous jump in summer TL at 500 Hz). Below the seasonal thermocline revealed a greater variation in all frequencies above 40 Hz. It is due to these below seasonal thermocline differences that variations in TL are much greater, between surface and deeper waters, in summer (4 – 8 dB) than they are in winter (0 – 4 dB), especially at frequencies above 63Hz.
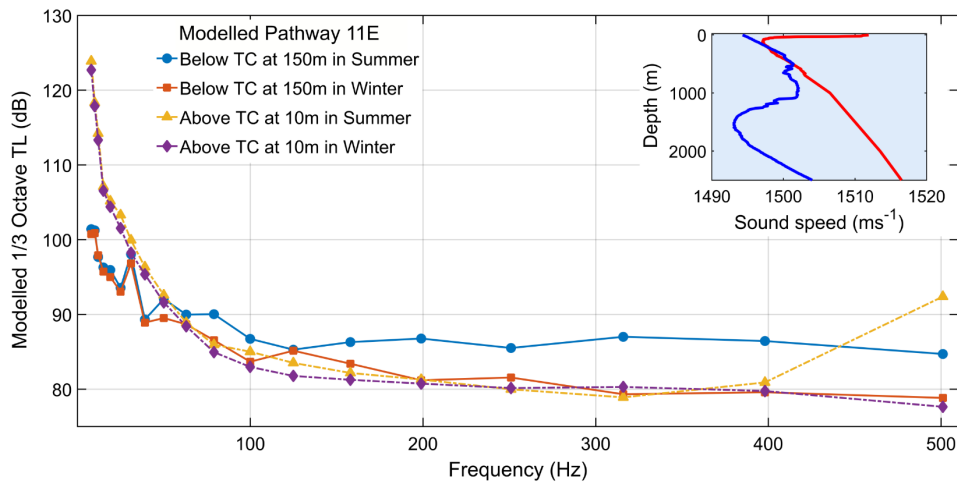


**Fig. 4.10.** Pathway 11E: modelled TL values per 1/3 octave centre frequency for values modelled above and below thermocline in both summer and winter. Insert plot displays sound speed profiles for summer (red) and winter (blue).

## 4.4. Discussion

### 4.4.1. *Porcupine Basin in the context of noise pollution*

Due to the PB's underlying geology and consequent interest shown in hydrocarbon exploration, it is important to understand the regional geoacoustic parameters that will moderate any anthropogenic noise propagation from continued seismic surveying. Topography, being a major control on sound propagation, varies in the PB from the flat or gently sloping deep basin centre rising to the more sharply inclined continental margin, which includes for example, submarine canyons and channels to the east. As part of a wider study on airgun signals, McCauley et al., (2000a, b) found upslope propagation values varied with slope by > 10 dB and further found values up to 30 dB greater on level pathways than the upslope values,

even at greater ranges; a caveat being that all these measurements were from shallow shelf waters (70 -160 m). Although the seismic survey source and receiver locations here only concern gentler slopes in deeper water, sound level variation  is still shown, even over slight differences in slope, for example a 2.17 dB modelled $TL_{broad}$ difference over a 1.21° change in slope between 11E and 13C, as also seen in 1/3 octave values (Fig. 4.9). Single frequency model outputs confirm the change in propagation patterns between up and down sloping bathymetry, where a greater number of reflections over a shallowing pathway result in a reduction and homogenisation of sound energy at a  given frequency (Fig. 4.8). The variation would become greater over steeper and/or more complex topography as exists around the Porcupine Seabight, the Porcupine Bank and the adjacent Rockall Trough, where submarine canyons may provide conditions for lateral reflections and resonance due to their geomorphology.

Other environmental parameters also play major roles in the control of sound propagation in the PB. Properties of the water column, specifically temperature, salinity and density and the resulting sound speed profile change both seasonally (seasonal thermocline), semi-diurnally (tidal) and dynamically (e.g., solitons of internal waves and internal tidal energy) (e.g., Thorpe et al., 1990; Huthnance et al., 2001). A stratified summer water column, through steeper gradient of density and thus sound speed, will strengthen the effect of the ocean as a wave guide including that of the deep sound channel (such as at latitudes covering the PB) compared to well mixed winter conditions (Jensen et al., 2011). Modelled TL values show how a variability of up to 8 dB can be found across a wide band of frequencies between winter and summer conditions on a single pathway (Fig. 4.10), calculated using real sound speed profiles from the region in both seasons. An 8 dB increase in sound intensity is considerable, especially for marine mammals, who's hearing sensitivities peak around the same frequency bands (e.g., low and mid frequency cetaceans) (Southall et al., 2007), considering that 10 dB is a ten-fold increase and a perceived doubling of intensity to humans and most likely cetaceans too. These summer to winter differences in noise propagation may alter behaviour patterns in addition to natural seasonal biological changes (e.g., Chen et al., 2017). Stratified summer conditions will also enhance the occurrence and magnitude of any internal waves, especially at the shelf edge known in this area for large internal wave generation (e.g., Thorpe et al., 1990; Holt and Thorpe 1997; Sharples et al., 2007; Aslam et al., 2018), which will in turn affect the propagation of any sound signal, including pulsed

anthropogenic noise. Luo et al., (2008), while investigating sound propagation through internal waves, found fluctuations of up to 15 dB corresponding to acoustic energy being redistributed in the horizontal, in what they term focussing and defocussing events. The Luo et al., (2008) study concerned shallower shelf depths compared to the PB but highlight the need to consider these dynamics in this region as well. Another interaction of sound in the water column is that of sea surface reflection, where increased surface roughness and bubble effects can reduce forward reflecting propagation (Jensen et al., 2011; Etter, 2013). The PB is located in an area of the NE North Atlantic that regularly experiences stormy conditions and wind driven surface waves, although seismic survey operators are limited by the same phenomena.

One of the main motivations for studying pulsed anthropogenic noise in the PB is the potential for it to cause harm and behavioural disturbance to resident and transient marine mammals in the region. Noise exposure criteria are the primary metrics used to measure the effects of anthropogenic noise on cetaceans and pinnipeds (Southall et al., 2007). A limitation of the observed data here is that noise levels at the closest ranges (pathway 18A: 158.3 dB (re:1 µPa) 0-peak and 143.4 dB (re: 1 µPa$^2$s) SEL$_{pulse}$ at 5 km) are below the suggested main injury thresholds (see Fig. 4.3a), those being 230 dB (re:1 µPa) 0-peak and 198 dB (re: 1 µPa$^2$s) SEL for PTS and 224 dB (re:1 µPa) 0-peak and 183 dB (re: 1 µPa$^2$s) SEL for TTS (Southall et al., 2007). Back extrapolation to threshold levels using a simple spreading model (see Fig. 4.3b) produced results with ranges very close to source (e.g., < 40 m for PTS) but are not considered meaningful as they do not account for the true and complex nature of sound propagation in the PB. Frequency weighting is another factor for consideration with cetaceans, where weighting functions are applied to data, so that sound levels reflect a specific marine mammal hearing group's sensitivity band, for example the low frequency cetacean group (LF) of most concern at the frequencies dominant to the seismic airguns studied here (Southall et al., 2019). The PB is a region of environmental significance, containing two of Ireland's five deep ocean Special Areas of Conservation (SACs), with the Hovland Mound Province SAC being approximately 85km away from the Polarcus survey's closest approach. It is also an area of known cetacean habitat. O'Cadhla et al., (2004), observing mostly in spring/summer, recorded many sightings of cetaceans, including fin, sei and minke whales around the northern margin of the PB. Through regulations, such as mitigating ramp up procedures for noise production, the

hydrocarbon exploration industry is compelled to engage with the surrounding environment. Although TTS criteria are most likely met at quite short ranges from an acoustic airgun array and when correct mitigation procedures are in place the occurrences of permanent or temporary injury are rare if any, these metrics do not consider all potential harm. Another criterion, that of behavioural disturbance, has been identified as an impact from seismic surveys that has a much wider set of ranges and effects. Behavioural disturbance is an active area of investigation, with ongoing work into having it a recognised and quantifiable metric in environmental impact assessment, regulation and mitigation measures in anthropogenic underwater noise. An example is the Behavioural Response of Australian Humpback Whales to Seismic Surveys (BRAHSS) project, which through an extensive four-year (2010 – 2014) field program, utilising taggings, sightings and acoustics, found disturbance, such as  slowed migration speeds and shorter dive times in response to seismic vessels occurred above SEL levels of 135 dB (re: 1 µPa$^2$s) and within 4km range (e.g., Dunlop et al., 2015; Dunlop et al., 2017). In what they term 'behavioural context', Ellison et al., (2012) advocate a wider approach to understanding behavioural response that considers metrics, such as animal activity and ambient noise, in addition to the more traditional use of single sound levels received by the animal. Future work following from this study aims to incorporate behavioural disturbance as a threshold guideline during noise propagation analysis.

By examining a set of pressure time-series consisting of a short sequence of individual shots, differences in shape, amplitude and presence of headwaves can be noted across varying pathway conditions. Contrasts are apparent on the two shorter range (10 km) pathways 18B and 19A, where the upslope 18B shot arrivals are much higher in amplitude than 19A downslope which has a secondary reflection of equal or higher amplitude than the initial one (Fig. 4.11a, b). The secondary arrivals in 19A are of a higher amplitude and less dissipated over time than those of 18B. It is unclear what is the driver of these differing arrivals, whether it is depth, slope angle, differing seabed properties or a combination of each. Water column properties are not thought to differ much over these temporal and spatial scales. 18B was more intense, with an observed time domain RL of 139.9 dB (SEL$_{pulse}$) and 0-peak of 156.4 dB (re: 1 µPa) compared to 19A values for RL and 0-peak of 138.8 and 155.0 dB, respectively. Shot signals received at longer ranges (see Fig. 4.11c, d) show a more defuse image, with multiple reflection arrivals spread out over a longer duration and with much lower amplitudes (note change in Y-axis limits). 22C
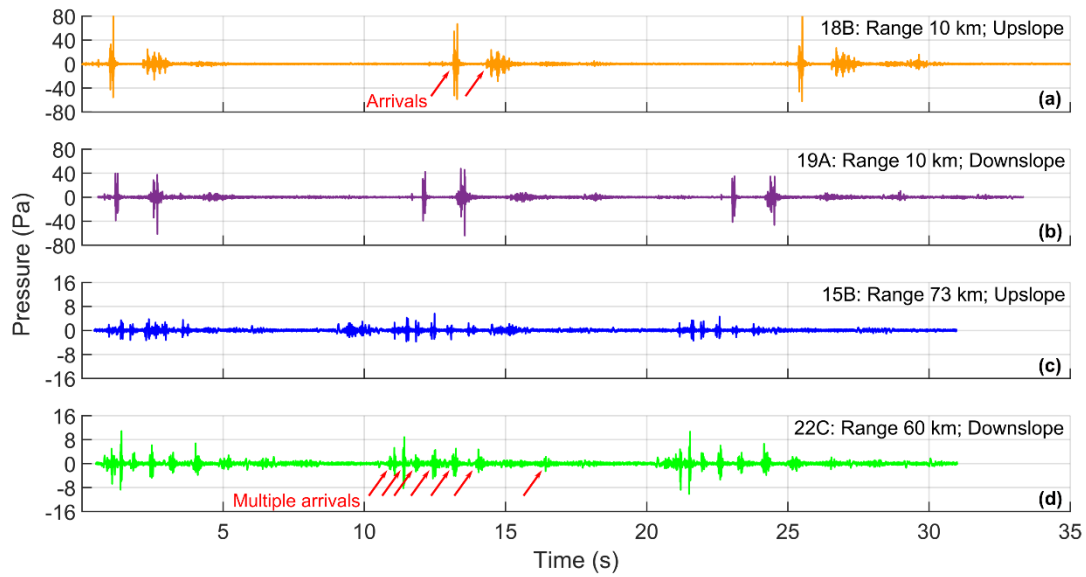
**Fig. 4.11**. Sets of pressure time-series shot arrivals. Peak pressure of first shot in each set has been approximately equalled as a start time. Note the change in y-axis scale from the shorter ranged (a) and (b) at 10 km, to the longer ranged (c) and (d) at 73 and 60 km, respectively. Examples of multiple arrivals from a single shot are indicated with red arrows.

appears to have a headwave arrival before the main arrival of peak amplitude. This headwave is likely a horizontally propagating, near surface, sub-seafloor shear wave returning sound energy to the water column. Also to note, from all shots in Fig. 4.11 that each shot is different within any given pathway, probably due to small changes in seabed or water column properties and explains the need to average a set of shots over a short time period to better characterise sound propagation. Observations here have highlighted how each propagation pathway across the northwest PB soundscape have different characteristics. Another example of this is in the shortest pathway 18A (5 km). In addition to the expected elevated power levels that all pathways have peaking around 50 Hz (Fig. 4.5), 18A has a further bulge between 200 and 300 Hz relative to other pathways in the figure. Again the reason for this is not answered here but is likely due directly to the close range and thus less complex reflection patterns experienced.

The composition of sub-seafloor layering controls the proportions of frequency dependent acoustic wave reflections and refractions crucial to understanding and tuning models of anthropogenic noise propagation. With only sparse data available for deep sub-seafloor parameters (i.e. two IODP boreholes) in the PB, assumptions must be made on the horizontal variability of these parameters and values tweaked

for model development. There are other inherent limitations to the methods used here. Ambient noise varies in the ocean and the PB but has not been quantified in this study as it is thought to add an insignificant margin of error to the results. All the source/receiver pathways investigated are gently sloping at most, providing no opportunity to investigate more extremes of topography, for example submarine canyons commonly found in the region, which may prove important moderators of sound propagation across the Irish continental margin. Subsequent studies are ongoing into this question of margin control on sound propagation in an Irish context.

### 4.4.2. Model functionality for the Porcupine Basin

Numerical 2D acoustic modelling has been a well-established discipline ever since the age of submarine naval operations. Many methods and models are available from simple energy spreading models, for example,  to the more advanced Normal Mode and Wave Integration models. While each 2D model has advantages in its optimal environmental conditions, they are all limited. One common limitation being that they only describe a single straight-line pathway from source to receiver. In order to minimise this limitation pseudo-3D models are a vast improvement on 2D but because they are based around a point source and due to the need for validation through observed measurements they have not been employed for this dataset. 3D modelling, such as finite element modelling in space and time, would be more accurate for complex modelling scenarios but would require advanced and extensive computing resources at the frequencies studied here, making the prospect very challenging. Ideally a fully 3D model could be developed for Irish waters, considering the regionally specific environmental parameters and designed to inform regulators and industry on predictive noise levels in the region for future seismic exploration.

Within the current scope of work, modelling through RAMGeo has been used to investigate the magnitude of noise level changes when altering various parameters, specifically slope effect, seasonal sound speed profiles and sub-seafloor composition in the vertical. Although the models used are not ideal at predicting observed values they are in general agreement (Fig. 4.7). This highlights the importance of constraining environmental parameters for refining any given acoustic model and for choosing an acoustic model capable of optimising the use

of available geoacoustic parameter data as discussed by (McCauley et al., 2000b). A feature of note is that pathway 14 has been wholly overestimated for TL by the RAMGeo model, all being below the equal value line (Fig. 4.7, purple boxed pathway). By comparing pathways 14 and 15B (of equal range and similar slope) using a rugosity index derived from detailed bathymetry data on a GIS platform following methods used by Daly et al., (2018), investigation took place into this being due to fine scale topography effects. Results could not confirm rugosity as a factor for pathway 14's anomaly, implying another geoacoustic property, such as sub-seafloor geology being responsible.

### 4.4.3. Regional scale benefits and outlook

Developments in marine acoustic research are ongoing. Methods are being refined and with increasing computational capacity available models are growing in their predictive capabilities, while modern instrumentation and digital communication has allowed for vastly improved recording and real-time streaming of underwater sound. These developments are important in understanding, monitoring and mitigating anthropogenic noise (both pulsed and continuous) in a warming and increasingly acidic ocean (e.g., Hester et al., 2008), coupled with greater knowledge of impacts to the marine environment (McCauley et al., 2000a), such as behavioural disturbance to marine mammals (Southall et al., 2019) or to abundance of base level organisms (McCauley et al., 2017). This study combined with previous work (Crawford 2016) has provided the required sound level metrics to allow crucial evaluation of a pulsed anthropogenic sound field for the northeast PB. Such a sound field can be used by industry and regulatory bodies as per requirements under the MSFD (Tasker et al., 2010) and on forming future mitigation strategies. The OSPAR Commission uses a pressure based impulsive noise indicator for measuring/mapping potential harm (OSPAR 2017). Sound level metrics measured here are not directly applicable to OSPARs unit of Pulse Block Days. OSPAR are, however, in the process of developing further indicators, for example a spatial risk assessment indicator (OSPAR 2017), which could benefit from the input of any regional scale studies, such as this one, to inform large scale modelling parameters for comparison with species distribution. Refined evaluation of regional sound fields coupled with focussed work on potential noise hotspots and development of 3D acoustic models will aid Irish sustainability and mitigation efforts in an increasingly noisy ocean.

## 4.5. Conclusion

This study has tailored a method of airgun shot identification and analysis for source and received acoustic data from an offshore seismic survey. 2D numerical modelling has been used to further investigate exaggerated slopes and seasonality. Although source levels from the seismic airgun array exceeded threshold levels of harm to marine mammals, received levels (all > 5 km range) did not, however these levels have potential for behavioural disturbance. Modelled idealised slope angles show higher sound energy, and variation over depth, from a deepening slope, compared to a shoaling one, while seasonal investigation indicated highest and most variable sound levels below seasonal thermocline depths in summer. Regional scale observational, monitoring, and modelling programmes in the Irish offshore are integral to Ireland's participation in international regulatory frameworks (e.g., MSDF) and marine environmental protection bodies (e.g., OSPAR).

# Chapter 4: Addendum and Erratum

**Addendum**

The rationale for this peer reviewed article was to investigate propagation controls (slope, bathymetry, water column seasonality), to examine what degree each effect sound transmission and to broaden the evaluation of a Porcupine Basin sound-field following a previous field campaign. It contributed sound level differences (especially for slope and seasonality) studied further in Chapter 5 and highlighted the need to focus work on the continental margin where variation would be greater.

The lead author contribution to the manuscript was:

- Re-processed and re-analysed all data using computational scripts (and more importantly: guidance) provided by the first co-author
- Developed new code
- Wrote the original draft in full and compiled all figures and tables.

For clarity, azimuthal differences in source levels from the airgun array were incorporated in calculating observed Transmission Loss (TL) throughout, but this should have been stated clearly within the methods section of Chapter 4.

**Erratum**

Following enquiries to the instrument manufacturer it was discovered (post-publishing) that the reference voltage ($V_{ref}$ = 1.17V) needed to convert the Analogue to Digital Converter's (ADC) output voltage to pressure (Pascals; Pa) was incorrect. There had been a mix-up, whereby 1.17V was actually the ADC's rms Voltage and the correct value was $V_{ref}$ = 1.65V (= $V_{rms}$ x $\sqrt{2}$). This resulted in all reported received pressure levels (RL) being too low by ~65% or 4.35 dB re: 1 µPa, and in turn, all observed TL values being 4.35 dB too high. This value needs to be added (RL) or subtracted (TL) from values in Figs. 4.3, 4.4, 4.6, 4.7 and 4.11. It is intended to publish this erratum in time for the next issue of the original publishing journal, IJES.

# Chapter 5: Evaluating Controls of Airgun Noise Propagation Across the Continental Margin

## 5.1. Background and Methodology

### 5.1.1. Introduction

Understanding how anthropogenic noise propagates across the continental margin is a key aspect in examining the potential harm it may cause to marine fauna within this ocean boundary region. There are various controls on noise propagation such as range, topography, sub-seafloor geology and water column structure, some of which are easier to constrain than others. For example, constraining density and other geoacoustic parameters of underlying sedimentary and clastic layers is not possible, beyond a first order estimate, due to lack of data in the region, whereas measuring range is relatively straight forward. It is these physical controls on noise propagation that provide the foundation for the hypothesis this chapter is premised on: To what degree, does the more extreme topography of a submarine canyon dominate control of noise propagation across the continental margin, in relation to other primary controls, such as range and water column dynamics and does the canyon enhance or inhibit cross slope propagation, each way, between deep ocean and shelf seas? To investigate this, various sound metrics from observed impulsive noise data are examined and compared over propagation pathways varying in range, slope, depth and topographic setting.

Ambient or background noise is a constant occurrence in the ocean but is increasing through anthropogenic influence by as much as 3 dB per decade (@ 40 Hz averaged over 40 years), mostly due to the increase in size of ships and fleet (Andrew et al., 2002; Erbe et al., 2019). Any natural or anthropogenic sound will transit from being dominant in the near-field to becoming part of the background noise at a given range, dependent on output amplitude and peak frequency band. The louder and/or more pervasive anthropogenic noises such as shipping, seismic airgun surveys or offshore development, can have the greatest general effect on ambient noise (Hildebrand, 2009). This noise in turn can have masking effects on marine mammals attempting to hunt or communicate (Erbe et al., 2016). Ambient

noise varies in the ocean, both in amplitude and spectrally, as a function of both natural and anthropogenic physical phenomena. Results presented and discussed in this chapter have identified variable and at times substantial ambient noise, which is most noticeable in the low frequency bands below 20 Hz but also throughout the lower decade bands up to 1000 Hz, with water currents thought to be a dominant driver in the absence of vessel noise. These ambient noise results must be considered quantitatively when assessing shot signal interpretation, but they also provide standalone information themselves, on differences between locations and temporally over the course of the deployment.

Having previously examined the wider, deeper and topographically smoother region of the north Porcupine Basin (PB) from pre-existing data in Chapter 4, the following chapter locally addresses the noise levels found using various metrics at each recorder location within a designed canyon/control site. This is followed by an in-depth comparison of pathways best placed to identify topographic controls. Ambient noise is characterised predominantly between a loud low frequency acoustic band (< 20 Hz) and a higher broader bandpass. Hydrography, dynamics (including IW structure) and derived water column sound speeds are assessed, followed by a detailed correlation study between acoustic and hydrographic instruments mounted on each mooring, in order to gauge potential relationships between ambient noise received and current/tide/internal wave changes to hydrographic parameters. Concluding the chapter is a synthesis of results and discussion of their interpretation and implications for constraining anthropogenic noise pollution.

### 5.1.2. PANiC Experiment and analysis

Propagation of Acoustic Noise in Canyons (PANiC) was a controlled acoustics experiment, carried out in June 2018, to quantify noise levels along the continental margin, using a seismic airgun and fixed acoustic mooring recorders. Acoustic mooring locations and the position of the source transect were designed to monitor noise propagation across both a submarine canyon and the adjacent slope. The upper slope (M1) and lower slope (M2) moorings are adjacent and parallel to axis of the upper canyon (M4) and lower canyon (M3) moorings, while M5 is placed on the shelf break at canyon head, as detailed in Fig. 5.1 here and further in Chapter 3. A seismic airgun source was deployed in a transect around the acoustic moorings (yellow line in Fig. 5.1) and pathways of specific interest were identified between

sources (labelled A1 – A13) and mooring receivers. By comparing the results of analysis between contrasting pathway topographies, using various sound metrics, an evaluation can be made of how propagation differs between them.
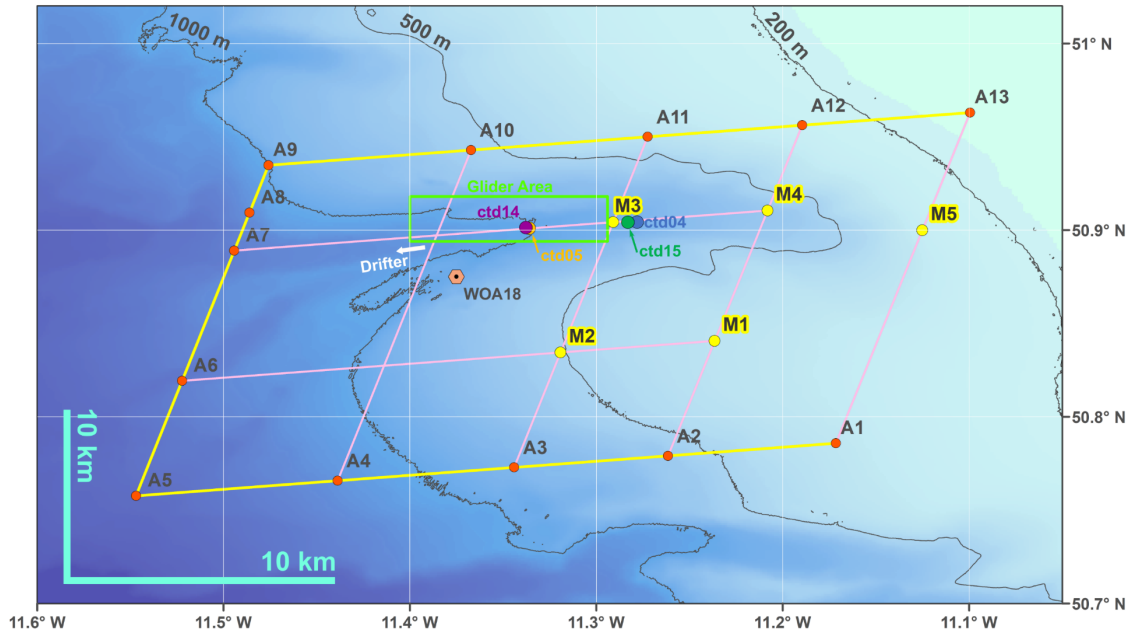


**Fig. 5.1.** Map of key locations within the survey area. Moorings M1-M5 are marked in yellow circles, airgun locations of interest A1-A13 in orange circles and airgun transect line in yellow. pink lines are theoretical propagation pathways of interest. The glider operational area is bounded by a green box and four CTD stations are labelled and colour coded, while the WOA18 Modelled winter station (see later in text and Figs. 5.16, 5.20) is denoted with an orange hexagon. The drifter deployment track is indicated with a white arrow in the direction of drift.

For interrogating noise propagation through received sound values, various metrics can be used. In the case of impulsive sounds, the metrics used here (following e.g., McCauley et al., 2000; Robinson et al., 2014) were zero-peak and 90% energy Sound Exposure Levels (SEL). Also carried out was a spectral density analysis of SEL values at stated frequency bins, including 1/3 octave frequencies, (see further details in Chapter 3.4.1). Zero-peak SPL values, being the instantaneous pressure difference from zero to peak pressure (Merchant et al., 2015), measure the maximum amplitude received from any given shot, providing an important metric of what a marine mammal will perceive as loudness. 90% Energy SELs are a pseudo measurement (between the 5% and 95% intervals and assuming specific acoustic impedance is constant) of acoustic energy transmitted through the water column in

the time domain. Incorporating spectral analysis through an FFT, in the form of a PSD, allows for investigation of specific bands of noise frequency convenient for excluding low frequency ambient noise, for example, or for identifying peak frequencies and variation of spectral densities.

## 5.2. Investigation of Controlled Seismic Airgun Noise

### 5.2.1. Airgun source levels

Source levels of impulsive noise emitted by bubble oscillations from the seismic airgun source (mini-GI gun, 40 in$^3$), are claimed by the manufacturers to be omnidirectional, negating the need for azimuthal variation in the analysis. Source level outputs modelled at 1 m from source were provided by the manufacturers, which gave a broadband, root-mean-squared Sound Pressure Level (SPL$_{rms}$) output of 201.1 dB (re: 1 µPa @ 1m),  which translates to a Sound Exposure Level (SEL) of 198.1 dB (re: 1 µPa$^2$s @ 1m) when integrated over a time duration of 0.5 s. Please see further single value metrics within the info box in Fig. 5.2. A signature (Fig. 5.2a), zoomed in spectra < 240 Hz (Fig. 5.2b) and broadband spectra (Fig. 5.2c), were also provided, along with permission to include here, but unfortunately after much communication, spectral or 1/3 octave levels were not forthcoming. This lack of frequency specific source data causes issues for spectral or 1/3 octave comparisons of source versus received values, transmission loss measurement and also discrete indicator frequencies for modelled transmission loss.

### 5.2.2. Received levels of airgun noise propagation

As a first pass appraisal of differences in propagation pathways, a pressure-time series can be viewed as the instantaneous sound pressure level received by each recorder's hydrophone and compared with results of recordings at different locations. Although the pressure-time series is not instantaneous, discrete recordings at a sufficiently high frequency sampling rate, when viewed over a long
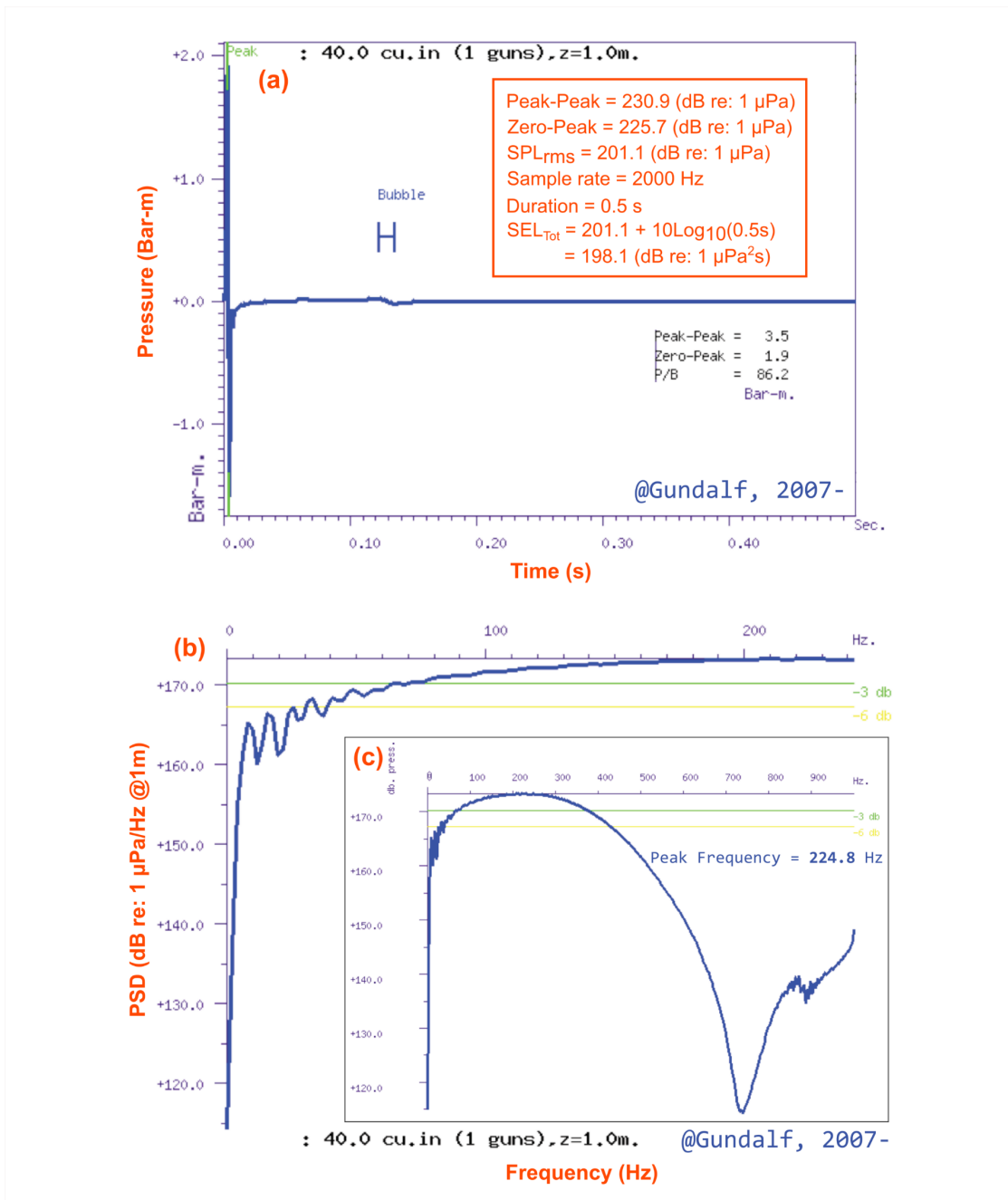
**Fig. 5.2.** Modelled airgun source outputs. (a) signature, (b) zoomed spectra and (c) broadband spectra. Enclosed info box contains durations, peaks and broadband values etc. These plots have been adapted from material provided by SERCEL Inc.'s Gundalf array modelling suite. Please note that this is an industry based source model concerned with downward propagation. The notch at ~720 Hz resulting from a (half wavelength) surface or 'ghost' reflection would prevent this output being useful to inform any horizontal propagation model such as this body of work is concerned with

enough time will appear so, and display some of the dominant characteristics (e.g., amplitude, number of arrivals per shot and background amplitude) of how seismic airgun noise differs between locations. As an example of this, the pathways of M2B (B = hydrophone placed just above bottom depth) and M1 from a source at A6 can

be visually compared with the pathways of M3B and M4 from a source at A7 of approximately equal respective ranges and over contrasting topography in Fig. 5.3. In both the pressure-time series and the adjoining spectrograms, the higher amplitude airgun signature and spectrally peaking arrivals at M3B and M4 (Fig. 5.3a, b) are appreciable when compared with the lower signatures and spectrograms of M2B and M1 (Fig. 5.3c, d) across each 5-min sample. The variance
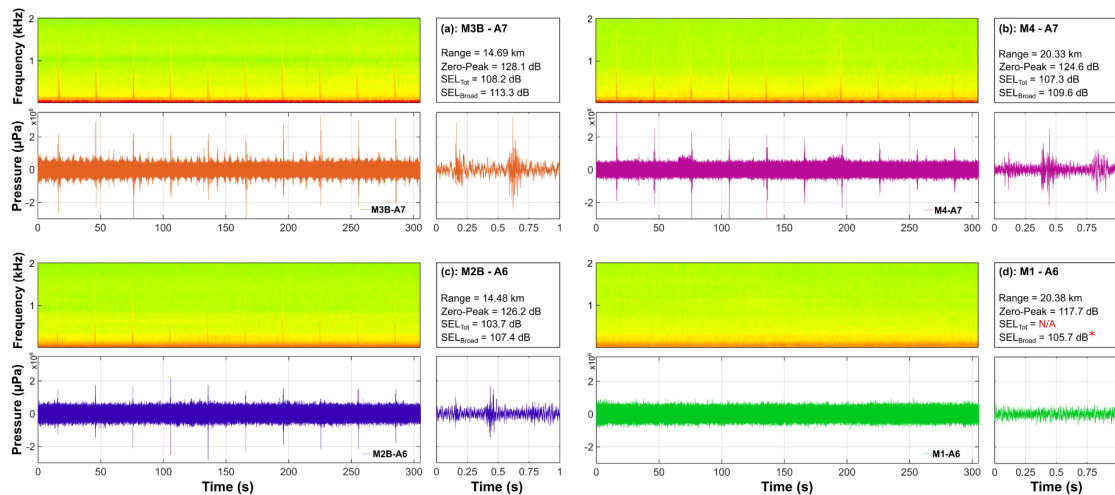


**Fig. 5.3.** Airgun shot spectrograms (top) and signatures (bottom) for four example pathways over varying topography, with (a) M3B-A7 and (b) M4-A7 over the canyon and with (c) M2B-A6 and (d) M1-A6 over a more typical slope. Bottom right-hand-side panel of each pathway is a single airgun shot zoomed into a 1 s duration. The enclosed info boxes contain ranges, zero-peak (re: 1 μPa), and Sound Exposure Levels (SEL) (re: 1 μPa$^2$s), described in detail later in the chapter.

between each individual shot's amplitude, seen at any single hydrophone, underlines the need to average over a given number of shots during sound metric analysis. Also of note is the difference in ambient or background noise seen in between shot arrivals in Fig. 5.3, which highlights the requirement of further analysis of ambient noise as part of measuring airgun shot arrivals.

As mentioned in Section 5.1.2., indicator pathways have been chosen to reflect differing topographic conditions, both along and across canyon axis. These indicator pathways are displayed within this section as map style scatter plots that show each of the three main metrics as size and colour intensified circles at every source-receiver pathway per location that are useful for visualising differences over range and depth. The entire set can be found in Appendix A.1. The two main
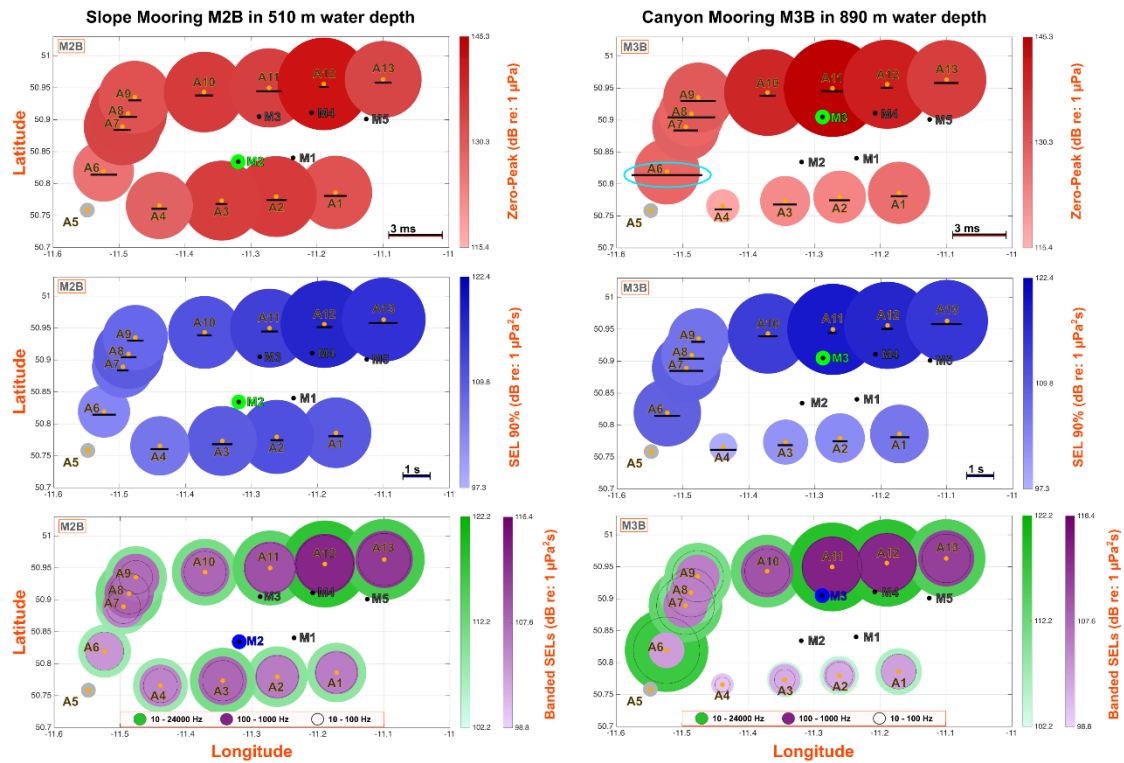
**Fig. 5.4.** Map scatter plots of sound levels received at M2B (left panels) and M3B (right panels) for all chosen pathways. Top panel is zero-peak levels, middle panel is 90% energy SELs and bottom panel shows banded SELs. Labelled black points are mooring locations and labelled orange points are airgun positions. Black horizontal bars in top and middle panels represent rise times of zero-peak and 90% energy respectively, while contour bars to the left of each panel are set to maximum and minimum values of the total set of moorings throughout.

pathways running parallel to the canyon axis, which best reflect these contrasting slope types are sources at A6 through M2 and M1, and at A7 through M3 and M4 over typical slope and canyon respectively (also see Fig. 5.1). It can be seen that at M2B (bottom hydrophone depth: 506 m), sound values along the typical slope pathway are faint in comparison to the values at M3B (bottom hydrophone depth 893 m) in canyon (Fig. 5.4). In fact, values received at M2B (Fig. 5.4, left panels) are stronger along a pathway from A7 than A6. At M3B (right panels) values are strong from both A7 and A6, although it must be noted that a strong low frequency ambient contingent of noise is seen in M3B-A6, especially where the broadband and first decade band (10 – 100 Hz) are large, whereas the 100 – 1000 Hz decade band is comparatively small (bottom panel of Fig. 5.4). This anomaly, also seen in the abnormally large zero-peak rise time (light blue oval in top RHS panel) is discussed further in the ambient section (Chapter 5.3).

As a general trend in Fig. 5.4, levels are relatively high on the lower slope mooring not only during the southerly slope airgun transect (east to west, A1 – A5), but also propagating from across the canyon during the northerly airgun transect (west to east, A9 – A13). This is in contrast with the M3B lower canyon mooring, where levels from the southerly airgun transect, propagating from the slope into the canyon are relatively weak in all three sound metrics, including 90% energy levels which have any low frequency ambient sound filtered out of analysis. Hydrophones placed higher in the water column (100m depth) at M2T and M3T, show very similar contrast characteristics between canyon and slope.

This incidence of higher values being received on the slope from across canyon, transverse to axis, is repeated at mooring M1 higher up slope, where all metrics of interest are significantly higher across canyon (e.g., A12), than from the much nearer gun location at A2 (Fig. 5.5). It is these differences in values, not consistent
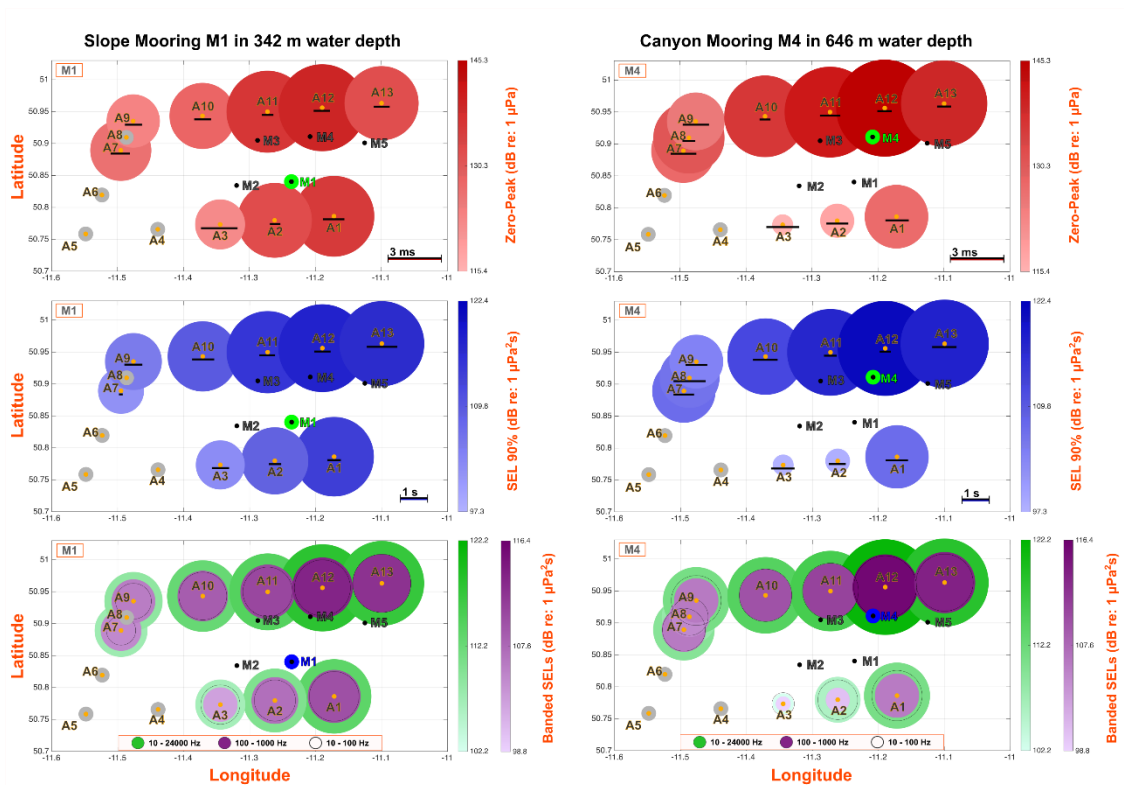


**Fig. 5.5.** Map scatter plots of sound levels received at M1 (left panels) and M4 (right panels) for all chosen pathways. Top panel is zero-peak levels, middle panel is 90% energy SELs and bottom panel shows banded SELs. Black dots are mooring locations. Black horizontal bars in top and middle panels represent rise times of zero-peak and 90% energy respectively, while contour bars to the left of each panel are set to maximum and minimum values of the total set of moorings throughout.

with range but consistent with topographic changes, that leads to the conclusion that topography has become a dominating control on noise propagation along with range itself. Where the noise appears to be louder propagating easterly through canyon axis compared to easterly over the slope it is most likely due to the morphology of the steeply sloping flanks of the submarine canyon and due in part, to the more gently sloping canyon axis. Additionally, noise propagates more strongly obliquely across canyon onto the opposite slope compared to propagation in the opposite direction. These relationships are examined further in the following sub-section and discussed in relation to other findings in the discussion chapter.

### *5.2.3 Direct comparison of airgun noise with range over varying topography*

Each indicator pathway has a different depth at source, receiver depth and range from source to receiver. Table 5.1 sets these out along with single value sound metrics and rise times calculated for each indicator pathway using methods described in Chapter 3.4.1. For a full set of mooring metadata and separately for sound levels, please refer to Tables A1, 2, 3 in Appendix A. Values of zero-peak pressure are all reduced considerably, due to transmission loss, from source level (225.7 dB re: 1 µPa) to receiver of between 107.9 – 80.6 dB. SEL levels result in similar transmission losses (92.2 – 76.6 dB) from a source of 198.1 dB re: 1 µPa$^2$s; and although SEL is not exactly comparable in this context (i.e. source is SPL$_{rms}$

**Table 5.1.** Comparison pathways.Metadata and sound level metrics.

| Pathway | Range | Depth | | | Zero-Peak* | | 90% Energy SELs** | | SEL Bands (Hz)** | | |
|---|---|---|---|---|---|---|---|---|---|---|---|
| | | Mooring | Phones | Airgun | Level | Rise Time | 1 s | Rise Time | 10 -24k | 10 -100 | 100 -1k |
| | (km) | (m) | (m) | (m) | (dB) | (s) | (dB) | (s) | (dB) | (dB) | (dB) |
| | | | | | re: 1uPa | | re: 1uPa$^2$s | | re: 1uPa$^2$s | re: 1uPa$^2$s | re: 1uPa$^2$s |
| M1-A2 | 6.98 | 344 | 100 | 603 | 132.52 | 0.000600 | 108.69 | 0.52 | 110.23 | 105.01 | 108.21 |
| M1-A6[#] | 20.38 | 344 | 100 | 1412 | 118.03 | 0.002723 | | | 105.79 | 103.25 | 100.81 |
| M1-A12 | 13.282 | 344 | 100 | 226 | 139.05 | 0.000925 | 117.57 | 0.62 | 118.09 | 111.06 | 117.01 |
| M2B-A6 | 14.484 | 511 | 506 | 1412 | 126.26 | 0.001521 | 103.65 | 0.84 | 107.38 | 104.11 | 103.75 |
| M2B-A7 | 13.79 | 511 | 506 | 1393 | 133.75 | 0.000962 | 106.79 | 0.46 | 107.94 | 102.73 | 105.89 |
| M3B-A6 | 19.145 | 898 | 893 | 1412 | 125.68 | 0.004073 | 108.68 | 0.94 | 116.67 | 116.44 | 102.91 |
| M3B-A7 | 14.689 | 898 | 893 | 1393 | 128.98 | 0.001402 | 108.21 | 0.86 | 113.26 | 111.96 | 106.88 |
| M4-A2 | 15.075 | 651 | 100 | 603 | 117.78 | 0.001263 | 97.75 | 0.64 | 105.87 | 104.52 | 98.79 |
| M4-A7 | 20.326 | 651 | 100 | 1393 | 127.63 | 0.001475 | 107.30 | 0.78 | 109.59 | 105.61 | 106.91 |
| M4-A12 | 5.188 | 651 | 100 | 226 | 145.15 | 0.000825 | 121.25 | 0.43 | 121.53 | 114.47 | 120.41 |

**Notes**:  \* Zero-peak of highpass filtered (>10 Hz) pressure series
\*\* 90% and Banded SELs calculated over a common 1s shot duration throughout
[#]M1-A6 had no shots present but was shot analysed for comparison purposes

derived whereas received is broadband) the differences are thought to be very small. Loudest received values of the entire survey were for pathway M4-A12, whereas the quietest pathway for this comparison was M1-A6, where airgun pulses were not detected but were processed anyway using the same methods, in an attempt to achieve comparable values, yet effectively reporting background levels (these levels have been highlighted in red in all tables and plots). The main comparison pathways investigated in this section have appreciable differences in received single value levels (Table 5.1) over very similar ranges. Metrics, such as zero-peak and broadband SEL, are not always concomitant between comparisons, highlighting the multi-controlled, non-linear and complicated nature of the problem. The greatest difference between range comparative pathways was the cross-canyon M1-A12 (stronger) versus the along-slope M4-A2 with variation in levels of 21.27 and 12.22 dB for zero-peak and broadband SEL respectively, and while considering there was a difference in range of 1.79 km, these differences are very large over opposing topographical paths. The next biggest difference was M4-A12 (stronger) versus M1-A2 (12.63 and 11.3 dB for zero-peak and broadband SEL respectively), again over comparable ranges.

In order to explore in detail, the differences in indicator pathways, spectral densities and 1/3 octave centre frequencies were employed for their ability to compare frequency component variation along with comparison to ambient noise. The first comparison here is that of the deep slope pathway M2B-A6 versus the pathway at the deep canyon opening M3B-A7 (Fig. 5.6). The pathway M3B-A7 is consistently stronger than M2B-A6 at all 1/3 octave values between 20 – 2000 Hz (Fig. 5.6a). Almost all individual Hz power levels up to 130 Hz and all remaining power levels up to and beyond 500 Hz (Fig. 5.6b) are also elevated. Here the power spectra have been zoomed into 50 – 500 Hz of greater interest with regards source output, to achieve finer resolution within the graph. Some spikes in the spectra (e.g., around 100 Hz) caused by ambient noise will be somewhat reflected in the 1/3 octave levels summed over that band but overall values are in line with differences seen in zero-peak levels (Fig. 5.6c) and in broadband SELs, being 5.3 dB from Table 5.1. Bathymetry is shoaling steeper over the slope pathway M2B-A6 here, compared to pathway M3B-A7 being aimed along the canyon thalweg (Fig. 5.6d, e). A steeper slope will create more surface/bottom reflections over a given range and thus lower received sound levels compared to a gentler (canyon thalweg) slope. However, the

differences found here are thought to be more than from slope angle alone and are scrutinised further in discussion Chapter 7, in relation to results found in Chapter 4.
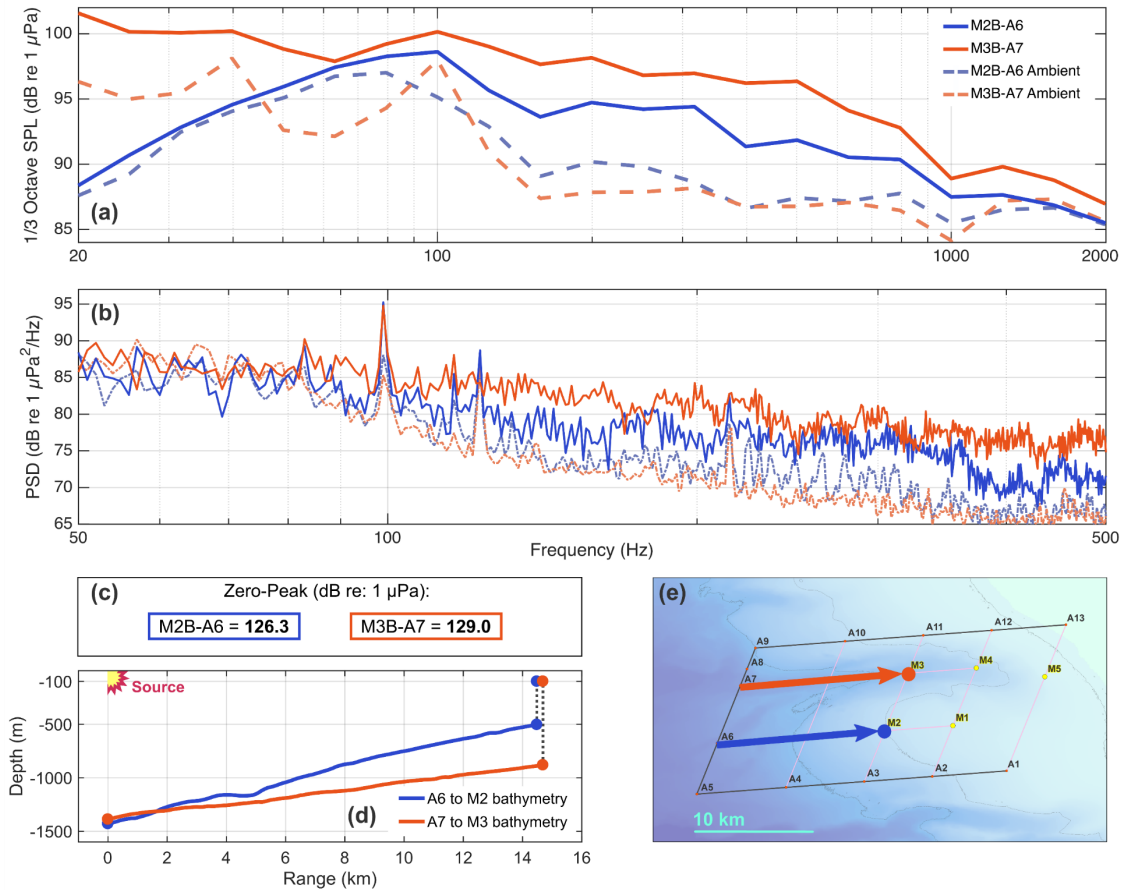


**Fig. 5.6.** Comparison of pathways M2B-A6 (blue) and M3B-A7 (orange) for shot averages (solid lines) and isolated ambient noise within 10 minutes of the event (dashed lines) over: (a) 1/3 Octave levels up to 2000 Hz and (b) Spectral densities zoomed into zone of interest. (c) Displays relative zero-peak values, while (d) plots bathymetry of each pathway, including source and receiver positions. (e) shows a plan view of pathways over a basic map backdrop with scalebar for range.

Recorded values from hydrophones mounted higher up on M2 and M3 moorings are displayed in Fig. 5.7. They show similar trends to the bottom recorders, with the exception of M3T decreasing from 60 back to 20 Hz unlike M3B but aligned with all M2 recordings. Above 100 Hz differences are even greater between canyon and slope pathways for the top mounted hydrophones. Results displayed in Figs. 5.6 and 5.7 indicate that topography does indeed affect propagation, allowing for stronger values from the canyon mooring at both airgun positions, but also
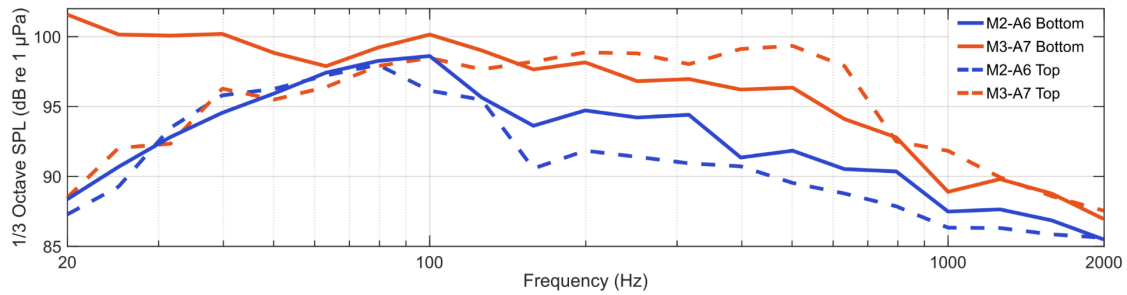
**Fig. 5.7.** Comparison of pathways M2B-A6 (blue) and M3B-A7 (orange) for Bottom hydrophones (solid lines) and top mounted hydrophones (dashed lines) over 1/3 Octave levels up to 2000 Hz.

highlights the prevalence of low frequency levels most prominently at hydrophone M3B.

Extending those pathways parallel to canyon axis from A6 and A7 over to M1 and M4 on the upper slope and canyon respectively, reveals a larger contrast in received levels, predominantly through the fact that no shots could be detected at M1 from A6, from either a pressure-time series, a spectrogram (Fig. 5.1d), or from headphone audio examination.

In order to make a form of comparison between these two pathways, M1-A6 was processed using the same method of shot extraction (without any shots present) by using the timings identified at M2T extended by the travel time (3.93 s) over the distance between M2T and M1 (5896 m), using a vertically averaged sound speed (1500.3 m s$^{-1}$) calculated from CTD profiles on the slope. Although this in no way guarantees correct timing of analysis to catch each of the 10 shots per airgun location, it does make a best attempt at setting a time framework for analysing shots, had they been present at M1 during the airgun transect at A6, even though resulting levels are effectively background levels as seen in the closely aligned dashed and solid green lines in Fig. 5.8. In 1/3 octave values between 125 – 316 Hz (i.e. peak airgun output), pathways M1-A6 against M4-A7 (Fig. 5.8a) show the largest differences seen in parallel axis comparisons, although examining a broader band, say 100 – 1260 Hz, differences are similar if not larger between M2T-A6 and M3T-A7 seen in Fig. 5.7. Both these differences make the greatest arguments for cross margin channelling of noise, at least within canyon, if not onto the shelf through the canyon pathways.
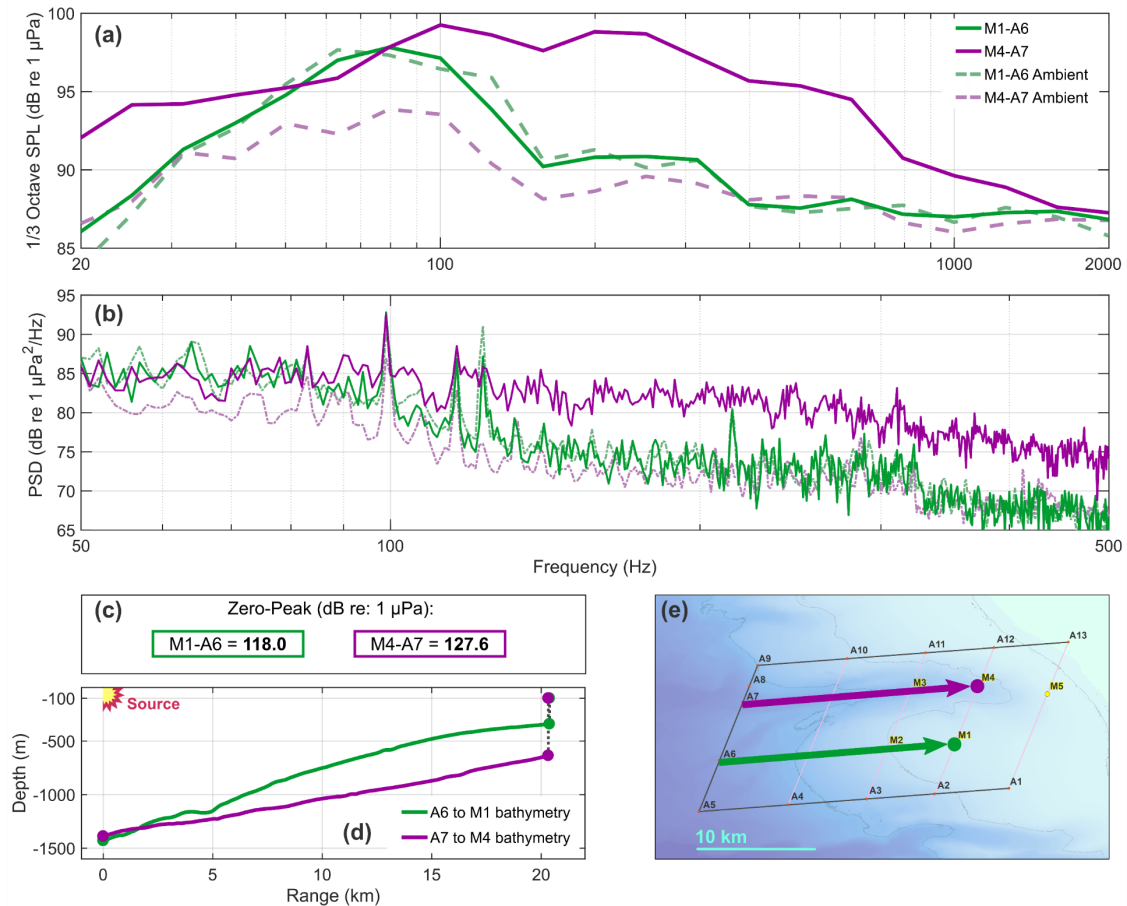
**Fig. 5.8.** Comparison of pathways M1-A6 (green) and M4-A7 (purple) for shot averages (solid lines) and isolated ambient noise within 10 minutes of the event (dashed lines) over: (a) 1/3 Octave levels up to 2000 Hz and (b) Spectral densities zoomed into zone of interest. (c) Displays relative zero-peak values, while (d) plots bathymetry of each pathway, including source and receiver positions. (e) shows a plan view of pathways over a basic map backdrop with scalebar for range.

The other propagation patterns of interest are those transverse to canyon axis. One of the loudest and clearest airgun signals occurs at M4 from the airgun at A12, as the sound travels down the flank of the canyon to the mooring at its axis nearby (5.19 km) (Fig. 5.9 pink line). The corresponding slope-based airgun position at A2 (in a straight line through moorings M1 to M4) holds considerably lower 1/3 octave and spectral values received at M4 (Fig. 5.9a, b, brown line). These results are not consistent with those of mooring M1 along the same straight-line path. Here pathway M1-A12 (light blue line) is considerably higher in values at a considerably longer range (13.28 km), across all frequencies of interest, propagating across the canyon to the slope on the other side where M1 is placed, compared with the much closer ranged (6.98 km) M1-A2 pathway (green line) propagating gently upslope.
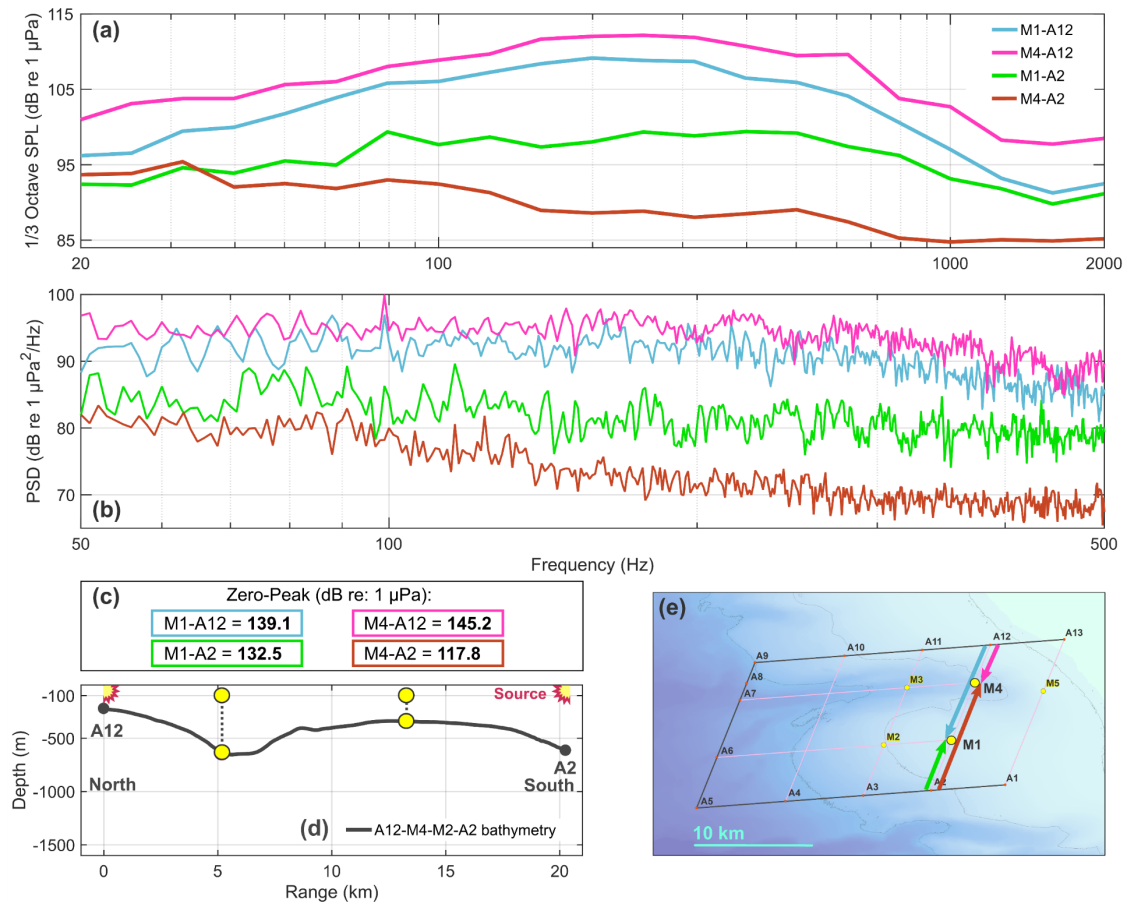
**Fig. 5.9.** Comparison of pathways M1-A6 (green) and M4-A7 (purple) for shot averages (solid lines) and isolated ambient noise within 10 minutes of the event (dashed lines) over: (a) 1/3 Octave levels up to 2000 Hz and (b) Spectral densities zoomed into zone of interest. (c) Displays relative zero-peak values, while (d) plots bathymetry of each pathway, including source and receiver positions. (e) shows a plan view of pathways over a basic map backdrop with scalebar for range.

The advantage of investigating these various pathways of similar range and contrasting topography, is that received values that are not consistent with a simple spreading model, (i.e. linear variation with range (technically log-linear)), are by that fact varied due to other controlling factors. If not only topography, then changes to subseafloor reflective layers that may enhance in-canyon propagation, will also be closely related to the geomorphology of an incised canyon compared to the typical slope. Other factors, for example, water column dynamics, including internal waves and solitons, effects of which are more difficult to constrain quantitatively, will also alter propagation and received levels, but most probably to a much lesser extent, as discussed at a later stage. Weather, such as rain or strong wind/wave action can also influence received values as can frequent marine mammal sounds through a rise in ambient levels, but none of these factors were observed during the PANiC survey which was calm and had only occasional and faint marine mammal calls.

## 5.3. Characterisation of Ambient Noise

Ambient noise at the study site was found to be quite strong and variable, especially in the very low frequencies (< ~15 Hz) and this component was the primary contributor to considerably high ambient levels of total or broadband noise. Because of these high levels, ambient noise was deemed prudent to analyse in full. To achieve this, 30 s long samples were taken every 10 min throughout the full deployment (including manual selection between airgun shots), at each recorder, and $SPL_{rms}$ then calculated from each sample. The low frequency component from some of the moorings showed a diurnal and/or potentially semi-diurnal (i.e. tidal) signals. Examples of this are observed at M1 and M4 across the entire deployment (Fig. 5.10), where $SPL_{rms}$ (maroon line) and the 3 – 20 Hz band (purple) are clearly seen to have two marked dips or undulations, 24 hrs apart with a minor dip 12 hours in between, especially in the M4 data. Although not consistent in amplitude, M1 holds somewhat of a similar pattern. These values are considerably high and periodically variable compared with the broadband values above 20 Hz (sky blue). Minor spikes are seen in broadband values that coincide with times when vessel
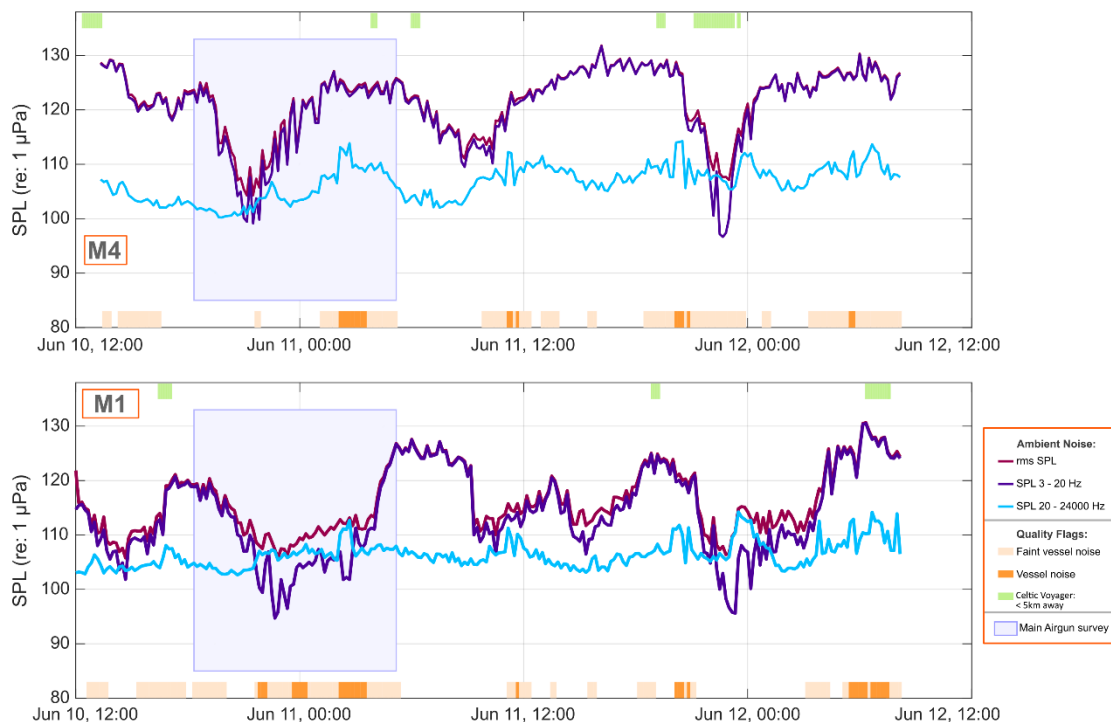


**Fig. 5.10.** $SPL_{rms}$ values from 30 s samples of ambient noise at M4 (above) and M1 (below), throughout deployment. See legend for details.

noise was observed in spectrograms (dark orange time periods along the bottom X-axis of graphs), for example, around June 11th, 00:00, 11:00 and again at 20:00 UTC, however some spikes did not have obvious ship noise in the spectrogram, for example June 12th 00:00. Vessel presence was visualised over long duration spectrograms using Sonic Visualizer (Cannam et al., 2010). These spikes superimposed on a general variation of between 5 – 8 dB in broadband ambient noise above 20 Hz are repeated at all mooring recorders and can be viewed within a full mooring set of ambient figures in Appendix A.2.

The M3 bottom hydrophone had abnormally high variation and more extreme minimum and maximum values of low frequency ambient noise, as seen in Fig. 5.11. This is coupled with the fact that M3B is the deepest recorder of the set, being at 893 m depth, approximately 4.5 m above the seafloor centred on the axis of the canyon, approximately halfway out from canyon head. This depth and position may well expose the hydrophone to focussed tidal current or bottom boundary currents. Although broadband levels above 20 Hz appear similar to other mooring levels, the sharp rise seen around June 10th 23:00 is most likely due to the low frequency oscillations exhibiting content above 20 Hz. A point to note is that during shot analysis (explained in detail in Chapter 3.4), mooring M3B during airgun transect A6 (June 10th 23:18) was the only occasion that zero-peak SPLs could not be calculated successfully using the 10 Hz highpass filter, but rather needed a 20Hz filter through the data, in order to decouple noise from the signal before measuring the signature for peak levels. To complicate analysis further this large variation from minimum to maximum and back again centered around June 11th 00:00, including the extra frequency content of very low frequency noise, coincides with the timing
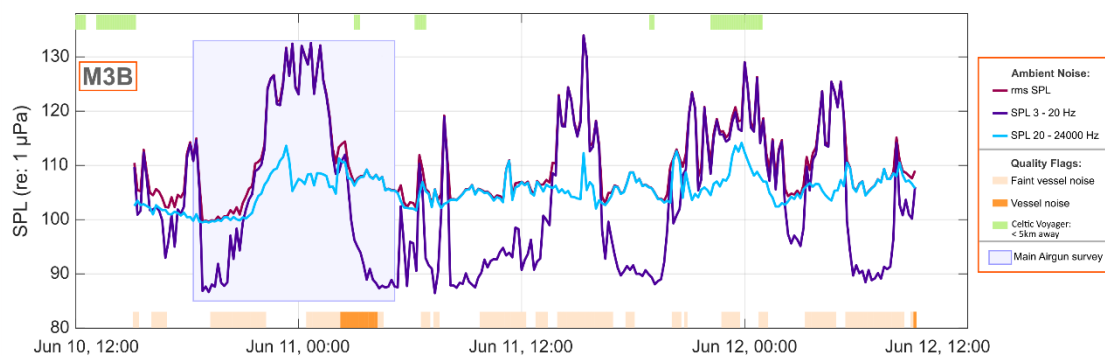


**Fig. 5.11.** SPL values of 30s samples of ambient noise at M3B, throughout deployment. See legend for details.

of the main airgun transect (shaded box in Fig. 5.11). This highlights the need to account for ambient noise, while analysing received levels of pulsed airgun signals. It is apparent, especially from observations at M3B, how the low frequency component drives the overall $SPL_{rms}$ level, when levels are above the broadband (> 20 Hz) ambient level, but do not observably affect the broadband level when fallen below. The very low values seen at somewhat diurnal intervals, are by far the lowest minimum values of low frequency ambient noise and are only mirrored somewhat at M2B (the second deepest hydrophone at 506 m on June 11th between 14:00 and 18:00.

In order to investigate the difference in ambient noise at both low and broadband frequencies between recorders sitting just above the seafloor and those placed at 100 m depth (moorings M2 and M3 only), Fig. 5.12 displays the 10 min interval values for the entire deployment. At both moorings, the deep recordings match the shallower recordings closely, indicating little variance with depth in ambient levels (> 20 Hz). The low frequency component varies less at the shallower recorders, although not by much and with approximate co-variance at M2. At M3, the bottom recorder does not seem to co-vary with the top recorder in low frequency ambient
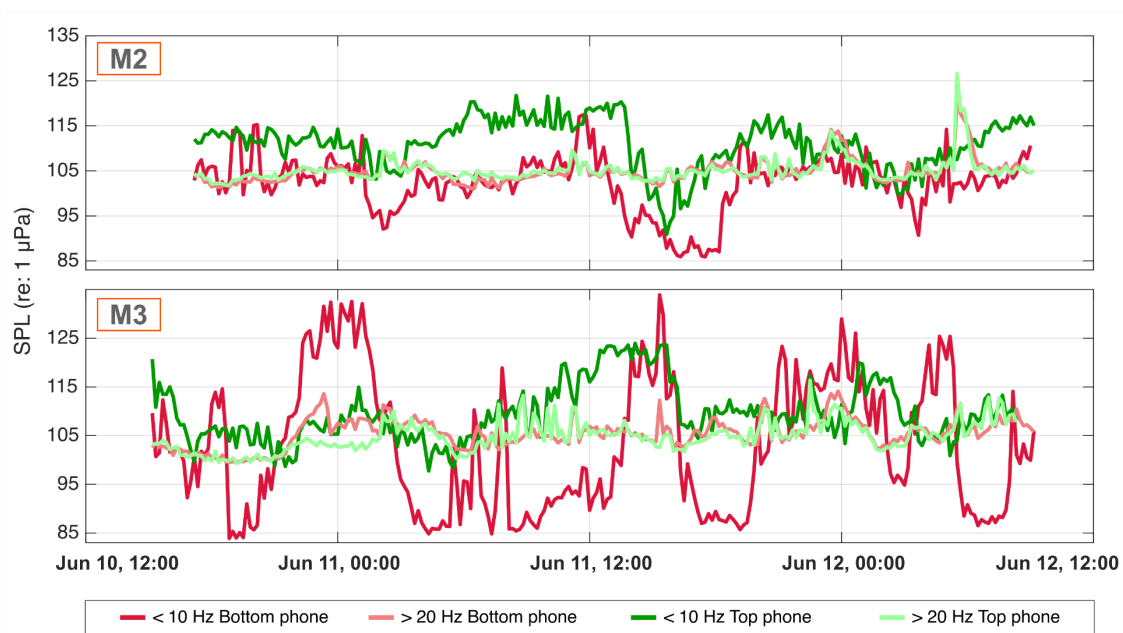


**Fig. 5.12.** SPL values of 30s samples of ambient noise at M2 (top) and M3 (bottom), throughout deployment. Values are included for bottom mounted (reds) and top (greens) mounted hydrophones. Results are split between low frequency (dark colours) and broadband > 20 Hz (light).

noise, suggesting that some other process is at play at the M3B hydrophone, as highlighted already in Fig. 5.11, through its extreme values and variance. Possible causes and effects of these findings are expanded on in Section 5.5.

As a comparison exercise, broadband and 1/3 octave ambient levels have been examined along with another study carried out on ambient noise in the region. The ObSERVE programme published plots of acoustic data from their Autonomous Multichannel Acoustic Recorders (AMARs) (Berrow et al., 2018), and used for comparison here is their Station 6 on the western flank of the Porcupine Bank in June of 2016. Ambient results found here were averaged across 1/3 octave bands combining separately the top and bottom hydrophones at deepest moorings M2 and M3 for the duration of deployment (Fig. 5.13a). ObSERVE's 1/3 octave levels hold elevated frequency content up to 2000 Hz (Fig. 5.13b), similar in shape to PANiC, although at slightly lower levels. Broadband SPL level from the ObSERVE mooring, for the month of June (~103 dB) (Fig. 5.13c), was comparable to ours (106 dB re: 1 µPa) and might have been closer, had ObSERVE's bandwidth been calculated only as far as our top end (24 kHz) rather than theirs (125 kHz).
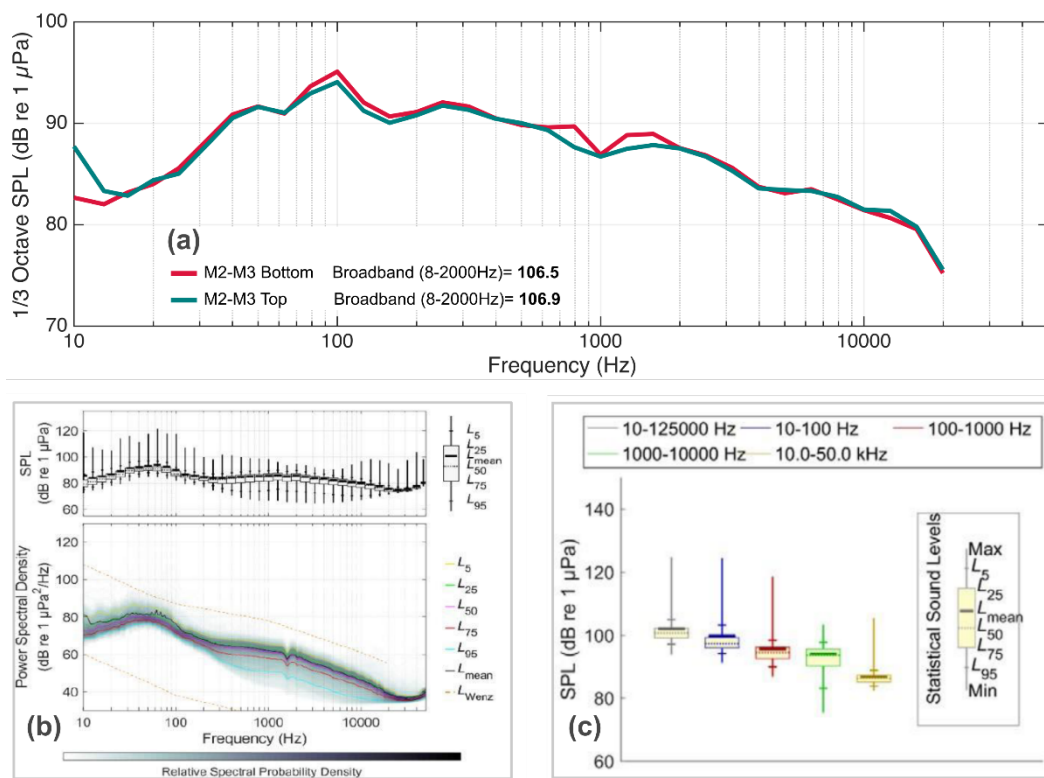


**Fig. 5.13. (a)** 1/3 octave and broadband levels from M2 and M3. **(B)** 1/3 octave and spectral levels and **(c)** banded levels of ambient noise from ObSERVE (Berrow et al., 2018)

## 5.4. Hydrography, Water Column Dynamics and Sound Speed

As highlighted previously, hydrography and associated dynamics are controls on sound propagation in the ocean. This is especially the case along the continental margin, where the changes in topography force a more dynamic water column, for example, as tidal currents transit from deep ocean to shallow shelf seas. This results in internal tidal energy manifesting as perturbations in the pycnocline (density field) that can take the form of IWs or solitary wave packets (solitons) (Sharples et al., 2007; White and Dorschel, 2010; Aslam et al., 2018). In turn, variation in density in the horizontal, especially when more strongly stratified or across a front in the summer/autumn seasons, will affect how sound propagates over the margin regardless of direction of propagation.

### *5.4.1. Hydrography at the study site*

In order to account for hydrographic conditions at the study site the PANiC survey utilised a submarine glider, vessel mounted CTD profiles and MicroCAT recorders for temperature/salinity, where some of the MicroCATs (M2 and M3) had additional pressure sensors included.

CTD transects were conducted along the axis of the canyon and in parallel along the adjacent slope and can be seen in the section plots of Fig. 5.14. Sections for both transects look very similar for all three properties, with the possible exception of temperature contours in the canyon transect appearing to be less horizontally uniform especially below 300 m, which might indicate greater baroclinicity. Also the deep sound speed minimum in the canyon transect may be shoaling eastwards from deep canyon opening to canyon head. Below the surface mixed layer, the watermass expected here would be a modified Eastern North Atlantic Water (ENAW; Harvey, 1982), although a temperature-salinity (TS) plot (Fig. 5.15) shows water only coincident with the 'Harvey Line' (boundaries of ENAW) at midwater depths. Those below show a more saline character at representative temperatures, for example, as densities tend towards $\sigma_t$ = 27.5, likely caused by mixing from northern filaments of Mediterranean Overflow Water (MOW). Shelf exchange of water, dynamic mixing and/or a passing slope current (thought to be weaker and more seasonal than over the Rockall Trough slope), might explain some of the divergence from ENAW. For example, the near-slope dipping isotherms (~400 −
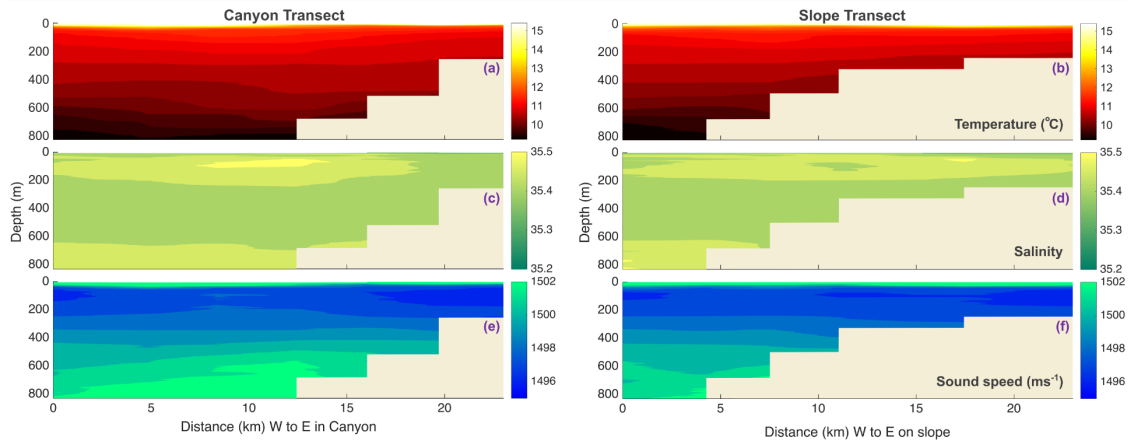
**Fig. 5.14.** Water property sections from CTD transects conducted in canyon (Left panels) and over the slope (right) with a point of view looking north. Transects approximately correspond with A7 to M5 (left) and A6 through M1 (right) as seen in Fig. 5.1. (a) and (b) are temperature (°C), (c) and (d) are salinity, (e) and (f) are sound speed (m s⁻¹).

600 m) could be influenced by the slope current and/or remnants of MOW. What remains clear is there is very little, if any, change in watermass between canyon and slope transects (Fig. 5.15).
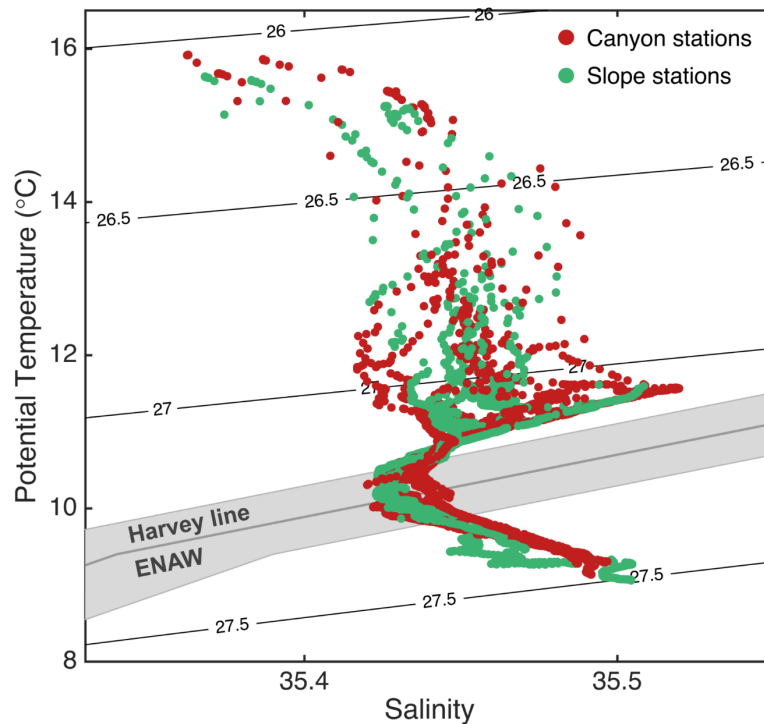


**Fig. 5.15.** Temperature-Salinity plot of all canyon (red) and slope (green) stations, with the 'Harvey line' and boundaries for ENAW indicated in grey (Harvey, 1982).

Repeat CTDs were conducted opportunistically at some stations along the transects to investigate potential changes in water column structure over time and are displayed here in conjunction with glider temperature data (Fig. 5.16). The glider was constricted to fly in an area within the canyon, just west of mooring M3, with this area chosen for having more depth and to avoid the M3 mooring itself, while remaining over the canyon axis. The flight path of the glider, along with the positions of M3, CTD stations and positions of the glider during CTD casts are shown in Fig. 5.16a, with a relative distance scale bar included. CTD profiles for stations CTD05 and CTD14, taken within the glider survey area (yellow and purple respectively) are shown (Fig. 5.16b) with various symbols at temperatures of interest every 0.25°C. At around 600 m there is a vertical displacement of 80 – 90 m at a temperature of 10.25°C (diamond symbols), between these casts taken ~14 hrs apart. Profiles for CTD04 and CTD15, located directly adjacent to mooring M3 (blue and green respectively) again display greatest vertical displacement at approximately 600 m (diamond symbols in Fig. 5.16c). All four profiles are displayed together at full depth (Fig. 5.16d), along with a modelled (WOA18; Locarnini et al., 2018) winter (month of Feb) profile taken close by (4 km SW of CTD05). A strong shallow seasonal thermocline can be seen in our CTD profiles ~20 – 50 m between 11.5 and 16°C, although varying in depth between stations, before a slower steady decrease in temperatures down to bottom depth with little or no indication of a permanent thermocline. As expected, the winter profile indicates a fully mixed water column. Glider temperature data, providing an ongoing stream of data for the area and covering all depths, is useful to identify the presence of internal waves or dynamic instability of isopycnals (isotherms being equivalent here). The contoured section of glider data does not identify any vertical displacement of temperature (Fig. 5.16e), however, by plotting actual glider values of temperature at selected intervals (pink contour lines) a diurnal fluctuation of temperature becomes apparent. On top of this signal there appears to be a positive phase shift from the larger vertical displacements seen at 10.25°C around 600 m to gentler displacements seen on the shallowest isotherm at 11.25°C. Although this positive upwards phase shift is somewhat undefined, its presence could signal a downward propagating beam of internal tidal energy to deeper waters from the shelf break (Pingree and New, 1989). Overlayed synchronously on the contoured glider temperature section is the CTD values of indicator temperatures, which are generally in agreement with the glider data. An anomalous displacement appears at 10.5°C between CTDs 04 and 05 (blue and yellow star symbols respectively) but must be taken in the context of these
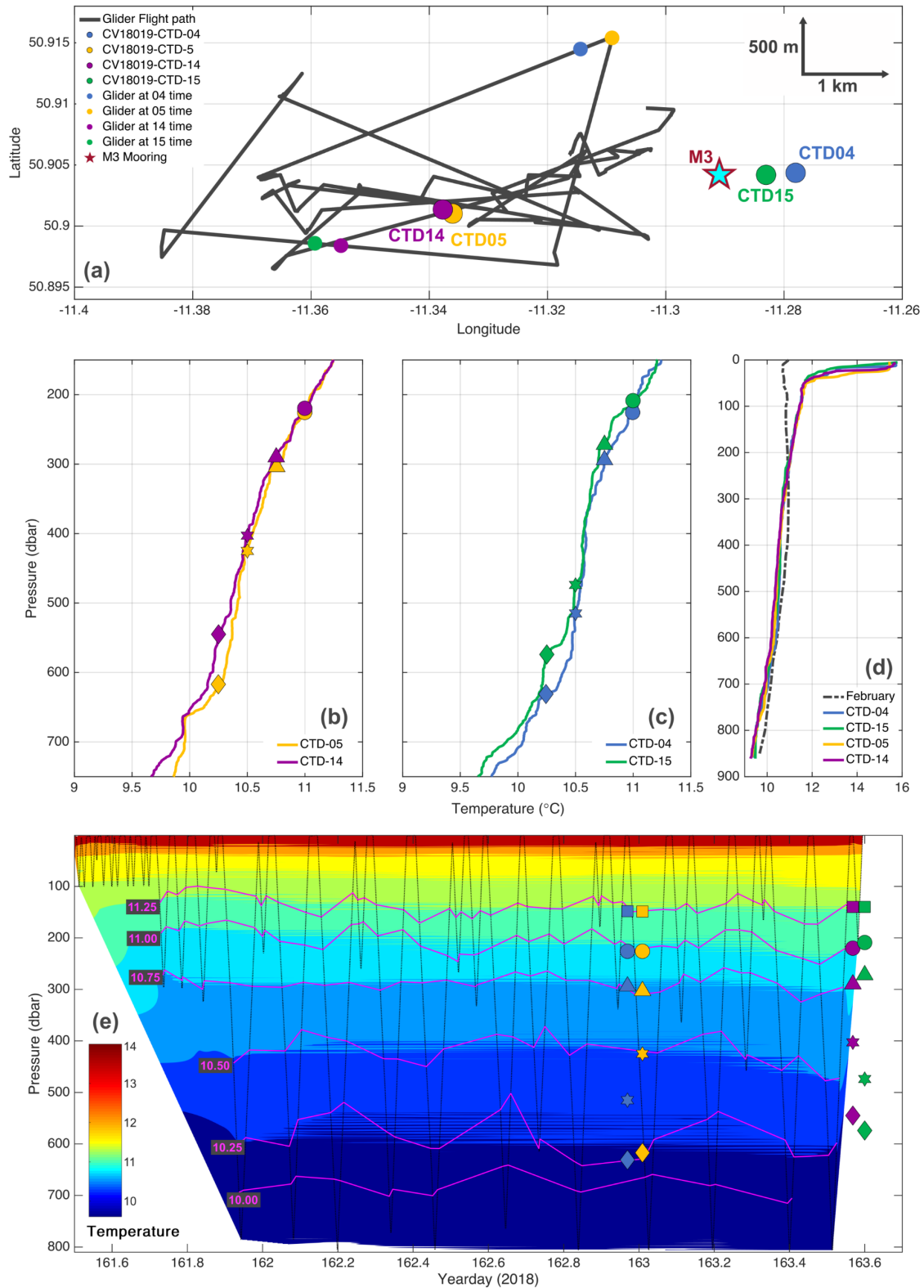
**Fig. 5.16. (a)** Glider flight path; **(b),(c),(d)** CTD profiles within the glider survey area including a winter modelled (WOA18) profile; **(e)** Glider temperature section with contours of glider temperature data (pink lines) and CTD profiles (coloured symbols as per (b) and (c)). Glider dives are shown as dotted black lines.

CTDs having been sampled at different locations (4097 m apart) and times (57 min apart). Superimposing CTD values on a glider section also highlights the limits in resolution of the glider data, for example, during the period between ~162.85 and 163 yeardays (~3.5 hrs) the glider did not survey at any depths below 330 m.

### 5.4.2. Water column dynamics

From the assessment of MicroCAT data, a feature of interest was the high frequency alterations of temperature measured by the instruments, seen especially in M2 around 09:00 on June 11th, and again from June 11th, 23:00 onwards (just over one semi-diurnal tidal period later) (Fig. 5.17). Rapid changes in temperature here (~0.1 – 0.3°C) translate to vertical displacement of the thermocline. For the M3 mooring, the average displacement of 0.1°C is 32.3 m at 11.55°C at an average depth of 79.5 m, calculated from the downcasts of the four CTDs (CTD04,05,14,15) taken within the region of M3 and the glider area. For the M2 mooring (averaged over CTD10 and CTD11), displacement was only 8 m at 11.4°C at an average depth of 81 m. These rapid temperature displacements at M2 and M3 are an indication of the possible presence of internal waves and thus provided the motivation to investigate further.

An event which displayed considerable high frequency temperature fluctuation was focussed on between 10:00 and 12:00 on the 11th of June. This was best seen at the M2 MicroCAT positioned at ~29 m depth and from the drifting buoy MicroCAT (D1 on Fig. 5.1) at 25 m depth (Fig. 5.8). The rapid changes in temperature seen
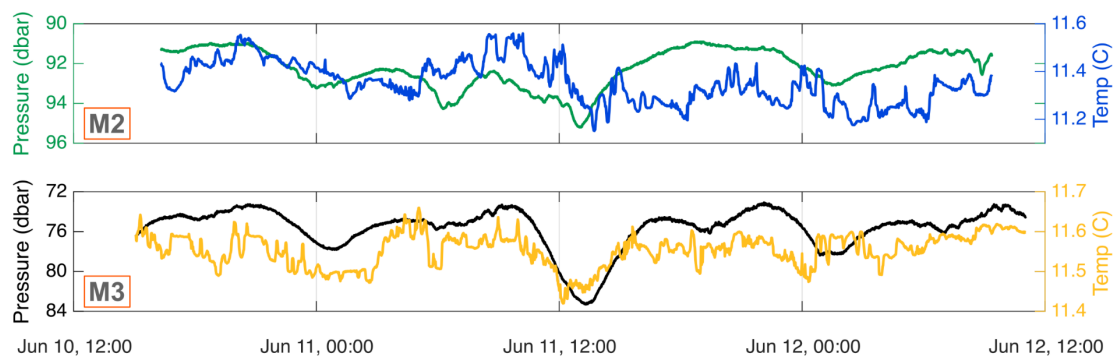


**Fig. 5.17.** Microcat time-series. LHS y-axis is pressure and RHS y-axis is temperature for M2 (top) and M3 (bottom) sensors. Both sensors were placed 102 m deep on the mooring lines but due to rope stretch they sat higher up in the water column.

here are most likely caused by a solitary wave packet (a soliton) propagating along the seasonal pycnocline and displacing a stratified water column as it passes the sensors. Using the times at the crests (or troughs for D1) of these temperature oscillations (arrows with time labels; Fig. 5.18), an approximate wave period could be estimated at 33 minutes for M2 and 24 minutes for the drifter D1, by averaging the duration between each peak for that event. It must be noted that the drifter data not only differed in average period from M2 but was also considerably less defined and open to conjecture as to where the peaks were. Nonetheless, the drifter data does display notable periodic temperature variation consistent with that of solitons found in the region (e.g., Figs. 12 and 13 from Pingree and Mardell, 1981). The fact that both sensors (9 km apart) experienced these oscillations at the same time eludes to the possibility that the soliton was initiated somewhere at the shelf edge at an equivalent distance from both sensors, assuming it is the same soliton. An estimate of vertical displacement ($D_L$) was made (Fig. 5.18b), using a nearby CTD profile (CTD11 at M2 mooring) by calculating the vertical temperature gradient centered around the mean depth of each Microcat as follows:

$$D_L = \left( \frac{\Delta T_{Mc}}{\frac{dT_{CTD}}{dz}} \right) \quad (m) \tag{E5.1}$$

where $\Delta T_{Mc} = T_{Mc} - \overline{T}_{Mc}$ is the MicroCAT temperature divergence from its mean (over all values, sampled at 60 s intervals), $dT_{CDT}$ is the difference in CTD profile temperature between the upper and lower values across a depth range (dz) here chosen as 10 m. Displacements were as expected for a passing soliton, where previous studies have shown peak displacements of > 60 m (Pingree et al., 1984), or crest to trough amplitudes of > 50 m (Sharples et al., 2007) at spring tides. Averaging over each displacement (coinciding with red and black arrows in Fig. 5.18), mean displacements of 43.5 and 20.9 m along with maximum displacements of 39 and 55 m were estimated for M2 and D1 respectively. Soliton wavelengths tend towards 1 km but can be as much as 2 km, can have phase speeds between 30 and 60 cm s$^{-1}$ (Pingree and Mardell, 1981; Sharples et al., 2007) and are not confined to generation from across slope barotropic tidal motions but can also form from along slope processes, especially over rugged topography (Holt and Thorpe, 1997).
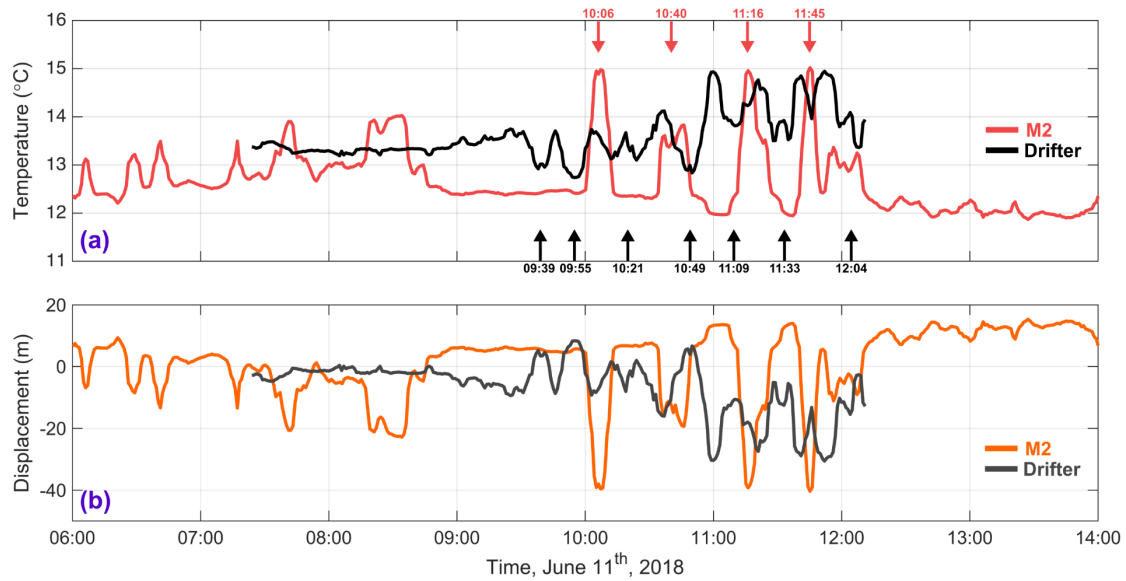
**Fig. 5.18.** Probable soliton event within MicroCAT data. (a) Temperature from the M2 MicroCAT at ~29 m depth (red) and from the drifter at 25 m depth (black). Rapid changes in temperature due to vertical displacement of a stratified water column are marked at peak with arrows, each with a time label included. (b) Vertical displacements of the water column, associated with a potential solitary wave packet, at each MicroCAT depth; M2 mooring in orange and drifter in grey.

To further investigate baroclinic structure and the potential presence of an internal tide at the site, normal mode analysis of CTD density profiles was undertaken (Fig. 5.19). Buoyancy frequency ($N^2$) (Fig. 5.19b) is used at discrete pressures to calculate modal structure and phase speeds (following Klinck, 1999). Phase speeds (mode 1) of the internal tide were calculated to be 55.8 and 59.4 cm s$^{-1}$ for CTD04 and CTD05 further west respectively, both generally in line with figures found for this region in the literature (e.g., Pingree et al., 1984). Pingree at al., 1984 also calculated internal tide wavelengths of ~30 km and found higher frequency oscillations (Solitary wave packets) during maximum outward barotropic tidal flows at spring tide, for an area along the southern slope of the Celtic Sea Shelf. Each of the first three vertical modes (Fig. 5.19c) have a peak between 500 and 740 m, approximately coinciding with the depths of greatest displacement (~600 m) seen in the glider temperature data (pink lines in Fig. 5.16e). Also at these depths, density increases at a faster rate and $N^2$ is slightly more variable then say from 100 – 600 m, which might indicate the starting depths of a permanent thermocline. Where horizontal velocity structure changes direction (i.e. crosses zero line), or where horizontal modes are superposed, can indicate depths of greatest internal wave shear or turbulence (Münnich et al., 1992). For example, between depths of 250 –
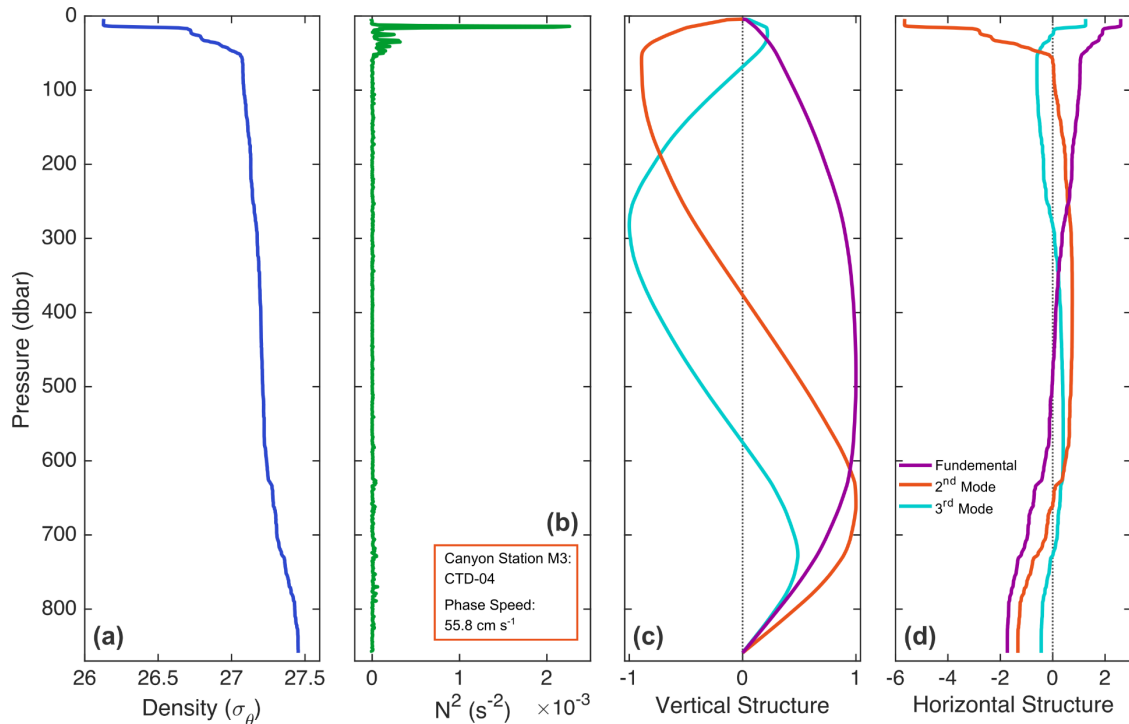
**Fig. 5.19.** CTD station 04. (a) Density; (b) Buoyancy frequency and info box with phase speed; (c) First three modes of vertical velocity structure; (d) First three modes of horizontal velocity structure.

400 m (Fig. 5.19d), where the first horizontal mode crosses the other modes and zero line, are at depths approximately similar to the upper slope and shelf break where internal waves are generated from. Although these results are not conclusive, Fig. 5.19 in combination with Figs. 5.17, 5.18 allude to an internal tide and the possibility that soliton generation may occur periodically around the shelf break within the survey site (although solitons will only manifest in the shallower layers associated with the seasonal pycnocline/thermocline). The northeast North Atlantic is already known to experience internal tidal energy and occurrence of IWs and solitons (e.g., Pingree and Mardell, 1981; Xing and Davies, 1996; White and Dorschel, 2010). One such study using gliders to measure IW energy dissipation, at the very location within the canyon surveyed here, found IW wavelengths of $\lambda =$ 36 km (mode 1) (R. Hall 2021, personal communication, 12th April). Solitons and IWs are discussed in relation to acoustic transmission loss in a later section here.

*5.4.3. Local sound speed profiles*

Sound speed profiles can be derived using data on the physical properties of the water column (temperature, salinity, pressure). In the case of vessel mounted CTDs, this variable was an intrinsic output of the processing software, whereas with glider data a basic routine was written to calculate sound speed using the UNESCO 1983 equations (Fofonoff and Millard Jr, 1983). The sound speed is minimum (~1497.5 ms$^{-1}$) at shallow depths (~50 m; approximately coinciding with the seasonal thermocline) and increases gradually down to bottom depth (Fig. 5.20a), whereas a sound speed derived from the winter modelled profile (WOA18; grey dashed line) has a considerably lower sound speed minimum (1493 ms$^{-1}$) very near the sea surface. The interpolated, contoured section of sound speed from glider data may suggest a slight shoaling of sound speed contours throughout the duration of glider deployment, although care must be taken interpreting these interpolated values, especially towards each end or away from dive lines (thin white dashed lines) (Fig. 5.20b).

The in-situ sound speed profile will dictate where the local sound channels sit and in turn moderate how internal refraction of sound rays occurs within the water column and at the boundaries, for example with a shallow sound speed minimum, sound rays will experience more surface reflections than with a considerably deeper minimum and associated deep ocean sound duct.
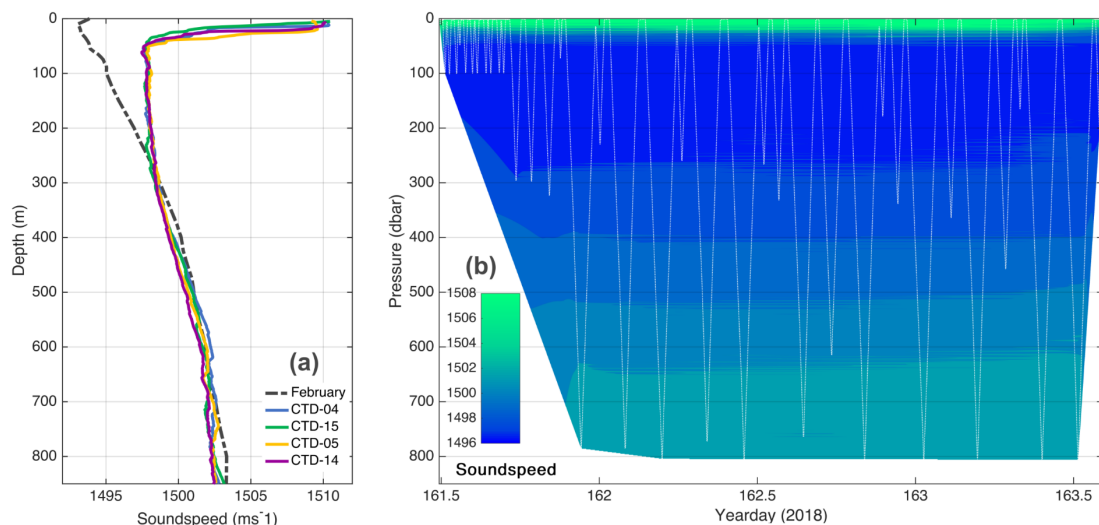


**Fig. 5.20.** (a) Sound speed profiles for glider area CTDs and modelled winter profile (dashed grey); (b) Sound speed section derived from glider data and including glider dives (thin white dashed lines).

## 5.5. Correlations Between Airgun/Ambient Noise, Range, Depth and Hydrography

While evaluating the MicroCAT data, it was apparent that there was semi-diurnal and potentially diurnal variation in both temperature and pressure variables at each mooring containing a pressure sensor (M2 and M3, Fig. 5.17). The change in pressure and in turn the lower frequency change in temperature at both moorings most likely results from the instruments being depressed to, and released from, deeper depths due to passing water currents dragging the mooring line laterally at the top in relation to its anchor and thus vertically in the water column, which can be seen best in the pressure series of M3. Theoretically, if the instrument were stationary in space, pressure would vary with tidal change in depth, estimated in this region at these water depths to be 1 – 1.2 m (Lynch et al., 2004). In order to assess the (somewhat) diurnal signals interpreted from the low frequency ambient noise, a linear regression study was undertaken using each variable of pressure and temperature at M2 and M3 as independent variables (separately) and using each of the seven moorings' low frequency (< 10 Hz) ambient noise levels calculated every ten minutes throughout deployment. From each dependent-independent pair, a linear regression analysis was conducted, including a positive and negative time lag each way of up to five hours in 10 min increments resulting in 61 (5 hrs x 6 increments x 2 ways + 1 centre/zero-lag) separate regressions per pair. To display these results, the highest related pairs for each independent variable have been plotted, with each column of tiles representing temperature and pressure respectively and top row being M2 and bottom row M3 (Fig. 5.21); please note change in x-axis limits for both temperature and pressure. Of interest here is that each of the four strongest correlations involved ambient data from the alternate mooring to the MicroCAT (i.e. M2 MicroCAT vs M3 ambient noise and vice versa), with the time lags of M3 being consistent but not those of M2. Also of note here is the inclusion of M3B correlating strongly with the M2 MicroCAT, considering its more extreme and less apparent diurnal relationship seen in Fig. 5.11. Although each of these variable pairs have strongly proven relationships (all p-values << 0.05), their actual correlations are not strong (e.g., maximum $R^2$ value of 0.54 at M3 MicroCAT vs M2B ambient) and regardless of strength must not be interpreted as cause and effect (i.e. cannot say that the reason for the changing pressure series is also what is causing the variation in ambient noise). However, the most likely cause is tidal current intensifying diurnally and/or semi-diurnally, causing noise

directly to the hydrophone receiver or through mooring self-noise being picked up by the phone.
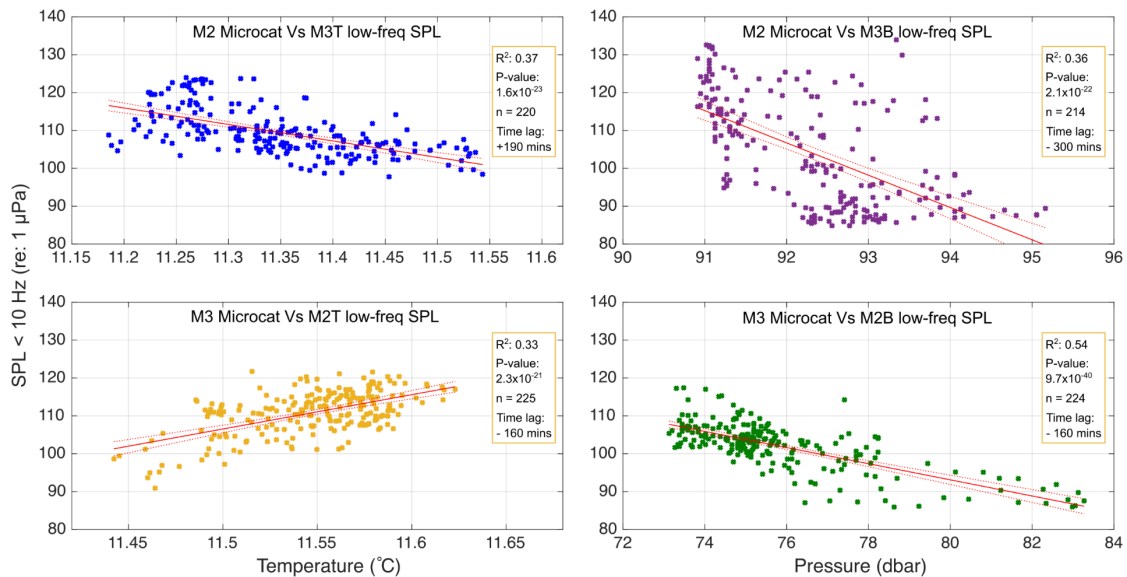


**Fig. 5.21.** Strongest regression plots for each independent variable. LHS column is temperature and RHS is pressure. Top row is M2 while bottom row is M3. Info boxes include time lag where a positive lag is ambient noise shifted ahead of MicroCATs.

Multiple linear regression was used to investigate relationships between single value received level metrics as dependent variables, including rise times, and spatial positioning of sources and receivers (range, water depth at gun and water depth difference, between source and receiver) as independent variables. $R^2$ values for variables (with outliers removed) show the strongest single pair relationships to be from water depth at gun, where the dependent variables of significance are zero-peak, 90% SEL and banded SELs, especially broad and 10 – 100 Hz bands (Table 5.2). These patterns are accentuated when running multiple regressions, especially the grouping of all three independent variables where $R^2$ values are regularly above 0.8. Of note is that neither of the rise time variables correlate strongly at all, indicating other controls on their variation. See Appendix A.2, Table A4 for $R^2$ results without any outliers removed, which mirror the table below but with weaker values throughout.

**Table 5.2.** Coefficients of Determination ($R^2$) from linear regression analysis of selected independent and dependent variables, using data with outliers removed

| Response Variables | Units | Simple Linear Regression (1) Range $R^2$ | Simple Linear Regression (2) Depth at gun $R^2$ | Simple Linear Regression (3) Δ Depth $R^2$ | Multiple Linear Regression (1 + 2) $R^2$ | Multiple Linear Regression (1 + 3) $R^2$ | Multiple Linear Regression (2 + 3) $R^2$ | Multiple Linear Regression (1 + 2 + 3) $R^2$ |
|---|---|---|---|---|---|---|---|---|
| Zero-peak | dB (re: 1 µPa) | 0.19 (4) | 0.57 (3) | 0.47 (6) | 0.58 (5) | 0.49 (4) | 0.58 (2) | 0.59 (5) |
| Zero-peak Rise time | s | 0.01 (3) | 0.05 (3) | 0.02 (3) | 0.11 (3) | 0.06 (3) | 0.11 (4) | 0.18 (4) |
| 90% SEL (manual) | dB (re: 1 µPa$^{2S}$) | 0.06 (4) | 0.82 (4) | 0.63 (9) | 0.85 (4) | 0.65 (5) | 0.87 (4) | 0.90 (4) |
| 90% SEL (1 s) | dB (re: 1 µPa$^{2S}$) | 0.07 (3) | 0.80 (4) | 0.61 (9) | 0.83 (4) | 0.64 (4) | 0.85 (4) | 0.87 (4) |
| 90% SEL (2 s) | dB (re: 1 µPa$^{2S}$) | 0.05 (3) | 0.79 (4) | 0.60 (8) | 0.83 (5) | 0.63 (4) | 0.85 (4) | 0.89 (5) |
| 90% SEL Rise time | s | 0.11 (5) | 0.17 (3) | 0.10 (2) | 0.52 (5) | 0.39 (5) | 0.25 (3) | 0.59 (5) |
| Broadband SEL | dB (re: 1 µPa$^{2S}$) | 0.004 (1) | 0.60 (6) | 0.36 (7) | 0.71 (4) | 0.43 (5) | 0.79 (7) | 0.89 (6) |
| SEL 10 -100 Hz | dB (re: 1 µPa$^{2S}$) | 0.03 (1) | 0.75 (3) | 0.49 (7) | 0.81 (3) | 0.54 (5) | 0.89 (6) | 0.95 (4) |
| SEL 100 -1k Hz | dB (re: 1 µPa$^{2S}$) | 0.001 (1) | 0.55 (6) | 0.33 (7) | 0.67 (5) | 0.41 (2) | 0.72 (6) | 0.83 (5) |
| SEL 1k -10k Hz | dB (re: 1 µPa$^{2S}$) | 0.03 (3) | 0.06 (4) | 0.002 (3) | 0.17 (5) | 0.05 (4) | 0.44 (4) | 0.54 (4) |

Notes:
1) In brackets are number of outliers (identified where residual intervals do not contain zero), such that the amount of points per regression is n = 73 - (number of outliers)
2) Yellow cells are where P-values are > 0.05, indicating the null hypothesis or no significant relationship present
3) See **Table A4** in Appendix I for $R^2$ values which include outliers

## 5.6. Synthesis of Results

Propagation of sound in the water column is primarily controlled by range from source to receiver through absorption, scattering, spreading and reflection of sound energy waves and is frequency dependent, where higher frequencies will be absorbed at shorter ranges than lower frequencies. Scattering occurs from particles in the water column, from the ocean-atmosphere interface and from the seafloor interface, each of which are related to their local environments (e.g., suspended material, weather and seafloor roughness). Simple spreading laws state that sound energy will spread spherically up to a range of approximately its water depth at source, where it will transition to cylindrical spreading (details in Chapter 3.4.3). On initial appraisal of received levels of sound metrics during airgun operation, it was clear that propagation did not hold a directly linear or simple spreading relationship with range from source to receiver, and that variation appeared to also depend on topography (Fig. 5.3). Interrogation of the map-scatter plots (Figs. 5.4 & 5.5) and further through direct comparisons (Figs. 5.6 – 5.9), show a defined relationship, with topography as a direct control on propagation both along and across canyon axis. However, it remains unquantified here as to what degree this relationship is due to direct changes in topography or due to changes in sub-seafloor geological layers, which will also be more heterogeneous around a submarine canyon compared to a typical slope. The magnitude of variability due to combined topographic and unknown sub-seabed changes was up to 21 dB re: 1 µPa zero-

peak levels and 12 dB re: 1 µPa$^2$s for broadband SEL as seen when comparing pathways M1-A12 and M4-A2. Nonetheless, mechanism of control will be location/environment specific. Also, the difference in slope angle will control the amount of bottom/surface bounces per given range, with the canyon thalweg rising more gently under deeper water in a more concave morphology (excepting the sharp rise at canyon head) compared to a typical slope which will rise more steadily (or convex like), causing more reflections and hence greater propagation loss. Reflection loss due to slope is considered only part of the situation here. Modelled results from Chapter 4 produced a 2.2 dB change in TL over a 1.21° slope, whereas here M2B-A6/M3B-A7 and M1-A6/M4-A7 showed differences of 5.9 and 3.8 dB over slope differences of 1.62° and 0.91° respectively, thus indicating further effects than simply in-canyon slope. What the results do clearly highlight is that in the region of a submarine canyon, anthropogenic noise propagation is stronger both up canyon and across canyon. In addition to these results, noise has been shown in Chapter 6 to propagate more strongly down canyon from a shelf edge bottom trawling source. The implications are that this canyon, and in turn similar canyons along the continental margin, are both focussing anthropogenic noise within them and providing a conduit for noise pollution to propagate both further onto the shallower continental shelf and further into the deep sound channel compared to gentler continental slopes. These rises in metrics, such as zero-peak or SELs, in and around submarine canyons will directly affect any marine fauna susceptible to adverse noise levels (Slabbekoorn *et al.*, 2010; Merchant *et al.*, 2015; Merchant *et al.*, 2020), not least resident or transient marine mammals known to frequent these canyon settings (Barlow and Gisiner, 2006; Cox et al., 2006; McCauley, 2015; Berrow et al., 2018).

While analysing the various metrics used to measure controlled airgun shots, many challenges were encountered, not least the prevalence of a loud low frequency ambient signature. For analysing impulsive underwater noise, for example airguns, a favoured metric is 90 % energy (blue circles in map-scatter plots (Figs 5.4, 5.5b). To measure the energy (or occurrence of 5 to 95% of it, as customary) purely from an airgun shot, the background noise level must be subtracted from the integrated squared pressure-time series (i.e. in the time domain). With many of the received data here, this was not possible because the unfiltered background noise was too strong (i.e. SNR was too weak). Therefore, all data required pre-filtering and in preparation for this, a testing regime was implemented to identify the best and least

intrusive filter (~20 Hz highpass, described in Chapter 3.3.2.). Likewise, an unfiltered pressure-time series deviated greatly from the zero line at very low frequencies, preventing accurate measurement of zero-peak levels, where a 10 Hz highpass filter had to be incorporated (with the exception of pathway M3B-A6, which needed a ~20 Hz filter). While investigating banded SELs, analysis was designed to include different durations of shot signal being a) time from 5 – 95% energy transmission; b) 1 second duration; c) 2 seconds. Although the choice to mostly report banded SELs using a 1s duration could be considered as arbitrary, it was felt it best represented the metric being reported. For example, using 5 – 95% energy start/finish times produces an inconsistent integration time per pathway and using 2 second values differed very little from 1 second values. This points to the need for a standardised methodology for impulsive noise analysis and highlights the requirement to report all methodology, including integration times with every piece of analysis. As part of this analysis, rise times (time taken to go from zero to peak or from 5 to 95% energy) were investigated to ascertain if they added understanding to how airgun noise propagates. The rise times for zero-peak and 90% energy levels are displayed as horizontal bars inside the red and blue map scatter-plot circles respectively (Figs. 5.4, 5.5), but did not yield any obvious relationships (Table 5.2) and raise the question of why not? Either rise times are completely unrelated to range from source to receiver, water depth at source and depth difference between source and receiver and are varied due to other propagation controls, or else there is a more complex, non-linear and less obvious relationship at play (see Appendix A.3. for regression plots of all these dependent and independent pairs).

Ambient noise will always be a consideration when attempting to assess the impacts of anthropogenic noise in the ocean, especially when it is loud or variable at frequencies of interest. In this study, low frequency ambient noise prevented the pure analysis of SELs and required a filtering regime in order to adequately conclude analysis. The variability found in ambient noise, in itself, provides an interesting study. The fact that the most variable and most extreme ambient noise was measured at the deepest hydrophone of the entire survey and directly within the canyon axis, points to the possibility of enhanced processes within the deep canyon causing the noise. The source of the localised low frequency noise is most probably water current or movement of the mooring caused by tidal changes. Through regression analysis it was shown that the strongest relationships were lagged. For example, the regression pairs at M3 MicroCAT, including the strongest

$R^2$ value (M3-pressure vs M2B-ambient noise), both had lag times of 2 hrs 40 mins, suggesting a north or north-easterly migration of peak currents. Although it must be noted, M2 hydrographic variables proved less consistent when regressed with M3 ambient noise, indicating a more complex situation. The extreme values at mooring recorder M3B compared to the other recorders indicate a tidal current which may be channelled along the canyon axis. Also of note were spectral peaks of ambient noise at approximately 110, 120 and 210 Hz, common to a number of pathways and recorders (Figs. 5.6 and 5.8). It is unclear where these peaks originate from but they may be harmonics of lower frequency water currents or mooring self-noise. Understanding and monitoring ambient noise is important, as anthropogenic noise in the ocean increases and general ambient noise increases due to it (e.g., Andrew et al., 2002; Hildebrand, 2009; Erbe et al., 2019). Although this survey only provides a snapshot of background noise conditions, it can provide a baseline for further measuring/monitoring, especially at these depths along the continental margin in areas of ecological concern. Increased levels of ambient noise caused by anthropogenic input can mask the ability of marine mammals to communicate (Erbe et al., 2016), especially in the lower frequency bands and hearing groups, where the masking does not need to occur locally but adds to the 'din' at greater ranges from source in deep waters (Ellison et al., 2012).

The northeast North Atlantic continental margin and associated incised canyons have been detailed as dynamic regions for internal tidal energy, including internal waves and solitons (e.g., Holt and Thorpe, 1997; Aslam et al., 2017). Work here (Section 5.3) confirms the presence of a dynamically stratified water column (i.e. IWs). Other ocean processes are also occurring, for example, the presence and variable strength of the European Continental Current, a branch of which is believed to (at least) intermittently pass the eastern margin of the Porcupine Basin (and our study area) (Mohn et al., 2002; White, 2006). These bring warmer, more saline water, which will in turn alter the density field in which any anthropogenic noise will propagate through, as do any ocean fronts in the area, such as a shelf edge front (Miller, 2009). Changes to hydrographic conditions at the study site (as with the entire continental margin at these latitudes), vary across temporal scales ranging from semi-diurnal tides to seasonal stratification changes due to insolation or input of wind forcing, and include the less predictable character of the continental slope current. In turn, these factors will affect when anthropogenic noise input is at its most damaging. Stronger propagation may occur during winter's fully mixed water

column similar to the 5 dB increase in cumulative SELs for two grey seals seen in the nearby Celtic Sea (albeit in shallower shelf waters) (Chen et al. 2017) or an increase of 16 dB transmission loss in summer modelled around the same area (Shapiro et al., 2014). Internal waves, most prevalent during spring tides in stratified waters along the margin, can have focussing and defocussing effects on noise propagation (e.g., Zhou et al., 1991; Luo et al., 2008, both in shelf depth waters). Mode coupling techniques were used to show that solitary wave packets can introduce a 20 dB modelled signal gain (Duda, 2004), although strongly dependent on depth of receiver, where greatest gain was at 100 m deep, unlike source depths on the PANiC survey (1 m depth). Near surface sources (similar to PANiC), which would usually attenuate more quickly through generation of higher modes can have energy "thrown" into lower (and further propagating) modes due to internal wave scattering (Lynch et al., 2006). Depth, sound speed, and associated sound ducting will differ over the deeper waters and more extreme topography of the continental margin compared with the studies cited above. However, IW action will have a focussing and/or defocussing effect on noise propagation at the study site, which, if compounded with other topographic controls in canyon, may increase the potential for damaging or disturbing levels of noise picked up by nearby marine mammals. Another compounding anthropogenic factor is long-term ocean warming and acidification due to human input of $CO_2$ to the atmosphere, in that a warmer, more acidic ocean can allow for stronger propagation of noise (Hester et al., 2008).

The continental margins of the northeast North Atlantic, including the eastern flank of the Porcupine Basin, is known to be a sensitive area of higher biodiversity and abundance relative to adjacent settings. Submarine canyons host a myriad of lifeforms usually associated with cold water corals or sponge fields. In turn, higher trophic level fauna are attracted there, including large marine mammals, which are known to visit these areas (O'Cadhla et al., 2004; McCauley, 2015; Berrow et al., 2018). Beaked whales are thought to especially favour canyon settings but are also thought to be particularly sensitive to impulsive anthropogenic noise (Barlow and Gisiner, 2006; Cox et al., 2006). Other sources of anthropogenic noise are also present, and although there are no major shipping lanes along this part of the margin, ships passage and more importantly bottom trawling (Chapter 6) are pervasive sources of noise that would augment any offshore seismic exploration, especially around sensitive canyon settings, which we have shown here to focus and channel that noise. It is hoped that evidence-based studies, as contained in this

chapter, can aid mitigation strategies and regulation of seismic surveying that could target specific sensitive areas, such as submarine canyons. This would benefit both the environment and industry through geographical targeting rather than blanket bans along the continental margin as discussed in further detail in the discussion chapter.

# Chapter 6:

# Bottom Trawling Noise: Are Fishing Vessels Polluting to Deeper Acoustic Habitats?

Eoghan Daly[1,2], Martin White[1,2]

[1]Earth and Ocean Sciences, Ryan Institute, National University of Ireland, Galway
[2]Irish Centre for Research in Applied Geosciences (iCRAG)

**Contributions:** E. Daly: Conceptualisation, Data curation, Formal analysis, Investigation, Methodology, Visualisation, Writing (original draft). M. White: Conceptualisation, Methodology, Project administration, Mentorship, Reviewing and editing.

## Abstract

The impact of bottom trawling noise was quantified on two surrounding marine acoustic habitats using fixed mooring acoustic recorders. Noise during trawling activity is shown to be considerably louder than ambient noise and a nearby underway research vessel. Estimated source levels were above cetacean damage thresholds. Measurements at a submarine canyon indicated potential noise focussing, inferring a role for such features to enhance down slope noise propagation at continental margin sites. Modelled sound propagates more efficiently when sourced from trawling gear dragging along the seabed relative to the vessel as a surface source. Results are contextualised with respect to marine mammal harm, to other anthropogenic ocean noise sources, topography and seasons. Noise energy emitted by bottom trawling activity is a source of pollution that requires further consideration, in line with other pervasive trawling pressures on marine species and seabed habitats, especially in areas of heightened ecological susceptibility.

## 6.1. Introduction

Anthropogenic noise in the ocean is a pervasive and ever-increasing source of pollution encroaching on the natural marine environment. Propagation of anthropogenic noise, as with all sound in the ocean, is controlled by physical factors, such as absorption, and reflection or refraction at the sea surface, in the water column and from sub-seafloor geological layers (Urick, 1983; Medwin and Clay, 1997; Jensen et al., 2011). Noise propagation is also a function of depth and topography, and is frequency dependent, where sound at low frequencies have been detected thousands of kilometres away across the span of ocean basins (Munk and Wunsch, 1979; Munk et al., 1994). Human derived noise energy input to the world's oceans come from a variety of sources (Wenz, 1962; Hildebrand, 2009; Merchant et al., 2016), including shipping, high powered sonar (Parsons, 2017; Bernaldo de Quirós et al., 2019), explosive ordnance (Lawrence, 2004; Bagocius, 2013), offshore hydrocarbon seismic surveys (e.g., Duncan and McCauley, 2000; McCauley et al., 2000; Nieukirk et al., 2004), drilling (Erbe and McPherson, 2017; MacDonnell, 2017), and piledriving for offshore development (Carstensen et al., 2006; Bailey et al., 2010). These noise sources can be divided into two categories, impulsive and non-impulsive (or continuous) while at relatively close ranges to source (Robinson et al., 2014), each with a differing character of disturbance to the marine environment. An example of non-impulsive ocean noise is that of shipping, where vessels create noise in the water column through engine vibration and propeller cavitation (Erbe et al., 2012, 2019; Merchant et al., 2012, 2014; Wang et al., 2012), with peak frequency outputs generally being lower with larger vessel size. Another example is that of bottom trawling, where in addition to vessel noise, heavy trawl gear is dragged along the seabed.

Worldwide, trawling for fish is the largest anthropogenic threat to marine species abundance and diversity (Watling and Norse, 1998; Kaiser et al., 2002) and its impacts on the seafloor are larger than all other human pressures combined (Eastwood et al., 2007; Halpern et al., 2008; Benn et al., 2010), surpassing the threats of microplastics or ocean acidification, for example. Bottom trawling, involving heavy gear contact with the seafloor (Gerritsen et al., 2013; O'Neill and Summerbell, 2011; Sala et al., 2019), not only effects the fauna along the trawl path but alters the seabed and surrounding water column to varying degrees (Pusceddu et al., 2005a, b; Oberle et al., 2016a, b, 2018). Trawling in deeper areas along the

shelf edge and slope is particularly invasive due to impacts on sensitive ecology (Haedrich et al., 2001; Morato et al., 2006), such as cold-water coral reef communities (Hall–Spencer et al., 2002), and additionally around submarine canyon ecosystems, where impacts, such as remobilisation, transportation of sediments and altered biogeochemistry down to the deeper ocean are enhanced (e.g., Puig et al., 2012, 2014; Martín et al., 2014a, b; Wilson et al., 2015; Daly et al., 2018; Arjona-Camas et al., 2019). Bottom trawl fishing in the Irish Exclusive Economic Zone (EEZ) mostly targets demersal white fish and prawns (Nephrops), undertaken by an international fleet of vessels, with the continental margin enduring larger trawlers with more powerful engines and heavier gear compared to more locally based coastal/shelf fishing fleets (European Commission, 2018; Marine Institute, 2019).

Trawler sourced acoustic noise generation has a distinct paucity of information in the literature, when compared to the wider effects of bottom trawling on the marine environment. As early as five decades ago, it was recognised that trawling noise had a behavioural effect on its target species (Buerkle, 1973, 1977), yet few studies have been carried out since. Single beam echo sounders have been used to track fish behaviour in response to an approaching fishing vessel (Ona and Toresen, 1988; Ona and Godø, 1990). More detailed measurement of trawler noise outputs, while the vessel was transiting, were carried out in line with published standards for vessel noise (Peña et al., 2011; Peng et al., 2018a, b), however these do not include active trawling. Further studies have included trawl activity, while still focussing on catch reduction due to scaring away the target species. Hovem et al., (2015) found a rise in 1/3 octave spectral values by as much as 10 dB during a bottom trawl at frequencies (80 – 1000 Hz) common to peak hearing sensitivity of some fish species (e.g., Bigeye Pempheris adspersa; 100 – 400 Hz; Putland et al., 2018) or to low frequency cetacean hearing groups (estimated: 10 Hz – 30 kHz; Finneran, 2016). Differences in overall and azimuthal values of propeller sound in a trawler have been found, depending on whether fishing or not (Pettersen, 2017). Abileah and Lewis, (1996) used the U.S. Navy's SOSUS array to identify illegal bottom trawling in the Bering sea. Contrary to trawling noise, general anthropogenic noise and its effects on marine fauna, including from passing vessels, is well documented. Various adverse effects such as hearing damage, avoidance, and stress are described on fish species (Slabbekoorn et al., 2010; Hawkins and Popper, 2017; Putland et al., 2018) and on marine mammals (e.g., Richardson et al., 2013; Blair

et al., 2016; Kavanagh et al., 2017; Erbe et al., 20.19). Acoustic habitats, and the measuring/monitoring of them, are important aspects of any given ecological setting, especially with regards acoustically sensitive species in contact with human sourced noise in the marine (and terrestrial) environment (Merchant et al., 2015).

The motivation for investigating anthropogenic noise across the continental margin is that the impacts on the marine environment, particularly on marine mammals, is yet to be fully understood. Loud anthropogenic sound in the water column, especially but not exclusively impulsive noise, can injure marine mammals (termed Temporary and Permanent Threshold Shifts: TTS and PTS) and even lead to mortality (Southall et al., 2007, 2019; Finneran, 2015, 2016; Tougaard, 2015). The less acute but wider spread impacts of behavioural disturbance to marine fauna (Ellison et al., 2012), which include avoidance, auditory masking, altered migration patterns and communication masking must also be considered (Southall et al., 2007; Stone and Tasker, 2006; Lucke et al., 2009; Erbe, 2013b), including consequences at a population level (Harwood et al., 2016). Effects are not limited to large marine mammals either, for example, vessel noise can negatively impact marine invertebrates down to the level of DNA integrity (Wale et al., 2019). It is due to this multitude of adverse impacts that anthropogenic noise is considered a pollutant across the global oceans. These impacts are currently being addressed by international bodies such as the OSPAR Commission (OSPAR, 2017) and more regionally by programmes such as JOMOPANS, JONAS or QUIETMED. Underwater noise pollution requires regulation (Erbe, 2013a; Sutton et al., 2013), which is carried out in Europe under various directives, most notably the Marine Strategy Framework Directive (MSFD) (Tasker et al., 2010; Van der Graaf et al., 2012) or the upcoming Maritime Spatial Planning Directive (MSPD). Both sites studied here are prone to noise pollution, being inhabited by marine mammals (Berrow, 2001; Berrow et al., 2010; O'Cadhla et al., 2004) along with other species including fisheries target catch. In particular, the continental margin site is in a sensitive area for resident and migrating marine mammals that include fin, sperm, smaller toothed whales and dolphins (McCauley, 2015; Berrow et al., 2018). The enigmatic and deep diving beaked whales (family Ziphiidae), whose behaviour and physiology are least well understood, may prefer canyon habitats and be particularly sensitive to anthropogenic noise (Barlow and Gisiner, 2006; Cox et al., 2006), and have been detected in the region along the eastern shelf break of the Porcupine Basin (McCauley, 2015; Berrow et al., 2018). Although beaked whales vocalise in

the range 13 – 40 kHz (Barlow et al., 2006), they are known to be most affected, through strandings, by mid frequency active sonar (~3.5 kHz) (Barlow and Gisiner, 2006; Cox et al., 2006) and potentially (through behavioural response, for example) by lower frequency bands that bottom trawling emits.

Having described sound recording and analysis methods, this paper reports received noise level results and trawler source level estimates from a trawling event at each study site. This is followed by a discussion that includes surface sourced noise from the vessel compared to bottom sourced noise from trawl gear, comparisons of each site and of levels with other noise sources, followed by consideration of noise impacts on the natural soundscape or acoustic habitat within the context of wider environmental impacts from trawling.

## 6.2. Methods and Materials

### 6.2.1. Study area

The two sites where trawling noise was measured (Fig. 6.1), are contrasting in geographical, temporal and geoacoustic parameters. The first site surveyed is located along the Celtic Sea shelf edge, on the eastern flank of the Porcupine Basin (hereafter known as the PANiC site; Fig. 6.1a) situated directly adjacent to a small submarine canyon, whose base meets the basin floor at approximately 1100 m and head cuts the shelf edge at 250 – 200 m depth. The canyon is one of a set of geomorphological slope types found in the northeast North Atlantic, where the underlying crust transitions from oceanic to continental (Sacchetti et al., 2013). The Porcupine Basin, being a deep sedimentary basin, hosts up to 10 km thick of Mesozoic and Cenozoic sediments above an extensional and thinning continental crust (Shannon, 1991; Van Rooij et al., 2007). Below the surface mixed layer, hydrography of the basin consists of East North Atlantic Water (ENAW; Harvey, 1982), above intermediate waters that can include a wedge of Mediterranean Overflow Water (MOW) between 800 – 1200 m (White, 2006) underlain by lower deep waters including Labrador Sea Water and North Atlantic Deep Water (Pollard et al., 1996). Hydrography in this region is dynamic with mesoscale variability and boundary currents (Vermeulen, 1997; Mitchell and Huthnance, 2008), along with
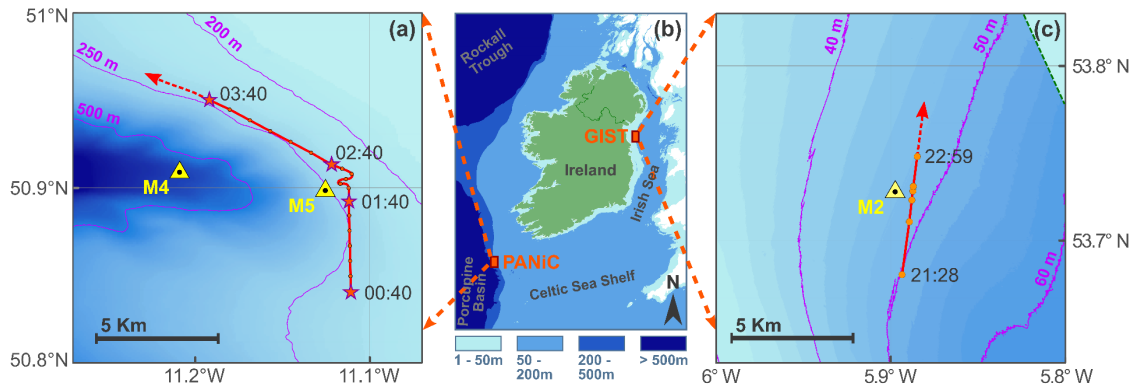
**Fig. 6.1.** Area maps. (a): PANiC survey area along the Celtic Sea margin, including acoustic receiver moorings (yellow triangles) and interpreted trawl track in red. Red stars are confirmed VMS positions of the trawler with times (UTM) on 11/06/2018. (b): Overview of both site locations and depth settings (colour key is for (b) only). (c): GIST survey site in the Irish Sea, with moored acoustic recorder (yellow triangle) and trawl track in red showing AIS points (orange dots) with time (UTM) on 25/10/2019.

tidal energy, which drives internal baroclinic tides and waves (White and Dorschel, 2010; Aslam et al., 2018). These watermass properties and processes control the in-situ sound speed profile, and in turn how anthropogenic noise propagates across the margin. The second site surveyed was approximately 22 km east of the Irish coast in the Irish Sea (hereafter known as the GIST site; Fig. 6.1b), in a region known as the Western Irish Sea Mud Belt, which is a depocenter for Holocene sediments (up to 40 m thick), overlaying glacial stratigraphy (McCabe et al., 2007; Coughlan et al., 2019). Hydrography was thought to be fully mixed during the GIST survey (end October) following stormy conditions. Seasonally, this area is a very active trawling grounds with predominantly small to mid-sized local trawlers fishing for Dublin Bay prawns or Langoustine (Nephrops norvegicus) (Marine Institute, 2019). The GIST site also holds strong potential for near future offshore wind farm development, with various consequences for local fishing grounds and for monitoring of anthropogenic noise in the water column, for example under the MSPD, due to the planned development and risk to marine fauna.

## 6.2.2. Data acquisition

Data were acquired for this study from two separate field campaigns, both of which used the same equipment and setup. In both cases, hydrophones and acoustic recorders were deployed on short-term fixed moorings for the duration of the campaigns and recovered on completion.

Propagation of Acoustic Noise in Canyons (PANiC) was a dedicated marine acoustics research survey carried out in June 2018 and provides the main dataset for this study as part of a larger project investigating anthropogenic noise propagation along the continental margin. Hydrophones and recorders were placed at 100 m below the sea surface, in 651 m and 251 m water depths, recording constantly for 47.05 and 31.68 hours, for moorings M4 and M5 respectively, over a small submarine canyon. The event studied here involved a mid-sized bottom trawler, most likely trawling for demersal whitefish along the 250 m isobath. The trawler's positional data were acquired from Vessel Monitoring System (VMS) provided by the Marine Institute of Ireland and confirm individual position, time and fishing status every hour over four hours, although vessel call sign and specifications remain classified. Further to confirmed VMS locations, position details in between hourly points were inferred from a screengrab of navigation software (MaxSea) on-board the R.V. Celtic Voyager, using automated identification data (AIS) and converted to latitude/longitude points in time every 10 minutes.

Geohazard Investigation in the Irish Sea using Seismic and Seabed Mapping Techniques (GIST) was a research survey on sediment dynamics and geohazard linked with proposed offshore windfarm development, executed in October/November 2019. The opportunity was seized to deploy fixed acoustic moorings as an adjunct project from this research cruise, in order to record all anthropogenic noise in the locality during the survey, including the survey itself. The short-term moored hydrophone and recorder were placed in 47 m of water, 4.5 m above the bottom, recording constantly for 15.18 hours. The trawl event captured here was from a 17 – 20 m long fishing vessel with a gross tonnage between 110 – 120 t, which was registered under an Irish flag and was actively bottom trawling for prawn. Positional data for the prawner were exclusively extracted from AIS data collected from the Celtic Voyager's MaxSea, using features of the software that provided real-time position, distance and bearing from the mooring.

The 'industry standard' hydrophone model used for both campaigns was the GeoSpectrum M14-600 with a factory set preamp gain of +35 dB and a frequency band low end of 2 Hz, with high end capped by sampling frequency. The hydrophones were calibrated using an in-water multipoint frequency sensitivity test with a projector and reference hydrophone. The recorder used was an RS-ORCA

rated to 3000 m with an on-board Analogue to Digital Converter (ADC) utilising adjustable sampling rate, duty cycling and front-end gain. For both campaigns, neither duty cycling, or front-end gain were added, and the sampling rate was set to 48 kHz, providing an effective pass band up to 24 kHz, once Nyquist frequency had been accounted for.

### 6.2.3. Analysis and sound outputs.

Data processing consisted of converting the raw 16 bit signed integer (N-bits) ADC output to a micro-pascal (µPa) pressure time-series, incorporating a single value calibration coefficient supplied with each individual hydrophone, providing a flat frequency response across bands of interest. This discrete Sound Pressure Level (SPL) time-series (48 thousand samples per second) provides the basis for all further metrics analysed.

In the time domain the main metric of interest is root mean square SPL (SPLrms), as is recommended for investigating non-impulsive noise in the ocean (Robinson et al., 2014). Here SPLrms is calculated over 60-second-long segments of data and reported in decibels (dB) relative to a reference value where:

$$SPL_{rms} = 10 \ \log_{10} \left( \frac{\bar{P}^{\,2}}{P_{ref}^2} \right) = 20 \ \log_{10} \left( \frac{\bar{P}}{P_{ref}} \right)$$

with $\bar{P}$ being a mean value of SPL across all samples of the 60 s segment and Pref being the reference value of 1 µPa (for underwater acoustics). Zero to peak SPL values are a measure of instantaneous pressure difference from zero to ± peak pressure (Merchant et al., 2015) and although more commonly used for impulsive noise, provide an additional metric convenient for analysing maximum sound pressures added to the water column due to trawling activity.

By analysing data in the frequency domain, spectral or banded frequency values can provide information on where the noise is strongest, useful especially in comparison with frequencies of known marine fauna sensitivities. Frequency based analysis commences with calculating Power Spectral Density (PSD), being a fast Fourier transform of the 60 s segment pressure time-series, which breaks up a signal into constituent frequencies. Here PSD is estimated with Welsh's method of

segment averaging (Welch, 1967), using a hamming window (zero overlap) producing a one-sided, discrete frequency set of values from 0 – 24 kHz. PSD is reported in dB re: 1 µPa2 Hz$^{-1}$. From PSD estimates, band analysis of SPL is calculated for various bands where SPL is simply the sum of values across frequencies within a given band before conversion to dB.

One third octave bands from 10 Hz to 10 kHz are also calculated as above but with PSD estimates interpolated to a 0.1 Hz resolution for finer extraction of 1/3 octave band centre frequency values of SPL which are particularly useful for combining with modelled transmission loss at individual frequencies.

Further to band analysis, exceedance levels are a method of statistically evaluating spectral samples within each band. Exceedance levels are the number of samples, as a percentage, that exceed a given value and as reported in the results here (as SPL in dB) are most commonly reported at standardised level pairs such as 95-5% or 75-25%. They are convenient here for showing the distribution of the bulk of sample values relative to minimum and maximum sample values per frequency band, albeit with very little variance between the exceedance levels themselves across all bands and all sources analysed.

### 6.2.4. Numerical Modelling.

Modelling of Transmission Loss (TL) was carried out on example pathways of sound propagation between source and receiver for each 1/3 octave centre frequency (10 – 10,000 Hz). The model selected for this application was RamGEO, which is a 'Range dependent Acoustic Model' (Collins, 1993) based on the Parabolic Equation suite of models run on AcTUP (Duncan and Maggi, 2006) and was range averaged (Harrison and Harrison, 1995) following validation in the Porcupine Basin (Crawford, 2016), although not at the survey site. For the PANiC area, sub-seafloor model parameters were used from a previous regional model for the Porcupine Basin (Crawford, 2016), while GIST area parameters were entered from various sources, with thicknesses of seabed layers calculated from Coughlan et al. (2019); see: Appendix B, Supplementary Table B.T1.

Given received levels (RL) and modelled TL at 1/3 octave frequencies, estimates of source levels (SL) of SPL (and Sound Exposure Levels; SEL) can be made, where

$$SL_{1/3} \ = \ RL_{1/3} \ + \ TL_{1/3} \ (dB)$$

for each 1/3 octave centre frequency, calculated from summed or time integrated values (SPL or SEL respectively) of RL and modelled from individual frequency TL. In this study SPL and SEL are linearly related (e.g., Madsen, 2005), due to the duration of analysed segments being uniform at one minute, where

$$SEL = SPL_{rms} + 10\log_{10}(60s) = \ SPL_{rms} + 17.78 \ dB \quad (re: 1 \ \mu Pa^2 s).$$

These trawling events were measured opportunistically, differing from standardised measurement of vessel noise in deep water (e.g., ISO, 2019).

## 6.3. Results

### 6.3.1. Received noise levels

6.3.1.1. PANiC area

Noise from the Trawling event recorded at M5 mooring at the PANiC survey site over a period of 3.5 hours is displayed in Fig. 6.2. The spectrogram of frequencies (< 10 kHz) over the duration of the event (Fig. 6.2a), shows elevated noise clearly apparent above both ambient levels and above airgun shots conducted (seismic source: 25.7 – 8.6 km west to west-northwest) over the same period. One-minute rms SPL levels (Fig. 6.2b) for the trawling event have been decoupled, in time, from the airgun shots taking place. A sharp rise in SPLrms is seen at 02:02 UTC with levels highly elevated until approximately 02:40, including a peak level of 126.85 dB (re: 1 μPa) at 02:21. For comparison, single value SPLrms values are included for the quietest background noise recorded during the entire survey (112.63 dB re: 1 μPa; 10th June, 15:13 UTC) and for the research vessel Celtic Voyager (117.64 dB re: 1 μPa) at 500 m range from receiver, just prior to mooring recovery. Distances from the trawler source to the mooring receiver are confirmed by VMS at four points (stars in Fig. 6.2c) and the grey line, being an inferred distance to receiver, has closest interval of ~605 m from receiver.
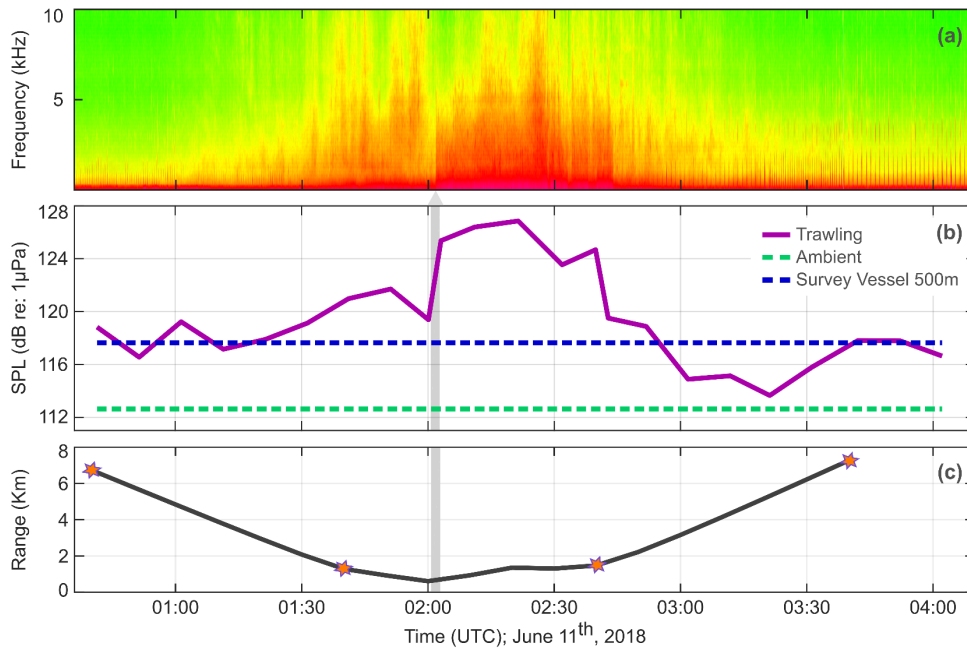
**Fig. 6.2.** Trawling noise in the water column for the PANiC area over a 3.5 hr period. (a): Spectrogram of scale dBV using a 1024 sample window with a 50% overlap. (b): Purple line is the rms SPL values from one-minute segments, avoiding any airgun content. Also shown are a single value for the lowest ambient one-minute rms SPL recorded at that mooring (Green dashed line) and a single value one-minute rms SPL, while the research vessel was approximately 500 m from receiver (Blue dashed). Light grey area and pointer indicates approximately the extent shown in Fig. 6.4. (c): Range from trawler source to receiver in kilometres, where the stars are confirmed VMS locations and the dark grey line is interpreted range using RV Celtic Voyager navigation software.

Power spectral densities for a one-minute segment of data at time of peak trawling indicated that trawling noise dominated the total spectra, containing highest densities across all frequencies above ~30 Hz (Fig. 6.3). Strongest values were centred around 240 Hz, but also elevated around 48 Hz, spiked at 100 Hz and were 20 dB higher than the survey vessel and 30 dB higher than background levels throughout the 100 – 1000 Hz band.

In an effort to focus on the sharp rise in noise levels seen around 02:02 UTC at ~650 m range, a two-minute section was extracted for finer temporal analysis around this event. The rapid change in spectral noise content (Fig. 6.4a) is mirrored in received values (Fig. 6.4b, c). Zero to peak SPL values increased by 5 dB within five seconds during the stepwise change (Fig. 6.4c). Broadband (10 – 24,000 Hz) and third decade band (100 – 1000 Hz) values both increase by approximately 7 dB over a 10 s interval across the shift in noise (Fig. 6.4c), where a 6 dB increase
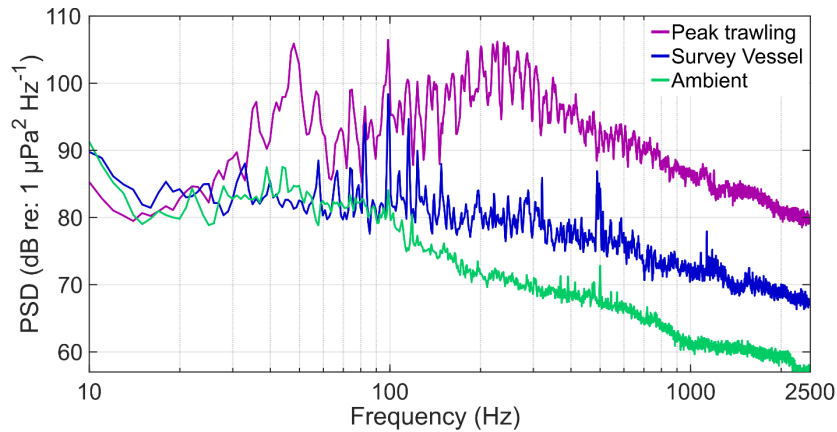
**Fig.6.3.** Power Spectral Density (PSD) curves for trawling noise at its peak (purple line), research vessel noise at 500 m from receiver (blue) and lowest recorded ambient noise (green), zoomed in to 10–2000 Hz. Dates and times of each one-minute PSD are as follows: Peak-trawling 11th June, 02:21; Survey vessel 11th June, 19:38; Ambient noise 10th June, 15:13.

in underwater SPL represents a doubling of sound pressure. To listen to a 40 s snippet of this change in noise, the reader is encouraged to open the Supplementary Audio file (PANiC_Trawl.wav). Also available for comparison are survey vessel and ambient audio file samples (PANiC_RV.wav and PANiC_Ambient.wav; as seen in Fig. 6.2b) [(Click here to Link) and found in Appendix B].
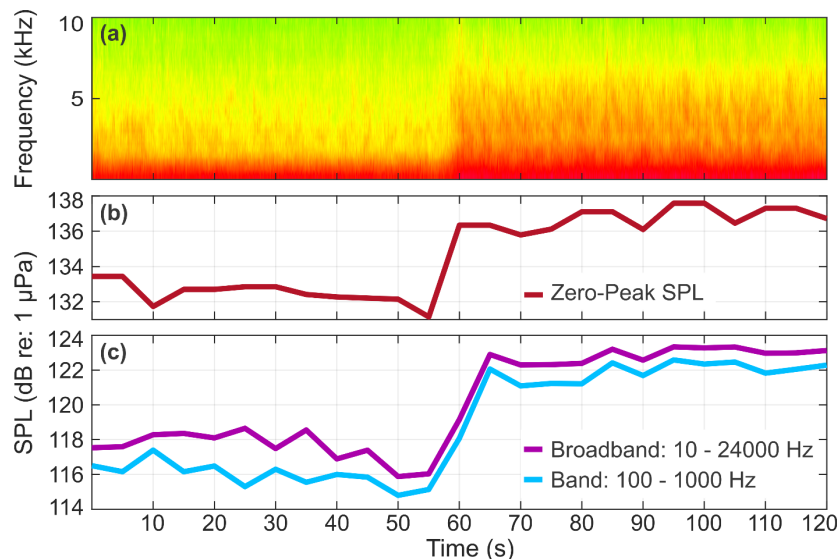


**Fig. 6.4.** Onset of trawling noise event zoomed to a two-minute time period (grey arrow in Fig. 6.2 above) centered around 02:02 UTC. (a): Spectrogram of scale dBV using a 1024 sample window with a 50% overlap. (b): Orange line is zero to peak SPL values every five seconds from a 10 s rolling window with 50% overlap. (c): Broadband (purple) and 100–1000 Hz band (blue) SPL values every 5 s from frequency analysis of 10 s sections with 50% overlap. [please find supplementary audio file (PANiC_Trawl.wav) to playback 40 seconds of recording centered around this event]

### 6.3.1.2 GIST area

Trawling noise for the event studied at the GIST survey site is presented in Fig. 6.5. The spectrogram shows harmonic striations characteristic of a passing ship (Fig. 6.5a). SPLrms levels across the hour of one-minute segments (orange line, Fig. 6.5b) are elevated by ~6 dB as the trawler passes the moored receiver, reaching a peak of 119.93 dB re: 1 µPa, while also showing shorter scale variability between segments. For comparison, the green dashed line indicates lowest ambient noise (109.76 dB re: 1 µPa) recorded at that mooring. Fig. 6.5c is a plot of distance from trawler source to moored receiver using navigation plotting software data points (orange circles), with closest approach being ~670 m. As with the PANiC survey, supplementary audio files can be accessed for peak trawling and ambient noise conditions at the GIST site (GIST_Trawl.wav and GIST_Ambient.wav; as seen in Fig. 6.5b).
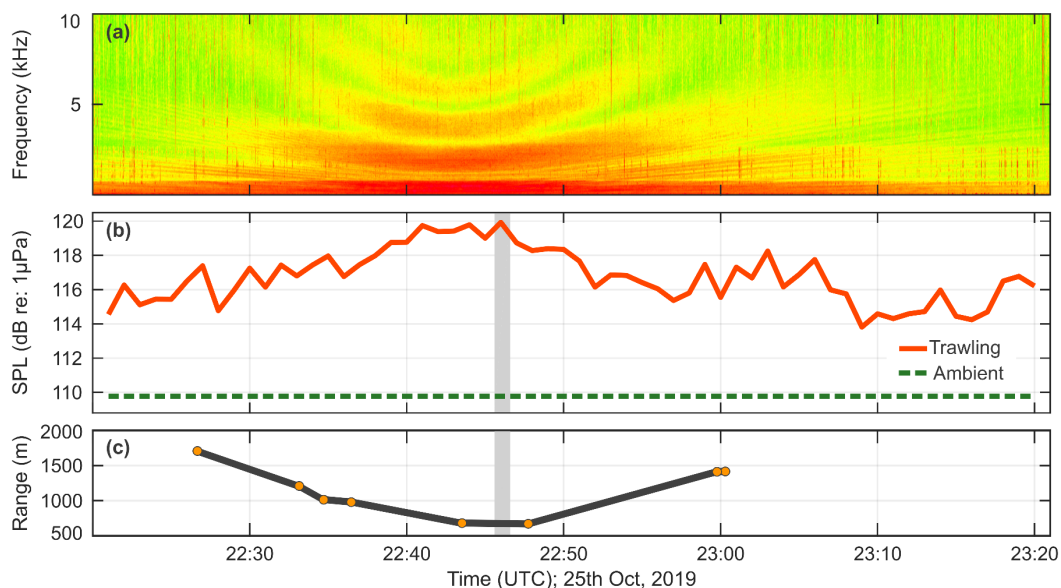


**Fig. 6.5.** Trawling noise in the water column for the GIST area over a one-hour period. (a): Spectrogram of scale dBV using a 1024 sample window with 50% overlap. (b): Orange line is rms SPL values from one-minute sections for each minute of the hour. Green dashed line represents a single value for the lowest ambient, one-minute rms SPL recorded at that mooring. Light grey vertical area indicates the one-minute section seen in Figs. 6.6 and 6.7. (c): Range from trawler source to receiver in metres, where the orange dots are confirmed AIS positions (with time) from the research vessel's bridge software MaxSea.

## 6.3.2 Spectral and 1/3 Octave outputs

Spectral sound analysis has been binned to 1/3 octave bands for comparison of noise frequency content from both study sites (Fig. 6.6). The shallower based GIST peak trawling event held highest SPL values up to 30 Hz, but the deeper canyon directed path of PANiC peak trawling dominates at higher frequencies. As with trawling values, ambient noise levels are also higher at the deeper, more topographically complex PANiC M5 mooring site. Although both trawling and ambient 1/3 octave SPLs are comparatively lower at the GIST site, frequency content of trawling there (orange line) surpasses the levels emitted from the research vessel in deeper water at PANiC (blue dashed line).
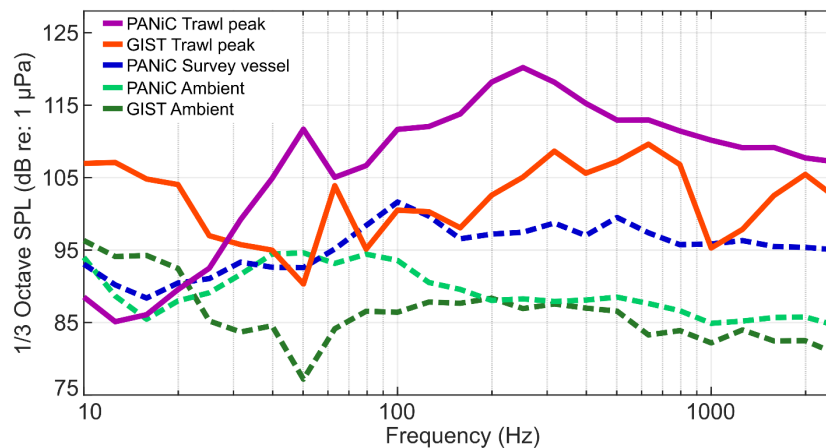


**Fig. 6.6.** One third octave SPL sound levels from one-minute spectral analysis at both survey sites, displaying 10 – 2500 Hz centre frequencies. Purple line is peak trawling along the shelf edge at the PANiC area; Orange line is peak trawling in the shallow shelf Irish Sea at the GIST site; The blue dashed line represents the survey vessel at 500 m range at PANiC; Light green and darker green dashed lines are lowest recorded ambient noise levels at PANiC and GIST respectively.

Further comparison between all events was made through statistical breakdown of spectral SPL values, derived from 1 Hz resolution PSD analysis, banded to mostly decade bands (Fig. 6.7). Broadband analysis (red horizontal bars) shows highest general exceedance levels (5%, 25%, 75% and 95%) at the PANiC peak trawling event followed by the GIST peak trawling event. Actual SPL levels (also known as $L_{eq}$) or 50% exceedance ($L_{50}$) are not displayed here but fall within the 25 – 75% horizontal bars. Of note is that in every anthropogenically sourced continuous noise, including the survey vessel, the 100 – 1000 Hz band (purple bars) is higher than all

other bands, with the PANiC trawling event being > 10 dB higher in that band then the decade bands each side of it.
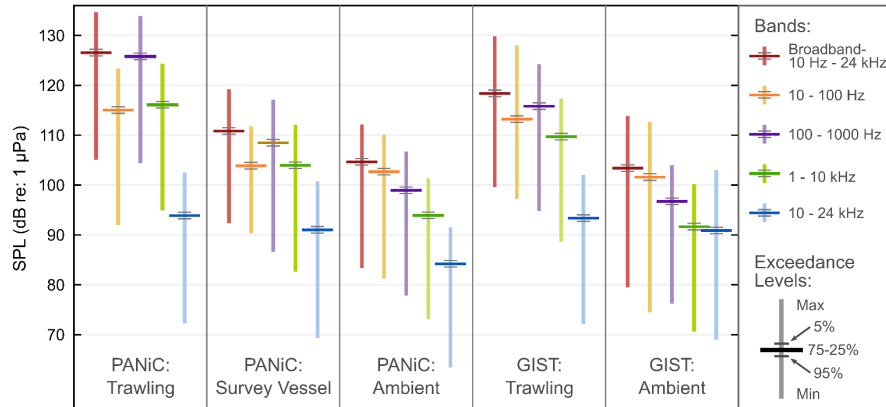


**Fig. 6.7.** Statistical SPL sound levels as a function of frequency band (per colour) for various one-minute sections as shown in Figs. 6.2, 6.4, 6.5 and 6.6 above. Vertical lines are drawn between minimum and maximum values occurring within each coloured band; Horizontal lines represent exceedance levels (see key to left of figure). Number of samples analysed was 60 x 48 kHz = 2.88 x106 for each of the 5 one-minute segments.

### 6.3.3. Source estimates from modelled transmission loss

6.3.3.1. Source levels across pathways

Estimation of source noise levels (SL) emanating from bottom trawling activity have been made through addition of modelled Transmission Loss (TL) with observed received levels. broadband source levels of SEL (at propeller depth) along with broadband RLs and modelled TL values are displayed in Table 6.1. RL, and consequently SL values, have also been auditory weighted (previous to integration of 1/3 octave levels) for the three cetacean groupings, following Southall et al. (2019), in order to access the risk of TTS and PTS. Sources are considerably higher in the PANiC area over relatively similar ranges to receiver. All source levels in the low frequency (LF) and very high frequency (VHF) cetacean groupings are above TTS at both sites and would cause temporary harm if the animal were at source. The PANiC area has values all considerably higher than TTS (> 10 dB) for LF and VHF groupings with paths 1 and 2 marginally above PTS thresholds. These high values imply a further distance from source to the boundaries of TTS and thus harm to marine mammals. Source levels show some variation, hence mean values (at

**Table 6.1.**

Values of trawler noise source level estimates, modelled TL and received levels of 1/3 octave SEL (calculated over 60s segments) for model pathways, along with spatial and temporal parameters for sources and receivers.

| | PANiC Area | | | | | GIST Area | | | |
|---|---|---|---|---|---|---|---|---|---|
| | Path 1 | Path 2 | Path 3 | Path 4 | Mean | Path 1 | Path 2 | Path 3 | Mean |
| **Spatial Parameters (m):** | | | | | | | | | |
| Range: Source to receiver | 1284 | 1475 | 2401 | 3358 | 2130 | 1712 | 722 | 1415 | 1283 |
| Source depth at surface | 4 | 4 | 4 | 4 | 4 | 3 | 3 | 3 | 3 |
| Receiver depth | 100 | 100 | 100 | 100 | 100 | 42.1 | 42.1 | 42.1 | 42.1 |
| Mooring depth | 251 | 251 | 251 | 251 | 251 | 46.6 | 46.6 | 46.6 | 46.6 |
| **Time (UTC)** | | | | | | | | | |
| PANiC: 11th June 2018 | 02:32 | 02:40 | 02:52 | 03:02 | | | | | |
| GIST: 25th Oct. 2019 | | | | | | 22:26 | 22:43 | 22:59 | |
| **Received SEL levels (dB re: 1 µPa²s ):** | | | | | | | | | |
| RL | 140.51 | 142.01 | 132.17 | 128.76 | 138.68 | 130.27 | 135.63 | 131.29 | 133.06 |
| RL LF* | 138.18 | 139.78 | 129.82 | 126.63 | 136.41 | 123.39 | 133.81 | 126.00 | 130.03 |
| RL HF* | 114.15 | 113.69 | 108.97 | 108.37 | 112.05 | 107.44 | 113.10 | 108.44 | 110.41 |
| RL VHF* | 109.06 | 108.11 | 104.34 | 103.79 | 106.91 | 103.92 | 108.44 | 104.13 | 106.03 |
| **Modelled Transmission Loss (dB):** | | | | | | | | | |
| TL | 96.28 | 95.55 | 98.02 | 101.28 | 98.08 | 87.26 | 82.41 | 85.74 | 85.37 |
| **Source SEL Estimates (dB re: 1 µPa²s ):** | | | | | | | | | |
| SL | 205.01 | 203.92 | 199.27 | 200.69 | 202.82 | 190.77 | 187.80 | 189.43 | 189.50 |
| SL LF* | 200.98 | 200.85 | 194.23 | 195.03 | 198.83 | 179.79 | 183.67 | 180.15 | 181.58 |
| SL HF* | 174.60 | 175.68 | 173.98 | 174.69 | 174.78 | 161.58 | 162.56 | 161.30 | 161.85 |
| SL VHF* | 169.43 | 169.95 | 169.48 | 170.13 | 169.76 | 158.12 | 157.69 | 156.95 | 157.61 |

*Auditory weighted values for cetacean groupings: LF (Low Frequency), HF (High Frequency), VHF (Very High Frequency), following Southall et al., (2019)

Notes: SEL levels for non-impulsive Temporary Threshold Shift (TTS): LF = 179, HF = 178, VHF = 153 (dB re: 1 µPa²s )

SEL levels for non-impulsive Permanent Threshold Shift (PTS): LF = 199, HF = 198, VHF = 173 (dB re: 1 µPa²s )

Coloured cells indicate:

| |
|---|
| Above TTS by up to 10 dB |
| Above TTS by 10 - 20 dB |
| Above PTS |

1/3 octave stage) have been calculated to address this variation and limitations potentially causing these inconsistencies are discussed in the next section. 1/3 octave SPL source estimates (dB re: 1 µPa @ 1 m) are also tabled and reported (see Appendix B, Supplementary Table B.T2).

## 6.3.3.2. Surface Vs Seabed Source Estimates

As part of source estimate analysis, a speculative study was made into the difference between a source emanating from the fishing vessel near the surface and emanating from the trawling gear being dragged along the seabed. Modelled TL was found to be lower from a bottom sourced noise than a surface sourced one, indicating stronger propagation through the water column and laterally through the sub-seafloor (Appendix B, Supplementary Table B.T3). Following a defined inversion between 12.6 and 15.9 Hz, all 1/3 octave TLs and resulting SLs were higher from surface sourced noise up to 200 Hz for both PANiC and GIST sites, while converging at higher frequencies (see: Appendix B, Supplementary Fig. B.1). As an example of these differences in TL model runs, Fig. 6.8 displays the strongest pathway (path 2) at PANiC, where it can be clearly seen how higher TL and therefore lower noise propagation occur through the water column from a surface

sourced noise (Fig. 6.8b) compared to a bottom sourced noise (Fig. 6.8c). In order to quantify this, an average TL exclusively from the water column was calculated across approximately two wavelengths in the horizontal (120 m) over full depth of water, centred at the receiver range from source (green rectangles, Fig. 6.8b, c). Surface sourced sound in the water column contained TLavg of 74.78 dB, whereas seabed sourced contained 60.38 dB, which in turn would deliver received propagation levels 14.4 dB higher from bottom sourced noise compared to surface.
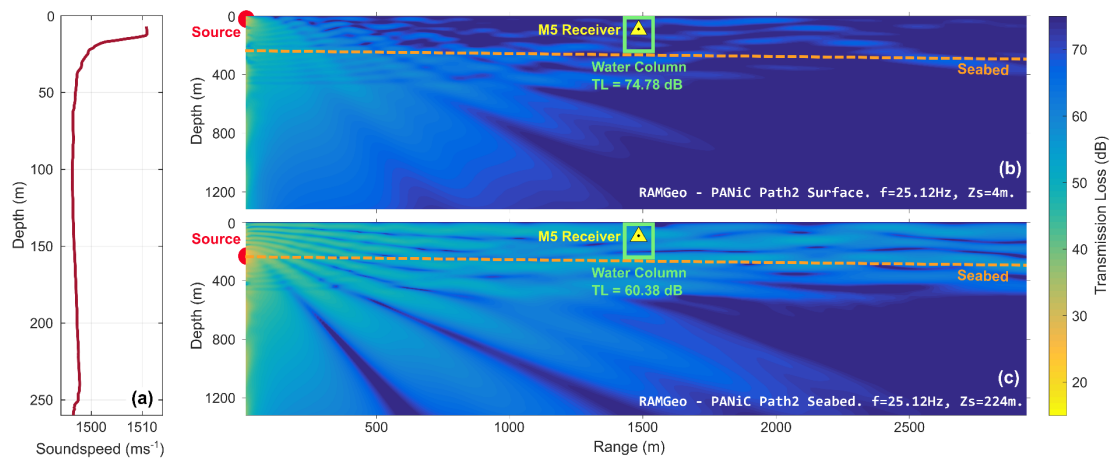


**Fig. 6.8.** RamGEO TL model outputs at 25 Hz for path 2 at the PANiC site. (a): Sound speed profile from ship-based CTD cast local to mooring M5 taken during survey; used for model runs at the PANiC site. (b): Source depth within the model positioned at the vessel (4 m deep). (c): Source depth positioned at the seabed (224 m deep). The red dots are source location, yellow triangles are receiver position in the water column, and green rectangles are water column TL averaged over full depth and two wavelengths wide, centred at receiver range.

## 6.4. Discussion

### 6.4.1. Noise propagation in canyon

Statistical SPL levels of the five noise sources investigated here display strongest noise signals from trawling activity (Fig. 6.7) with PANiC values the greatest, while

all anthropogenic sources examined (including the research vessel) have elevated values in the 100 – 1000 Hz decade band, compared to ambient levels. This is reflected by peaks in 1/3 octave received trawling SPLs at 251 Hz (Fig. 6.6) and further in spectral densities (Fig. 6.3), where trawling shows a bulged peak around 240 Hz and sustained levels considerably higher than ambient to above 2.5 kHz. A consideration here for elevated RLs from trawling at the shelf break is the proximity and geometry to the adjacent canyon head and axis, where sloping topography becomes more extreme and possibly drives focussing or channelling of noise propagation down canyon. As part of a wider associated project investigating pulsed airgun noise propagation in canyon and onto the shelf, a mooring (marked M4 in Fig. 6.1) was deployed further down the canyon axis and displayed is a spectrogram of that receiver during the trawling event (Fig. 6.9). Apparent is a higher noise content, while the trawler was at the canyon head (~02:00 – 02:40 UTC) compared to when it was trawling nearer to M4 (03:40, see also Fig. 6.1a). Full analysis of trawling noise at M4 proved inconsistent and was not therefore reported here as results. The inability to definitively discern the trawling component at this station was believed to be due to a combination of issues including range from source, varying ambient noise, low frequency mooring system noise (caused by strong water currents) and the closer presence of the airgun survey; the latter seen as vertical shot lines every 30 – 60 s (Fig. 6.9). Although not conclusive, the spectrogram does however indicate stronger noise propagation down canyon from a shelf edge source, in comparison to source being orthogonal or oblique to canyon axis. This highlights canyon slope features as potential conduits for down-slope noise propagation along the continental margin.
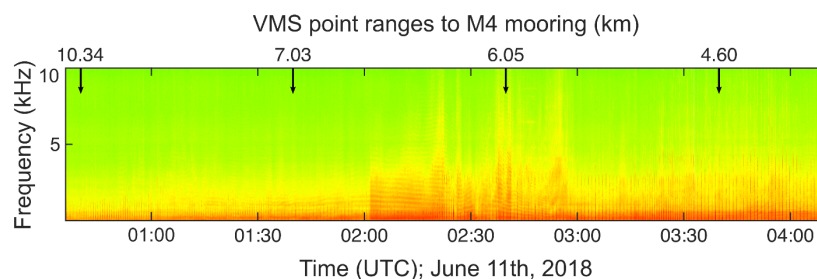


**Fig. 6.9.** Spectrogram of mooring M4 deployed in canyon. Receiver at 100m below surface in 651 m depth. Black arrows and range in km correspond to VMS point data seen in Figs. 6.1 and 6.2c.

## 6.4.2. Source level estimates and geometry

Source levels here are estimates and must be viewed within their inherent limitations, a major one being generalised assumptions made within the TL models, for example homogeneously layered substrata across range used in modelling runs, or models validated within the region but not on-site. Notwithstanding limitations, estimating source levels is a key step in estimating noise pollution by elucidating potential levels of harm to nearby marine fauna and advising on levels for noise pollution management. Auditory weighted source estimates reported in Table 6.1 are consistently > 10 dB higher than the onset of temporary threshold shifts (TTS) for both LF and VHF cetaceans in all modelled pathways in the PANiC survey area, with levels breaching PTS on two of the pathways. However, these are 'at source' levels. To put this into further context, if a LF cetacean remained at a 500 m radius from source at PANiC, it would take 14 hours to reach a cumulative SEL above auditory weighted TTS onset, and 107 hours at 1000 m (backwards calculated from SL, using range averaged TLs). However, levels of harm and other adverse effects are not limited to TTS and PTS metrics. An example of behavioural disturbance resulting from anthropogenic noise (including active bottom trawling) is that of communication masking, where a marine mammal's ability to communicate at range is impaired due to artificially elevated background noise and can require the animal to alter its communication strategy (Erbe et al., 2016 and references within). This can be a consequence of locally sourced noise or from a more global rise in ambient noise, which may be increasing by as much as 3 dB per decade from shipping noise (again including trawling)(Erbe et al., 2019 and references within).

When assessing sound energy emitted by a fishing vessel while actively trawling, the noise sources of vessel and gear, and the relative position of each, must be considered distinctly. Results here have shown seabed sourced sound to propagate more efficiently than a source at the surface, while in reality received levels will be a combination of both in different  proportions, depending on relative location to receiver and acoustic propagation parameters. The fact that the bottom sourced gear noise contributes more efficiently, adds potential for trawling activity to impinge negatively on the surrounding aquatic environment. Radiated noise fields from a non-impulsive source, such as a ship or trawler will not be isotropic (equal in all directions) and will increase in complexity as frequency increases (Arveson and Vendittis, 2000) which could explain further why source levels reported here differ

over pathways from the same source vessel (Table 6.1; Appendix B, Supplementary Table B.T3), although sub-seafloor and water column changes must also be considered. Another complexity to consider from bottom trawling compared to general shipping noise, is the use of additional equipment, such as winches on deck vibrating through the hull, or various types of gear used on the trawl itself. These include the heavy trawl doors (can be > 1 tonne each) that keep the net open and footropes or chains, which may have rockhoppers (large rubber discs to prevent snagging on rocks) attached (Watling and Norse, 1998; O'Neill and Summerbell, 2011; Sala et al., 2019). Trawl warps (cables connecting net to vessel) may create a humming noise in the water column due to cable tension, potentially explaining the elevated high frequency content.

### 6.4.3. Comparison of survey sites

When comparing the two sites there are various differences that become apparent, not least how geoacoustic parameters differ widely (Appendix B, Supplementary Table B.T1). Topography at the deeper PANiC site is varied from smoother slopes to an incised canyon and associated gullies. In contrast the shallower GIST site is on relatively flat ground. Fishing vessel length, engine power and gear size will be larger in the offshore region surrounding the PANiC site (Gerritsen and Lordan, 2014) and have a bigger environmental impact (Watling and Norse, 1998). Fishing effort (hrs/km$^2$) calculated from acquired VMS records, and filtered to only include active bottom trawling, shows a considerable difference between locations (Fig. 6.10). Differences occur both in intensity and geographical spread, where the GIST location (fished 17268 hrs over the years 2018 and 2019) is more heavily fished than the PANiC location (5920 hrs) but is also more evenly fished. VMS data at PANiC shows heaviest fishing between the 250 and 500 m contours and is probably limited by slope angle around the canyon's head and flanks, where trawlers can be limited to slopes below 15 – 20° (Daly et al., 2018). There is some seasonality in the VMS data, with GIST seeing a large rise over summer months (Jul, Aug, Sept), with a peak in August at 4312 hours over the two years. Fishing at PANiC is bimodal, with high efforts in summer (May, Jun, Jul) and winter (Dec, Jan). The effect of trawl fishing is noisier along the continental margin than on the Irish sea, as seen here through spectrograms, reported RLs and estimated SLs, including auditory weighted SELs. Spectrograms highlighted difference in the presence (GIST) or absence (PANiC) of tonal lines or 'striations' and of 'U shaped' patterns of
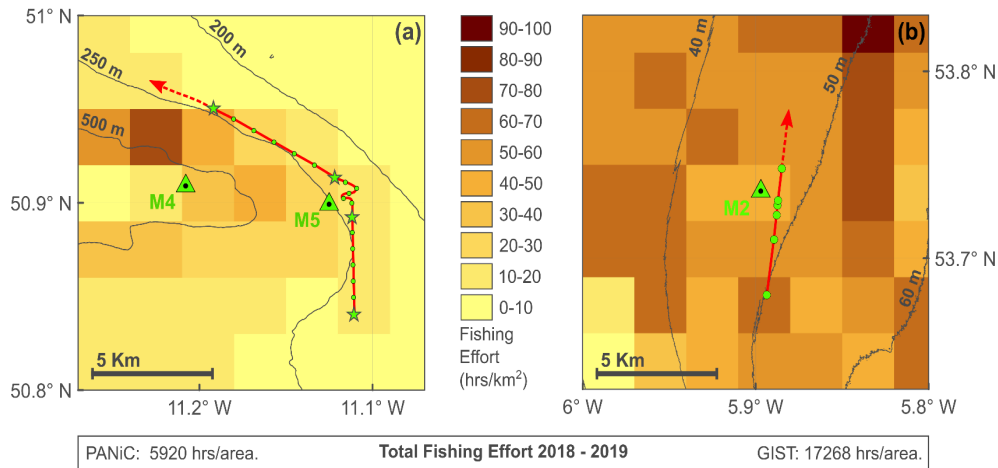
**Fig. 6.10.** Fishing Effort per area from VMS data for the years 2018 and 2019 as per map areas and objects in Fig. 6.1. PANiC area (a) and GIST area (b) fishing effort in hrs per km2 (see key). Included are totals per area summed over the two years.

interference at the two trawl locations. These are seen clearly in the GIST spectrogram as harmonics of primary frequencies and of dipole sourced (Lloyd mirror effect) destructive and constructive interference, generated at least in part by propeller cavitation, which appear similar to that seen in shipping (McKenna et al., 2012; Simard et al., 2016). However the U patterns and striations seem thicker and appear to reach higher frequencies than some of those previously published (e.g., here Fig. 6.5a; McKenna et al., 2012 Fig. 2a, b top; Simard et al., 2016 Fig. 2). This is perhaps due to the fact that the overall noise here is comprised of broader band signals from towing trawl gear, in addition to tonal frequencies from propeller cavitation and/or engine vibration. In contrast, the 3.5 hour spectrogram for the PANiC trawl event (Fig. 6.2a) shows no dipole U patterns and very faint striations, which may be due to the abrasive towing of heavy fishing gear over hard ground being a competitive or masking noise to propeller and engine. This may be due in part to factors mentioned earlier, such as depth, topography, door size and the frequency dependency of each. However, the lack of U patterns may also be due in part to vessel heading relative to mooring M5 as seen in the meandering vessel track in Fig. 6.1.

### 6.4.4. Trawling relative to other non-impulsive sources

Although there are examples in the literature of spectral source levels from fishing vessels (e.g., Hovem et al., 2015; Peng et al., 2018a, b), unfortunately for this study

they do not provide comparative broadband levels that focus on vessels actively trawling. Therefore, other somewhat similar sources of non-impulsive anthropogenic noise are examined here and compared with the mean (averaged across pathways) source level of 185 dB (re: 1 µPa @ 1 m, 10 – 10,000 Hz) for the main PANiC trawling event. Values for shipping noise vary, for example, from 188.1 dB  (re: 1 µPa2, 20 – 1000 Hz) for a 298 m long container ship (McKenna et al., 2012) to an average of 197.1 dB (re: 1 µPa @ 1 m, 20 – 500 Hz) for multiple ships passage through a merchant shipping lane (Simard et al., 2016). Erbe et al. (2013) found levels of 188 dB (re: 1 µPa @ 1 m, 20 – 2500 Hz, 5th percentile) for a Floating Production Storage and Offloading (FPSO) vessel, while MacDonnell (2017) reported 187.7 dB (re: 1 µPa @ 1 m, 10 –3 2,000 Hz) from an active mobile offshore drilling unit and its offshore support vessels. When compared to the larger sound sources mentioned above, the noise remains considerable from a single mid-sized trawler engaged in fishing along the Porcupine margin. Active bottom trawling along the continental margin, such as the event measured here, may compound the generation of noise pollution compared to a faster moving ship travelling directly across the slope or a point sourced drill operation, due to trawling's pervasive and near ubiquitous presence in the region, as quantified from VMS records. This may be compounded further in the vicinity of environmentally sensitive topographic features such as submarine canyons, enhanced even more by a component of source content propagating strongly from the seabed. Other factors, such as time of year and water column properties/processes can further enhance the effect of noise energy input. Chen et al. (2017) found higher sound levels in winter from a commercial cargo ship due to seasonal hydrographic conditions in the Celtic Sea, while in the Porcupine Basin, lower 1/3 octave modelled TL values were found in winter using in-situ seasonal sound speed profiles (Daly et al., 2020). This coupled with the fact that December and January are two of the three busiest months fishing in the PANiC area, and that bottom trawling is concentrated along the shelf edge and slope (Gerritsen and Lordan, 2014) makes trawling potentially quite hazardous to the region's acoustic habitat. Winter months (Nov–Mar) in the Porcupine region experience a south-westerly migratory pattern for Humpback whales and an over-winter presence of other cetacean species, such as Fin and Blue whales (O'Cadhla et al., 2004; Charif and Clark, 2009).

*6.4.5. Implications for the marine environment*

The impact of bottom trawling on the natural marine environment is multifaceted. Trawling generated noise pollution is a facet that augments human pressure on marine ecology globally. This is especially true in sensitive regions such as the western European continental margin that provides favoured habitats and migration pathways for a diverse collection of marine mammals (O'Cadhla et al., 2004; Berrow et al., 2018). Hazards outlined here, additional to other trawling pressures, such as seafloor changes, trawl plumes, sediment transport and altered biogeochemistry (e.g., Stelzenmüller et al., 2008; Wilson et al., 2015; Daly et al., 2018; Arjona-Camas et al., 2019), identifies this human activity as a growing concern requiring further measurement and monitoring, both in terms of impact on the regional soundscape (Tasker et al., 2010; Sutton et al., 2013) and direct impact on communities and ecosystems, especially in sensitive areas along the continental margin.

Mitigation measures are being developed to reduce the impacts on the seafloor from contact with heavy trawl gear. An example is the PORTES project in the Palamós region of the Mediterranean, where scientists and fishermen have collaborated to trial semi-pelagic and pelagic trawl doors, which have little or no contact with the seabed, while engaged in demersal or bottom fishing (Palanques et al., 2018). This, by extension, could see a reduction in trawl door dragging noise input to the water column, along with the intended benefits of reduction in seafloor damage, sediment transport and horsepower/fuel.

The aim of the work presented here is to add trawler noise to the list of anthropogenic stressors on the marine acoustic habitat (Merchant et al., 2015), that includes ship noise (Erbe et al., 2019), pile driving (e.g., Bailey et al., 2010) and seismic surveys (Gordon et al., 2003; Madsen et al., 2006; Cato et al., 2013) responsible for the behavioural disturbance and ultimate harm (Southall et al., 2007; Finneran, 2015; Tougaard et al., 2015) to marine mammals and other marine fauna. In an ocean already faced with plastic pollution and climate change, where a warming, more acidic ocean might drive an even noisier acoustic habitat (Hester et al., 2008), a better understanding of trawler noise pollution will underline it as another known anthropogenic stressor. At a policy level there is a lack of regulation around noise pollution in the ocean from all anthropogenic sources, including bottom trawling, although various management strategies are becoming more widely recognised as necessary mitigation tools (Merchant, 2019). In addition to

continent-wide regulations (such as the MSFD and the MSPD), strategies at a national/regional level can further address noise pollution, an example being the OSPAR Commission's Impulsive Noise Register (INR) (Merchant et al., 2020). Other initiatives, such as the work output on underwater noise proposed by Canada (MEPC 75/14) to the International Maritime Organisation (IMO), that aims to deal with vessel noise mitigation by enhancing existing international guidelines (IMO, 2014), which encourage both technological solutions (e.g., propeller and hull improvements) and avoidance of sensitive areas. The work carried out in this paper highlights bottom trawling as a source of noise that needs consideration for any future mitigation strategies being developed. It also highlights submarine canyons as areas that focus or channel noise and warrant inclusion to any upcoming avoidance strategies, for example, through Special Areas of Conservation (SACs) or deep water Marine Protected Areas (MPAs) (e.g., Williams et al., 2015) aimed at preserving the marine environment.

In conclusion, this paper has displayed results of observed noise levels emanating from two trawling events in contrasting settings, along with control measures of ambient and research vessel noise. Bottom trawling is found to be louder than all other sources measured and above potential levels of harm to marine fauna, in particular resident and transient marine mammals. Modelling techniques have allowed for source estimates from active trawling that are comparable to other noise polluting sources, such as shipping noise or offshore hydrocarbon extraction. Seabed sourced sounds from trawl gear dragging along the bottom is modelled as propagating more efficiently than fishing vessel sounds at the surface. Submarine canyons are identified as potential hotspots for noise focussing along the continental margin. Trawling noise outputs are highlighted here as cause for concern, being a source of pollution that compounds the existing stressors imposed by the trawl fishing industry on the regional marine environment, especially in ecologically sensitive settings, such as the European continental margin.

## Acknowledgements

**6.5. Supplement** (for thesis manuscript only)

The lead author's contribution to the work was:

- Led Scientific rationale and survey design following a preparatory desk study and securing the required equipment

- The successful competitive ship-time proposal was written in the most part by the lead author

- Led experimental design and procurement equipment including the seismic source

- Analysis and interpretation of observational data (acoustic and hydrographic including the Glider)

- Structured the layout, writing, literature review and figure plotting with the co-author advising on structure or layout when needed and thoroughly reviewing the literary process

- The lead author coordinated with the publishers and peer reviewers, making the necessary manuscript changes to resubmit the final, accepted draft

# Chapter 7: Synthesis and Future Study

## 7.1. Synthesis of Key Findings

This project has investigated anthropogenic noise as it propagates through the ocean's water column, across the continental margin between deep ocean and shallow waters. Moving from a wider study of an industrial seismics noise field in the deeper north Porcupine Basin (PB), a localised experiment has focussed on the varying topographies (submarine canyon and slope) of the margin from offshore seismics and trawling industries on the PB's eastern flank. This study of human noise, unique to the region, has used novel analysis methods to provide greater understanding of the physical processes of sound propagation, especially within canyons, and to draw attention to new sources of harmful noise not described in the literature.

### 7.1.1. The Porcupine Basin sound field

To assess the regional scale sound field of the north PB using medium to long-range pathways (5 – 73 km) of seismic survey sourced noise, a pre-existing dataset (Crawford, 2016) was utilised and re-analysed. The purpose being to quantify variation in received sound with range, depth, and slope angle, along with the added benefit of providing a foundation for the overall project with respect to underwater acoustic processing, analysis and modelling. As part of this process, a tailored method of manually identifying airgun shots through computer code was developed and further refined for later experiment analysis.

No received levels of noise from Chapter 4 (Daly et al., 2020) were above TTS levels, reinforcing both the need to view these findings in terms of behavioural disturbance and the limitations of the available data, such as not being any closer to source than 5 km. First order estimations of PTS onset were put at approximately 40 m from source but were not rigorous enough for reporting as results. Received levels were found to be higher over a deepening slope than a shoaling one of similar range (~10 dB re: 1 µPa$^2$s between 5° up Vs down-slope) and highest below the thermocline in summer (~8 dB re: 1 µPa$^2$s between summer and winter), identifying

seasonality and slope angle as components of sound propagation in the PB. However, results in this respect are frequency dependent and not fully consistent, suggesting the need to contextualise findings within an envelope of values, or with an associated level of uncertainty when assessing direction or seasonality per range.

The complex nature of the results found in Chapter 4, for example, the signatures and arrival times of shots discussed in the final section, identifies a non-trivial relationship between the multifaceted controls of noise propagation in this region. Findings reported on the PB sound field provided a backdrop of deep ocean and long-range pathways that the following chapters could be built upon. Non-damaging levels at greater ranges, comparison of slope variation and seasonal differences showed that a more localised study across margin over differing topography would be required to greater understand the variation and potential harm from anthropogenic noise propagation.

### 7.1.2. Across margin controls on anthropogenic noise

The primary emphasis in Chapter 5 was to investigate the differences in received sound levels between a submarine canyon and a typical slope, both along and transverse to canyon axis on contrasting pathways, some of which were at comparable ranges. Levels were higher both up canyon towards the shelf edge and across canyon compared to slope values of similar range from source, indicating topography as a major control on propagation within the study area. As with many of the findings of the overall project, due to the complex nature of ocean sound propagation and the multiple physical control types, the results were neither straight forward nor linear. For example, 90% energy SELs from time domain analysis were not directly proportional to banded SELs from spectral analysis. Rise times from zero to peak and from 5 to 95% energy were likewise not proportional over similar ranges. Hence, there is a need for further work as discussed in section 7.2.

Ambient noise levels, while similar in comparison to the ObSERVE survey site just outside the PB (Berrow et al., 2018), were found to be considerably variable (both spatially and temporally) prompting the further, more in-depth analysis of this noise. Analysis carried out at the PANiC site was conveniently utilised in Chapter 6 (Daly and White, 2021), when comparing 1/3 octave levels of sound with trawling activity

and the nearby research vessel. Levels were not directly comparable to Chapter 4 due to the fact that for the north PB sound field, ambient levels were orders of magnitude lower than the received airgun signal (even at long range) and were considered insignificant and consequently were not analysed in detail.

Hydrography was examined in detail using all available oceanographic data, and although watermass properties were consistent throughout the survey area, there was strong indication of a dynamically stratified water column, including the probable presence of IWs and solitons. Tidally induced perturbations in the pycnocline in turn will introduce further variability in sound propagation, additional to variation already caused by the contrasting topography. To what degree IWs will alter received sound levels as a control compared to topography has not been constrained quantitatively in this study and would need further analysis following methods used in similar studies (e.g. Zhou et al., 1991; Lynch et al., 2003; Duda, 2004). However, the presence and potential location of IW generation could be tentatively eluded to using timing differences of solitons at various moorings.

Findings from Chapter 5 were very much informed by the previous work carried out in Chapter 4, not only in terms of identifying the more varied topography of the margin as an area that needed examination. Chapter 4 provided evidence from an industrial airgun array, convenient for comparison with our single gun used during PANiC. A crucial aspect found during the PANiC airgun analysis is how noise is channelled up-canyon, and when combined with the results of the trawling analysis in Chapter 6, highlights submarine canyon topography as a mechanism for two-way enhancement of anthropogenic noise propagation across the continental margin. One of the key implications of topography being identified as a critical propagation control is that these canyon settings may be more susceptible to harmful noise levels for any marine fauna present, for instance beaked whales (Barlow and Gisiner, 2006; Cox et al., 2006). The fact that canyons may channel noise through them and potentially focus noise within canyon, through resonance or reflection forced by steep topography, holds biological implications for these ecological hotspots.

*7.1.3. Trawling noise*

Trawling noise has been presented here as a considerable source of sound energy, within a sensitive ecological setting, through analysis carried out in Chapter 6, in a manner that has not been described previously. Not only are sound levels high when compared to ambient or research vessel noise, and channel noise down-canyon as mentioned previously but are considerable when compared to other sources of human noise, such as shipping or drilling for hydrocarbons (Parnum et al., 2013; Erbe et al., 2019). The fact that trawling noise has been found through modelling to propagate more efficiently when sourced on the seabed (i.e. trawl gear), underpins the idea that bottom trawling holds potential to increase disturbance to marine life when compared to shipping.

Trawling noise is not the only adverse anthropogenic impact. Bottom trawling is known to hold the greatest impact on the oceans, with effects greater than all other human activity combined (Halpern et al., 2008; Benn et al., 2010). Work carried out on bottom trawling at a larger canyon system approximately 220 km to the south at Whittard Canyon, has found statistical relationships between trawling and seafloor rugosity, that infer anthropogenic smoothing of the seafloor around canyon interfluves that are more heavily fished (see Appendix B; Daly et al., 2018). Trawl plumes of suspended sediment, holding enhanced turbulent energy and density overturns, were detected at depths much greater than the fishing occurrence, which as a result heterogeneously altered food source supply to benthic organisms found in-canyon (Appendix B). A possible benefit of such activity in the context of global climate change is the potential for trawling to transport and sequester carbon rich sediments to the deeper abyssal ocean floor (e.g. Holt et al., 2009).

The contrasting anthropogenic source types investigated here between impulsive or transient airgun shots and continuous trawling noise, not only required differing analysis methods and sound metrics but furthermore reflected the different effects and implications between them. Trawling noise is mostly localised and less intensive at range from source, although it is more pervasive and most commonly located in areas along the shelf edge coincident with enhanced marine mammal activity. Offshore seismic surveys, in contrast, are more sporadic, more seasonal and often over deeper water, away from slope or canyon but hold greater potential for PTS and TTS with range, due to highly intensive noise outputs (McCauley et al., 2000).

Canyons at these latitudes are known for their diverse assemblage of marine fauna based around cold water coral and sponge habitats (Freiwald et al., 2004), and as a popular setting for deep diving whales (e.g. Barlow and Gisiner, 2006). Bottom trawling, propagating noise down-canyon from the shelf break will expose these sensitive marine mammals to levels well above the natural background noise. With the potential for this noise to get ducted into the deep sound channel and increase general ocean levels of ambient noise, coupled with the particularly pervasive presence of trawling along the shelf edge (e.g. Fig. 2.4 from Chapter 2), makes them a notable source of disturbance potential, for instance through communication masking (Erbe et al., 2016b).

The principle findings and key implications from the three main results chapters outlined herein, hold significance both in terms of our understanding of physical propagation processes across margin within this thesis and in aligning with current policy and mitigation measures discussed in the following section.

## 7.2. Significance of results

Have the core research questions been answered or comprehensively addressed? Principally they have, in that they provide analytical results and findings significant to the objectives of each study component. Long-range and shorter sonic pathways vary in propagation (or transmission loss) when compared over equal range and/or differing slope angles and depths, illustrating that levels picked up by a receiver (hydrophone or mammal) will not only depend on distance from source. Canyons have been identified as locations of enhanced noise propagation, albeit in a complex manner, being a function of many independent physical parameters. Bottom trawling, as a source of anthropogenic noise needs to be added to the already large list of known adverse impacts on the natural marine environment resulting from this activity. All of the above findings have different grades of usefulness and implications for current and future policy and mitigation strategy development. Policies like the MSFD recognised globally as being at the forefront of regulating anthropogenic noise pollution (Van der Graaf et al., 2012), or nationally in Ireland through the (soon to be published) National Marine Planning Framework (NMPF), aim to limit the damage from human development and extraction of natural

resources from the ocean. Mitigation measures, for example, seismic survey exclusion zones or areas requiring extra protection of their ecosystems (e.g. MPAs; Williams et al., 2015; Marine Protected Area Advisory Group, 2020), can be expanded or reduced in size and finely tuned using evidence-based research, including from the findings herein. This could allow continuation of activity related to societal benefit, such as provision of food or energy supply, while further protecting sensitive ecosystems and maintaining biodiversity, when compared to strategies of the past (or lack thereof). Another mitigation strategy which Chapter 6 has helped draw attention to, is that of using pelagic or semi-pelagic trawl doors that 'float' or 'glide' just above the seafloor while keeping the trawl net open, an example of which is being pioneered in the Mediterranean between scientists and fishermen (Palanques et al., 2018). These would replace the heavier, more destructive demersal trawl door, which drags along the bottom, impacting the seabed, the wildlife and as we now know, addition of sound energy to the acoustic habitat.

A further issue that this project has helped identify is the difficulties in measuring, monitoring and modelling ocean noise that any signatory nation of afore mentioned directives must adhere to. These difficulties have been found to be multifaceted. The sheer time, effort and expense of launching an acoustics observation platform, even for a short-term deployment over a small geographical area, coupled with the analysis and disseminating of the resulting large dataset is very substantial, as this project has demonstrated. The resources required to long-term monitor Ireland's offshore expanse (or even vaster, to regionally monitor across the European continental margin and shelf), in terms of finance, technology and expertise are massive and as yet are far short of what the MSFD stipulates as required for addressing anthropogenic noise pollution in the near future. This is where acoustic modelling might assist, however, it is suspected that 3D full waveform modelling is not yet near capable of the task (see next section for details), nor is 2D range dependent modelling capacity realistic over the varied depths, geomorphologies, water column dynamics and immense size of the continental margin and adjacent deep ocean and shelf seas. Modelling capacity, no matter how useful it is for understanding transmission loss on individual studies, does not provide a unique solution to long-term (or seasonal) large scale monitoring or prediction of underwater noise, especially without validation using observed data.

In order to successfully monitor noise or refine marine mammal threshold assessment, it is essential to assess the natural variability and sources of error involved. As already underlined, this variability is complexly distributed in space, time and frequency, especially across the changing and more extreme topography of the continental margin and from varying source types, both natural and anthropogenic. These complexities introduce a natural uncertainty envelope within the findings, caused to a large degree by the variable and interdependent sound controls acting on noise propagation. Some errors have been impossible to constrain quantitively, for instance, possible instrument and mooring self-noise, or assessing to what degree parasitic water current noise (as it passes over the hydrophones) varies with respect to temporal background noise variation at low to very low frequencies. Modelling comes with its own assumptions and limitations, and though it is believed that the best model choice and geoacoustic parameters have been used, there remains intrinsic model error purely from being derived independently of observed sound values. Parameters used for calculating values from a number of sound metrics have been somewhat arbitrary, while still making a best attempt at accurate measurement. For example, using 60 s segments for assessing continuous noise is not a standardised duration and only used in some studies (e.g. MacDonnell, 2017). This stresses the difficulties the marine acoustic research community has had in fully standardising analysis (and modelling) methods, metrics and parameters across many differing research applications (Robinson et al., 2014; Wang et al., 2019).

Assessing damage thresholds for marine mammals has involved considerable work from many research groups over the years and still relies on some very wide assumptions in understanding the physiology of large and wild marine megafauna (e.g. Southall et al., 2007, 2019 and references within). Assessing behavioural disturbance in its many forms, from various anthropogenic sources, is yet more difficult still. Work is only at early stages and perhaps a long way off achieving a defined set of threshold levels. Nonetheless it is hoped that work from this PhD project can inform and feed into such studies to help evaluate potential harm to the natural marine environment.

One of the benefits experienced during this project, through sharing of data and knowledge, is that of industrial engagement in relation to seismic surveys and the environment. Industry representatives have displayed a genuine interest and

eagerness to engage with environmental protection and mitigation against damage. This engagement is clearly required and will need to be encouraged (or enforced?) within the fishing industry and for contractors involved in near-future piledriving for offshore windfarm development.

The suitability of using a single airgun as a controlled source for the PANiC survey as a proxy for a full industrial survey may be brought into question. Granting these sources are not directly scalable in noise terms; the source generated from an airgun array and a single gun share many similar characteristics and are qualitatively comparable. The fact that successful findings were achieved with a single gun, to demonstrate the impacts of human noise pollution in the vicinity of a sensitive submarine canyon, can only prove that an industrial airgun array would impose considerably higher magnitude impacts.

Acoustic modelling of underwater sound is a powerful tool in understanding and monitoring anthropogenic noise. Even though this PhD project has relied heavily on observed and recorded acoustic data, it has also used 2D Parabolic Equation (PE) modelling to examine, contrast and infer many propagation processes and controls. Some of the findings of note from the modelling work were the source estimates from trawling and the differentiating between sources at the sea surface and seafloor. Similarly, real and exaggerated up and down-slope propagation models from Chapter 4 provided variance in levels used to further understand the topographic effects of canyons in Chapter 5.

## 7.3. Future research and outlook

Future regional scale monitoring, incorporating new technologies (e.g. real-time data retrieval) needs feasibility assessment and development now. For example, compiling baseline studies, including this one and others (e.g. McCauley, 2015; Berrow et al., 2018), could initiate the monitoring of long-term change in ocean noise in the Irish EEZ due to anthropogenic forcing and help develop any regional noise registers in line with the NMPF in Ireland. Similar to existing guidelines on impulsive noise, new guidelines will need to be developed that take into consideration new mitigation technologies. For instance, upcoming piledriving activity which should

make use of bubble curtains to dampen horizontal noise propagation. Naval active sonar is another noise source that urgently needs tackling to prevent further marine mammal strandings, but efforts will most likely be stifled by strategic military operations taking precedence over environmental concerns. There are recent and upcoming initiatives with standardised sets of metrics to quantify anthropogenic noise in the Northeast Atlantic (OSPAR, 2017; Thomisch et al., 2021), where existing and future stand-alone studies (including this one) could be adjusted to align with these programmes. A biological aspect and expertise could be added to projects like this one, to assess damage or disturbance, not only to marine mammals but to other fauna, such as fisheries target species, who use the continental margin for spawning grounds and to disperse their larvae using physical oceanographic processes (e.g. Bartsch and Coombs, 1997). Climate change and atmospheric $CO_2$ input to the North Atlantic will drive a warmer ocean and altered large scale circulation, continental margin processes and seasonal stratification. This in turn will have a greater control on how noise propagates across the margin and onto shelf seas requiring further research into the future.

Complexities and differences in sound metric values (e.g. peak levels, SPL, SEL, and rise times), per pathway (already discussed), were not consistent with common range or topography in this study. What causes these inconsistencies and non-linear relationships between individual metrics per pathway or per range? What methods can be used to assess these and would it be a viable gain of knowledge and research output? To answer these questions a technical follow-up from results found here is suggested. Ambient spikes in spectral densities identified in Chapter 5 between 100 and 250 Hz would likewise benefit from further research to ascertain where they are sourced from. Are they mooring, vessel or background noise or harmonics of one of these? Are they from far off storms and what is their overall significance? It may be possible to use rise times of zero-peak and 90% energy SELs to investigate the occurrence of resonance or focussing of noise within canyon. These and other metrics may be combined with advanced or upcoming modelling systems to ground-truth and broaden understanding of in-canyon noise.

As part of this project, a feasibility study was carried out into applying a 3D acoustic model to the canyon and adjacent slope in collaboration with Dr. Florian Le Pape, a researcher with DIAS Geophysics (Dublin Institute for Advanced Studies). As a test case, Le Pape developed a finite element, full waveform 3D model for the study

area using the software SPECFEM-3D, which is more often applied to lower frequencies from seismic events. Screenshots of the model run at 2 s intervals show the progression of acoustic waves from a 5 Hz source ($\lambda$ = ~500 m) upslope through the canyon from the bottom left of each image (F. Le Pape 2021, personal communication) (Fig. 7.1; with permission). One interesting feature of note is at T = 13 s into the run there appears to be a higher intensity deviation of propagation direction into a minor gully on the northern flank of the canyon underlining the model's potential to identify topographic controls. It was found that computational overheads limited the model to a maximum of ~25 – 30 Hz for the entire area of the PANiC site. It was also found that by cutting the area size down to a narrow patch directly over the canyon, a frequency of up to 50 Hz was feasible. Adding real data for water column sound speed and using observed sound levels for training the model would be relatively straight forward to implement and not computationally expensive (although these were not carried out on this test case). The main issue remained that the number of finite elements that needed processing through the model algorithms grew exponentially with increasing frequency (i.e. shorter wavelengths). This imposes a major limitation on modelling seismic survey or trawling noise that peak within the 100 – 1000 Hz decade band and extend well beyond it. Notwithstanding these limitations, with future improvements in computation capacity, model refinement and possibly using a less detailed model choice, 3D modelling could become more viable. For instance, over small, focussed areas of ecological concern or over shelf water windfarm developments and piledriving in an effort to help Ireland meet its commitments to monitor and regulate anthropogenic ocean noise.

The future outlook for marine acoustics research in Ireland will depend on further and strengthened collaborations within and outside of national research institutes and state agencies, in order to build capacity, expertise and management strategies and to comply with EU directives. Initiatives such as JONAS (JONAS, 2019) and SATURN (SATURN, 2021), which are regional international collaborations between acoustic and biological impact research groups (both coordinated from Ireland) go a long way to mounting a comprehensive effort to tackle the impacts of noise pollution. A word of caution may be included for any future programmes monitoring the Irish offshore soundscape, where models, ideally open-source, are observationally validated and sufficient to reflect at least some of the natural envelope of noise levels at a local geographical scale, as discussed earlier within
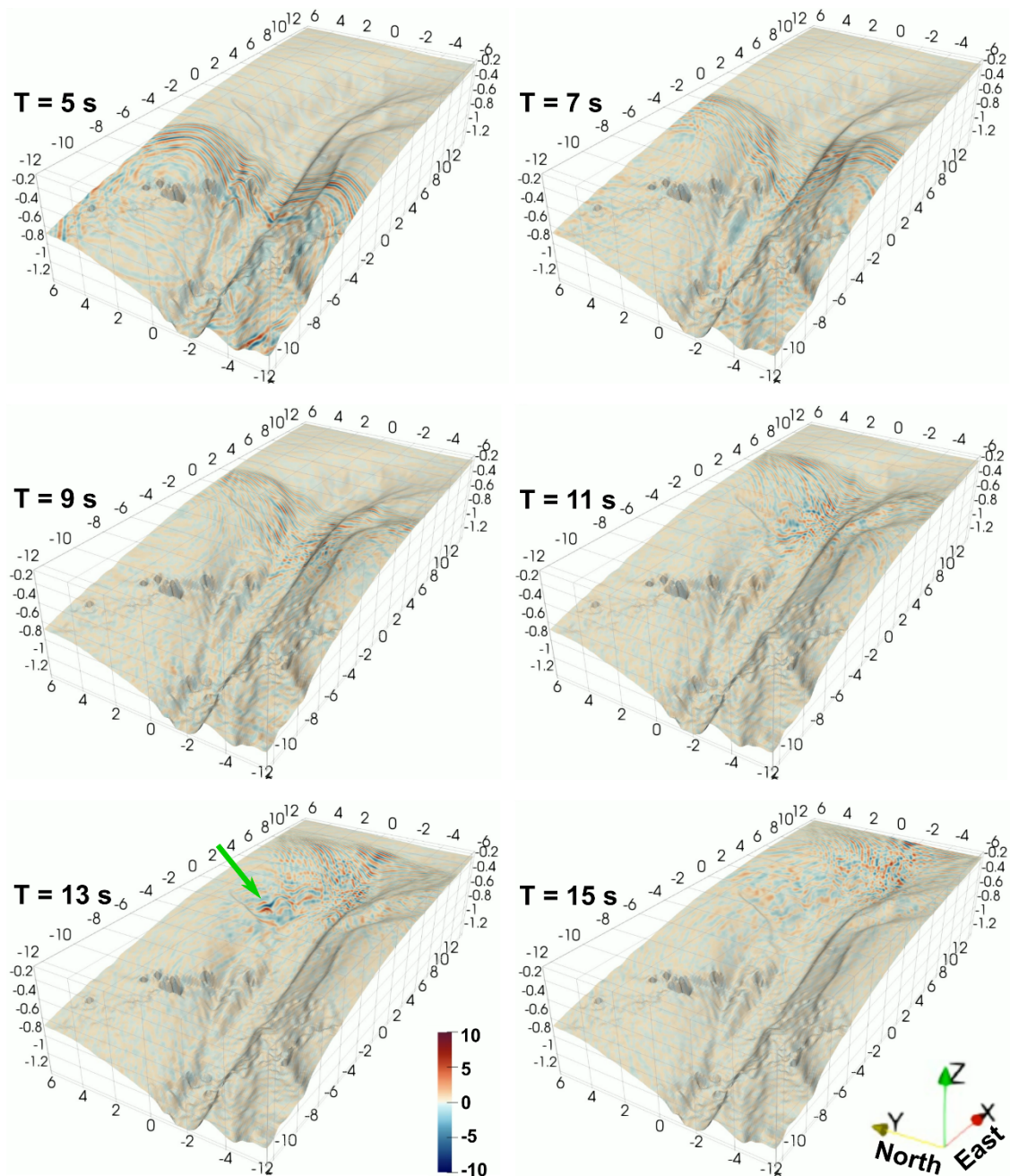
**Fig. 7.1.** SPECFEM-3D model run at 5 Hz at 2 s intervals starting at T = 5 s into the run. Source position is (-12, 0, 0) in the X-Y-Z space, or at the bottom left of each tile at the sea surface. The model slice displayed here is at or just above bottom depths. Green arrow indicates probable focussing of higher intensity levels at a northern gully off the main axis at T = 13. Please zoom in for better detail if viewing an electronic version of the manuscript. Adapted with permission from Florian Le Pape.

the context of complex propagation controls. Perhaps a working-group or framework for operational modelling of sound, at a national level, could attain consensus from key research groups and governing bodies for a future roadmap to

monitoring the environmental status of ocean noise pollution (or even improve it). Within Ireland the new NMPF will include an impulsive noise register to address these sources of noise. Any impulsive noise register developed for the Irish ocean territory should explicitly aim to comply with and feed into existing noise registers, play an active role in developing standardised criteria and consider adding a continuous noise register or similar mechanism to its framework. For example, the Open Portal to Underwater Soundscapes (OPUS) (Thomisch et al., 2021), is an upcoming initiative closely aligned with where Irish marine acoustics research could aim to achieve or collaborate with.

It is the responsibility of a scientist in this field, not only to investigate and understand the physical processes and impacts of ocean noise pollution but to publicly communicate and provide evidence-based research to policy makers in this regard (please see Appendix D for a list of public engagement activities conducted as part of this PhD project). This is especially true when the research is publicly funded. That said, the burden of responsibility lies on those policy makers and governance to tackle ocean noise pollution head on, through regulation and enforcement and by incentivising collaboration and engagement across the sector, including relevant research disciplines and directly within industry.

## 7.4. Conclusions

The aim of this project has been to enhance our understanding of anthropogenic noise propagation in the ocean, especially across the Irish continental margin, where geomorphology and ecological susceptibility are heightened. To do this, noise propagation has been characterised in terms of source type, physical controls, background noise and geoacoustic parameters using observed data through offshore experiment, modelling tools and building on previous work. Topography has been highlighted as a major control, in both directions across the margin, with submarine canyons identified as a focus for noise and a conduit for noise propagation. By reporting sound levels from various human sources and ambient noise, this project can join previous work as a baseline study on the effects of ocean noise. With these findings and through collaborations forged during the project, capacity can be built for measuring, monitoring and modelling noise in an

Irish context, while identifying areas of concern or that require further development, such as 3D modelling.

It is planned that this project in some way helps to protect the marine ecosystems found along the continental margin, by providing evidence for prevention and mitigation measures for harm and widespread disturbance. By further developing and resourcing projects such as this, it is hoped that Ireland cannot just comply with but lead in protecting its resident and transient marine mammals, for instance through deep water MPAs or SACs around hotspots for biodiversity and noise, including submarine canyons. This action will lessen the anthropogenic impact on the natural marine acoustic habitat. In an ocean enduring a myriad of human pressures, worsening year on year, the onus is on us as marine scientists to push through with cutting edge research and innovation to help combat the huge environmental crises that the planet and humanity are facing.

# References:

Abileah, R., Lewis, D., 1996. Monitoring high-seas fisheries with long-range passive acoustic sensors. Presented at the OCEANS 96 MTS/IEEE Conference Proceedings. The Coastal Ocean-Prospects for the 21st Century, IEEE, pp. 378–382. https://doi.org/10.1109/oceans.1996.572776

Ainslie, M., de Jong, C., Miksis-Olds, J., 2019. IQOE Workshop Report: Guidelines for Observation of Ocean Sound, 13 July 2019, Park Hotel, Den Haag, Netherlands.

Ainslie, M.A., 2010. Principles of sonar performance modelling. Springer.

Amaro, T., de Stigter, H., Lavaleye, M., Duineveld, G., 2015. Organic matter enrichment in the Whittard Channel; its origin and possible effects on benthic megafauna. Deep Sea Research Part I: Oceanographic Research Papers 102, 90–100. https://doi.org/10.1016/j.dsr.2015.04.014

Amaro, T., Huvenne, V.A.I., Allcock, A.L., Aslam, T., Davies, J.S., Danovaro, R., De Stigter, H.C., Duineveld, G.C.A., Gambi, C., Gooday, A.J., Gunton, L.M., Hall, R., Howell, K.L., Ingels, J., Kiriakoulakis, K., Kershaw, C.E., Lavaleye, M.S.S., Robert, K., Stewart, H., Van Rooij, D., White, M., Wilson, A.M., 2016. The Whittard Canyon – A case study of submarine canyon processes. Progress in Oceanography 146, 38–57. https://doi.org/10.1016/j.pocean.2016.06.003

Andrew, R., Howe, B., Mercer, J., Dzieciuch, M., 2002. Ocean ambient sound: comparing the 1960s with the 1990s for a receiver off the California coast. ARLO 3: 65.

Andrew, R.K., Howe, B.M., Mercer, J.A., Dzieciuch, M.A., 2002. Ocean ambient sound: Comparing the 1960s with the 1990s for a receiver off the California coast. Acoustics Research Letters Online 3, 65–70. https://doi.org/10.1121/1.1461915

Arhan, M., King, B., 1995. Lateral mixing of the Mediterranean Water in the eastern North Atlantic. Journal of Marine Research 53, 865–895. https://doi.org/10.1357/0022240953212990

Arjona-Camas, M., Puig, P., Palanques, A., Emelianov, M., Durán, R., 2019. Evidence of trawling-induced resuspension events in the generation of nepheloid layers in the Foix submarine canyon (NW Mediterranean). Journal of Marine Systems 196, 86–96. https://doi.org/10.1016/j.jmarsys.2019.05.003

Arveson, P.T., Vendittis, D.J., 2000. Radiated noise characteristics of a modern cargo ship. The Journal of the Acoustical Society of America 107, 118–129. https://doi.org/10.1121/1.428344

Aslam, T., Hall, R.A., Dye, S.R., 2018. Internal tides in a dendritic submarine canyon. Progress in Oceanography, Bridging the gap between the shallow and deep oceans: The key role of submarine canyons 169, 20–32. https://doi.org/10.1016/j.pocean.2017.10.005

Au, W.W.L., Banks, K., 1998. The acoustics of the snapping shrimp Synalpheus parneomeris in Kaneohe Bay. The Journal of the Acoustical Society of America 103, 41–47. https://doi.org/10.1121/1.423234

Azevedo, A., da Silva, J.C., New, A.L., 2002. Possible generation sites of internal solitary waves observed by ERS SAR in the central region of the Bay of Biscay. Presented at the IEEE International Geoscience and Remote Sensing Symposium, IEEE, pp. 1600–1602.

Badiey, M., Katsnelson, B.G., Lin, Y.-T., Lynch, J.F., 2011. Acoustic multipath arrivals in the horizontal plane due to approaching nonlinear internal waves. The Journal of the Acoustical Society of America 129, EL141–EL147. https://doi.org/10.1121/1.3553374

Badiey, M., Mu, Y., Lynch, J., Apel, J., Wolf, S., 2002. Temporal and azimuthal dependence of sound propagation in shallow water with internal waves. IEEE Journal of Oceanic Engineering 27, 117–129. https://doi.org/10.1109/48.989898

Bagocius, D., 2013. Underwater noise generated by the detonation of historical ordnance in the Baltic Sea, Lithuania: potential ecological impacts on marine life. Baltica 26, 187–192. https://doi.org/10.5200/baltica.2013.26.19

Bailey, H., Senior, B., Simmons, D., Rusin, J., Picken, G., Thompson, P.M., 2010. Assessing underwater noise levels during pile-driving at an offshore windfarm and its potential effects on marine mammals. Marine pollution bulletin 60, 888–897. https://doi.org/10.1016/j.marpolbul.2010.01.003

Baines, M., Reichelt, M., Griffin, D., 2017. An autumn aggregation of fin (Balaenoptera physalus) and blue whales (B. musculus) in the Porcupine Seabight, southwest of Ireland. Deep Sea Research

# References

Part II: Topical Studies in Oceanography, Abundance, distribution and habitats of Atlantic and Mediterranean marine megafauna 141, 168–177. https://doi.org/10.1016/j.dsr2.2017.03.007

Barile, C., Berrow, S., Parry, G., O'Brien, J., 2021. Temporal acoustic occurrence of sperm whales Physeter macrocephalus and long-finned pilot whales Globicephala melas off western Ireland. Marine Ecology Progress Series 661, 203–227. https://doi.org/10.3354/meps13594

Barlow, J., Ferguson, M.C., Perrin, W.F., Ballance, L., Gerrodette, T., Joyce, G., Macleod, C.D., Mullin, K., Palka, D.L., Waring, G., 2005. Abundance and densities of beaked and bottlenose whales (family Ziphiidae). Journal of Cetacean Research and Management 7, 263.

Barlow, J., Gisiner, R., 2006. Mitigating, monitoring and assessing the effects of anthropogenic sound on beaked whales. Journal of Cetacean Research and Management 7, 239–249.

Bartsch, J., Coombs, S., 1997. A numerical model of the dispersion of blue whiting larvae, Micromesistiuspoutassou (Risso), in the eastern North Atlantic. Fisheries Oceanography 6, 141–154. https://doi.org/10.1046/j.1365-2419.1997.00036.x

Beck, S., O'Connor, I., Berrow, S., O'Brien, J., 2013. Assessment and monitoring of ocean noise in Irish waters. STRIVE Report Series No. 120.

Benn, A.R., Weaver, P.P., Billet, D.S., Van Den Hove, S., Murdock, A.P., Doneghan, G.B., Le Bas, T., 2010. Human activities on the deep seafloor in the North East Atlantic: an assessment of spatial extent. PloS one 5, e12730. https://doi.org/10.1371/journal.pone.0012730

Bernaldo de Quirós, Y., Fernandez, A., Baird, R., Brownell Jr, R., Aguilar de Soto, N., Allen, D., Arbelo, M., Arregui, M., Costidis, A., Fahlman, A., 2019. Advances in research on the impacts of anti-submarine sonar on beaked whales. Proceedings of the Royal Society B 286, 20182533. https://doi.org/10.1098/rspb.2018.2533

Berrow, S., 2001. Biological diversity of cetaceans (whales, dolphins and porpoises) in Irish waters. Presented at the Marine biodiversity in Ireland and adjacent waters. Proceedings of a conference, pp. 115–119.

Berrow, S., O'Brien, J., Meade, R., Delarue, R., Kowarski, K., Martin, B., Moloney, J., Wall, D., Gillespie, D., Leaper, R, Gordon, J, Lee, A, Porter, L, 2018. Acoustic Surveys of Cetaceans in the Irish Atlantic Margin in 2015–2016: Occurrence, distribution and abundance. Department of Communications, Climate Action & Environment and the National Parks and Wildlife Service (NPWS), Department of Culture, Heritage and the Gaeltacht, Dublin, Ireland.

Berrow, S., Whooley, P., O'Connell, M., Wall, D., 2010. Irish Cetacean Review (2000-2009). Irish Whale and Dolphin Group, 60pp.

Billett, D., Lampitt, R., Rice, A., Mantoura, R., 1983. Seasonal sedimentation of phytoplankton to the deep-sea benthos. Nature 302, 520–522. https://doi.org/10.1038/302520a0

Blair, H.B., Merchant, N.D., Friedlaender, A.S., Wiley, D.N., Parks, S.E., 2016. Evidence for ship noise impacts on humpback whale foraging behaviour. Biology letters 12, 20160005. https://doi.org/10.1098/rsbl.2016.0005

Boyd, I.L., Frisk, G., Urban, E., Tyack, P., Ausubel, J., Seeyave, S., Cato, D., Southall, B., Weise, M., Andrew, R., 2011. An international quiet ocean experiment. Oceanography 24, 174–181. https://doi.org/10.5670/oceanog.2011.37

Breitzke, M., Bohlen, T., 2010. Modelling sound propagation in the Southern Ocean to estimate the acoustic impact of seismic research surveys on marine mammals. Geophysical Journal International 181, 818–846.

Buerkle, U., 1977. Detection of trawling noise by Atlantic cod (Gadus morhua L.). Marine & Freshwater Behaviour & Phy 4, 233–242. https://doi.org/10.1080/10236247709386955

Buerkle, U., 1973. Gill-net catches of cod (Gadus morhua L.) in relation to trawling noise. Marine & Freshwater Behaviour & Phy 2, 277–281. https://doi.org/10.1080/10236247309386930

Burgess, A.S., Kewley, D.J., 1983. Wind-generated surface noise source levels in deep water east of Australia. The Journal of the Acoustical Society of America 73, 201–210. https://doi.org/10.1121/1.388840

Canals, M., Puig, P., de Madron, X.D., Heussner, S., Palanques, A., Fabres, J., 2006. Flushing submarine canyons. Nature 444, 354–357. https://doi.org/10.1038/nature05271

Cannam, C., Landone, C., Sandler, M., 2010. Sonic visualiser: An open source application for viewing, analysing, and annotating music audio files. Presented at the Proceedings of the 18th ACM international conference on Multimedia, pp. 1467–1468.

# References

Carbone, N.M., Hodgkiss, W.S., 2000. Effects of tidally driven temperature fluctuations on shallow-water acoustic communications at 18 kHz. IEEE Journal of Oceanic Engineering 25, 84–94. https://doi.org/10.1109/48.820739

Carey, W.M., 2006. Sound sources and levels in the ocean. IEEE Journal of Oceanic Engineering 31, 61–75. https://doi.org/10.1109/JOE.2006.872214

Carey, W.M., 1995. Standard definitions for sound levels in the ocean. IEEE Journal of Oceanic Engineering 20, 109–113. https://doi.org/10.1109/48.376673

Carey, W.M., Evans, R.B., 2011. The Measurement of Oceanic Ambient Noise, in: Ocean Ambient Noise. Springer, pp. 45–98.

Carstensen, J., Henriksen, O., Teilmann, J., 2006. Impacts of offshore wind farm construction on harbour porpoises: acoustic monitoring of echolocation activity using porpoise detectors (T-PODs). Marine Ecology Progress Series 321, 295–308. https://doi.org/10.3354/meps321295

Carter, G.S., Gregg, M.C., 2002. Intense, Variable Mixing near the Head of Monterey Submarine Canyon. Journal of Physical Oceanography 32, 3145–3165. https://doi.org/10.1175/1520-0485(2002)032<3145:IVMNTH>2.0.CO;2

Cato, D., Noad, M., Dunlop, R., McCauley, R., Gales, N., Salgado Kent, C., Kniest, H., Paton, D., Jenner, C., Noad, J., 2013. A study of the behavioural response of whales to the noise of seismic air guns: Design, methods and progress. Acoustics Australia 41, 88–97.

Cato, D.H., 2008. Ocean ambient noise: its measurement and its significance to marine animals. Proceedings of the Institute of Acoustics 30, 1–9.

Cato, D.H., McCauley, R.D., 2002. Australlan research in ambient sea noise. Acoustics Australia 30, 13–20.

Cato, D.H., McCauley, R.D., Noad, M., 2004. Potential effects of noise from human activities on marine animals. Presented at the Annual Conference of the Australian Acoustical Society, pp. 369–374.

Chapman, N.R., Price, A., 2011. Low frequency deep ocean ambient noise trend in the Northeast Pacific Ocean. The Journal of the Acoustical Society of America 129, EL161–EL165. https://doi.org/10.1121/1.3567084

Charif, R.A., Clapham, P.J., Clark, C.W., 2001. Acoustic Detections of Singing Humpback Whales in Deep Waters Off the British Isles. Marine Mammal Science 17, 751–768. https://doi.org/10.1111/j.1748-7692.2001.tb01297.x

Charif, R.A., Clark, C.W., 2009. Acoustic monitoring of large whales in deep waters north and west of the British Isles: 1996–2005. Cornell Lab Ornithol 8, 40.

Chen, F., Shapiro, G.I., Bennett, K.A., Ingram, S.N., Thompson, D., Vincent, C., Russell, D.J.F., Embling, C.B., 2017. Shipping noise in a dynamic sea: a case study of grey seals in the Celtic Sea. Marine Pollution Bulletin 114, 372–383. https://doi.org/10.1016/j.marpolbul.2016.09.054

Chin-Bing, S.A., King, D.B., Davis, J.A., Evans, R.B., 1993. PE Workshop II. Proceedings of the Second Parabolic Equation Workshop. Naval Research Lab Stennis Space Center Ms.

Collins, M.D., 1995. User's Guide for RAM Versions 1.0 and 1.0 p. Naval Research Lab, Washington, DC 20375, 14.

Collins, M.D., 1993. A split-step Padé solution for the parabolic equation method. The Journal of the Acoustical Society of America 93, 1736–1742. https://doi.org/10.1121/1.406739

Compton, R., Goodwin, L., Handy, R., Abbott, V., 2008. A critical examination of worldwide guidelines for minimising the disturbance to marine mammals during seismic surveys. Marine Policy 32, 255–262. https://doi.org/10.1016/j.marpol.2007.05.005

Conte, M.H., Dickey, T.D., Weber, J.C., Johnson, R.J., Knap, A.H., 2003. Transient physical forcing of pulsed export of bioreactive material to the deep Sargasso Sea. Deep Sea Research Part I: Oceanographic Research Papers 50, 1157–1187. https://doi.org/10.1016/S0967-0637(03)00141-9

Cornuelle, B.D., Worcester, P.F., Dzieciuch, M.A., 2008. Ocean acoustic tomography. Presented at the Journal of Physics: Conference Series, IOP Publishing, p. 012002.

Coughlan, M., Wheeler, A.J., Dorschel, B., Long, M., Doherty, P., Mörz, T., 2019. Stratigraphic model of the Quaternary sediments of the Western Irish Sea Mud Belt from core, geotechnical and acoustic data. Geo-Marine Letters 39, 223–237. https://doi.org/10.1007/s00367-019-00569-z

# References

Cox, T.M., Ragen, T., Read, A., Vos, E., Baird, R.W., Balcomb, K., Barlow, J., Caldwell, J., Cranford, T., Crum, L., 2006. Understanding the impacts of anthropogenic sound on beaked whales. Space and Naval Warfare Systems Center San Diego Ca.

Cranford, T.W., Amundin, M., Norris, K.S., 1996. Functional morphology and homology in the odontocete nasal complex: Implications for sound generation. Journal of Morphology 228, 223–285. https://doi.org/10.1002/(SICI)1097-4687(199606)228:3<223::AID-JMOR1>3.0.CO;2-3

Crawford, S., 2016. Development of a sound propagation model to monitor seismic survey noise in Irish waters. MSc Thesis. National University of Ireland, Galway.

Crawford, S., Brown, C., McKeown, E., Stapleton, F., Duncan, A., McCauley, R., White, M., 2016. Development of a sound propagation model to monitor seismic survey noise in Irish waters. Presented at the Proceedings of Meetings on Acoustics 4ENAL, ASA, p. 070025. https://doi.org/10.1121/2.0000490

Crocker, S.E., Fratantonio, F.D., 2016. Characteristics of sounds emitted during high-resolution marine geophysical surveys. Naval Undersea Warfare Center Division Newport United States.

Croker, P., Shannon, P., 1987. The evolution and hydrocarbon prospectivity of the Porcupine Basin, offshore Ireland. Presented at the Conference on petroleum geology of North West Europe. 3, pp. 633–642.

Croker, P.F., Shannon, P.M., 1995. The petroleum geology of Ireland's offshore basins: introduction. Geological Society, London, Special Publications 93, 1–8.

CTBTO.org, n.d. CTBTO Preparatory Commission [WWW Document]. URL https://www.ctbto.org/ (accessed 3.21.21).

Curtis, K.R., Howe, B.M., Mercer, J.A., 1999. Low-frequency ambient sound in the North Pacific: Long time series observations. The Journal of the Acoustical Society of America 106, 3189–3200.

DAHG, 2014. Guidance to Manage the Risk to Marine Mammals from Man-made Sound Sources in Irish Waters. Dublin, Ireland, Department of Arts, Heritage and the Gaeltacht 58pp. http://dx.doi.org/10.25607/OBP-176

Daly, E., Johnson, M.P., Wilson, A.M., Gerritsen, H.D., Kiriakoulakis, K., Allcock, A.L., White, M., 2018. Bottom trawling at Whittard Canyon: Evidence for seabed modification, trawl plumes and food source heterogeneity. Progress in Oceanography, Bridging the gap between the shallow and deep oceans: The key role of submarine canyons 169, 227–240. https://doi.org/10.1016/j.pocean.2017.12.010

Daly, E., Jordan, S.C., White, M., 2020. Seismic Survey Sound Propagation: A Porcupine Basin Noise-field. Irish Journal of Earth Sciences 38, 25–39. https://doi.org/10.3318/ijes.2020.38.4

Daly, E., White, M., 2021. Bottom trawling noise: Are fishing vessels polluting to deeper acoustic habitats? Marine Pollution Bulletin 162, 111877. https://doi.org/10.1016/j.marpolbul.2020.111877

Davies, A.J., Roberts, J.M., Hall-Spencer, J., 2007. Preserving deep-sea natural heritage: Emerging issues in offshore conservation and management. Biological Conservation 138, 299–312. https://doi.org/10.1016/j.biocon.2007.05.011

Davies, J.S., Howell, K.L., Stewart, H.A., Guinan, J., Golding, N., 2014. Defining biological assemblages (biotopes) of conservation interest in the submarine canyons of the South West Approaches (offshore United Kingdom) for use in marine habitat mapping. Deep Sea Research Part II: Topical Studies in Oceanography, Submarine Canyons: Complex Deep-Sea Environments Unravelled by Multidisciplinary Research 104, 208–229. https://doi.org/10.1016/j.dsr2.2014.02.001

De Leo, F.C., Smith, C.R., Rowden, A.A., Bowden, D.A., Clark, M.R., 2010. Submarine canyons: hotspots of benthic biomass and productivity in the deep sea. Proceedings of the Royal Society B: Biological Sciences 277, 2783–2792. https://doi.org/10.1098/rspb.2010.0462

Dekeling, R., Tasker, M., Van der Graaf, A., Ainslie, M., Andersson, M., André, M., Borsani, J., Brensing, K., Castellote, M., Cronin, D., 2014a. Monitoring guidance for underwater noise in European seas, Part 1: Executive Summary. JRC Sci. Policy Rep. EUR 26557 EN, Luxembourg: Publications Office of the European Union.

Dekeling, R., Tasker, M., Van der Graaf, A., Ainslie, M., Andersson, M., André, M., Borsani, J., Brensing, K., Castellote, M., Cronin, D., 2014b. Monitoring guidance for underwater noise in European Seas, Part II: Monitoring guidance specifications. JRC Scientific and Policy Report EUR 26555 EN, Luxembourg: Publications Office of the European Union.

## References

DeRuiter, S.L., Hansen, M., Koopman, H.N., Westgate, A.J., Tyack, P.L., Madsen, P.T., 2010. Propagation of narrow-band-high-frequency clicks: Measured and modeled transmission loss of porpoise-like clicks in porpoise habitats. The Journal of the Acoustical Society of America 127, 560–567. https://doi.org/10.1121/1.3257203

DeRuiter, S.L., Southall, B.L., Calambokidis, J., Zimmer, W.M.X., Sadykova, D., Falcone, E.A., Friedlaender, A.S., Joseph, J.E., Moretti, D., Schorr, G.S., Thomas, L., Tyack, P.L., 2013. First direct measurements of behavioural responses by Cuvier's beaked whales to mid-frequency active sonar. Biology Letters 9, 20130223. https://doi.org/10.1098/rsbl.2013.0223

Di Iorio, L., Clark, C.W., 2010. Exposure to seismic survey alters blue whale acoustic communication. Biology Letters 6, 51–54. https://doi.org/10.1098/rsbl.2009.0651

Dillon, T.M., 1982. Vertical overturns: A comparison of Thorpe and Ozmidov length scales. Journal of Geophysical Research: Oceans 87, 9601–9613. https://doi.org/10.1029/JC087iC12p09601

Doney, S.C., 2010. The Growing Human Footprint on Coastal and Open-Ocean Biogeochemistry. Science 328, 1512–1516. https://doi.org/10.1126/science.1185198

Dragoset, B., 2000. Introduction to air guns and air-gun arrays. The Leading Edge 19, 892–897. http://dx.doi.org/10.1190/1.1438741

Dragoset, W.H., 1990. Air-gun array specs: a tutorial. The Leading Edge 9, 24–32. http://dx.doi.org/10.1190/1.1439671

Du Preez, C., 2015. A new arc–chord ratio (ACR) rugosity index for quantifying three-dimensional landscape structural complexity. Landscape Ecol 30, 181–192. https://doi.org/10.1007/s10980-014-0118-8

Duarte, C.M., Chapuis, L., Collin, S.P., Costa, D.P., Devassy, R.P., Eguiluz, V.M., Erbe, C., Gordon, T.A.C., Halpern, B.S., Harding, H.R., Havlik, M.N., Meekan, M., Merchant, N.D., Miksis-Olds, J.L., Parsons, M., Predragovic, M., Radford, A.N., Radford, C.A., Simpson, S.D., Slabbekoorn, H., Staaterman, E., Van Opzeeland, I.C., Winderen, J., Zhang, X., Juanes, F., 2021. The soundscape of the Anthropocene ocean. Science 371, eaba4658. https://doi.org/10.1126/science.aba4658

Duda, T.F., 2004. Acoustic mode coupling by nonlinear internal wave packets in a shelfbreak front area. IEEE Journal of Oceanic Engineering 29, 118–125. https://doi.org/10.1109/JOE.2003.822975

Duineveld, G., Lavaleye, M., Berghuis, E., de WILDE, P., 2001. Activity and composition of the benthic fauna in the Whittard Canyon and the adjacent continental slope (NE Atlantic). Oceanologica Acta 24, 69–83. https://doi.org/10.1016/S0399-1784(00)01129-4

Duineveld, G.C.A., Jeffreys, R.M., Lavaleye, M.S.S., Davies, A.J., Bergman, M.J.N., Watmough, T., Witbaard, R., 2012. Spatial and tidal variation in food supply to shallow cold-water coral reefs of the Mingulay Reef complex (Outer Hebrides, Scotland). Marine Ecology Progress Series 444, 97–115. https://doi.org/10.3354/meps09430

Duncan, A., 2009. Combined Sound Exposure Level Modelling for Simultaneous Operation of Two Seismic Survey Vessels in the Eendracht 3D Survey (No. C2009-28).

Duncan, A., McCauley, R., 2008. Environmental impact assessment of underwater sound: Progress and pitfalls. Presented at the Annual Conference of the Australian Acoustical Society, Australian Acoustical Society, pp. 1–8.

Duncan, A., McCauley, R., 2000. Characterisation of an air-gun as a sound source for acoustic propagation studies. Presented at the UDT Pacific 2000 Conference, Sydney Australia, pp. 7–9.

Duncan, A.J., Gavrilov, A.N., McCauley, R.D., Parnum, I.M., Collis, J.M., 2013. Characteristics of sound propagation in shallow water over an elastic seabed with a thin cap-rock layer. The Journal of the Acoustical Society of America 134, 207–215. https://doi.org/10.1121/1.4809723

Duncan, A.J., Maggi, A.L., 2006. A consistent, user friendly interface for running a variety of underwater acoustic propagation codes. Proceedings of Acoustics 2006 471–477.

Dunlop, R.A., Noad, M.J., McCauley, R.D., Kniest, E., Paton, D., Cato, D.H., 2015. The behavioural response of humpback whales (Megaptera novaeangliae) to a 20 cubic inch air gun. Aquatic Mammals 41, 412.

Dunlop, R.A., Noad, M.J., McCauley, R.D., Kniest, E., Slade, R., Paton, D., Cato, D.H., 2017. The behavioural response of migrating humpback whales to a full seismic airgun array. Proceedings of the Royal Society B: Biological Sciences 284, 20171901. https://doi.org/10.1098/rspb.2017.1901

# References

Dunn, D., Halpin, P., 2009. Rugosity-based regional modeling of hard-bottom habitat. Marine Ecology Progress Series 377, 1–11. https://doi.org/10.3354/meps07839

Duros, P., Fontanier, C., de Stigter, H.C., Cesbron, F., Metzger, E., Jorissen, F.J., 2012. Live and dead benthic foraminiferal faunas from Whittard Canyon (NE Atlantic): Focus on taphonomic processes and paleo-environmental applications. Marine Micropaleontology 94–95, 25–44. https://doi.org/10.1016/j.marmicro.2012.05.004

Duros, P., Fontanier, C., Metzger, E., Pusceddu, A., Cesbron, F., de Stigter, H.C., Bianchelli, S., Danovaro, R., Jorissen, F.J., 2011. Live (stained) benthic foraminifera in the Whittard Canyon, Celtic margin (NE Atlantic). Deep Sea Research Part I: Oceanographic Research Papers 58, 128–146. https://doi.org/10.1016/j.dsr.2010.11.008

Eastwood, P., Mills, C., Aldridge, J., Houghton, C., Rogers, S., 2007. Human activities in UK offshore waters: an assessment of direct, physical pressure on the seabed. ICES Journal of Marine Science 64, 453–463. https://doi.org/10.1093/icesjms/fsm001

Ellett, D.J., Edwards, A., Bowers, R., 1986. The hydrography of the Rockall Channel—an overview. Proceedings of the Royal Society of Edinburgh, Section B: Biological Sciences 88, 61–81. https://doi.org/10.1017/S0269727000004474

Ellett, D.J., Kruseman, P., Prangsma, G.J., Pollard, R.T., van Aken, H.M., Edwards, A., Dooley, H.D., Gould, W.J., Harvey, J.G., Woods, J.D., Businger, J.A., Charnock, H., Pollard, R.T., 1983. Water masses and mesoscale circulation of North Rockall Trough waters during JASIN 1978. Philosophical Transactions of the Royal Society of London. Series A, Mathematical and Physical Sciences 308, 231–252. https://doi.org/10.1098/rsta.1983.0002

Ellison, W., Southall, B., Clark, C., Frankel, A., 2012. A new context-based approach to assess marine mammal behavioral responses to anthropogenic sounds. Conservation Biology 26, 21–28. https://doi.org/10.1111/j.1523-1739.2011.01803.x

Erbe, C., 2013a. International Regulations of Underwater Noise. Acoustics Australia 41.

Erbe, C., 2013b. Underwater noise of small personal watercraft (jet skis). The Journal of the Acoustical Society of America 133, EL326–EL330. https://doi.org/10.1121/1.4795220

Erbe, C., 2013c. Underwater passive acoustic monitoring & noise impacts on marine fauna-a workshop report. Acoustics Australia 41, 113–9.

Erbe, C., 2011. Underwater Acoustics: Noise and the Effects on Marine Mammals, a Pocket Handbook. Jasco Applied Sciences: Halifax, NS, Canada.

Erbe, C., Liong, S., Koessler, M.W., Duncan, A.J., Gourlay, T., 2016a. Underwater sound of rigid-hulled inflatable boats. The Journal of the Acoustical Society of America 139, EL223–EL227. https://doi.org/10.1121/1.4954411

Erbe, C., MacGillivray, A., Williams, R., 2012. Mapping cumulative noise from shipping to inform marine spatial planning. The Journal of the Acoustical Society of America 132, EL423–EL428. https://doi.org/10.1121/1.4758779

Erbe, C., Marley, S., Schoeman, R., Smith, J.N., Trigg, L., Embling, C.B., 2019. The Effects of Ship Noise on Marine Mammals—A Review. Frontiers in Marine Science 6, 606. https://doi.org/10.3389/fmars.2019.00606

Erbe, C., McCauley, R., McPherson, C., Gavrilov, A., 2013. Underwater noise from offshore oil production vessels. The Journal of the Acoustical Society of America 133, EL465–EL470. https://doi.org/10.1121/1.4802183

Erbe, C., McPherson, C., 2017. Underwater noise from geotechnical drilling and standard penetration testing. The Journal of the Acoustical Society of America 142, EL281–EL285. https://doi.org/10.1121/1.5003328

Erbe, C., Reichmuth, C., Cunningham, K., Lucke, K., Dooling, R., 2016b. Communication masking in marine mammals: A review and research strategy. Marine pollution bulletin 103, 15–38. https://doi.org/10.1016/j.marpolbul.2015.12.007

Erbe, C., Williams, R., Parsons, M., Parsons, S.K., Hendrawan, I.G., Dewantama, I.M.I., 2018. Underwater noise from airplanes: An overlooked source of ocean noise. Marine Pollution Bulletin 137, 656–661. https://doi.org/10.1016/j.marpolbul.2018.10.064

Etter, P.C., 2018. Underwater Acoustic Modeling and Simulation, 5th ed. CRC Press. https://doi.org/10.1201/9781315166346

Etter, P.C., 2013. Underwater Acoustic Modeling and Simulation, 4th ed. CRC Press, Boca Raton, Fla.

# References

Etter, P.C., 2012. Advanced Applications for Underwater Acoustic Modeling. Advances in Acoustics and Vibration 2012, e214839. https://doi.org/10.1155/2012/214839

EU, 2016/2336, 2016. Council Regulation 2016/2336 of the European Parliament of 14 December 2016 establishing specific conditions for fishing for deep-sea stocks in the north-east Atlantic and provisions for fishing in international waters of the north-east Atlantic and repealing Council Regulation (EC) No 2347/2002, OJ L.

EU Atlas of the Seas, 2021. European Atlas of the Seas; interactive web-based marine geographic data application. URL https://ec.europa.eu/maritimeaffairs/atlas_en (accessed 3.21.21).

European Commission, 2008. Directive 2008/56/EC of the European Parliament and of the Council of 17 June 2008 establishing a framework for community action in the field of marine environmental policy (Marine Strategy Framework Directive). Official Journal of the European Communities 164, 19–40.

European Commission, 2018. Facts and Figures on the Common Fisheries Policy-Basic Statistical Data. https://doi.org/doi:10.2771/294952

Expedition Scientists, 2005. Modern carbonate mounds: Porcupine drilling. IODP Prel. Rept 307, 58.

Farcas, A., Thompson, P.M., Merchant, N.D., 2016. Underwater noise modelling for environmental impact assessment. Environmental Impact Assessment Review 57, 114–122. https://doi.org/10.1016/j.eiar.2015.11.012

Faulkner, R.C., Farcas, A., Merchant, N.D., 2018. Guiding principles for assessing the impact of underwater noise. Journal of Applied Ecology 55, 2531–2536. https://doi.org/10.1111/1365-2664.13161

Findlay, C.R., Ripple, H.D., Coomber, F., Froud, K., Harries, O., van Geel, N.C.F., Calderan, S.V., Benjamins, S., Risch, D., Wilson, B., 2018. Mapping widespread and increasing underwater noise pollution from acoustic deterrent devices. Marine Pollution Bulletin 135, 1042–1050. https://doi.org/10.1016/j.marpolbul.2018.08.042

Finette, S., Oba, R., Shen, C., Evans, T., 2007. Acoustic propagation under tidally driven, stratified flow. The Journal of the Acoustical Society of America 121, 2575–2590. https://doi.org/10.1121/1.2713724

Finneran, J.J., 2016. Auditory weighting functions and TTS/PTS exposure functions for marine mammals exposed to underwater noise. Space and Naval Warfare Systems Center Pacific San Diego United States.

Finneran, J.J., 2015. Noise-induced hearing loss in marine mammals: A review of temporary threshold shift studies from 1996 to 2015. The Journal of the Acoustical Society of America 138, 1702–1726. https://doi.org/10.1121/1.4927418

Finneran, J.J., Mulsow, J., Schlundt, C.E., Houser, D.S., 2011. Dolphin and sea lion auditory evoked potentials in response to single and multiple swept amplitude tones. The Journal of the Acoustical Society of America 130, 1038–1048. https://doi.org/10.1121/1.3608117

Finneran, J.J., Schlundt, C.E., Dear, R., Carder, D.A., Ridgway, S.H., 2002. Temporary shift in masked hearing thresholds in odontocetes after exposure to single underwater impulses from a seismic watergun. The Journal of the Acoustical Society of America 111, 2929–2940. https://doi.org/10.1121/1.1479150

Fofonoff, N.P., Millard Jr, R., 1983. Algorithms for the computation of fundamental properties of seawater. Unesco technical papers in marine science, 44, 58pp.

Freiwald, A., Fossa, J.H., Grehan, A., Roberts, T.K. and J.M., 2004. Cold Water Coral Reefs: Out of Sight-No Longer Out of Mind.

Galbraith, P.S., Kelley, D.E., 1996. Identifying Overturns in CTD Profiles. Journal of Atmospheric and Oceanic Technology 13, 688–702. https://doi.org/10.1175/1520-0426(1996)013<0688:IOICP>2.0.CO;2

Gedamke, J., Gales, N., Frydman, S., 2011. Assessing risk of baleen whale hearing loss from seismic surveys: The effect of uncertainty and individual variation. The Journal of the Acoustical Society of America 129, 496–506. https://doi.org/10.1121/1.3493445

Gerritsen, H., Lordan, C., 2014. Atlas of commercial fisheries around Ireland. Marine Institute.

Gerritsen, H., Lordan, C., 2011. Integrating vessel monitoring systems (VMS) data with daily catch data from logbooks to explore the spatial distribution of catch and effort at high resolution. ICES Journal of Marine Science 68, 245–252. https://doi.org/10.1093/icesjms/fsq137

# References

Gerritsen, H.D., Minto, C., Lordan, C., 2013. How much of the seabed is impacted by mobile fishing gear? Absolute estimates from Vessel Monitoring System (VMS) point data. ICES Journal of Marine Science 70, 523–531. https://doi.org/10.1093/icesjms/fst017

Gordon, J., Gillespie, D., Potter, J., Frantzis, A., Simmonds, M.P., Swift, R., Thompson, D., 2003. A Review of the Effects of Seismic Surveys on Marine Mammals. Marine Technology Society Journal 37, 16–34. https://doi.org/10.4031/002533203787536998

Grassle, J.F., Maciolek, N.J., 1992. Deep-Sea Species Richness: Regional and Local Diversity Estimates from Quantitative Bottom Samples. The American Naturalist 139, 313–341. https://doi.org/10.1086/285329

Gregg, M.C., Carter, G.S., Kunze, E., 2005. CORRIGENDUM. Journal of Physical Oceanography 35, 1712–1715. https://doi.org/10.1175/JPO2789.1

Gunton, L.M., Gooday, A.J., Glover, A.G., Bett, B.J., 2015. Macrofaunal abundance and community composition at lower bathyal depths in different branches of the Whittard Canyon and on the adjacent slope (3500m; NE Atlantic). Deep Sea Research Part I: Oceanographic Research Papers 97, 29–39. https://doi.org/10.1016/j.dsr.2014.11.010

Haedrich, R., Merrett, N., O'Dea, N., 2001. Can ecological knowledge catch up with deep-water fishing? A North Atlantic perspective. Fisheries Research 51, 113–122. https://doi.org/10.1016/s0165-7836(01)00239-9

Hall, R.A., Aslam, T., Huvenne, V.A.I., 2017. Partly standing internal tides in a dendritic submarine canyon observed by an ocean glider. Deep Sea Research Part I: Oceanographic Research Papers 126, 73–84. https://doi.org/10.1016/j.dsr.2017.05.015

Hall–Spencer, J., Allain, V., Fosså, J.H., 2002. Trawling damage to Northeast Atlantic ancient coral reefs. Proceedings of the Royal Society of London. Series B: Biological Sciences 269, 507–511. https://doi.org/10.1098/rspb.2001.1910

Halpern, B.S., Walbridge, S., Selkoe, K.A., Kappel, C.V., Micheli, F., D'Agrosa, C., Bruno, J.F., Casey, K.S., Ebert, C., Fox, H.E., Fujita, R., Heinemann, D., Lenihan, H.S., Madin, E.M.P., Perry, M.T., Selig, E.R., Spalding, M., Steneck, R., Watson, R., 2008. A Global Map of Human Impact on Marine Ecosystems. science 319, 948–952. https://doi.org/10.1126/science.1149345

Hanrahan, M., Morgan, C., 2015. Status of exploration offshore Ireland and new data. Atlantic Ireland.

Harding, Harry. R, Gordon, Timothy. A. C, Havlik, Michelle. N, Predragovic, Milica, Devassy, Reny. P, Radford, Andrew. N, Simpson, Stephen. D, Duarte, Carlos. M, 2021. A systematic literature assessment on the effects of human-altered soundscapes on marine life. https://doi.org/10.5281/ZENODO.4080965

Harrison, C., Harrison, J., 1995. A simple relationship between frequency and range averages for broadband sonar. The Journal of the Acoustical Society of America 97, 1314–1317. https://doi.org/10.1121/1.412172

Harvey, J., 1982. θ-S relationships and water masses in the eastern North Atlantic. Deep Sea Research Part A. Oceanographic Research Papers 29, 1021–1033. https://doi.org/10.1016/0198-0149(82)90025-5

Harwood, J., King, S., Booth, C., Donovan, C., Schick, R.S., Thomas, L., New, L., 2016. Understanding the population consequences of acoustic disturbance for marine mammals, in: The Effects of Noise on Aquatic Life II. Springer, pp. 417–423.

Hastings, M.C., 2004. Noise exposure metrics for auditory and nonauditory damage in aquatic animals. The Journal of the Acoustical Society of America 116, 2533–2533. https://doi.org/10.1121/1.4785107

Hawkins, A.D., Popper, A.N., 2017. A sound approach to assessing the impact of underwater noise on marine fishes and invertebrates. ICES Journal of Marine Science 74, 635–651. https://doi.org/10.1093/icesjms/fsw205

Hester, K.C., Peltzer, E.T., Kirkwood, W.J., Brewer, P.G., 2008. Unanticipated consequences of ocean acidification: A noisier ocean at lower pH. Geophysical research letters 35. https://doi.org/10.1029/2008gl034913

Hildebrand, J.A., 2009. Anthropogenic and natural sources of ambient noise in the ocean. Marine Ecology Progress Series 395, 5–20. https://doi.org/doi:10.3354/meps08353

Hill, A.E., Mitchelson-Jacob, E.G., 1993. Observations of a poleward-flowing saline core on the continental slope west of Scotland. Deep Sea Research Part I: Oceanographic Research Papers 40, 1521–1527. https://doi.org/10.1016/0967-0637(93)90127-O

# References

Holliday, P., Pollard, R.T., Read, J.F., Leach, H., 2000. Water mass properties and fluxes in the Rockall Trough, 1975–1998. Deep Sea Research Part I: Oceanographic Research Papers 47, 1303–1332. https://doi.org/10.1016/S0967-0637(99)00109-0

Holt, J., Wakelin, S., Huthnance, J., 2009. Down-welling circulation of the northwest European continental shelf: A driving mechanism for the continental shelf carbon pump. Geophysical Research Letters 36.

Holt, J.T., Thorpe, S.A., 1997. The propagation of high frequency internal waves in the Celtic Sea. Deep Sea Research Part I: Oceanographic Research Papers 44, 2087–2116. https://doi.org/10.1016/S0967-0637(97)00091-5

Houser, D.S., Yost, W., Burkard, R., Finneran, J.J., Reichmuth, C., Mulsow, J., 2017. A review of the history, development and application of auditory weighting functions in humans and marine mammals. The Journal of the Acoustical Society of America 141, 1371–1413.

Hovem, J.M., Vågsholm, R., Sørheim, H., Haukebø, B., 2015. Measurements and analysis of underwater acoustic noise of fishing vessels, in: OCEANS 2015 - Genova. Presented at the OCEANS 2015 - Genova, pp. 1–6. https://doi.org/10.1109/OCEANS-Genova.2015.7271675

Hunter, W.R., Jamieson, A., Huvenne, V.A.I., Witte, U., 2013. Sediment community responses to marine vs. terrigenous organic matter in a submarine canyon. Biogeosciences 10, 67–80. https://doi.org/10.5194/bg-10-67-2013

Huthnance, J.M., 1986. The Rockall slope current and shelf-edge processes. Proceedings of the Royal Society of Edinburgh, Section B: Biological Sciences 88, 83–101. https://doi.org/10.1017/S0269727000004486

Huthnance, J.M., 1984. Slope Currents and "JEBAR." Journal of Physical Oceanography 14, 795–810. https://doi.org/10.1175/1520-0485(1984)014<0795:SCA>2.0.CO;2

Huthnance, J.M., Coelho, H., Griffiths, C.R., Knight, P.J., Rees, A.P., Sinha, B., Vangriesheim, A., White, M., Chatwin, P.G., 2001. Physical structures, advection and mixing in the region of Goban spur. Deep Sea Research Part II: Topical Studies in Oceanography 48, 2979–3021. https://doi.org/10.1016/S0967-0645(01)00030-3

Huvenne, V.A.I., De Mol, B., Henriet, J.-P., 2003. A 3D seismic study of the morphology and spatial distribution of buried coral banks in the Porcupine Basin, SW of Ireland. Marine Geology, Geosphere-Biosphere Coupling: Cold Seep Related Carbonate and Mound Formation and Ecology 198, 5–25. https://doi.org/10.1016/S0025-3227(03)00092-6

Huvenne, V.A.I., Tyler, P.A., Masson, D.G., Fisher, E.H., Hauton, C., Hühnerbach, V., Bas, T.P.L., Wolff, G.A., 2011. A Picture on the Wall: Innovative Mapping Reveals Cold-Water Coral Refuge in Submarine Canyon. PLOS ONE 6, e28755. https://doi.org/10.1371/journal.pone.0028755

IMO, M., 2014. Guidelines for the reduction of underwater noise from commercial shipping to address adverse impacts on marine life. International Maritime Organization.

International Organization for Standardization, 2019. Underwater Acoustics—Quantities and Procedures for Description and Measurement of Underwater Sound From Ships—Part 2: Determination of Source Levels From Deep Water Measurements (ISO 17208-2). Geneva: International Organization for Standardization.

International Organization for Standardization, 2017. Underwater Acoustics–Terminology. International Organization for Standardization Geneva, Switzerland.

Ismail, A., Stumpf, A., Bauer, R., 2014. Seismic characterization of glacial sediments in central Illinois. Journal of Applied Geophysics 101, 1–10. https://doi.org/10.1016/j.jappgeo.2013.11.009

ISPSG, 2005. Deep water environment to the west of Ireland (No. Report to the Irish Shelf Petroleum Studies Group Project IS03/21).

Jensen, F., 1982. Numerical Models of Sound Propagation in Real Oceans, in: OCEANS 82. Presented at the OCEANS 82, pp. 147–154. https://doi.org/10.1109/OCEANS.1982.1151749

Jensen, F.B., Kuperman, W.A., Porter, M.B., Schmidt, H., 2011. Computational ocean acoustics. Springer Science & Business Media.

Jensen, F.H., Johnson, M., Ladegaard, M., Wisniewska, D.M., Madsen, P.T., 2018. Narrow Acoustic Field of View Drives Frequency Scaling in Toothed Whale Biosonar. Current Biology 28, 3878-3885.e3. https://doi.org/10.1016/j.cub.2018.10.037

Jiménez-Arranz, G., Glanfield, R., Banda, C., Wyatt, R., 2018. Review on Existing Data on Underwater Sounds Produced by the Oil and Gas Industry (E&P Sound & Marine Life (JIP)).

# References

Johnson, D.T., 1994. Understanding air-gun bubble behavior. Geophysics 59, 1729–1734. http://dx.doi.org/10.1190/1.1443559

Johnson, M.P., White, M., Wilson, A., Würzberg, L., Schwabe, E., Folch, H., Allcock, A.L., 2013. A Vertical Wall Dominated by Acesta excavata and Neopycnodonte zibrowii, Part of an Undersampled Group of Deep-Sea Habitats. PLOS ONE 8, e79917. https://doi.org/10.1371/journal.pone.0079917

JONAS, 2019. JONAS – Joint Framework for Ocean Noise in the Atlantic Seas [WWW Document]. URL https://www.jonasproject.eu/ (accessed 4.14.21).

Jones, J.B., 1992. Environmental impact of trawling on the seabed: A review. New Zealand Journal of Marine and Freshwater Research 26, 59–67. https://doi.org/10.1080/00288330.1992.9516500

Kaiser, M.J., Collie, J.S., Hall, S.J., Jennings, S., Poiner, I.R., 2002. Modification of marine habitats by trawling activities: prognosis and solutions. Fish and Fisheries 3, 114–136. https://doi.org/10.1046/j.1467-2979.2002.00079.x

Kannan, R., Sanjana, M.C., Latha, G., 2015. Passive Acoustic Recognition of Fishing Vessel Activity in the Shallow Waters of the Arabian Sea: A Statistical Approach. Fluct. Noise Lett. 14, 1550035. https://doi.org/10.1142/S0219477515500352

Kasumyan, A.O., 2008. Sounds and sound production in fishes. J. Ichthyol. 48, 981–1030. https://doi.org/10.1134/S0032945208110039

Kavanagh, A.S., Noad, M.J., Blomberg, S.P., Goldizen, A.W., Kniest, E., Cato, D.H., Dunlop, R.A., 2017. Factors driving the variability in diving and movement behavior of migrating humpback whales (Megaptera novaeangliae): Implications for anthropogenic disturbance studies. Marine mammal science 33, 413–439. https://doi.org/10.1111/mms.12375

Kavanagh, A.S., Nykänen, M., Hunt, W., Richardson, N., Jessopp, M.J., 2019. Seismic surveys reduce cetacean sightings across a large marine ecosystem. Scientific Reports 9, 19164. https://doi.org/10.1038/s41598-019-55500-4

Khripounoff, A., Vangriesheim, A., Crassous, P., Etoubleau, J., 2009. High frequency of sediment gravity flow events in the Var submarine canyon (Mediterranean Sea). Marine Geology 263, 1–6. https://doi.org/10.1016/j.margeo.2009.03.014

Kihslinger, R.L., Klimley, A.P., 2002. Species identity and the temporal characteristics of fish acoustic signals. Journal of Comparative Psychology 116, 210.

Kinsler, L.E., Frey, A.R., Coppens, A.B., Sanders, J.V., 1999. Fundamentals of acoustics. Fundamentals of Acoustics, 4th Edition, by Lawrence E. Kinsler, Austin R. Frey, Alan B. Coppens, James V. Sanders, pp. 560. ISBN 0-471-84789-5. Wiley-VCH, December 1999. 560.

Kiriakoulakis, K., Blackbird, S., Ingels, J., Vanreusel, A., Wolff, G.A., 2011. Organic geochemistry of submarine canyons: The Portuguese Margin. Deep Sea Research Part II: Topical Studies in Oceanography 58, 2477–2488. https://doi.org/10.1016/j.dsr2.2011.04.010

Kiriakoulakis, K., Freiwald, A., Fisher, E., Wolff, G.A., 2007. Organic matter quality and supply to deep-water coral/mound systems of the NW European Continental Margin. Int J Earth Sci (Geol Rundsch) 96, 159–170. https://doi.org/10.1007/s00531-006-0078-6

Kiriakoulakis, K., Marshall, J., Wolff, G., 2000. Biomarkers in a Lower Jurassic concretion from Dorset (UK). Journal of the Geological Society 157, 207–220. http://dx.doi.org/10.1144/jgs.157.1.207

Kiriakoulakis, K., Vilas, J.C., Blackbird, S.J., Arístegui, J., Wolff, G.A., 2009. Seamounts and organic matter—Is there an effect? The case of Sedlo and Seine seamounts, Part 2. Composition of suspended particulate organic matter. Deep Sea Research Part II: Topical Studies in Oceanography 56, 2631–2645. https://doi.org/10.1016/j.dsr2.2008.12.024

Klinck, J., 1999. Dynmodes. m—Ocean Dynamic Vertical Modes, in: Woods Hole (MA): Woods Hole Science Center—SEA-MAT—Matlab Tools for Oceanographic Analysis.

Koenig, S., Fernández, P., Company, J.B., Huertas, D., Solé, M., 2013. Are deep-sea organisms dwelling within a submarine canyon more at risk from anthropogenic contamination than those from the adjacent open slope? A case study of Blanes canyon (NW Mediterranean). Progress in Oceanography 118, 249–259. https://doi.org/10.1016/j.pocean.2013.07.016

Korakas, A., Hovem, J.M., 2013. Comparison of modeling approaches to low-frequency noise propagation in the ocean. Presented at the 2013 MTS/IEEE OCEANS-Bergen, IEEE, pp. 1–7.

Lawrence, M.W., 2004. Acoustic monitoring of the global ocean for the CTBT. Presented at the Proceedings of Acoustics, pp. 455–460.

## References

Lee, I.-H., Lien, R.-C., Liu, J.T., Chuang, W., 2009. Turbulent mixing and internal tides in Gaoping (Kaoping) Submarine Canyon, Taiwan. Journal of Marine Systems, Fate of Terrestrial Substances on the Gaoping (Kaoping) Shelf/Slope and in the Gaoping Submarine Canyon off SW Taiwan 76, 383–396. https://doi.org/10.1016/j.jmarsys.2007.08.005

Lepper, P., Gordon, J., Booth, C., Theobald, P., Robinson, S., Northridge, S., Wang, L., 2014. Establishing the sensitivity of cetaceans and seals to acoustic deterrent devices in Scotland. Loughborough University.

Levin, L.A., Dayton, P.K., 2009. Ecological theory and continental margins: where shallow meets deep. Trends in Ecology & Evolution 24, 606–617. https://doi.org/10.1016/j.tree.2009.04.012

Levin, L.A., Sibuet, M., 2011. Understanding Continental Margin Biodiversity: A New Imperative. Annu. Rev. Mar. Sci. 4, 79–112. https://doi.org/10.1146/annurev-marine-120709-142714

Levin, L.A., Sibuet, M., Gooday, A.J., Smith, C.R., Vanreusel, A., 2010. The roles of habitat heterogeneity in generating and maintaining biodiversity on continental margins: an introduction. Marine Ecology 31, 1–5. https://doi.org/10.1111/j.1439-0485.2009.00358.x

Li, Z., Zhang, R., Peng, Z., Li, X., 2004. Anomalous sound propagation due to the horizontal variation of seabed acoustic properties. Science in China Series G: Physics, Mechanics and Astronomy 47, 571–580.

Locarnini, M., Mishonov, A., Baranova, O., Boyer, T., Zweng, M., Garcia, H., Seidov, D., Weathers, K., Paver, C., Smolyar, I., 2018. World ocean atlas 2018, volume 1: Temperature. A. Mishonov Technical Ed.; NOAA Atlas NESDIS 52 pp.

Lucke, K., Siebert, U., Lepper, P.A., Blanchet, M.-A., 2009. Temporary shift in masked hearing thresholds in a harbor porpoise (Phocoena phocoena) after exposure to seismic airgun stimuli. The Journal of the Acoustical Society of America 125, 4060–4070. https://doi.org/10.1121/1.3117443

Lueck, R.G., Osborn, T.R., 1985. Turbulence measurements in a submarine canyon. Continental Shelf Research 4, 681–698. https://doi.org/10.1016/0278-4343(85)90036-6

Luís, A.R., Silva, C., Andrade, F.F. de, Santos, M.E. dos, 2008. Influence zones of pile-drive noise on a resident population of bottlenose dolphins in the Sado estuary, Portugal. Proceedings of the Institute of Acoustics 43–51.

Luo, J., Badiey, M., Karjadi, E.A., Katsnelson, B., Tskhoidze, A., Lynch, J.F., Moum, J.N., 2008. Observation of sound focusing and defocusing due to propagating nonlinear internal waves. The Journal of the Acoustical Society of America 124, EL66–EL72. https://doi.org/10.1121/1.2963087

Lynch, D.R., Smith, K.W., Cahill, B., 2004. Seasonal mean circulation on the Irish shelf—a model-generated climatology. Continental Shelf Research, Recent Developments in Physical Oceanographic Modelling: Part I 24, 2215–2244. https://doi.org/10.1016/j.csr.2004.07.022

Lynch, J.F., Colosi, J.A., Gawarkiewicz, G.G., Duda, T.F., Pierce, A.D., Badiey, M., Katsnelson, B.G., Miller, J.E., Siegmann, W., Chiu, C.-S., Newhall, A., 2006. Consideration of fine-scale coastal oceanography and 3-D acoustics effects for the ESME sound exposure model. IEEE Journal of Oceanic Engineering 31, 33–48. https://doi.org/10.1109/JOE.2006.872207

Lynch, J.F., Newhall, A.E., Sperry, B., Gawarkiewicz, G., Fredricks, A., Tyack, P., Chiu, C.S., Abbot, P., 2003. Spatial and temporal variations in acoustic propagation characteristics at the New England shelfbreak front. IEEE Journal of Oceanic Engineering 28, 129–150. https://doi.org/10.1109/JOE.2003.808833

Ma, B.B., Nystuen, J.A., Lien, R.-C., 2005. Prediction of underwater sound levels from rain and wind. The Journal of the Acoustical Society of America 117, 3555–3565. https://doi.org/10.1121/1.1910283

MacDonald, D.G., Carlson, J., Goodman, L., 2013. On the heterogeneity of stratified-shear turbulence: Observations from a near-field river plume. Journal of Geophysical Research: Oceans 118, 6223–6237.

MacDonnell, J., 2017. Shelburne Basin Venture Exploration Drilling Project: Sound Source Characterization, 2016 Field Measurements of the Stena IceMAX. Document 01296, Version 3.0. Technical report by JASCO Applied Sciences for Shell Canada Limited. (Document 01296).

MacGillivray, A.O., 2006. Acoustic modelling study of seismic airgun noise in Queen Charlotte Basin (Thesis).

MacGillivray, A.O., Chapman, N.R., 2012. Modeling underwater sound propagation from an airgun array using the parabolic equation method. Canadian Acoustics 40, 19–25.

# References

Macleod, C.D., 2000. Review of the distribution of Mesoplodon species (order Cetacea, family Ziphiidae) in the North Atlantic. Mammal Review 30, 1–8. https://doi.org/10.1046/j.1365-2907.2000.00057.x

Madsen, P., 2005. Marine mammals and noise: Problems with root mean square sound pressure levels for transients. The Journal of the Acoustical Society of America 117, 3952–3957. https://doi.org/10.1121/1.1921508

Madsen, P., Møhl, B., Nielsen, B., Wahlberg, M., 2002. Male sperm whale behaviour during exposures to distant seismic survey pulses. Aquatic mammals 28, 231–240.

Madsen, P.T., Johnson, M., de Soto, N.A., Zimmer, W.M.X., Tyack, P., 2005. Biosonar performance of foraging beaked whales (Mesoplodon densirostris). Journal of Experimental Biology 208, 181–194. https://doi.org/10.1242/jeb.01327

Madsen, P.T., Johnson, M., Miller, P., Aguilar Soto, N., Lynch, J., Tyack, P., 2006. Quantitative measures of air-gun pulses recorded on sperm whales (Physeter macrocephalus) using acoustic tags during controlled exposure experiments. The Journal of the Acoustical Society of America 120, 2366–2379. https://doi.org/10.1121/1.2229287

Madsen, P.T., Wahlberg, M., 2007. Recording and quantification of ultrasonic echolocation clicks from free-ranging toothed whales. Deep Sea Research Part I: Oceanographic Research Papers 54, 1421–1444. https://doi.org/10.1016/j.dsr.2007.04.020

Marine Institute, 2019. The Stock Book 2019: Annual Review of Fish Stocks in 2019 with Management Advice for 2020. Marine Institute, Galway, Ireland.

Marine Protected Area Advisory Group, 2020. Expanding Ireland's Marine Protected Area Network: A report by the Marine Protected Area Advisory Group. Report for the Department of Housing, Local Government and Heritage, Ireland.

Martín, J., Puig, P., Masqué, P., Palanques, A., Sánchez-Gómez, A., 2014a. Impact of bottom trawling on deep-sea sediment properties along the flanks of a submarine canyon. PloS one 9, e104536. https://doi.org/10.1371/journal.pone.0104536

Martín, J., Puig, P., Palanques, A., Giamportone, A., 2014b. Commercial bottom trawling as a driver of sediment dynamics and deep seascape evolution in the Anthropocene. Anthropocene 7, 1–15. https://doi.org/10.1016/j.ancene.2015.01.002

Martín, J., Puig, P., Palanques, A., Masqué, P., García-Orellana, J., 2008. Effect of commercial trawling on the deep sedimentation in a Mediterranean submarine canyon. Marine Geology 252, 150–155. https://doi.org/10.1016/j.margeo.2008.03.012

Martín, J., Puig, P., Palanques, A., Ribó, M., 2014c. Trawling-induced daily sediment resuspension in the flank of a Mediterranean submarine canyon. Deep Sea Research Part II: Topical Studies in Oceanography, Submarine Canyons: Complex Deep-Sea Environments Unravelled by Multidisciplinary Research 104, 174–183. https://doi.org/10.1016/j.dsr2.2013.05.036

Mater, B.D., Schaad, S.M., Venayagamoorthy, S.K., 2013. Relevance of the Thorpe length scale in stably stratified turbulence. Physics of Fluids 25, 076604. https://doi.org/10.1063/1.4813809

Mater, B.D., Venayagamoorthy, S.K., Laurent, L.S., Moum, J.N., 2015. Biases in Thorpe-Scale Estimates of Turbulence Dissipation. Part I: Assessments from Large-Scale Overturns in Oceanographic Data. Journal of Physical Oceanography 45, 2497–2521. https://doi.org/10.1175/JPO-D-14-0128.1

McCabe, A.M., Clark, P.U., Clark, J., Dunlop, P., 2007. Radiocarbon constraints on readvances of the British–Irish Ice Sheet in the northern Irish Sea Basin during the last deglaciation. Quaternary Science Reviews 26, 1204–1211. https://doi.org/10.1016/j.quascirev.2007.01.010

McCauley, R., 2015. Offshore Irish noise logger program (March to September 2014): Analysis of cetacean presence, and ambient and anthropogenic noise sources. Centre for Marine Science and Technology (CMST), Curtin University for RPS MetOcean/Woodside Energy (Ireland) Pty Ltd.

McCauley, R., Fewtrell, J., Duncan, A., Jenner, C., Jenner, M., Penrose, J., Prince, R., Adhitya, A., Murdoch, J., McCabe, K., 2000a. Marine seismic surveys—a study of environmental implications. The APPEA Journal 40, 692–708. https://doi.org/10.1071/aj99048

McCauley, R.D., Day, R.D., Swadling, K.M., Fitzgibbon, Q.P., Watson, R.A., Semmens, J.M., 2017. Widely used marine seismic survey air gun operations negatively impact zooplankton. Nature Ecology & Evolution 1, 1–8. https://doi.org/10.1038/s41559-017-0195

McCauley, R.D., Fewtrell, J., Duncan, A.J., Jenner, C., Jenner, M.-N., Penrose, J.D., McCabe, K., 2000b. Marine seismic surveys: analysis and propagation of air-gun signals; and effects of air-

gun exposure on humpback whales, sea turtles (No. R99-15). Centre for Marine Science and Technology, Curtin University, Western Australia.

McCauley, R.D., Fewtrell, J., Popper, A.N., 2003. High intensity anthropogenic sound damages fish ears. The Journal of the Acoustical Society of America 113, 638–642. https://doi.org/10.1121/1.1527962

McDonald, M.A., Hildebrand, J.A., Mesnick, S., 2009. Worldwide decline in tonal frequencies of blue whale songs. Endangered Species Research 9, 13–21. https://doi.org/10.3354/esr00217

McDonald, M.A., Hildebrand, J.A., Wiggins, S.M., 2006. Increases in deep ocean ambient noise in the Northeast Pacific west of San Nicolas Island, California. The Journal of the Acoustical Society of America 120, 711–718. https://doi.org/10.1121/1.2216565

McGrath, T., Nolan, G., McGovern, E., 2012. Chemical characteristics of water masses in the Rockall Trough. Deep Sea Research Part I: Oceanographic Research Papers 61, 57–73. https://doi.org/10.1016/j.dsr.2011.11.007

McKenna, M.F., Ross, D., Wiggins, S.M., Hildebrand, J.A., 2012. Underwater radiated noise from modern commercial ships. The Journal of the Acoustical Society of America 131, 92–103. https://doi.org/10.1121/1.3664100

Medwin, H., Clay, C.S., 1997. Fundamentals of acoustical oceanography. Academic press.

Mercer, J.A., Colosi, J.A., Howe, B.M., Dzieciuch, M.A., Stephen, R., Worcester, P.F., 2009. LOAPEX: The long-range ocean acoustic propagation experiment. IEEE Journal of Oceanic Engineering 34, 1–11.

Merchant, N.D., 2019. Underwater noise abatement: Economic factors and policy options. Environmental Science & Policy 92, 116–123. https://doi.org/10.1016/j.envsci.2018.11.014

Merchant, N.D., Andersson, M.H., Box, T., Le Courtois, F., Cronin, D., Holdsworth, N., Kinneging, N., Mendes, S., Merck, T., Mouat, J., 2020. Impulsive noise pollution in the Northeast Atlantic: Reported activity during 2015–2017. Marine Pollution Bulletin 152, 110951. https://doi.org/10.1016/j.marpolbul.2020.110951

Merchant, N.D., Blondel, P., Dakin, D.T., Dorocicz, J., 2012. Averaging underwater noise levels for environmental assessment of shipping. The Journal of the Acoustical Society of America 132, EL343–EL349. https://doi.org/10.1121/1.4754429

Merchant, N.D., Brookes, K.L., Faulkner, R.C., Bicknell, A.W.J., Godley, B.J., Witt, M.J., 2016. Underwater noise levels in UK waters. Scientific reports 6, 36942. https://doi.org/10.1038/srep36942

Merchant, N.D., Fristrup, K.M., Johnson, M.P., Tyack, P.L., Witt, M.J., Blondel, P., Parks, S.E., 2015. Measuring acoustic habitats. Methods in Ecology and Evolution 6, 257–265. https://doi.org/10.1111/2041-210x.12330

Merchant, N.D., Pirotta, E., Barton, T.R., Thompson, P.M., 2014. Monitoring ship noise to assess the impact of coastal developments on marine mammals. Marine Pollution Bulletin 78, 85–95. https://doi.org/10.1016/j.marpolbul.2013.10.058

Miller, P., 2009. Composite front maps for improved visibility of dynamic sea-surface features on cloudy SeaWiFS and AVHRR data. Journal of Marine Systems, Special Issue on Observational Studies of Oceanic Fronts 78, 327–336. https://doi.org/10.1016/j.jmarsys.2008.11.019

Mitchell, N.C., Huthnance, J.M., 2008. Oceanographic currents and the convexity of the uppermost continental slope. Journal of Sedimentary Research 78, 29–44. https://doi.org/10.2110/jsr.2008.006

Møhl, B., Wahlberg, M., Madsen, P.T., Heerfordt, A., Lund, A., 2003. The monopulsed nature of sperm whale clicks. The Journal of the Acoustical Society of America 114, 1143–1154. https://doi.org/10.1121/1.1586258

Møhl, B., Wahlberg, M., Madsen, P.T., Miller, L.A., Surlykke, A., 1999. Sperm whale clicks: Directionality and source level revisited. The Journal of the Acoustical Society of America 107, 638–648. https://doi.org/10.1121/1.428329

Mohn, C., Bartsch, J., Meincke, J., 2002. Observations of the mass and flow field at Porcupine Bank. ICES Journal of marine Science 59, 380–392.

Mooney, T.A., Hanlon, R., Madsen, P.T., Christensen-Dalsgaard, J., Ketten, D.R., Nachtigall, P.E., 2012. Potential for sound sensitivity in cephalopods, in: The Effects of Noise on Aquatic Life. Springer, pp. 125–128.

# References

Moran, S.B., Charette, M.A., Pike, S.M., Wicklund, C.A., 1999. Differences in seawater particulate organic carbon concentration in samples collected using small- and large-volume methods: the importance of DOC adsorption to the filter blank. Marine Chemistry 67, 33–42. https://doi.org/10.1016/S0304-4203(99)00047-X

Morato, T., Watson, R., Pitcher, T.J., Pauly, D., 2006. Fishing down the deep. Fish and fisheries 7, 24–34. https://doi.org/10.1111/j.1467-2979.2006.00205.x

Munk, W., Wunsch, C., 1979. Ocean acoustic tomography: A scheme for large scale monitoring. Deep Sea Research Part A. Oceanographic Research Papers 26, 123–161. https://doi.org/10.1016/0198-0149(79)90073-6

Munk, W.H., Spindel, R.C., Baggeroer, A., Birdsall, T.G., 1994. The heard island feasibility test. The Journal of the Acoustical Society of America 96, 2330–2342. https://doi.org/10.1063/1.881317

MÜnnich, M., WÜest, A., Imboden, D.M., 1992. Observations of the second vertical mode of the internal seiche in an alpine lake. Limnology and Oceanography 37, 1705–1719. https://doi.org/10.4319/lo.1992.37.8.1705

National Research Council, 2003. Ocean noise and marine mammals. National Academies Press (US).

National Research Council, 2000. Marine mammals and low-frequency sound: Progress since 1994. National Academies Press (US).

National Research Council (U.S.), National Academies Press (U.S.) (Eds.), 2005. Marine mammal populations and ocean noise: determining when noise causes biologically significant effects. National Academies Press, Washington, D.C.

Naylor, D., Murphy, N., 2002. Porcupine-Goban Region: A standard structural nomenclature system. Department of the Marine and Natural Resources, Petroleum Affairs Division.

Nédélec, C., Prado, J., 1990. Definition and classification of fishing gear categories. Définition et classification des categories d'engins de péche. Definición y clasificación de las diversas categorías de artes de pesca. FAO Fisheries Technical Paper.

Nedwell, J., Needham, K., Turnpenny, A., Thompson, D., 1999. Measurement of sound during a 3D seismic survey in blocks 14/14a of the North Sea. Subacoustech Ltd., Hampshire, UK, Tech. Rep. 356R0108.

New, A.L., Da Silva, J.C.B., 2002. Remote-sensing evidence for the local generation of internal soliton packets in the central Bay of Biscay. Deep Sea Research Part I: Oceanographic Research Papers 49, 915–934. https://doi.org/10.1016/S0967-0637(01)00082-6

New, L., Lusseau, D., Harcourt, R., 2020. Dolphins and Boats: When Is a Disturbance, Disturbing? Front. Mar. Sci. 7. https://doi.org/10.3389/fmars.2020.00353

Nieukirk, S.L., Stafford, K.M., Mellinger, D.K., Dziak, R.P., Fox, C.G., 2004. Low-frequency whale and seismic airgun sounds recorded in the mid-Atlantic Ocean. The Journal of the Acoustical Society of America 115, 1832–1843. https://doi.org/10.1121/1.1675816

Nowacek, D.P., Bröker, K., Donovan, G., Gailey, G., Racca, R., Reeves, R.R., Vedenev, A.I., Weller, D.W., Southall, B.L., 2013. Responsible practices for minimizing and monitoring environmental impacts of marine seismic surveys with an emphasis on marine mammals. Aquatic Mammals 39, 356.

Nowacek, D.P., Thorne, L.H., Johnston, D.W., Tyack, P.L., 2007. Responses of cetaceans to anthropogenic noise. Mammal Review 37, 81–115. https://doi.org/10.1111/j.1365-2907.2007.00104.x

Oba, R., Finette, S., 2002. Acoustic propagation through anisotropic internal wave fields: Transmission loss, cross-range coherence, and horizontal refraction. The Journal of the Acoustical Society of America 111, 769–784.

Oberle, F., Puig, P., Martín, J., 2017. Submarine Geomorphology: Fishing Activities. pp. 503–534. https://doi.org/10.1007/978-3-319-57852

Oberle, F.K., Storlazzi, C.D., Hanebuth, T.J., 2016a. What a drag: Quantifying the global impact of chronic bottom trawling on continental shelf sediment. Journal of Marine Systems 159, 109–119. https://doi.org/10.1016/j.jmarsys.2015.12.007

Oberle, F.K., Swarzenski, P.W., Reddy, C.M., Nelson, R.K., Baasch, B., Hanebuth, T.J., 2016b. Deciphering the lithological consequences of bottom trawling to sedimentary habitats on the shelf. Journal of Marine Systems 159, 120–131. https://doi.org/10.1016/j.jmarsys.2015.12.008

# References

Oberle, F.K.J., Puig, P., Martín, J., 2018. Fishing Activities, in: Micallef, A., Krastel, S., Savini, A. (Eds.), Submarine Geomorphology, Springer Geology. Springer International Publishing, Cham, pp. 503–534. https://doi.org/10.1007/978-3-319-57852-1_25

O'Brien, J., Berrow, S., McGrath, D., Evans, P., 2009. Cetaceans in Irish waters: A review of recent research. Presented at the Biology and Environment: Proceedings of the Royal Irish Academy, JSTOR, pp. 63–88. https://doi.org/10.3318/bioe.2009.109.2.63

O'Cadhla, O., Mackey, M., Aguilar de Soto, N., Rogan, E., Connolly, N., 2004. Cetaceans and seabirds of Ireland's Atlantic margin. Volume II—Cetacean distribution and abundance. Report on research carried out under the Irish Infrastructure Programme (PIP): Rockall Studies Group (RSG) projects 98.

Okal, E.A., 2008. The generation of T waves by earthquakes, in: Dmowska, R. (Ed.), Advances in Geophysics. Elsevier, pp. 1–65. https://doi.org/10.1016/S0065-2687(07)49001-X

Ona, E., Godø, O.R., 1990. Fish reaction to trawling noise: the significance for trawl sampling. ICES.

Ona, E., Toresen, R., 1988. Reactions of herring to trawling noise. ICES.

O'Neill, F.G., Summerbell, K., 2011. The mobilisation of sediment by demersal otter trawls. Marine Pollution Bulletin 62, 1088–1097. https://doi.org/10.1016/j.marpolbul.2011.01.038

OSPAR, 2017. Distribution of Reported Impulsive Sounds. Intermediate Assessment 2017. [WWW Document]. URL https://oap.ospar.org/en/ospar-assessments/intermediate-assessment-2017/pressures-human-activities/distribution-reported-impulsive-sounds-sea/

Palanques, A., 1994. Distribution and heavy metal pollution of the suspended particulate matter on the barcelona continental shelf (North-Western Mediterranean). Environmental Pollution 85, 205–215. https://doi.org/10.1016/0269-7491(94)90087-6

Palanques, A., Martín, J., Puig, P., Guillén, J., Company, J.B., Sardà, F., 2006. Evidence of sediment gravity flows induced by trawling in the Palamós (Fonera) submarine canyon (northwestern Mediterranean). Deep Sea Research Part I: Oceanographic Research Papers 53, 201–214. https://doi.org/10.1016/j.dsr.2005.10.003

Palanques, A., Masqué, P., Puig, P., Sanchez-Cabeza, J.A., Frignani, M., Alvisi, F., 2008. Anthropogenic trace metals in the sedimentary record of the Llobregat continental shelf and adjacent Foix Submarine Canyon (northwestern Mediterranean). Marine Geology 248, 213–227. https://doi.org/10.1016/j.margeo.2007.11.001

Palanques, A., Puig, P., Arjona, M., 2018. Self-regulated deep-sea trawling fishery management in La Fonera Canyon (NW Mediterranean) towards reduction of sediment resuspension and seabed impact.

Palanques, A., Puig, P., Guillén, J., Demestre, M., Martín, J., 2014. Effects of bottom trawling on the Ebro continental shelf sedimentary system (NW Mediterranean). Continental Shelf Research 72, 83–98. https://doi.org/10.1016/j.csr.2013.10.008

Parnum, I.M., Wilkes, D., Duncan, A., 2013. Prediction of underwater noise associated with the operation of a drilling rig in the Great Australian Bight (Report 2013-10).

Parsons, E., 2017. Impacts of Navy Sonar on Whales and Dolphins: Now beyond a Smoking Gun? Frontiers in Marine Science 4, 295. https://doi.org/10.3389/fmars.2017.00295

Payo-Payo, M., Jacinto, R.S., Lastras, G., Rabineau, M., Puig, P., Martín, J., Canals, M., Sultan, N., 2017. Numerical modeling of bottom trawling-induced sediment transport and accumulation in La Fonera submarine canyon, northwestern Mediterranean Sea. Marine Geology 386, 107–125. https://doi.org/10.1016/j.margeo.2017.02.015

Peña, H., Øvredal, J., Totland, B., Olav, N., Handegard, N., 2011. Underwater sound measurements from fishing vessel "Brennholm." Report Prepared for: Institute of Marine Research, Norway.

Peng, Z., Fan, J., Wang, B., 2018a. a Analysis and modelling on radiated noise of a typical fishing boat measured in shallow water inspired by AQUO Project's Model. Archives of Acoustics 43. https://doi.org/doi:10.24425/122374

Peng, Z., Wang, B., Fan, J., 2018b. b Modeling of low-frequency source levels from fishing vessels using an acoustic observatory in the East China Sea. Noise Control Engineering Journal 66, 27–32. https://doi.org/10.3397/1/37663

Peterson, T.D., Crawford, D.W., Harrison, P.J., 2011. Mixing and biological production at eddy margins in the eastern Gulf of Alaska. Deep Sea Research Part I: Oceanographic Research Papers 58, 377–389. https://doi.org/10.1016/j.dsr.2011.01.010

## References

Pettersen, Ø.S., 2017. A Study of Radiated Noise from Fishing Vessels. (Master's thesis, NTNU).

Pham, C.K., Ramirez-Llodra, E., Alt, C.H.S., Amaro, T., Bergmann, M., Canals, M., Company, J.B., Davies, J., Duineveld, G., Galgani, F., Howell, K.L., Huvenne, V.A.I., Isidro, E., Jones, D.O.B., Lastras, G., Morato, T., Gomes-Pereira, J.N., Purser, A., Stewart, H., Tojeira, I., Tubau, X., Rooij, D.V., Tyler, P.A., 2014. Marine Litter Distribution and Density in European Seas, from the Shelves to Deep Basins. PLOS ONE 9, e95839. https://doi.org/10.1371/journal.pone.0095839

Pilskaln, C.H., Churchill, J.H., Mayer, L.M., 1998. Resuspension of Sediment by Bottom Trawling in the Gulf of Maine and Potential Geochemical Consequences. Conservation Biology 12, 1223–1229. https://doi.org/10.1046/j.1523-1739.1998.0120061223.x

Pingree, R.D., 1993. Flow of surface waters to the west of the British Isles and in the Bay of Biscay. Deep Sea Research Part II: Topical Studies in Oceanography 40, 369–388. https://doi.org/10.1016/0967-0645(93)90022-F

Pingree, R.D., Griffiths, D.K., Mardell, G.T., 1984. The Structure of the Internal Tide at the Celtic Sea Shelf Break. Journal of the Marine Biological Association of the United Kingdom 64, 99–113. https://doi.org/10.1017/S002531540005966X

Pingree, R.D., Mardell, G.T., Cartwright, D.E., Peregrine, D.H., Swallow, J.C., Currie, R.I., Gill, A.E., Simpson, J.H., 1981. Slope turbulence, internal waves and phytoplankton growth at the Celtic Sea shelf-break. Philosophical Transactions of the Royal Society of London. Series A, Mathematical and Physical Sciences 302, 663–682. https://doi.org/10.1098/rsta.1981.0191

Pingree, R.D., New, A.L., 1989. Downward propagation of internal tidal energy into the Bay of Biscay. Deep Sea Research Part A. Oceanographic Research Papers 36, 735–758. https://doi.org/10.1016/0198-0149(89)90148-9

Pingree, R.D., Sinha, B., Griffiths, C.R., 1999. Seasonality of the European slope current (Goban Spur) and ocean margin exchange. Continental Shelf Research 19, 929–975. https://doi.org/10.1016/S0278-4343(98)00116-2

Pollard, R., Pu, S., 1985. Structure and circulation of the upper Atlantic Ocean northeast of the Azores. Progress in Oceanography 14, 443–462. https://doi.org/10.1016/0079-6611(85)90022-9

Pollard, R.T., Griffhths, M., Cunningham, S.A., Read, J., Pérez, F.F., Ríos, A.F., 1996. Vivaldi 1991- A study of the formation, circulation and ventilation of Eastern North Atlantic Central Water. Progress in Oceanography 37, 167–192. https://doi.org/10.1016/s0079-6611(96)00008-0

Popper, A.N., Fewtrell, J., Smith, M.E., McCauley, R.D., 2003. Anthropogenic Sound: Effects on the Behavior and Physiology of Fishes. Marine Technology Society Journal 37, 35–40. https://doi.org/10.4031/002533203787537050

Popper, A.N., Hastings, M.C., 2009. The effects of human-generated sound on fish. Integrative Zoology 4, 43–52. https://doi.org/10.1111/j.1749-4877.2008.00134.x

Popper, A.N., Hawkins, A.D., 2019. An overview of fish bioacoustics and the impacts of anthropogenic sounds on fishes. Journal of Fish Biology 94, 692–713. https://doi.org/10.1111/jfb.13948

Puig, P., Canals, M., Company, J.B., Martin, J., Amblas, D., Lastras, G., Palanques, A., Calafat, A.M., 2012. Ploughing the deep sea floor. Nature 489, 286–289. https://doi.org/10.1038/nature11410

Puig, P., Palanques, A., Martín, J., 2014. Contemporary Sediment-Transport Processes in Submarine Canyons. Annual review of marine science 6, 53–77. https://doi.org/10.1146/annurev-marine-010213-135037

Purser, A., Thomsen, L., 2012. Monitoring strategies for drill cutting discharge in the vicinity of cold-water coral ecosystems. Marine Pollution Bulletin 64, 2309–2316. https://doi.org/10.1016/j.marpolbul.2012.08.003

Pusceddu, A., Bianchelli, S., Martín, J., Puig, P., Palanques, A., Masqué, P., Danovaro, R., 2014. Chronic and intensive bottom trawling impairs deep-sea biodiversity and ecosystem functioning. PNAS 111, 8861–8866. https://doi.org/10.1073/pnas.1405454111

Pusceddu, Antonio, Fiordelmondo, C., Danovaro, R., 2005a. Sediment Resuspension Effects on the Benthic Microbial Loop in Experimental Microcosms. Microb Ecol 50, 602–613. https://doi.org/10.1007/s00248-005-5051-6

Pusceddu, A, Fiordelmondo, C., Polymenakou, P., Polychronaki, T., Tselepides, A., Danovaro, R., 2005b. Effects of bottom trawling on the quantity and biochemical composition of organic matter in coastal marine sediments (Thermaikos Gulf, northwestern Aegean Sea). Continental Shelf Research 25, 2491–2505. https://doi.org/10.1016/j.csr.2005.08.013

## References

Putland, R.L., Merchant, N.D., Farcas, A., Radford, C.A., 2018. Vessel noise cuts down communication space for vocalizing fish and marine mammals. Global change biology 24, 1708–1721. https://doi.org/10.1111/gcb.13996

Quattrini, A.M., Nizinski, M.S., Chaytor, J.D., Demopoulos, A.W.J., Roark, E.B., France, S.C., Moore, J.A., Heyl, T., Auster, P.J., Kinlan, B., Ruppel, C., Elliott, K.P., Kennedy, B.R.C., Lobecker, E., Skarke, A., Shank, T.M., 2015. Exploration of the Canyon-Incised Continental Margin of the Northeastern United States Reveals Dynamic Habitats and Diverse Communities. PLOS ONE 10, e0139904. https://doi.org/10.1371/journal.pone.0139904

Ramirez-Llodra, E., Reid, W.D.K., Billett, D.S.M., 2005. Long-term changes in reproductive patterns of the holothurian Oneirophanta mutabilis from the Porcupine Abyssal Plain. Marine Biology 146, 683–693. https://doi.org/10.1007/s00227-004-1470-z

Ramirez-Llodra, E., Tyler, P.A., Baker, M.C., Bergstad, O.A., Clark, M.R., Escobar, E., Levin, L.A., Menot, L., Rowden, A.A., Smith, C.R., Dover, C.L.V., 2011. Man and the Last Great Wilderness: Human Impact on the Deep Sea. PLOS ONE 6, e22588. https://doi.org/10.1371/journal.pone.0022588

Reichmuth, C., Ghoul, A., Sills, J.M., Rouse, A., Southall, B.L., 2016. Low-frequency temporary threshold shift not observed in spotted or ringed seals exposed to single air gun impulses. The Journal of the Acoustical Society of America 140, 2646–2658. https://doi.org/10.1121/1.4964470

Reid, G.S., Hamilton, D., 1990. A reconnaissance survey of the Whittard Sea Fan, Southwestern Approaches, British Isles. Marine Geology 92, 69–86. https://doi.org/10.1016/0025-3227(90)90027-H

Richardson, W.J., Greene Jr, C.R., Malme, C.I., Thomson, D.H., 2013. Marine mammals and noise. Academic press.

Richter, C., Dawson, S., Slooten, E., 2006. Impacts of Commercial Whale Watching on Male Sperm Whales at Kaikoura, New Zealand. Marine Mammal Science 22, 46–63. https://doi.org/10.1111/j.1748-7692.2006.00005.x

Robert, K., Jones, D.O.B., Tyler, P.A., Van Rooij, D., Huvenne, V.A.I., 2015. Finding the hotspots within a biodiversity hotspot: fine-scale biological predictions within a submarine canyon using high-resolution acoustic mapping techniques. Mar Ecol 36, 1256–1276. https://doi.org/10.1111/maec.12228

Robinson, S.P., Lepper, P.A., Hazelwood, R.A., 2014. Good Practice Guide for Underwater Noise Measurement. NPL Good Practices Guide,133, National Measurement Office, Marine Scotland, The Crown Estate. https://doi.org/10.25607/OBP-21

Rodríguez-Pérez, A., Delgado-Restituto, M., Medeiro, F., 2011. Power Efficient ADCs for Biomedical Signal Acquisition. Biomedical Engineering, Trends in Electronics, Communications and Software 171–192.

Rolland, R.M., Parks, S.E., Hunt, K.E., Castellote, M., Corkeron, P.J., Nowacek, D.P., Wasser, S.K., Kraus, S.D., 2012. Evidence that ship noise increases stress in right whales. Proceedings of the Royal Society B: Biological Sciences 279, 2363–2368. https://doi.org/10.1098/rspb.2011.2429

Ross, D., 1993. On ocean ambient noise. Acoustics Bulletin 18, 5–5.

Sacchetti, F., Benetti, S., Georgiopoulou, A., Shannon, P.M., O'Reilly, B.M., Dunlop, P., Quinn, R., Ó Cofaigh, C., 2012. Deep-water geomorphology of the glaciated Irish margin from high-resolution marine geophysical data. Marine Geology 291–294, 113–131. https://doi.org/10.1016/j.margeo.2011.11.011

Sacchetti, F., Benetti, S., Quinn, R., Cofaigh, C.Ó., 2013. Glacial and post-glacial sedimentary processes in the Irish Rockall Trough from an integrated acoustic analysis of near-seabed sediments. Geo-Marine Letters 33, 49–66. https://doi.org/10.1007/s00367-012-0310-2

Sala, A., Notti, E., Bonanomi, S., Pulcinella, J., Colombelli, A., 2019. Trawling in the Mediterranean: An Exploration of Empirical Relations Connecting Fishing Gears, Otterboards and Propulsive Characteristics of Fishing Vessels. Frontiers in Marine Science 6, 534. https://doi.org/10.3389/fmars.2019.00534

Sanchez-Vidal, A., Canals, M., Calafat, A.M., Lastras, G., Pedrosa-Pàmies, R., Menéndez, M., Medina, R., Company, J.B., Hereu, B., Romero, J., Alcoverro, T., 2012. Impacts on the Deep-Sea Ecosystem by a Severe Coastal Storm. PLOS ONE 7, e30395. https://doi.org/10.1371/journal.pone.0030395

## References

Sañé, E., Martín, J., Puig, P., Palanques, A., 2013. Organic biomarkers in deep-sea regions affected by bottom trawling: pigments, fatty acids, amino acids and carbohydrates in surface sediments from the La Fonera (Palamós) Canyon, NW Mediterranean Sea. Biogeosciences 10, 8093–8108. https://doi.org/10.5194/bg-10-8093-2013

SATURN, 2021. SATURN: Solutions At Underwater Radiated Noise [WWW Document]. MaREI. URL https://www.marei.ie/project/saturn-solutions-at-underwater-radiated-noise/ (accessed 4.14.21).

Schumann, K., Stipp, M., Behrmann, J.H., Klaeschen, D., Schulte-Kortnack, D., 2014. P and S wave velocity measurements of water-rich sediments from the Nankai Trough, Japan. Journal of Geophysical Research: Solid Earth 119, 787–805. https://doi.org/10.1002/2013jb010290

Scrimger, P., Heitmeyer, R.M., 1991. Acoustic source-level measurements for a variety of merchant ships. The Journal of the Acoustical Society of America 89, 691–699. https://doi.org/10.1121/1.1894628

SERCEL, 2015. Mini Gi Gun Operational Manual. Toulon, France: SERCEL Inc. (Revision A). 12–18.

Shannon, P., 1991. The development of Irish offshore sedimentary basins. Journal of the Geological Society 148, 181–189. https://doi.org/10.1144/gsjgs.148.1.0181

Shannon, P., Corcoran, D., Haughton, P.D., 2001. The petroleum exploration of Ireland's offshore basins: introduction. Geological Society, London, Special Publications 188, 1–8. http://dx.doi.org/10.1144/GSL.SP.2001.188.01.01

Shannon, P.M., Naylor, D., 1998. An Assessment of Irish Offshore Basins and Petroleum Plays. Journal of Petroleum Geology 21, 125–152. https://doi.org/10.1111/j.1747-5457.1998.tb00651.x

Shapiro, G., Chen, F., Thain, R., 2014. The effect of ocean fronts on acoustic wave propagation in the Celtic Sea. Journal of Marine Systems 139, 217–226. https://doi.org/10.1016/j.jmarsys.2014.06.007

Sharples, J., Moore, C.M., Hickman, A.E., Holligan, P.M., Tweddle, J.F., Palmer, M.R., Simpson, J.H., 2009. Internal tidal mixing as a control on continental margin ecosystems. Geophysical Research Letters 36. https://doi.org/10.1029/2009GL040683

Sharples, J., Scott, B.E., Inall, M.E., 2013. From physics to fishing over a shelf sea bank. Progress in Oceanography 117, 1–8. https://doi.org/10.1016/j.pocean.2013.06.015

Sharples, J., Tweddle, J.F., Green, J.A.M., Palmer, M.R., Kim, Y.-N., Hickman, A.E., Holligan, P.M., Moore, C.M., Rippeth, T.P., Simpson, J.H., Krivtsov, V., 2007. Spring-neap modulation of internal tide mixing and vertical nitrate fluxes at a shelf edge in summer. Limnology and Oceanography 52, 1735–1747. https://doi.org/10.4319/lo.2007.52.5.1735

Sherwin, T.J., Aleynik, D., Dumont, E., Inall, M.E., 2015. Deep drivers of mesoscale circulation in the central Rockall Trough. Ocean Science 11, 343–359. https://doi.org/10.5194/os-11-343-2015

Sherwin, T.J., Read, J.F., Holliday, N.P., Johnson, C., 2012. The impact of changes in North Atlantic Gyre distribution on water mass characteristics in the Rockall Trough. ICES Journal of Marine Science 69, 751–757. https://doi.org/10.1093/icesjms/fsr185

Simard, Y., Roy, N., Gervaise, C., Giard, S., 2016. Analysis and modeling of 255 source levels of merchant ships from an acoustic observatory along St. Lawrence Seaway. The Journal of the Acoustical Society of America 140, 2002–2018. https://doi.org/10.1121/1.4962557

Simpson, S.D., Radford, A.N., Nedelec, S.L., Ferrari, M.C.O., Chivers, D.P., McCormick, M.I., Meekan, M.G., 2016. Anthropogenic noise increases fish mortality by predation. Nature Communications 7, 10544. https://doi.org/10.1038/ncomms10544

Širović, A., Hildebrand, J.A., Wiggins, S.M., 2007. Blue and fin whale call source levels and propagation range in the Southern Ocean. The Journal of the Acoustical Society of America 122, 1208–1215. https://doi.org/10.1121/1.2749452

Slabbekoorn, H., Bouton, N., van Opzeeland, I., Coers, A., ten Cate, C., Popper, A.N., 2010. A noisy spring: the impact of globally rising underwater sound levels on fish. Trends in ecology & evolution 25, 419–427. https://doi.org/10.1016/j.tree.2010.04.005

Solé, M., Lenoir, M., Fontuño, J.M., Durfort, M., van der Schaar, M., André, M., 2016. Evidence of Cnidarians sensitivity to sound after exposure to low frequency noise underwater sources. Scientific Reports 6, 37979. https://doi.org/10.1038/srep37979

Sousa, A.C.A., Oliveira, I.B., Laranjeiro, F., Takahashi, S., Tanabe, S., Cunha, M.R., Barroso, C.M., 2012. Organotin levels in Nazaré canyon (west Iberian Margin, NE Atlantic) and adjacent coastal area. Marine Pollution Bulletin 64, 422–426. https://doi.org/10.1016/j.marpolbul.2011.11.013

# References

Southall, B.L., 2005. Shipping noise and marine mammals: a forum for science, management, and technology. Presented at the Final report of the National and Atmospheric Administration (NOAA) International Symposium.

Southall, B.L., Bowles, A.E., Ellison, W.T., Finneran, J.J., Gentry, R.L., Greene Jr, C.R., Kastak, D., Ketten, D.R., Miller, J.H., Nachtigall, P.E., 2007. Marine mammal noise-exposure criteria: initial scientific recommendations. Bioacoustics 17, 273–275. https://doi.org/10.1080/09524622.2008.9753846

Southall, B.L., Finneran, J.J., Reichmuth, C., Nachtigall, P.E., Ketten, D.R., Bowles, A.E., Ellison, W.T., Nowacek, D.P., Tyack, P.L., 2019. Marine mammal noise exposure criteria: updated scientific recommendations for residual hearing effects. Aquatic Mammals 45, 125–232. https://doi.org/10.1578/am.45.2.2019.125

Souza, A.J., Simpson, J.H., Harikrishnan, M., Malarkey, J., 2001. Flow structure and seasonalityin the Hebridean slope current. Oceanologica Acta 24, 63–76. https://doi.org/10.1016/S0399-1784(00)01103-8

Spiga, I., 2015. Ocean Acoustics Modelling for EIAs: a Review. https://doi.org/10.13140/RG.2.2.16861.72168

Stelzenmuller, V., Rogers, S.I., Mills, C.M., 2008. Spatio-temporal patterns of fishing pressure on UK marine landscapes, and their implications for spatial planning and management. ICES Journal of Marine Science 65, 1081–1091. https://doi.org/10.1093/icesjms/fsn073

Stephen, R.A., 1988. A review of finite difference methods for seismo-acoustics problems at the seafloor. Rev. Geophys. 26, 445. https://doi.org/10.1029/RG026i003p00445

Stevenson, A., 2012. The European marine observation and data network: geological data. Baltica 25, 87–90. https://doi.org/DOI: 10.5200/baltica.2012.25.08

Stone, C.J., Tasker, M.L., 2006. The effects of seismic airguns on cetaceans in UK waters. Journal of Cetacean Research and Management 8, 255.

Sutton, G., Folegot, T., Jessopp, M., Clorennec, D., 2013. Mapping the spatiotemporal distribution of underwater noise in Irish Waters (STRIVE 121). Environ. Protection Agency.

Talley, L.D., McCartney, M.S., 1982. Distribution and Circulation of Labrador Sea Water. Journal of Physical Oceanography 12, 1189–1205. https://doi.org/10.1175/1520-0485(1982)012<1189:DACOLS>2.0.CO;2

Tasker, M., Amundin, M., Andre, M., Hawkins, A., Lang, W., Merck, T., Scholik-Schlomer, A., Teilmann, J., Thomsen, F., Werner, S., 2010. MARINE STRATEGY FRAMEWORK DIRECTIVE Task Group 11 Report Underwater noise and other forms of energy. Report No. EUR 24341, 2010. https://doi.org/doi:10.2788/87079

Thode, A.M., D'Spain, G.L., Kuperman, W.A., 2000. Matched-field processing, geoacoustic inversion, and source signature recovery of blue whale vocalizations. The Journal of the Acoustical Society of America 107, 1286–1300. https://doi.org/10.1121/1.428417

Thomisch, K., Flau, M., Heß, R., Traumueller, A., Boebel, O., 2021. OPUS - An Open Portal to Underwater Soundscapes to explore and study sound in the global ocean, in: EPIC35th Data Science Symposium, Virtual Meeting, 2021-01-22-2021-01-22. Presented at the 5th Data Science Symposium, virtual meeting.

Thompson, P., Brookes, K., Cheney, B., Cândido, A., Bates, H., Richardson, N., Barton, T., 2010. Assessing the potential impact of oil and gas exploration operations on cetaceans in the Moray Firth. First year Report for DECC, Scottish Government, COWRIE, and Oil & Gas UK, University of Aberdeen, Institute of Biological & Environmental Sciences, Lighthouse Field Station, Cromarty, Ross-shire IV11 8YJ.

Thomson, D.J.M., Barclay, D.R., 2020. Real-time observations of the impact of COVID-19 on underwater noise. The Journal of the Acoustical Society of America 147, 3390–3396. https://doi.org/10.1121/10.0001271

Thorpe, S., 1977. Turbulence and mixing in a Scottish loch. Philosophical Transactions of the Royal Society of London A: Mathematical, Physical and Engineering Sciences 286, 125–181.

Thorpe, S.A., Hall, P., White, M., Charnock, H., Edmond, J.M., McCave, I.N., Rice, A.L., Wilson, T.R.S., 1990. The variability of mixing at the continental slope. Philosophical Transactions of the Royal Society of London. Series A, Mathematical and Physical Sciences 331, 183–194. https://doi.org/10.1098/rsta.1990.0064

# References

Tindle, C.T., Deane, G.B., 1985. Sound propagation over a sloping bottom using rays with beam displacement. The Journal of the Acoustical Society of America 78, 1366–1374. https://doi.org/10.1121/1.392907

Tønnesen, P., Oliveira, C., Johnson, M., Madsen, P.T., 2020. The long-range echo scene of the sperm whale biosonar. Biology Letters 16, 20200134. https://doi.org/10.1098/rsbl.2020.0134

Tougaard, J., Wright, A.J., Madsen, P.T., 2015. Cetacean noise criteria revisited in the light of proposed exposure limits for harbour porpoises. Marine pollution bulletin 90, 196–208. https://doi.org/10.1016/j.marpolbul.2014.10.051

Tubau, X., Canals, M., Lastras, G., Rayo, X., Rivera, J., Amblas, D., 2015. Marine litter on the floor of deep submarine canyons of the Northwestern Mediterranean Sea: The role of hydrodynamic processes. Progress in Oceanography 134, 379–403. https://doi.org/10.1016/j.pocean.2015.03.013

Tyack, P.L., 2008. Implications for Marine Mammals of Large-Scale Changes in the Marine Acoustic Environment. Journal of Mammalogy 89, 549–558. https://doi.org/10.1644/07-MAMM-S-307R.1

Udovydchenkov, I.A., Stephen, R.A., Duda, T.F., Bolmer, S.T., Worcester, P.F., Dzieciuch, M.A., Mercer, J.A., Andrew, R.K., Howe, B.M., 2012. Bottom interacting sound at 50 km range in a deep ocean environment. The Journal of the Acoustical Society of America 132, 2224–2231. https://doi.org/10.1121/1.4747617

Ullgren, J.E., White, M., 2010. Water mass interaction at intermediate depths in the southern Rockall Trough, northeastern North Atlantic. Deep Sea Research Part I: Oceanographic Research Papers 57, 248–257. https://doi.org/10.1016/j.dsr.2009.11.005

Urick, R.J., 1983. Principles of underwater sound 3rd edition. Peninsula Publising Los Atlos, California 22, 23–24.

van Aken, H.M., 2000. The hydrography of the mid-latitude northeast Atlantic Ocean: I: The deep water masses. Deep Sea Research Part I: Oceanographic Research Papers 47, 757–788. https://doi.org/10.1016/S0967-0637(99)00092-8

van Aken, H.M., Becker, G., 1996. Hydrography and through-flow in the north-eastern North Atlantic Ocean: the NANSEN project. Progress in Oceanography 38, 297–346. https://doi.org/10.1016/S0079-6611(97)00005-0

Van der Graaf, A., Ainslie, M., André, M., Brensing, K., Dalen, J., Dekeling, R., Robinson, S., Tasker, M., Thomsen, F., Werner, S., 2012. European Marine Strategy Framework Directive-Good Environmental Status (MSFD GES): Report of the Technical Subgroup on Underwater noise and other forms of energy. Brussels.

Van Rooij, D., Blamart, D., Kozachenko, M., Henriet, J.-P., 2007. Small mounded contourite drifts associated with deep-water coral banks, Porcupine Seabight, NE Atlantic Ocean. Geological Society, London, Special Publications 276, 225–244. https://doi.org/10.1144/gsl.sp.2007.276.01.11

van Weering, Tj.C.E., Hall, I.R., de Stigter, H.C., McCave, I.N., Thomsen, L., 1998. Recent sediments, sediment accumulation and carbon burial at Goban Spur, N.W. European Continental Margin (47–50°N). Progress in Oceanography 42, 5–35. https://doi.org/10.1016/S0079-6611(98)00026-3

Vermeulen, N., 1997. Hydrography, Surface Geology and Geomorphology of the Deep Water Sedimentary Basins to the West of Ireland. Marine Institute.

Versluis, M., Schmitz, B., Heydt, A. von der, Lohse, D., 2000. How Snapping Shrimp Snap: Through Cavitating Bubbles. Science 289, 2114–2117. https://doi.org/10.1126/science.289.5487.2114

Vetter, E.W., Smith, C.R., Leo, F.C.D., 2010. Hawaiian hotspots: enhanced megafaunal abundance and diversity in submarine canyons on the oceanic islands of Hawaii. Marine Ecology 31, 183–199. https://doi.org/10.1111/j.1439-0485.2009.00351.x

Vlasenko, V., Stashchuk, N., 2015. Internal tides near the Celtic Sea shelf break: A new look at a well known problem. Deep Sea Research Part I: Oceanographic Research Papers 103, 24–36. https://doi.org/10.1016/j.dsr.2015.05.003

Volkman, J.K., Barrett, S.M., Blackburn, S.I., Mansour, M.P., Sikes, E.L., Gelin, F., 1998. Microalgal biomarkers: A review of recent research developments. Organic Geochemistry 29, 1163–1179. https://doi.org/10.1016/S0146-6380(98)00062-X

Volkman, J.K., Johns, R.B., 1977. The geochemical significance of positional isomers of unsaturated acids from an intertidal zone sediment. Nature 267, 693–694. https://doi.org/10.1038/267693a0
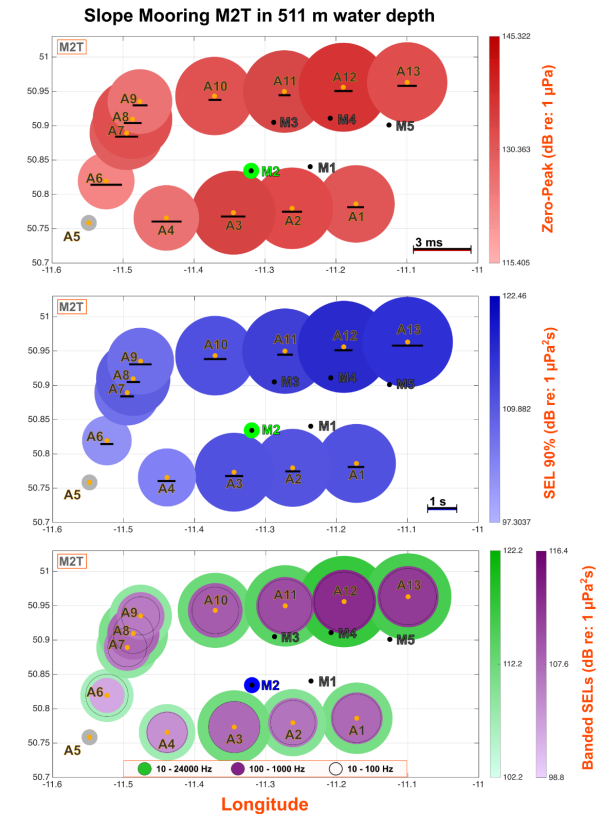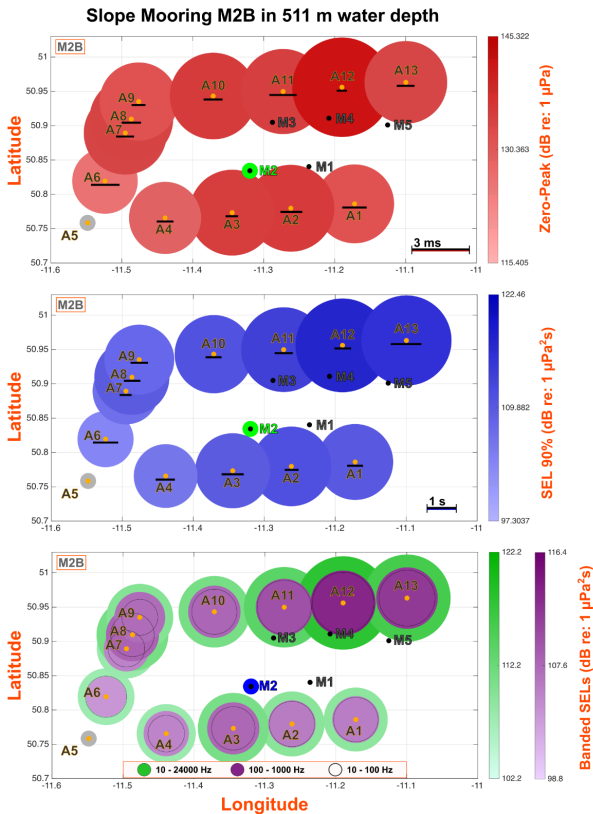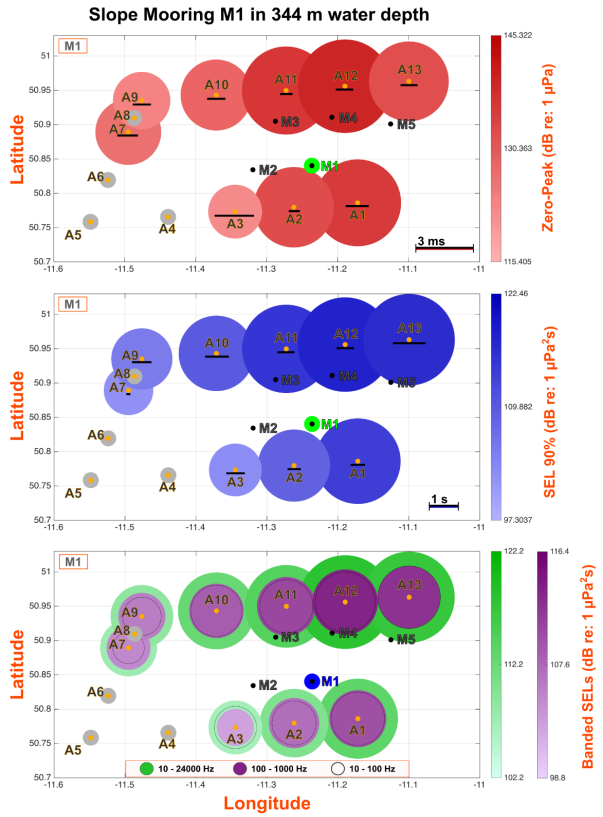
# References

Wagstaff, R.A., 1981. Low-frequency ambient noise in the deep sound channel—The missing component. The Journal of the Acoustical Society of America 69, 1009–1014. https://doi.org/10.1121/1.385680

Wale, M.A., Briers, R.A., Hartl, M.G., Bryson, D., Diele, K., 2019. From DNA to ecological performance: Effects of anthropogenic noise on a reef-building mussel. Science of The Total Environment 689, 126–132. https://doi.org/10.1016/j.scitotenv.2019.06.380

Wang, L., Ward, J., Robinson, S., 2019. Standard for data processing of measured data (Draft). Report of the EU INTERREG Joint Monitoring Programme for Ambient Noise North Sea (JOMOPANS), https://northsearegion.eu/jomopans/output-library/.

Wang, L.S., Robinson, S.P., Theobald, P., Lepper, P.A., Hayman, G., Humphrey, V.F., 2012. Measurement of radiated ship noise. Presented at the Proceedings of Meetings on Acoustics ECUA2012, ASA, p. 070091. https://doi.org/10.1121/1.4792663

Wartzok, D., Ketten, D.R., 1999. Marine mammal sensory systems. Biology of marine mammals 1, 117–175.

Watling, L., Norse, E.A., 1998. Disturbance of the Seabed by Mobile Fishing Gear: A Comparison to Forest Clearcutting. Conservation Biology 12, 1180–1197. https://doi.org/10.1046/j.1523-1739.1998.0120061180.x

Welch, P., 1967. The use of fast Fourier transform for the estimation of power spectra: a method based on time averaging over short, modified periodograms. IEEE Transactions on audio and electroacoustics 15, 70–73. https://doi.org/10.1109/tau.1967.1161901

Wenz, G.M., 1962. Acoustic ambient noise in the ocean: Spectra and sources. The Journal of the Acoustical Society of America 34, 1936–1956. https://doi.org/10.1121/1.1909155

White, M., 2006. Benthic dynamics at the carbonate mound regions of the Porcupine Sea Bight continental margin. Int J Earth Sci (Geol Rundsch) 96, 1. https://doi.org/10.1007/s00531-006-0099-1

White, M., 2003. Comparison of near seabed currents at two locations in the Porcupine Sea Bight--implications for benthic fauna. Marine Biological Association of the United Kingdom. Journal of the Marine Biological Association of the United Kingdom 83, 683. https://doi.org/10.1017/S0025315403007641h

White, M., Bowyer, P., 1997. The shelf-edge current north-west of Ireland. Presented at the Annales Geophysicae, Springer, pp. 1076–1083.

White, M., Dorschel, B., 2010. The importance of the permanent thermocline to the cold water coral carbonate mound distribution in the NE Atlantic. Earth and Planetary Science Letters 296, 395–402. https://doi.org/10.1016/j.epsl.2010.05.025

Wieczorek, A.M., Morrison, L., Croot, P.L., Allcock, A.L., MacLoughlin, E., Savard, O., Brownlow, H., Doyle, T.K., 2018. Frequency of Microplastics in Mesopelagic Fishes from the Northwest Atlantic. Front. Mar. Sci. 5. https://doi.org/10.3389/fmars.2018.00039

Wilcock, W.S.D., Stafford, K.M., Andrew, R.K., Odom, R.I., 2014. Sounds in the Ocean at 1–100 Hz. Annu. Rev. Mar. Sci. 6, 117–140. https://doi.org/10.1146/annurev-marine-121211-172423

Williams, Rob, Erbe, C., Ashe, E., Clark, C.W., 2015. Quiet (er) marine protected areas. Marine Pollution Bulletin 100, 154–161. https://doi.org/10.1016/j.marpolbul.2015.09.012

Williams, R., Wright, A.J., Ashe, E., Blight, L.K., Bruintjes, R., Canessa, R., Clark, C.W., Cullis-Suzuki, S., Dakin, D.T., Erbe, C., Hammond, P.S., Merchant, N.D., O'Hara, P.D., Purser, J., Radford, A.N., Simpson, S.D., Thomas, L., Wale, M.A., 2015. Impacts of anthropogenic noise on marine life: Publication patterns, new discoveries, and future directions in research and management. Ocean & Coastal Management, Making Marine Science Matter: Issues and Solutions from the 3rd International Marine Conservation Congress 115, 17–24. https://doi.org/10.1016/j.ocecoaman.2015.05.021

Wilson, A.M., Kiriakoulakis, K., Raine, R., Gerritsen, H.D., Blackbird, S., Allcock, A.L., White, M., 2015a. Anthropogenic influence on sediment transport in the Whittard Canyon, NE Atlantic. Marine pollution bulletin 101, 320–329. https://doi.org/10.1016/j.marpolbul.2015.10.067

Wilson, A.M., Raine, R., Mohn, C., White, M., 2015b. Nepheloid layer distribution in the Whittard Canyon, NE Atlantic Margin. Marine Geology 367, 130–142. https://doi.org/10.1016/j.margeo.2015.06.002

# References

Wilson, M.F.J., O'Connell, B., Brown, C., Guinan, J.C., Grehan, A.J., 2007. Multiscale Terrain Analysis of Multibeam Bathymetry Data for Habitat Mapping on the Continental Slope. Marine Geodesy 30, 3–35. https://doi.org/10.1080/01490410701295962

Wilson, O.B., Wolf, S.N., Ingenito, F., 1985. Measurements of acoustic ambient noise in shallow water due to breaking surf. The Journal of the Acoustical Society of America 78, 190–195. https://doi.org/10.1121/1.392557

Wisniewska, D.M., Johnson, M., Teilmann, J., Siebert, U., Galatius, A., Dietz, R., Madsen, P.T., 2018. High rates of vessel noise disrupt foraging in wild harbour porpoises ( Phocoena phocoena ). Proc. R. Soc. B. 285, 20172314. https://doi.org/10.1098/rspb.2017.2314

Wollast, R., 1998. Evaluation and comparison of the global carbon cycle in the coastal zone and in the open ocean. The sea 10, 213–252.

Wollast, R., Chou, L., 2001. The carbon cycle at the ocean margin in the northern Gulf of Biscay. Deep Sea Research Part II: Topical Studies in Oceanography 48, 3265–3293. https://doi.org/10.1016/S0967-0645(01)00040-6

Wood, S., 2018. Mixed GAM computation vehicle with GCV/AIC/REML smoothness estimation and GAMMs by REML/PQL. R package version 1–8.

Wood, S.N., 2017. Generalized Additive Models: An Introduction with R, 2nd ed. CRC press.

Wood, S., 2006. Generalized Additive Models: An Introduction with R, 1st ed. CRC Press.

Wood, S.N., Augustin, N.H., 2002. GAMs with integrated model selection using penalized regression splines and applications to environmental modelling. Ecological Modelling 157, 157–177. https://doi.org/10.1016/S0304-3800(02)00193-X

Wright, A.J., Cosentino, A.M., 2015. JNCC guidelines for minimising the risk of injury and disturbance to marine mammals from seismic surveys: We can do better. Marine Pollution Bulletin 100, 231–239. https://doi.org/10.1016/j.marpolbul.2015.08.045

Xing, J., Davies, A.M., 1996. Processes influencing the internal tide, its higher harmonics, and tidally induced mixing on the Malin-Hebrides Shelf. Progress in Oceanography 38, 155–204. https://doi.org/10.1016/S0079-6611(97)00001-3

Xu, J.P., Noble, M.A., Rosenfeld, L.K., 2004. In-situ measurements of velocity structure within turbidity currents. Geophysical Research Letters 31. https://doi.org/10.1029/2004GL019718

Yamamuro, M., Kayanne, H., 1995. Rapid direct determination of organic carbon and nitrogen in carbonate-bearing sediments with a Yanaco MT-5 CHN analyzer. Limnology and Oceanography 40, 1001–1005. https://doi.org/10.4319/lo.1995.40.5.1001

Zhao, Z., D'Asaro, E.A., Nystuen, J.A., 2014. The Sound of Tropical Cyclones. Journal of Physical Oceanography 44, 2763–2778. https://doi.org/10.1175/JPO-D-14-0040.1

Zhou, J., Zhang, X., Rogers, P.H., 1991. Resonant interaction of sound wave with internal solitons in the coastal zone. The Journal of the Acoustical Society of America 90, 2042–2054. https://doi.org/10.1121/1.401632

# Appendix A: Supplementary to Chapter 5

**Appendix A.1.** Map scatter plots of sound levels received at all mooring recorders, for all chosen pathways. Top panel (red) is zero-peak levels, middle panel (blue) is 90% energy SELs and bottom panel (purple/green) shows banded SELs. Black horizontal bars in top and middle panels represent rise times of zero-peak and 90% energy respectively, while contour bars to the left of each panel are set to maximum and minimum values of the total set of moorings throughout.

Canyon Mooring M3B in 898 m water depth



Canyon Mooring M3T in 898 m water depth



Canyon Mooring M4 in 651 m water depth



Shelf Edge Mooring M5 in 250 m water depth
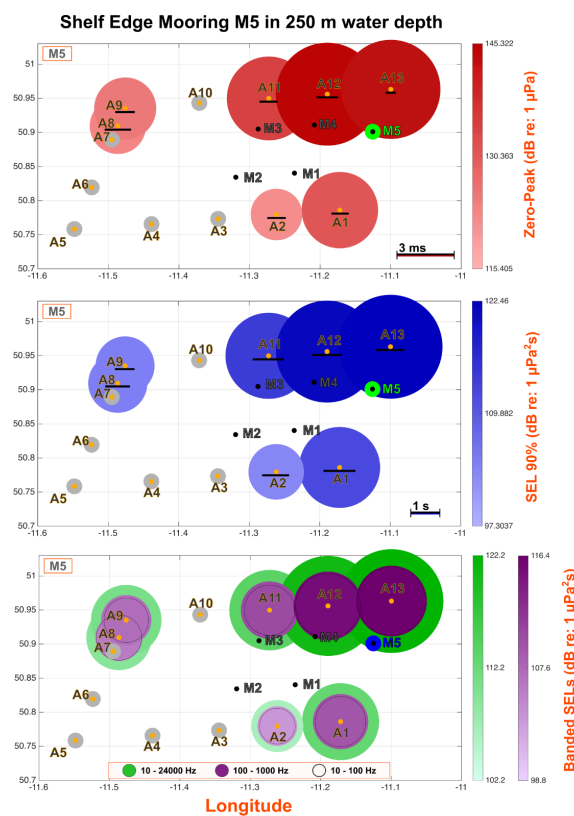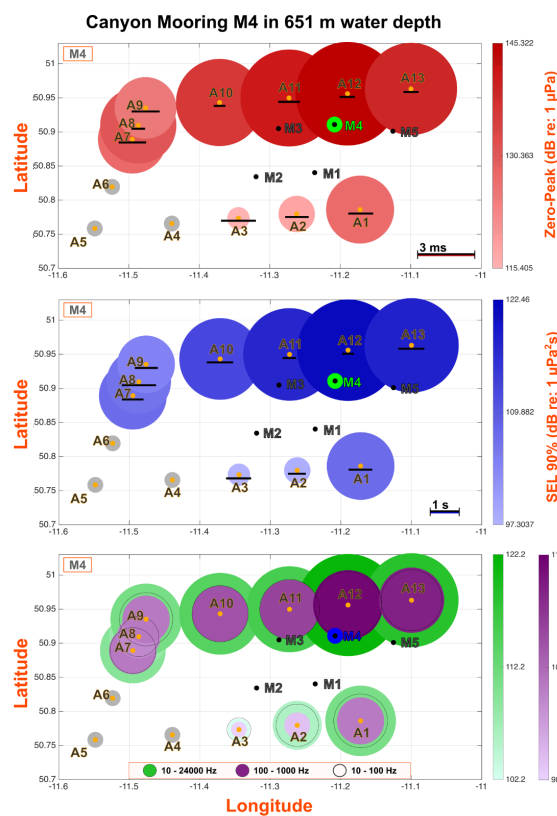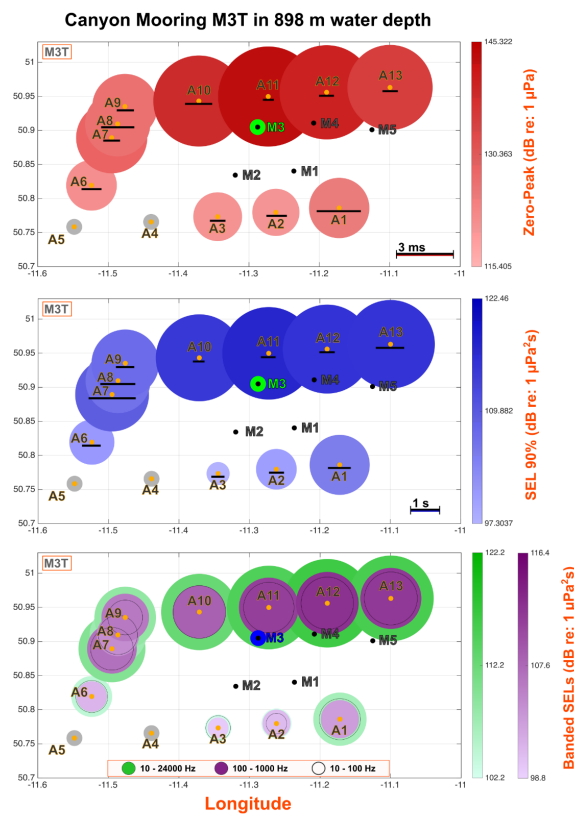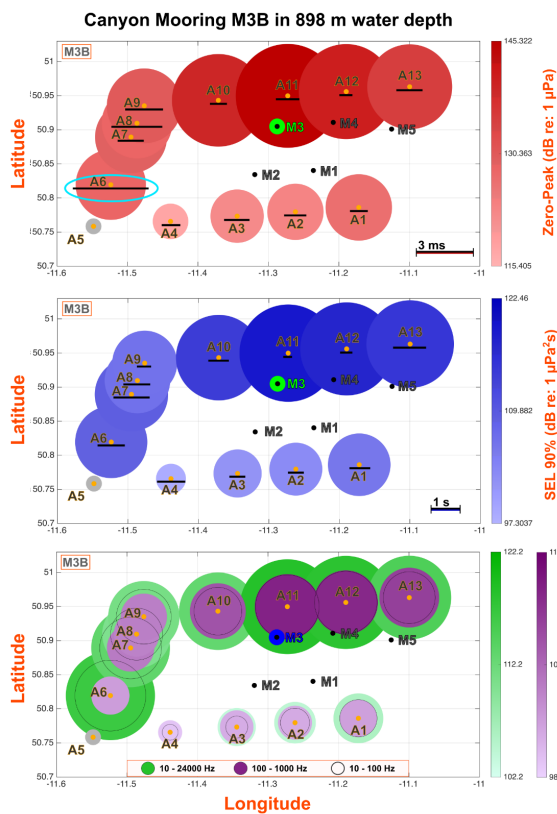
Table A1. Mooring and airgun locations. Spatial and temporal data

| | Date | Time | Position | | Depth | | |
|---|---|---|---|---|---|---|---|
| | | | Longitude | Latitude | Water | Bottom Phone | Top phone |
| | (June 2018) | (UTC) | (Deg) | (Deg) | (m) | (m) | (m) |
| Mooring Locations | | | | | | | |
| M1 | 10th - 12th | | -11.237 | 50.841 | 344 | | 100 |
| M2 | 10th - 12th | | -11.319 | 50.834 | 511 | 506 | 100 |
| M3 | 10th - 12th | | -11.291 | 50.904 | 898 | 893 | 100 |
| M4 | 10th - 12th | | -11.208 | 50.910 | 651 | | 100 |
| M5 | 10th - 12th | | -11.125 | 50.900 | 250 | | 100 |
| | | | | | | | |
| Airgun Locations | | | | | | | |
| A1 | 10th | 18:18:40 | -11.172 | 50.786 | 312 | | |
| A2 | 10th | 19:14:10 | -11.262 | 50.779 | 603 | | |
| A3 | 10th | 20:07:20 | -11.344 | 50.773 | 831 | | |
| A4 | 10th | 21:05:20 | -11.439 | 50.765 | 1186 | | |
| A5 | 10th | 22:14:20 | -11.548 | 50.758 | 1571 | | |
| A6 | 10th | 23:17:50 | -11.523 | 50.819 | 1412 | | |
| A7 | 11th | 00:31:10 | -11.495 | 50.889 | 1393 | | |
| A8 | 11th | 00:52:50 | -11.486 | 50.909 | 1221 | | |
| A9 | 11th | 01:19:10 | -11.476 | 50.935 | 957 | | |
| A10 | 11th | 02:21:20 | -11.371 | 50.943 | 535 | | |
| A11 | 11th | 03:22:10 | -11.272 | 50.950 | 362 | | |
| A12 | 11th | 04:16:10 | -11.189 | 50.956 | 226 | | |
| A13 | 11th | 05:18:40 | -11.099 | 50.963 | 180 | | |

**Table A2.** Pathways to slope moorings: Sound level metrics and rise times

| Pathway | Zero-Peak | | 90% Energy SELs | | | | SEL Bands (Hz)$ | | | | |
|---|---|---|---|---|---|---|---|---|---|---|---|
| | Level | Rise-time | Manual* | 1 s | 2 s | Rise-time** | 10 -24k | 10 -100 | 100 -1k | 1k -10k | 10k -24k |
| | (dB) | (s) | (dB) | (dB) | (dB) | (s) | (dB) | (dB) | (dB) | (dB) | (dB) |
| | re: 1uPa | | re: 1uPa$^2$s | re: 1uPa$^2$s | re: 1uPa$^2$s | | re: 1uPa$^2$s | re: 1uPa$^2$s | re: 1uPa$^2$s | re: 1uPa$^2$s | re: 1uPa$^2$s |
| M1-A1 | 135.62 | 0.00123 | 113.73 | 113.78 | 113.85 | 0.53 | 113.53 | 108.24 | 111.82 | 97.46 | 84.05 |
| M1-A2 | 132.52 | 0.00060 | 108.64 | 108.69 | 108.89 | 0.52 | 110.23 | 105.01 | 108.21 | 98.49 | 84.31 |
| M1-A3 | 122.24 | 0.00210 | 102.79 | 102.74 | 103.23 | 0.64 | 106.76 | 104.37 | 102.35 | 93.76 | 83.70 |
| M1-A6# | 118.03 | 0.00272 | 102.96 | 105.80 | 108.66 | | 105.79 | 103.25 | 100.81 | 95.21 | 85.44 |
| M1-A7 | 126.35 | 0.00110 | 101.97 | 102.52 | 103.07 | 0.43 | 107.41 | 101.48 | 105.16 | 97.57 | 85.36 |
| M1-A9 | 123.38 | 0.00097 | 105.09 | 105.13 | 105.53 | 0.71 | 108.76 | 103.25 | 106.62 | 97.11 | 84.41 |
| M1-A10 | 128.41 | 0.00096 | 109.81 | 109.70 | 109.99 | 0.74 | 112.56 | 107.49 | 110.38 | 101.27 | 83.83 |
| M1-A11 | 136.20 | 0.00066 | 114.93 | 114.98 | 115.03 | 0.64 | 114.32 | 108.22 | 112.85 | 99.27 | 85.47 |
| M1-A12 | 139.05 | 0.00092 | 117.58 | 117.57 | 117.63 | 0.62 | 118.09 | 111.06 | 117.01 | 100.21 | 84.90 |
| M1-A13 | 132.23 | 0.00091 | 116.29 | 115.47 | 116.34 | 0.80 | 117.18 | 112.17 | 115.39 | 98.83 | 86.04 |
| M2B-A1 | 131.80 | 0.00131 | 109.97 | 109.97 | 110.03 | 0.57 | 109.05 | 105.05 | 106.53 | 94.10 | 83.32 |
| M2B-A2 | 135.62 | 0.00116 | 111.36 | 111.34 | 111.40 | 0.48 | 109.33 | 105.32 | 106.73 | 95.73 | 83.75 |
| M2B-A3 | 135.09 | 0.00067 | 109.67 | 109.65 | 109.83 | 0.76 | 110.86 | 104.74 | 109.16 | 99.22 | 83.16 |
| M2B-A4 | 128.87 | 0.00090 | 105.89 | 105.83 | 106.12 | 0.60 | 107.89 | 102.71 | 105.78 | 96.37 | 83.50 |
| M2B-A6 | 126.26 | 0.00152 | 103.67 | 103.65 | 104.51 | 0.84 | 107.38 | 104.11 | 103.75 | 94.91 | 84.77 |
| M2B-A7 | 133.75 | 0.00096 | 106.73 | 106.79 | 106.94 | 0.46 | 107.94 | 102.73 | 105.89 | 95.67 | 84.29 |
| M2B-A8 | 134.00 | 0.00103 | 109.65 | 109.63 | 109.68 | 0.58 | 111.11 | 104.78 | 109.64 | 96.68 | 83.88 |
| M2B-A9 | 131.54 | 0.00074 | 107.91 | 107.91 | 108.13 | 0.63 | 109.77 | 102.59 | 108.47 | 95.72 | 83.72 |
| M2B-A10 | 135.46 | 0.00101 | 110.85 | 110.90 | 111.00 | 0.58 | 111.04 | 105.29 | 109.26 | 98.62 | 84.43 |
| M2B-A11 | 134.73 | 0.00146 | 113.40 | 113.39 | 113.47 | 0.64 | 113.65 | 108.54 | 111.80 | 97.51 | 84.38 |
| M2B-A12 | 142.31 | 0.00055 | 117.28 | 117.30 | 117.35 | 0.60 | 117.98 | 111.63 | 116.71 | 100.38 | 83.22 |
| M2B-A13 | 133.58 | 0.00095 | 115.71 | 114.59 | 115.74 | 0.72 | 115.79 | 109.32 | 114.60 | 95.58 | 82.98 |
| M2T-A1 | 131.15 | 0.00090 | 111.09 | 111.09 | 111.13 | 0.59 | 110.99 | 106.42 | 108.97 | 93.87 | 82.94 |
| M2T-A2 | 133.04 | 0.00107 | 110.73 | 110.73 | 110.78 | 0.53 | 109.85 | 105.08 | 107.67 | 97.12 | 82.66 |
| M2T-A3 | 134.14 | 0.00131 | 111.10 | 111.12 | 111.23 | 0.64 | 111.58 | 107.53 | 108.84 | 99.71 | 83.12 |
| M2T-A4 | 126.27 | 0.00160 | 104.22 | 104.25 | 104.65 | 0.64 | 107.32 | 103.76 | 104.23 | 94.86 | 83.41 |
| M2T-A6 | 123.13 | 0.00168 | 102.01 | 102.61 | 103.38 | 0.76 | 106.61 | 104.42 | 101.64 | 94.23 | 84.56 |
| M2T-A7 | 129.59 | 0.00123 | 106.47 | 106.53 | 106.63 | 0.49 | 108.54 | 103.37 | 106.58 | 94.95 | 84.09 |
| M2T-A8 | 132.04 | 0.00095 | 109.35 | 109.34 | 109.45 | 0.48 | 110.45 | 103.68 | 109.19 | 95.21 | 83.65 |
| M2T-A9 | 125.95 | 0.00079 | 106.89 | 106.87 | 107.10 | 0.79 | 108.71 | 103.17 | 106.86 | 95.39 | 83.44 |
| M2T-A10 | 131.57 | 0.00069 | 111.36 | 111.35 | 111.54 | 0.79 | 112.01 | 105.75 | 110.50 | 98.85 | 84.84 |
| M2T-A11 | 133.48 | 0.00064 | 113.62 | 113.66 | 113.73 | 0.56 | 113.88 | 108.24 | 112.28 | 98.21 | 84.33 |
| M2T-A12 | 136.67 | 0.00098 | 116.54 | 116.51 | 116.58 | 0.61 | 117.21 | 110.62 | 116.02 | 98.82 | 83.22 |
| M2T-A13 | 132.43 | 0.00104 | 115.79 | 114.29 | 115.80 | 0.73 | 115.61 | 109.41 | 114.33 | 95.85 | 82.64 |

**Notes:**

* Manual refers to manually picking individual shot start and finish times using a filtered time-pressure series

** Rise Time here is for 1 s duration 90% energy levels

$SEL Bands here are standardised to 1 s shot duration

#M3B-A6 Pathway had no shots present but has been shot analysed for comparison purposes

**Table A3.** Pathways to canyon moorings: Sound level metrics and rise times

| Pathway | Zero-Peak | | 90% Energy SELs | | | | SEL Bands (Hz)[$] | | | | |
|---|---|---|---|---|---|---|---|---|---|---|---|
| | Level | Rise-time | Manual* | 1 s | 2 s | Rise-time** | 10 -24k | 10 -100 | 100 -1k | 1k -10k | 10k -24k |
| | (dB) | (s) | (dB) | (dB) | (dB) | (s) | (dB) | (dB) | (dB) | (dB) | (dB) |
| | re: 1uPa | | re: 1uPa$^2$s | re: 1uPa$^2$s | re: 1uPa$^2$s | | re: 1uPa$^2$s | re: 1uPa$^2$s | re: 1uPa$^2$s | re: 1uPa$^2$s | re: 1uPa$^2$s |
| M3B-A1 | 126.76 | 0.00095 | 105.65 | 105.56 | 105.80 | 0.71 | 106.00 | 102.99 | 102.51 | 92.12 | 83.21 |
| M3B-A2 | 123.15 | 0.00119 | 102.92 | 102.92 | 103.09 | 0.56 | 104.55 | 100.98 | 101.34 | 92.97 | 83.42 |
| M3B-A3 | 122.23 | 0.00136 | 101.72 | 101.91 | 102.37 | 0.71 | 104.00 | 99.64 | 101.15 | 93.73 | 85.37 |
| M3B-A4 | 117.61 | 0.00100 | 98.26 | 97.88 | 98.79 | 0.77 | 102.23 | 98.79 | 98.36 | 92.96 | 83.61 |
| M3B-A6 | 125.68 | 0.00407 | 108.79 | 108.68 | 110.84 | 0.94 | 116.67 | 116.44 | 102.91 | 95.50 | 85.76 |
| M3B-A7 | 128.98 | 0.00140 | 109.22 | 108.21 | 109.57 | 0.86 | 113.26 | 111.96 | 106.88 | 96.10 | 85.29 |
| M3B-A8 | 128.46 | 0.00273 | 106.59 | 106.11 | 107.01 | 0.74 | 110.39 | 107.87 | 106.02 | 96.23 | 84.24 |
| M3B-A9 | 130.23 | 0.00203 | 106.38 | 107.13 | 107.69 | 0.79 | 111.10 | 108.95 | 106.37 | 96.35 | 84.21 |
| M3B-A10 | 138.86 | 0.00091 | 113.96 | 113.91 | 113.99 | 0.64 | 112.91 | 106.29 | 111.45 | 100.41 | 84.58 |
| M3B-A11 | 145.32 | 0.00126 | 119.22 | 119.26 | 119.30 | 0.39 | 118.72 | 112.89 | 117.17 | 103.50 | 86.24 |
| M3B-A12 | 140.23 | 0.00070 | 117.25 | 117.28 | 117.33 | 0.45 | 118.11 | 112.33 | 116.54 | 103.13 | 84.77 |
| M3B-A13 | 134.91 | 0.00140 | 114.82 | 113.85 | 114.85 | 0.77 | 114.87 | 107.80 | 113.75 | 98.30 | 84.13 |
| M3T-A1 | 124.56 | 0.00237 | 104.91 | 104.72 | 105.14 | 0.78 | 106.71 | 104.08 | 102.86 | 92.18 | 82.98 |
| M3T-A2 | 120.42 | 0.00110 | 100.10 | 100.22 | 100.66 | 0.65 | 102.93 | 99.42 | 99.40 | 92.46 | 83.51 |
| M3T-A3 | 120.88 | 0.00083 | 97.38 | 98.85 | 99.66 | 0.82 | 102.57 | 100.06 | 97.64 | 92.08 | 83.81 |
| M3T-A6 | 121.42 | 0.00107 | 101.05 | 101.19 | 101.91 | 0.73 | 104.43 | 101.66 | 100.19 | 93.29 | 84.54 |
| M3T-A7 | 128.69 | 0.00090 | 109.39 | 108.75 | 109.45 | 0.95 | 109.90 | 104.56 | 108.03 | 96.57 | 84.88 |
| M3T-A8 | 126.35 | 0.00178 | 106.40 | 106.07 | 106.38 | 0.80 | 107.43 | 103.52 | 104.67 | 94.23 | 84.46 |
| M3T-A9 | 126.32 | 0.00093 | 107.23 | 107.17 | 107.26 | 0.63 | 108.56 | 102.33 | 107.02 | 95.60 | 83.92 |
| M3T-A10 | 138.11 | 0.00146 | 114.55 | 114.54 | 114.62 | 0.40 | 112.51 | 108.09 | 109.94 | 101.41 | 85.32 |
| M3T-A11 | 143.15 | 0.00059 | 117.05 | 117.05 | 117.11 | 0.53 | 114.78 | 107.23 | 113.71 | 98.62 | 85.05 |
| M3T-A12 | 139.84 | 0.00080 | 115.46 | 115.51 | 115.61 | 0.57 | 116.44 | 107.99 | 115.53 | 102.58 | 85.60 |
| M3T-A13 | 135.09 | 0.00083 | 115.24 | 114.30 | 115.30 | 0.71 | 115.47 | 108.20 | 114.48 | 96.47 | 85.23 |
| M4-A1 | 127.37 | 0.00134 | 107.26 | 107.08 | 107.47 | 0.72 | 110.90 | 108.53 | 106.85 | 94.57 | 85.24 |
| M4-A2 | 117.78 | 0.00126 | 97.76 | 97.75 | 98.56 | 0.64 | 105.87 | 104.52 | 98.79 | 93.66 | 85.06 |
| M4-A3 | 115.40 | 0.00188 | 97.30 | 97.05 | 98.49 | 0.78 | 102.17 | 99.97 | 96.70 | 91.70 | 84.65 |
| M4-A7 | 127.63 | 0.00148 | 107.30 | 107.30 | 107.79 | 0.78 | 109.59 | 105.61 | 106.91 | 96.13 | 86.61 |
| M4-A8 | 130.83 | 0.00074 | 106.19 | 105.39 | 106.44 | 0.76 | 108.03 | 103.77 | 105.15 | 95.90 | 86.19 |
| M4-A9 | 125.05 | 0.00150 | 104.20 | 103.99 | 104.36 | 0.67 | 111.10 | 108.37 | 106.90 | 98.09 | 86.46 |
| M4-A10 | 136.05 | 0.00063 | 112.38 | 112.25 | 112.73 | 0.84 | 114.21 | 109.55 | 111.59 | 104.43 | 87.35 |
| M4-A11 | 141.29 | 0.00117 | 117.04 | 117.07 | 117.15 | 0.49 | 115.60 | 111.09 | 113.40 | 101.02 | 86.23 |
| M4-A12 | 145.15 | 0.00083 | 121.23 | 121.25 | 121.26 | 0.43 | 121.53 | 114.47 | 120.41 | 105.85 | 87.43 |
| M4-A13 | 138.69 | 0.00081 | 117.87 | 117.42 | 117.94 | 0.76 | 118.41 | 111.58 | 117.30 | 100.13 | 86.35 |
| M5-A1 | 130.87 | 0.00092 | 112.10 | 111.18 | 112.25 | 0.78 | 112.75 | 107.26 | 111.13 | 96.65 | 84.68 |
| M5-A2 | 121.66 | 0.00099 | 103.62 | 103.16 | 104.05 | 0.73 | 106.48 | 102.59 | 103.52 | 95.03 | 84.78 |
| M5-A8 | 123.11 | 0.00141 | 104.60 | 104.62 | 105.74 | 0.89 | 109.49 | 105.51 | 106.70 | 96.57 | 84.77 |
| M5-A9 | 125.10 | 0.00105 | 104.54 | 104.72 | 105.62 | 0.81 | 110.87 | 105.23 | 108.36 | 102.02 | 87.74 |
| M5-A11 | 134.33 | 0.00096 | 114.18 | 113.94 | 114.60 | 0.93 | 113.83 | 107.25 | 112.41 | 100.90 | 84.10 |
| M5-A12 | 144.70 | 0.00116 | 121.47 | 121.09 | 121.49 | 0.86 | 120.74 | 113.43 | 119.73 | 103.32 | 86.23 |
| M5-A13 | 142.48 | 0.00054 | 122.46 | 122.22 | 122.46 | 0.90 | 122.23 | 115.23 | 121.20 | 101.72 | 85.61 |

**Notes:**
* Manual refers to manually picking individual shot start and finish times using a filtered time-pressure series
** Rise Time here is for 1 s duration 90% energy levels
[$] SEL Bands here are standardised to 1 s shot duration

**Appendix A.2.** SPL$_{rms}$ values from 30 s samples of ambient noise at each mooring recorder for duration of deployment at various frequency bins. Please see legend to the right-hand side for details
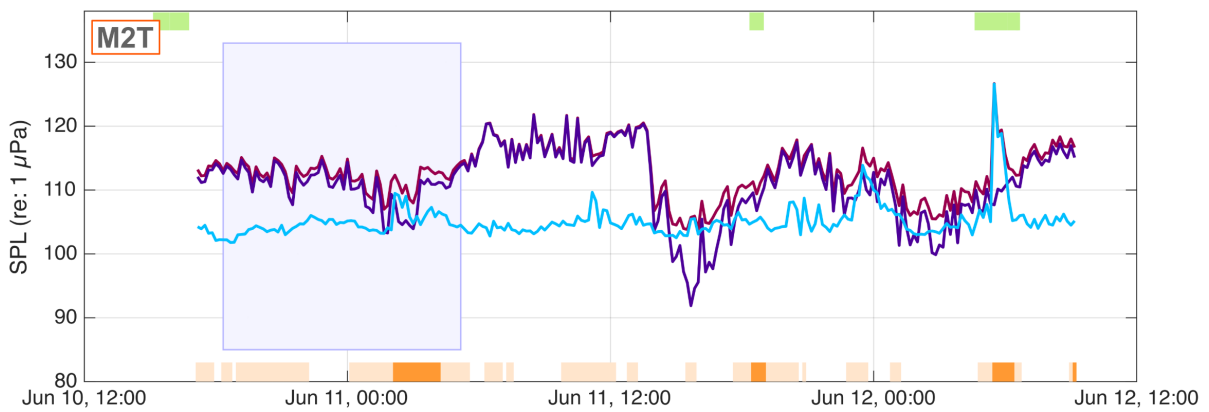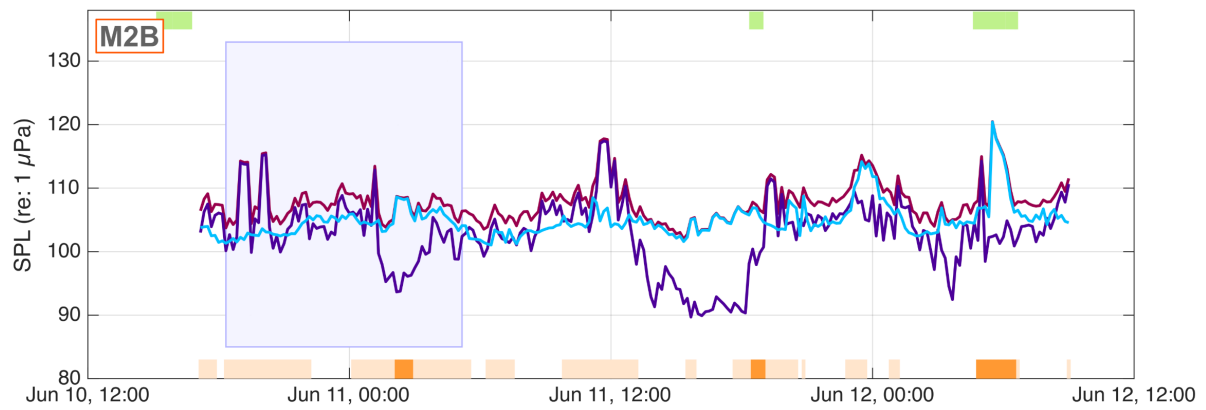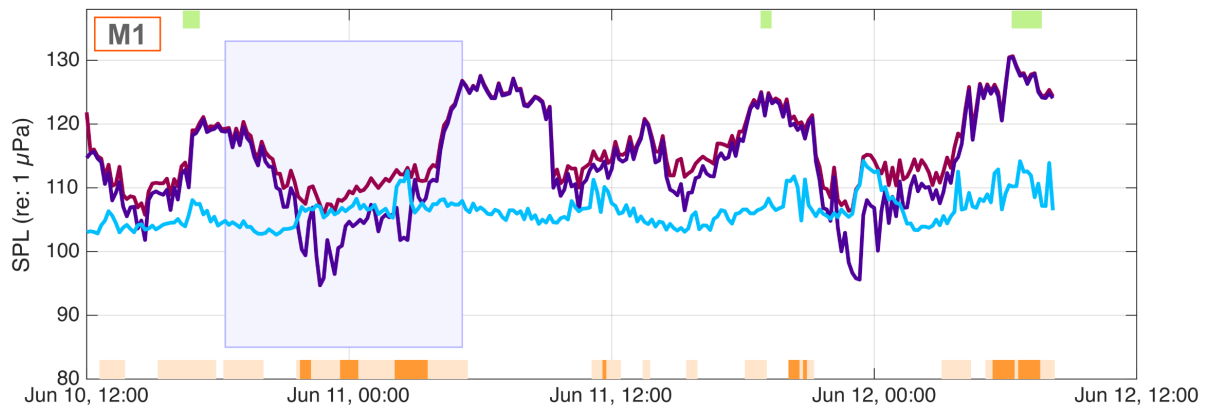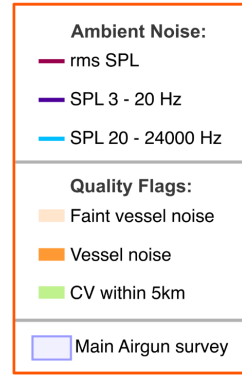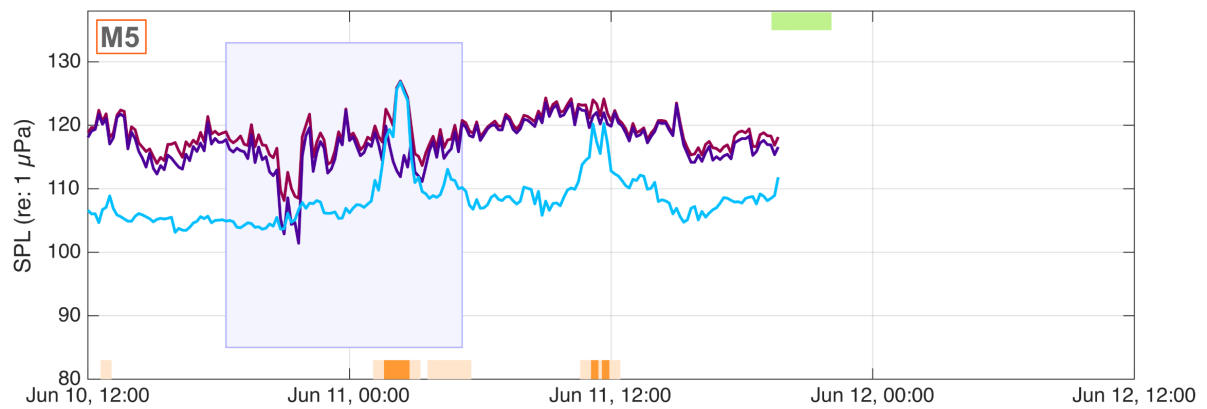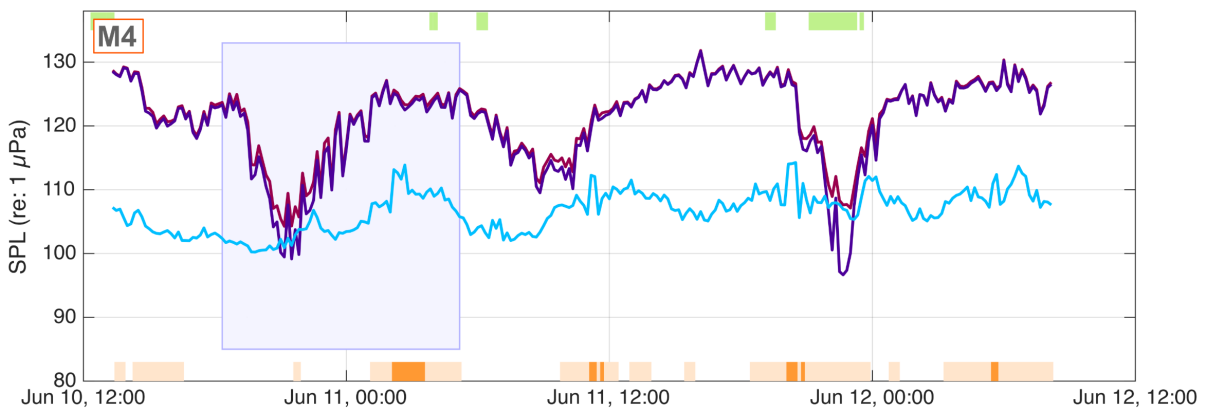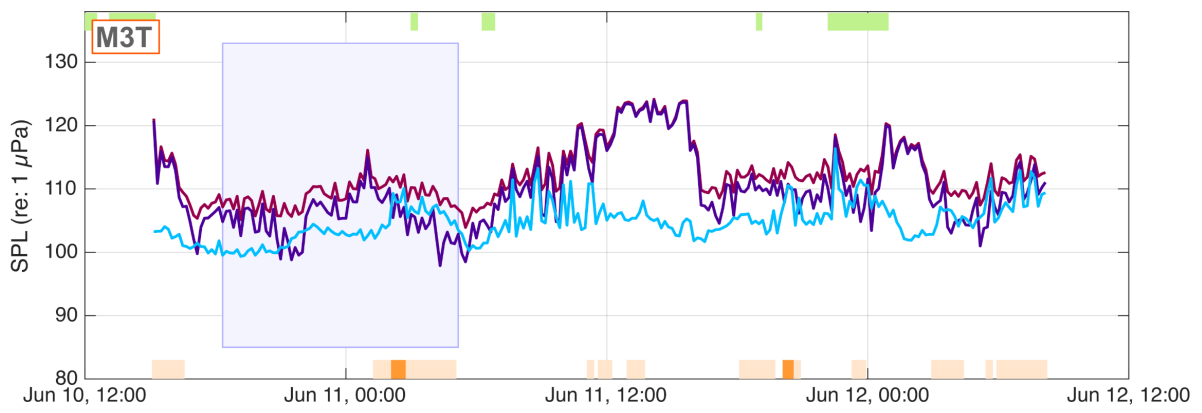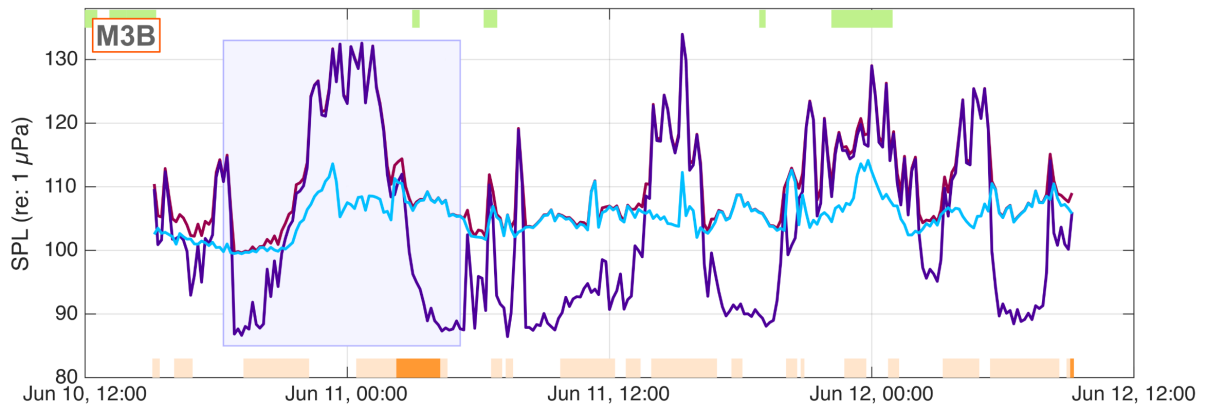
**Table A4.** Coefficients of Determination ($R^2$) from linear regression analysis of selected independent and dependent variables

| Response Variables | | Predictor Variables | | | | | | |
|---|---|---|---|---|---|---|---|---|
| | | Simple Linear Regression | | | Multiple Linear Regression | | | |
| | | (1) Range | (2) Depth at gun | (3) Δ Depth | (1 + 2) | (1 + 3) | (2 + 3) | (1 + 2 + 3) |
| | Units | $R^2$ | $R^2$ | $R^2$ | $R^2$ | $R^2$ | $R^2$ | $R^2$ |
| Zero-peak | dB (re: 1 µPa) | 0.40 | 0.31 | 0.24 | 0.51 | 0.49 | 0.32 | 0.52 |
| Zero-peak  Rise time | s | 0.04 | 0.13 | 0.02 | 0.13 | 0.05 | 0.19 | 0.20 |
| 90% SEL (manual) | dB (re: 1 µPa$^{2S}$) | 0.26 | 0.43 | 0.29 | 0.51 | 0.41 | 0.43 | 0.51 |
| 90% SEL (1 s) | dB (re: 1 µPa$^{2S}$) | 0.28 | 0.43 | 0.29 | 0.52 | 0.42 | 0.43 | 0.52 |
| 90% SEL (2 s) | dB (re: 1 µPa$^{2S}$) | 0.25 | 0.42 | 0.29 | 0.49 | 0.40 | 0.42 | 0.49 |
| 90% SEL Rise time | s | 0.20 | 0.03 | 0.03 | 0.20 | 0.20 | 0.03 | 0.20 |
| Broadband SEL | dB (re: 1 µPa$^{2S}$) | 0.13 | 0.33 | 0.22 | 0.35 | 0.27 | 0.33 | 0.36 |
| SEL 10 -100 Hz | dB (re: 1 µPa$^{2S}$) | 0.09 | 0.23 | 0.19 | 0.25 | 0.22 | 0.24 | 0.26 |
| SEL 100 -1k Hz | dB (re: 1 µPa$^{2S}$) | 0.16 | 0.39 | 0.22 | 0.42 | 0.29 | 0.40 | 0.43 |
| SEL 1k -10k Hz | dB (re: 1 µPa$^{2S}$) | 0.20 | 0.17 | 0.09 | 0.27 | 0.22 | 0.18 | 0.27 |

Notes:
1) n = 73 data points for each regression

2) Yellow cells are where P-values are > 0.05, indicating the null hypothesis or no significant relationship present

3) Refer to Ch. 6 **Table 6.2** for $R^2$ values with outliers removed

**Appendix A.3.** Single linear regression plots for each predictor (columns and X-axis) and response variable (rows and Y-axis) pair, as analysed and displayed in **Table 6.2** and in **Table A4** above.
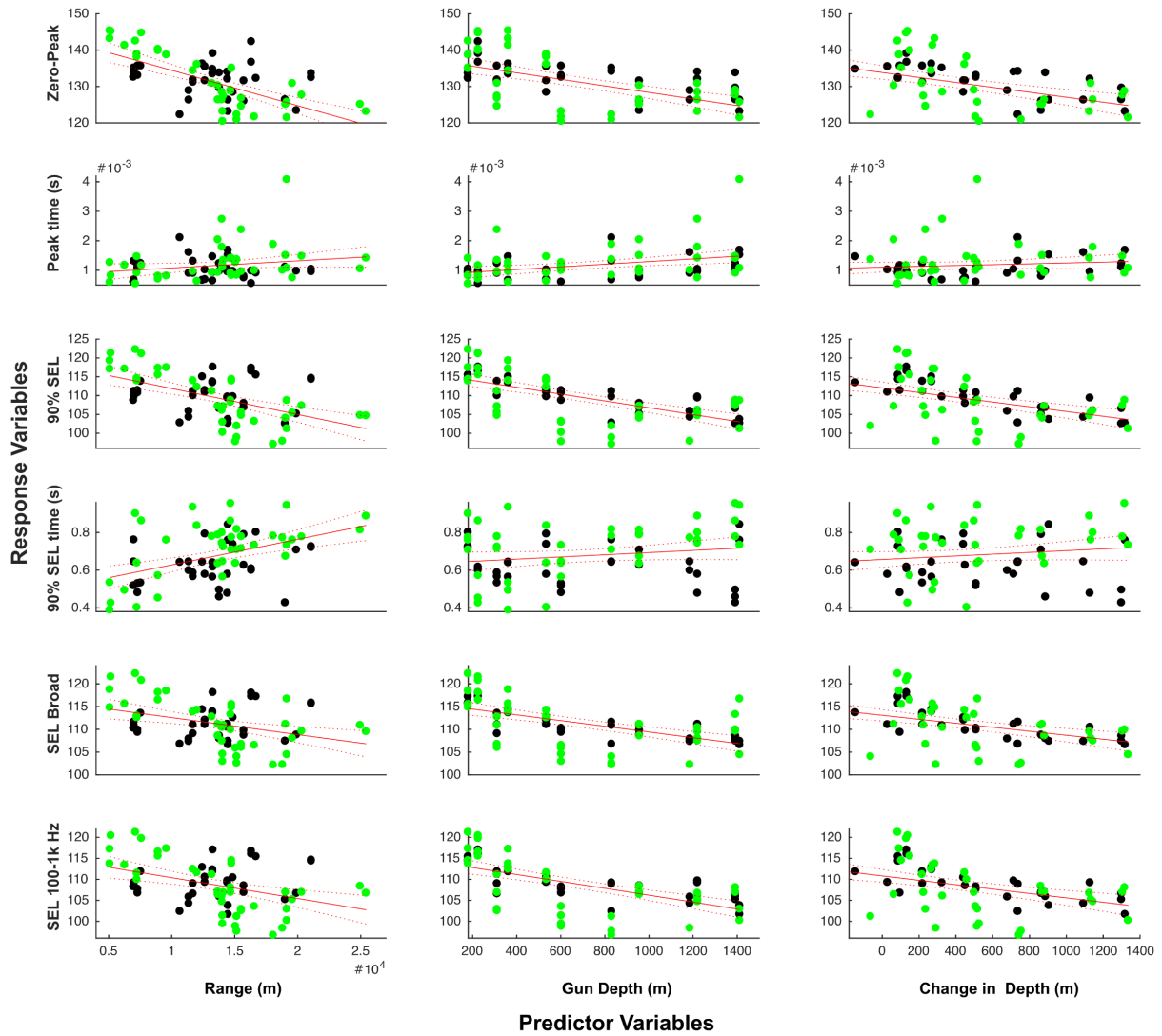
# Appendix B: Supplementary to Chapter 6

**Supplementary Table B.T1.**

Geoacoustic parameters used for RamGEO TL modelling

| | PANiC | | | GIST | | | |
|---|---|---|---|---|---|---|---|
| | Layer 1 | Layer 2 | Layer 3 | Layer 1 | Layer 2 | Layer 3 | Layer 4 |
| Description | Clay | Sand, silt clay | Halfspace | Holocene mud | Sandy mud | Sand & gravel | Halfspace |
| Thickness (m) | 50 | 200 | | 13 | 5 | 11 | |
| Compressional Sound speed (m s$^{-1}$) | 1549 - 1612 | 1642 - 1863 | 1950 | 1820 | 1600 | 2000 | 1950 |
| Density (kg m$^{-3}$) | 1488 | 1596 | 2100 | 2120 | 2310 | 2200 | 2100 |
| Compressional wave absorption (dB/λ) | 0.1 | 0.2 | 0.4 | 0.2 | 0.2 | 0.2 | 0.4 |
| Primary data source | Crawford *et al.*, 2016 | Crawford *et al.*, 2016 | Crawford *et al.*, 2016 | Coughlan *et al.*, 2019; | Coughlan *et al.*, 2019; | Coughlan *et al.*, 2019; | Crawford *et al.*, 2016 |
| Secondary data source | | | | *Pers. Comms.* Coughlan | e.g. Schumann *et al.*, 2014 | e.g. Ismail *et al.*, 2014 | |

**Supplementary Table B.T2.**

1/3 octave source level SPL estimates and broadband levels for all modelled pathways

| | PANiC | | | | GIST | | |
|---|---|---|---|---|---|---|---|
| Centre Frequencies (Hz) | Path 1 | Path 2 | Path 3 | Path 4 | Path 1 | Path 2 | Path 3 |
| 10 | 102.56 | 104.48 | 104.56 | 102.12 | 110.86 | 107.80 | 110.75 |
| 12.59 | 109.47 | 109.01 | 102.11 | 104.62 | 114.29 | 108.91 | 111.19 |
| 15.85 | 164.37 | 164.59 | 163.13 | 166.99 | 167.94 | 161.57 | 167.06 |
| 19.95 | 166.33 | 168.44 | 164.91 | 168.82 | 168.45 | 161.02 | 165.63 |
| 25.12 | 167.57 | 168.10 | 167.56 | 167.77 | 160.82 | 154.30 | 157.42 |
| 31.62 | 166.71 | 166.75 | 164.54 | 165.63 | 159.92 | 154.37 | 158.26 |
| 39.81 | 175.79 | 173.37 | 168.94 | 165.99 | 157.07 | 151.05 | 157.69 |
| 50.12 | 179.81 | 176.54 | 171.43 | 178.40 | 145.29 | 144.84 | 143.64 |
| 63.10 | 172.68 | 165.85 | 163.11 | 165.04 | 161.74 | 162.13 | 152.78 |
| 79.43 | 175.13 | 172.80 | 174.61 | 169.22 | 151.26 | 149.04 | 162.38 |
| 100 | 177.95 | 176.42 | 173.34 | 173.89 | 156.22 | 151.92 | 151.70 |
| 125.89 | 172.84 | 170.60 | 170.50 | 169.96 | 156.54 | 158.43 | 156.32 |
| 158.49 | 175.15 | 172.04 | 168.07 | 168.49 | 153.95 | 147.03 | 151.00 |
| 199.53 | 176.89 | 177.11 | 164.07 | 168.99 | 152.96 | 154.16 | 150.53 |
| 251.19 | 174.84 | 176.57 | 169.30 | 170.74 | 149.71 | 157.75 | 151.55 |
| 316.23 | 173.78 | 171.62 | 165.43 | 165.93 | 154.40 | 154.70 | 153.05 |
| 398.11 | 172.27 | 171.93 | 166.07 | 166.82 | 150.73 | 155.27 | 151.44 |
| 501.19 | 172.47 | 169.36 | 164.41 | 165.28 | 151.01 | 158.08 | 154.10 |
| 630.96 | 174.94 | 173.14 | 163.14 | 161.50 | 149.18 | 159.42 | 149.37 |
| 794.33 | 172.01 | 175.13 | 161.26 | 160.36 | 147.91 | 153.17 | 149.43 |
| 1000 | 166.77 | 169.33 | 159.77 | 159.33 | 142.84 | 142.49 | 146.83 |
| 1258.93 | 167.71 | 165.29 | 160.33 | 162.69 | 145.90 | 145.47 | 148.95 |
| 1584.89 | 169.53 | 171.77 | 164.43 | 165.71 | 146.99 | 150.66 | 148.12 |
| 1995.26 | 164.44 | 166.23 | 163.83 | 162.65 | 143.15 | 154.70 | 143.95 |
| 2511.89 | 164.39 | 167.49 | 158.91 | 159.96 | 137.96 | 152.29 | 144.32 |
| 3162.28 | 160.02 | 162.75 | 159.29 | 161.60 | 139.40 | 145.05 | 145.43 |
| 3981.07 | 157.10 | 160.07 | 157.95 | 159.13 | 140.92 | 149.79 | 144.56 |
| 5011.87 | 154.25 | 155.47 | 155.53 | 155.71 | 142.03 | 142.38 | 146.95 |
| 6309.57 | 155.10 | 153.59 | 154.43 | 155.26 | 140.97 | 140.54 | 140.59 |
| 7943.28 | 152.63 | 150.37 | 154.41 | 154.35 | 140.54 | 141.39 | 139.68 |
| 10000 | 149.73 | 148.67 | 150.68 | 151.61 | 143.80 | 138.50 | 139.61 |
| Broadband (Hz) | | | | | | | |
| 10 - 10000 | 187.23 | 186.14 | 181.49 | 182.91 | 172.98 | 170.02 | 171.65 |

Note: All values are SLs (dB re: 1 µPa @ 1 m) calculated from received 1/3 octave summed 60 second segment PSDs plus TL values

**Supplementary Table B.T3.**

Modelled TL values and source level estimates for  comparing surface with seabed generated noise,  from received levels of SPL & SEL for all modelled pathways.

| | PANiC Area | | | | GIST Area | | |
|---|---|---|---|---|---|---|---|
| | Path 1 | Path 2 | Path 3 | Path 4 | Path 1 | Path 2 | Path 3 |
| Spatial Parameters: | | | | | | | |
| Surface source depth (m) | 4 | 4 | 4 | 4 | 3 | 3 | 3 |
| Seabed source depth (m) | 217 | 224 | 233 | 245 | 48.5 | 48 | 47.5 |
| Received levels: | | | | | | | |
| RL rms SPL* (dB re: 1 µPa ) | 122.73 | 124.23 | 114.39 | 110.98 | 112.49 | 117.85 | 113.51 |
| RL SEL** (dB re: 1 µPa²/s ) | 140.51 | 142.01 | 132.17 | 128.76 | 130.27 | 135.63 | 131.29 |
| Modelled Transmission Loss (dB): | | | | | | | |
| TL modelled at surface | 96.28 | 95.55 | 98.02 | 101.28 | 87.26 | 82.41 | 85.74 |
| TL modelled at seabed | 88.79 | 89.18 | 92.36 | 94.38 | 87.12 | 80.19 | 84.30 |
| Source rms SPL* Estimates (dB re: 1 µPa ): | | | | | | | |
| SL from surface TL model | 187.23 | 186.14 | 181.49 | 182.91 | 172.98 | 170.02 | 171.65 |
| SL from seabed TL model | 182.13 | 183.72 | 177.23 | 175.32 | 173.56 | 168.12 | 171.27 |
| Source SEL** Estimates (dB re: 1 µPa²/s ): | | | | | | | |
| SEL from surface TL model | 205.01 | 203.92 | 199.27 | 200.69 | 190.77 | 187.80 | 189.43 |
| SEL from seabed TL model | 199.91 | 201.50 | 195.01 | 193.10 | 191.34 | 185.90 | 189.05 |

\* All rms SPL values are averaged over 60 seconds

\*\* All SEL values are integrated over a 60 second interval

Note: All broadband levels reported above are calculated from summed 1/3 octave values (10 – 10000 Hz), before conversion to dB
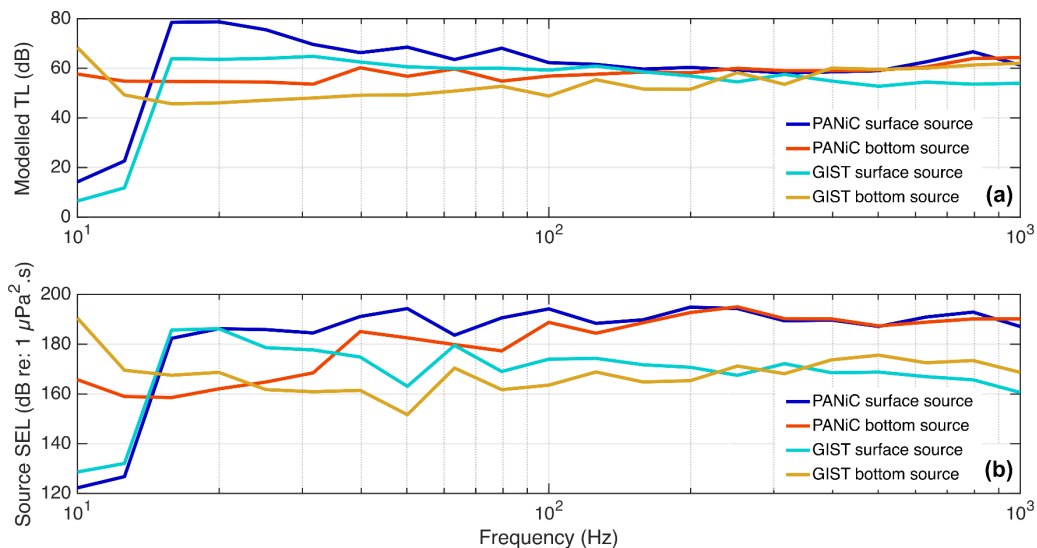


**Supplementary Fig. B.1.** (a): Modelled TL at 1/3 octave frequencies for both PANiC (blue)  and GIST (orange) sites contrasting surface (darker colour) and seabed (lighter) sourced noise. (b): Resulting 1/3 octave SL values as per colours above.

Supplementary audio files can be accessed through the (open access) online version of the publication (Click here to Link).

- Panic_Trawl.wav
- PANiC_RV.wav
- PANiC_Ambient.wav
- GIST_Trawl.wav
- GIST_Ambient.wav

# Appendix C:

# Bottom trawling at Whittard Canyon: evidence for seabed modification, trawl plumes and food source heterogeneity

Eoghan Daly[1,2], Mark P. Johnson[1], Annette Wilson[3], Hans D. Gerritsen[4], Konstadinos Kiriakoulakis[5], A. Louise Allcock[6] and Martin White[1,2].

[1]Earth and Ocean Sciences, Ryan Institute - School of Natural Sciences, National University of Ireland, Galway, Ireland.
[2]Irish Centre for Research in Applied Geoscience (ICRAG), National University of Ireland, Galway, Ireland.
[3]Alfred Wegener Institute, Biologische Anstalt Helgoland, 27498 Helgoland, Germany.
[4]Marine Institute, Rinville, Oranmore, Co. Galway, Ireland.
[5]Natural Sciences and Psychology, Liverpool John Moores University, UK.
[6]Ryan Institute and Zoology Department, School of Natural Sciences, National University of Ireland, Galway, Ireland.

**Contributions:** E. Daly: Conceptualisation, Data curation, Formal analysis, Investigation, Methodology, Visualisation, Writing (original draft and edits); A. Wilson: Biogeochemical analysis, Methodology, Writing (original draft, reviewing and editing); M. White: Conceptualisation, Methodology, Thorp analysis and interpretation, Project administration, Mentorship, Writing (original draft, reviewing and editing); M. Johnson: Statistical analysis and support, Reviewing and editing; H. Gerritsen: VMS data provision and interpretation, Reviewing and editing; K. Kiriakoulakis: Biogeochemical support; L. Allcock: Biological oversight.

**Keywords:** Trawling Plumes; Whittard Canyon; Suspended Particulate Matter; Vessel Monitoring System; Rugosity Index; Lipid Biomarkers

## Abstract

Fishing vessels are attracted to the dendritic Whittard Canyon system due to the abundance and diversity of species found there. Both midwater and bottom trawling are commonplace, including on deep canyon channel floors. Bottom trawling is identified here as a possible cause of changes to seafloor roughness along the canyon interfluves. An Arc Chord Ratio (ACR) rugosity index is calculated for the Whittard area and correlated with Vessel Monitoring System (VMS) data using various statistical models. Over higher slopes or rougher ground the heavily fished locations show a more homogeneous rugosity distribution than those lightly fished, indicating possible smoothing of the seabed.

Bottom trawling activity on adjacent interfluves/shelf is known to generate energetic turbid, sediment plumes within the canyon branches to 2500 m depth, with elevated Suspended Particulate Matter (SPM) concentrations in the water column up to 400 m above the seabed. Lipid biomarker analysis of organic material collected from these plumes showed higher concentrations of total lipids at sites that are intensively trawled (east). In comparison to sites that are less intensively trawled (west), higher contributions of fatty alcohols were detected. While lower concentrations of unsaturated fatty acids were detected, biomarkers indicative of phytoplankton accounted for 93.4±0.7% of total lipids identified from eastern samples suggesting rapid transport labile compounds. Intensive trawling, altering material loads and energetics at certain sites, can have implications for biochemical properties, sediment transport and distributions of local ecosystems in canyon systems, far from coastal zones.

## C.1. Introduction

The continental margin, occupying a little over 10% of the ocean surface area, connects the shelf seas (and hence coastal regions) to the deep sea, plays a significant role in the provision of food and energy resources, is a site for biogeochemical cycling (including carbon sequestration), and hosts a range of diverse ecosystem habitats and associated ecosystem services (e.g. Levin and Dayton, 2009; Benn et al., 2010; Levin and Sibuet, 2012). The margin is an area of heterogeneous habitat driven, in part, by the variation in continental morphology and topographic features, including slope variations, banks, mounds, seeps and canyons (Levin et al., 2010). In particular, sedimentary slopes are the most extensive margin habitat and contain the most numerous and diverse benthic communities (Grassle and Maciolek, 1997; Levin and Sibuet, 2012). There is a growing anthropogenic impact at these margin environments (e.g. Eastwood et al., 2007; Benn et al., 2010; Doney, 2010; Ramirez-Llodra et al., 2011). In particular, the spatial expansion of bottom trawling (Morato et al., 2006) into the deeper environment has been recognized as a significant element in modifying both seabed morphology and the sediment flux across the margin (e.g. Benn et al., 2010; Puig et al., 2012; Martín et al., 2014b; Oberle et al., 2016a). Both anthropogenic and natural drivers of ecosystem change at the continental margin require further

quantification as a foundation for offshore resource management and conservation (e.g., Davies et al., 2007; Benn et al., 2010).

Bottom trawling covers ground area comparable to between half (Watling and Norse, 1998) and three quarters (Kaiser et al., 2002) of the world's continental shelves, can globally drive sediment flux similar in quantity to fluvial input (Oberle et al., 2016a) and can have greater impact on the seabed than all other anthropogenic pressures combined (Eastwood et al., 2007; Halpern et al., 2008; Benn et al., 2010). These impacts are exacerbated in deeper, off-shelf waters where background energy levels and species resilience is lower and habitat recovery time slower (Kaiser et al., 2002). Bottom trawling gear makes direct contact with the seafloor and is responsible for the sorting and layering of sediments, for overturning, breaking up sediment fabric and causing bed armouring (Martín et al., 2014a; Oberle et al., 2016b). The degree to which the seafloor is affected depends on bottom type, gear design and ground contact (Gerritsen et al., 2013), with trawl doors causing the most acute damage (O'Neill and Summerbell, 2011), while sweep lines, bridals and footropes cause the most widespread damage (Martín et al., 2014b). In addition to physical alterations, trawling activity can also alter the biogeochemical composition of local sediments (Pusceddu et al., 2005a, b), with compositional changes being more influential than the seasonal input of organic matter in some areas (Sañe et al., 2013). Fishing grounds commonly have lower concentrations of flocculent Organic Carbon (OC) due to winnowing and oxygenation (Martín et al., 2014a; Pusceddu et al., 2014). Given these significant changes, the resuspension of organic matter from coastal and shelf regions by bottom trawling will likely increase OC export rates to the deep (Martín et al., 2008; Palanques et al., 2014). Furthermore, heavy metals and other pollutants buried in coastal sediments can be released by trawling activity and transported to deeper more vulnerable areas (Jones, 1992; Palanques et al., 1994).

Submarine canyons provide a conduit for sediment flux between shelf and deep ocean along the world's continental margins and, as such, both the deep sea and submarine canyons are now recognised as potential major repositories for anthropogenic wastes and marine litter, including plastics (e.g. Pham et al., 2014). There are many natural transport processes that control sediment erosion, transportation and deposition adjacent to, and within, submarine canyons, such as storm waves (Sanchez-Vidal et al., 2012), river input (Khripounoff et al., 2009),

dense shelf water cascading (Canals et al., 2006) and slope failure, each dependent on local or regional physical conditions. When compared to natural canyon transport processes that drive sediment flux, several studies have discussed anthropogenic impact, through bottom trawling, as a major, if not dominant, process, especially on human time scales (e.g. Halpern et al., 2008; Puig et al., 2012; Martín et al., 2014b; Puig et al., 2014). Additionally, bottom trawling in proximity to submarine canyons has been found to smooth out the seascape on large spatial scales, for example, at La Fonera Canyon (Puig et al., 2012; Martín et al., 2014a; Martín et al., 2014c; Payo-Payo et al., 2017), where changes to topography are now clearly visible on high resolution bathymetry maps (Puig et al., 2012). Trawler induced sediment gravity flows in La Fonera Canyon have been described in detail by Martín et al. (2014c). Payo-Payo et al. (2017) highlighted, through modelling anthropogenic sediment resuspension/transport, the ability of bottom trawling to affect wider areas than the fishing grounds, contrasting localised resettling on-shelf and over canyon flanks with widespread and distal displacement from sediment turbidity currents, especially over the steeper slopes.

Changes to morphology and biogeochemistry caused by bottom trawling in submarine canyons can affect ecosystem functioning and massively reduce benthic habitat heterogeneity (Watling and Norse, 1998; Puig et al., 2012 and references within). Trawling of the seafloor, negatively impacts on the biodiversity and abundance of life found there (Watling and Norse, 1998; Puig et al., 2012; Pusceddu et al., 2014); greatly reducing infaunal communities (O'Neill and Summerbell, 2011) when compared to untrawled areas.

In this paper the potential impacts of fishing on seabed morphology and down-canyon sediment distribution and associated biogeochemical parameters at the Whittard Canyon system on the Celtic Sea margin, NE Atlantic (Fig. C.1) have been assessed.  The Whittard Canyon is a dendritic system with canyon heads cutting the shelf at 180 – 200 m and a main channel axis opening onto deep ocean floor at 3600 – 4400 m (Reid and Hamilton, 1990; Amaro et al., 2016). Whittard Canyon has limited sediment input from fluvial processes due to its distance (~ 300 km) from land but does experience significant off-shelf material flux. This is due to high overlying pelagic productivity (Sharples et al., 2013) and dynamical processes such as boundary currents and internal waves which drive transport via nepheloid layers (Wilson 2015b; Hall et al., 2017), slope failure and sediment gravity flows (Amaro

et al., 2016). Additionally, Wilson et al. (2015a) observed Enhanced bottom Nepheloid Layers (ENLs) with significantly higher sediment concentrations in 2 branches of Whittard Canyon. These ENLs were correlated with fishing activity, via Vessel Monitoring System (VMS) data, to determine their anthropogenic origin but no detailed analysis of the plume dynamics were made at that time.
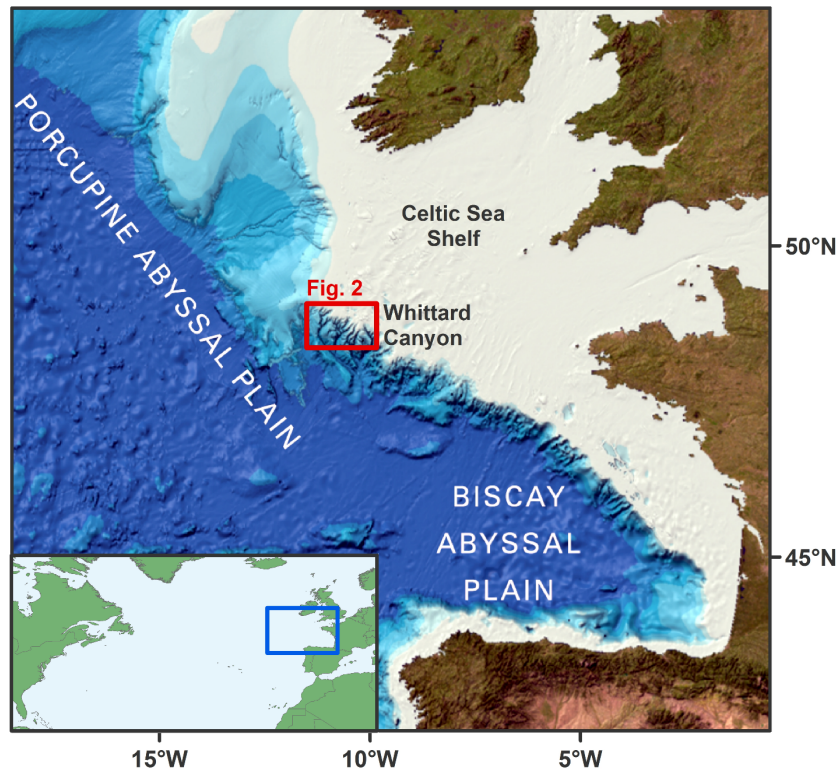


**Fig. C.1.** General overview of the Celtic Margin off the northwest European Continental Shelf. The red box is Fig. C.2: Whittard Canyon. Image reproduced from the GEBCO world map 2014, www.gebco.net.

Results presented here are in two parts; (i) a statistical comparison of fishing intensity and seafloor rugosity is carried out through a generalized additive model (GAM) fit, and (ii) a brief assessment is made of the dynamical and biogeochemical characteristics of the resulting trawl-induced sediment plumes found in the Whittard canyon branches. Results are discussed with respect to potential issues in interpretation of suspended sediment distribution patterns, biogeochemical signatures and potential impacts on ecosystem functioning within this and similar canyon systems.

## C.2. Methods

### C.2.1. Spatially distributed fishing intensity and seafloor roughness

Vessel Monitoring Systems (VMS) are used internationally for tracking vessel activity including fishing vessels. In the Whittard region, the fishing activity consists of northern and southern European fishing fleets. The spatial distribution of fishing fleets can change due to factors such as targeting different specific species or the cost of fuel (Gerritsen and Lordan, 2011). VMS monitoring is administered within the Irish Exclusive Economic Zone (EEZ) by the Irish Navel Service. Speed and position data are sent via satellite from each vessel at a minimum frequency of once every two hours. VMS data for this study were extracted for the period from January 2006 to February 2016 and then linked to logbook data to identify the gear type used (following methods described by Gerritsen and Lordan, 2011). Only bottom trawling vessels (which directly affect the seafloor) were retained in the dataset. Gear types used were bottom otter trawls (OTB), bottom pair trawls (PTB) and otter twin trawls (OTT) (Nédélec and Prado, 1990).  Fishing effort was defined according to Gerritsen and Lordan (2011). Each VMS record was assigned an effort value that was equal to the time interval since the previous record (generally 2 h). Records with time intervals > 4 h were given an effort value of 4 h. The data were then filtered to exclude vessel speeds < 0.5 knots or > 4.5 knots in order to retain only the records that correspond to fishing activity. VMS data were then gridded to their provided resolution of 0.01 x 0.01 decimal degrees, or 740 m (east/west) x 1110 m (north/south) at these latitudes, for analysis using Geographical Information System (GIS) applications (Fig. C.2b). It might be expected that the size of the grid cells should be approximately equal to the distance that a vessel can travel between successive VMS records, otherwise the vessel could travel over a number of grid cells without being recorded, leading to bias. However, this is not the case. Instead, each VMS record is a *sample* of a vessel's location (a systematic sample over time) and the number of VMS observations in each grid cell will therefore be proportional to the amount of time the vessels have spent in that cell. The resolution of the spatial grid is therefore not limited by the distance that a vessel can travel between successive VMS records, but instead by the number of records in each grid cell. Because the data are essentially count data, the precision can be estimated using a Poisson distribution. At the current resolution, 95% of grid cells in the study area

had at least 10 VMS records (relative standard error: 32%) and the mean number of records was 47 (relative standard error: 15%).
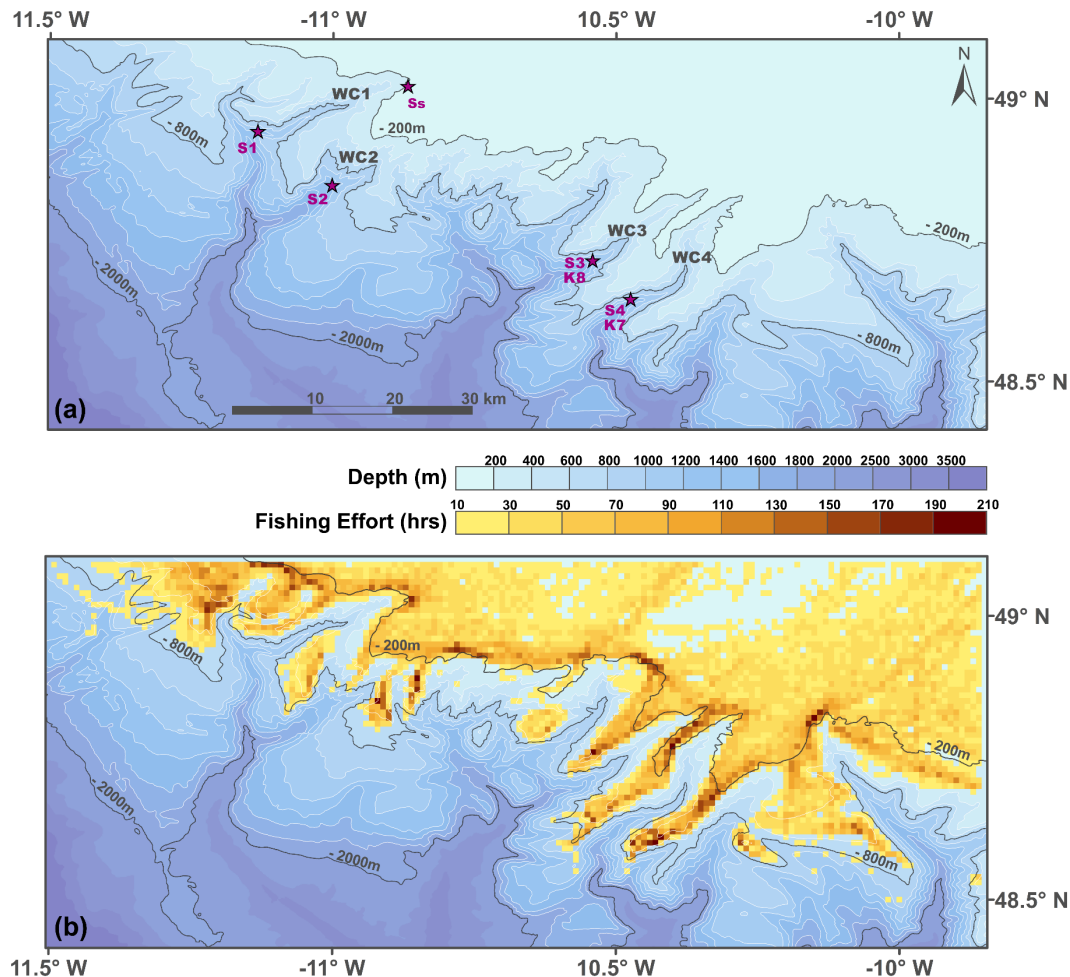


**Fig. C.2.** Area map of Whittard Canyon: (a) showing contoured bathymetry (in blue), SPM sample location labels: Ss = surface SPM; S1–4 = SPM samples from WC1–4 and turbulent energy analysis locations: K8 (Fig. C.8) & K9 (Fig. C.9). (b) Bathymetry overlaid with bottom trawling fishing hours from light in yellow to heavy in brown, with a minimum of 10 h shown.

Bathymetry was obtained from the Irish National Seabed Survey (INSS) for the Whittard Canyon region (extent: 48.416 to 49.105 N; −11.505 to −9.846 E). The INSS was carried out between 1999 and 2005, covering the majority of the Irish marine continental area and is freely accessible through the Geological Survey of Ireland (GSI) at a resolution of 0.001 x 0.001 degrees (~ 74 m by 111 m). Rugosity, a non-standardised (unitless) descriptor for seafloor roughness, was extracted using bathymetry data, point averaged down to VMS grid resolution and then analysed for correlations with VMS fishing effort. Here an Arc-Chord Ratio (ACR)

rugosity index was derived through a dedicated toolbox developed by Du Preez (2012) on an ArcGIS platform. The advantage of an ACR rugosity index is that it decouples background slope from the rugosity determination using a plane of best fit, rather than a more traditional horizontal plane. It is scale independent, therefore, making it well suited for use over the complex topographical features found around the Whittard Canyon.

Individual canyon branch polygons were drawn up within the canyon system to further scrutinise variation in fishing and potential sediment remobilisation across each location. These polygons (Labelled: WC1–WC4 in Fig. C.2a) were delineated using depth contours and distance from canyon branch channels. The deep ends of the canyon branch polygons were bound to the 2000 m depth contour. The polygons' sides make a line orthogonal to depth contours where the contours turn most sharply, stepping down from the canyon interfluves. The upper end of the polygons (where not touching another polygon) are defined to be a VMS grid cell above or touching the 200 m contour, in order to include those VMS cells as part of that canyon branch analysis. Although this approach is somewhat subjective, it is a best attempt at placing boundaries between these complexly shaped spurs and channels. Further polygons were drawn within these canyon branch divisions in an effort to focus on trawled areas that have the largest effect on sediment transport into the canyon channels. One approach here was to alter the original polygons by using a 10 hour VMS fishing contour as the inner or channel-side boundary, in order to isolate, for analysis, the regularly fished interfluves of the original polygon from the canyon axis. A second approach was to identify areas at the steepest limits of fishing occurrence over slopes with greatest potential for down canyon sediment supply; these strips are approximately 500 m wide and situated directly above areas of > 20° slope. Fishing rarely occurred anywhere steeper than a 20° slope angle (Fig. C.3a).

Potential influences on the rugosity of the seabed were considered to be broad scale geographic gradients, slope and fishing intensity. Estimates of the contributions of these variables were made using generalized additive models (GAMs). An example of a GAM in general form is as follows:

$$\mu_i \equiv E(R_i); \qquad g(\mu_i) = X_i\beta + S(x_{1i}) + S_2(x_{2i}, x_{3i}) + Ln_i S_3(x_4) + \dots \qquad \text{(C.1)}$$

Where $\mu_i$ is the expected value of the response variable $R_i$ and g is a known, monotonic, link function; $X_i\beta$ represents any fully parametric components of the linear predictor while $S_{1i,2i,3i...}$ are the smooth functions of the predictor variables ($x_{1i,2i,3i...}$); $Ln_i$ is included here as an example linear functional of $s_{3i}$, where there can be multiple or no such linear functional terms throughout the model (Wood and Augustin 2002; Wood 2006; Wood 2018). $R_i$ here is the interpolated rugosity value for each fished VMS grid cell. Predictors ($x_{1i-4i}$) were the latitude and longitude of each grid square (for geographic patterns), the estimated slope and the total fishing hours. GAMs were used because they provide a flexible statistical modelling framework for investigation of potentially nonlinear relationships, including interactions between predictor variables. Fitted GAMs are smoothed functions through the data using penalised regression splines, such that for example:

$$S(x) = \sum_{i=1} f_i(x)\beta_i \qquad\qquad\qquad\qquad\qquad\qquad (C.2)$$

Where the smooth function S constitutes values for the unknown parameters $\beta_i$ and where $f_i$ are chosen and known 'basis functions' on which the smoothing formulae rely on (Wood 2006; Wood 2018).

Screening of the data suggested that the data were not normally distributed. GAMs were therefore estimated (in R package mgcv, Wood, 2017) using a log-link to reflect the log-normal response variable. A number of models are possible given the four predictor variables investigated. The comparisons of interest were defined as a purely geographic pattern (predictors: latitude and longitude), a model based on just slope and fishing hours, and models where variables were allowed to interact in pairs or with all four variables together. Interaction terms test the hypothesis that the relationship of the response variable to a predictor is not fixed, but depends on a further predictor or predictors. The most informative of the alternative models was selected using the generalized cross validation (GCV) score, with low values indicating the best model (Wood, 2018). GCV scores penalize additional degrees of freedom, so the most complex model is not necessarily chosen as the most informative.
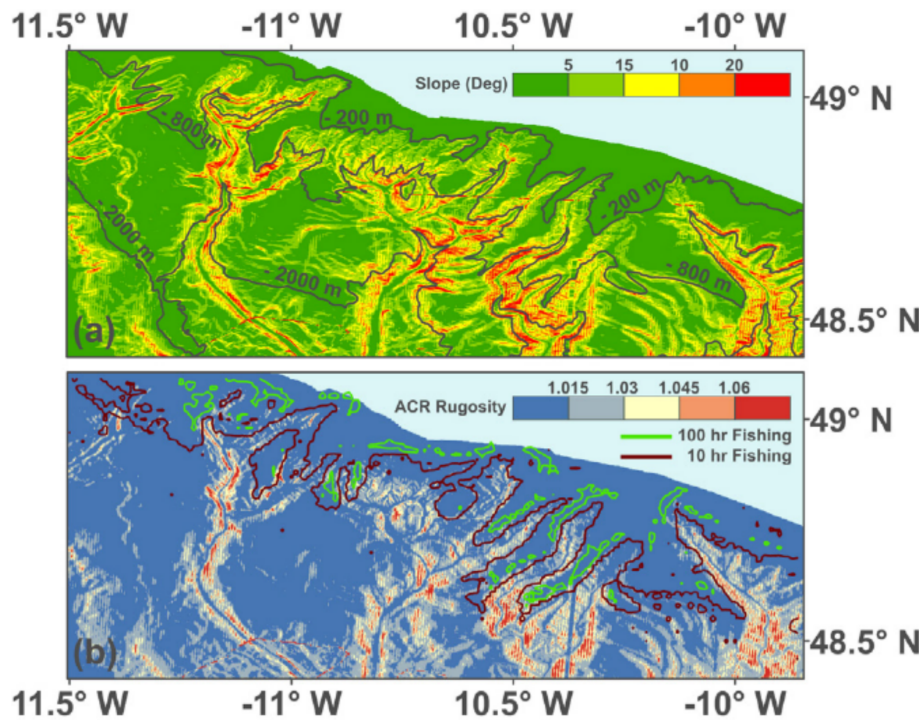
**Fig. C.3.** (a) Map image of slope angle at Whittard Canyon, with areas in red being greater than 20°. (b): Map image of ACR rugosity index; contours of VMS fishing effort are superimposed at 10 h (brown) and 100 h (green).

*C.2.2. Hydrographic observations*

Four branches of the Whittard Canyon were surveyed during summer 2013 (CE13008: 9–17th June 2013) & 2016 (CE16006: 29th May–15th June 2016) on the *RV Celtic Explorer*. Suspended Particulate Matter (SPM) was estimated from transmissometer measurements (C-star, WET labs; 0.25 m path length, operating at 650 nm) in conjunction with hydrographic measurements made with a CTD (Seabird SBE 911) and SBE32 rosette. Raw values (volts) were converted to SPM (µg L$^{-1}$) following the linear regression of beam attenuation values and the mass of SPM obtained from filtered water samples (Wilson et al., 2015b).

An assessment of the dynamical characteristics of recent trawling plumes measured was made using vertical CTD profiles. The turbulent length scales and first order estimation of magnitude in turbulent kinetic energy dissipation were quantified through Thorpe Length scale ($L_T$) analysis (Thorpe, 1977; Dillon, 1982). This method estimates the characteristic length scale ($L_T$) of density overturns within a CTD profile of sufficient vertical resolution (here 0.25m CTD data was used). $L_T$ is determined by reordering a profile of individual density values ($\rho_i$ at

depth $z_i$) into one where density increases monotonically with depth ($\rho_i$ at depth $z_o$). A corresponding profile of density displacements ($z_i - z_o$) is produced. $L_T$ is then defined as the RMS displacement value over an appropriate averaging process. This averaging is typically over individual overturns in a 'packet' of finite vertical extent where the sum of the individual Thorpe displacements equals zero, and that are not associated with instrument noise (e.g. Galbraith and Kelley, 1996; Mater et al., 2013). Furthermore, a simple estimate of the energy dissipation ($\varepsilon$) can be made following the arguments of Dillon (1982) and assuming $L_T$ is proportional to the Ozmidov length scale, $L_O$, which is used to describe the scale of turbulence in a stably stratified flow. Here we note caution in that $L_T$ is principally a method to estimate the vertical eddy size from the density profiles and only a limited method to fully quantify the turbulence (e.g. Mater et al., 2013).

Assuming that $L_T$ and $L_O$ are proportional, $\varepsilon$ can be found from a measurement of $L_T$,

$$\varepsilon = 0.64 * L_T^2 * N^{-3} \tag{C.3}$$

where N is the buoyancy frequency ($N^2 = [-g/\rho_0] * d\rho/dz$).

### C.2.3. Biogeochemical analysis of suspended particulate material

Suspended particulate organic matter (sPOM) was collected using a Stand Alone Pump System (SAPS; Challenger Oceanic), deployed by a winch on the CTD wire or attached to the CTD. Large volumes of water (163–1143 L) were filtered through two stacked pre-combusted (400 °C; > 6 hrs) glass fibre GF/F (Whatman, 293 mm diameter) filters at the surface and near bottom depths (7–22 m above the seabed). Filters were folded into quarters, wrapped in pre-combusted aluminium foil on recovery and stored at −80 °C for the duration of the cruise. Filters were subsequently freeze-dried and stored at −20 °C until analysis.

Elemental and molecular analysis was carried out on sPOM collected from Bottom Nepheloid Layers (BNLs) between 1310–1370 m water depth (< 20 m above the seabed) from the four branches and a surface sample (locations: Fig. C.2a). Particulate organic carbon (POC) and particulate nitrogen (PN) were measured from punched circles (113 mm$^2$) in homogeneous areas at the middle and edge of

the top filter only. Analyses were carried out using a CEInstruments NC 2500 CHN analyser in duplicates and the mean value was taken. POC values were obtained after de-carbonation of the filters (HCl vapour method; Yamamuro and Kayanne, 1995), whereas PN values were determined without de-carbonation. Mean values of the middle and edge filter samples were taken to eliminate filtrations artefacts. Concentrations below the limit of detection (< 0.01) were considered nil. Values were not corrected for dissolved organic material due to the large volumes of water filtered (Moran et al., 1999).

Lipid extractions and analyses of suspended Particulate Organic Matter (sPOM) were carried out according to the methods of Kiriakoulakis et al. (2007; 2009; 2011) to determine the total fatty acid and alcohol content. Briefly, portions (1/4) of the SAPS filter (~ 6.21–7.75 g) were spiked with 20 µl of internal standard (100 ng/µl 5α(H)-Cholestane; Sigma) and extracted by sonication (30 min @ 30 °C; x 3) in ~ 20 ml dichloromethane:methanol (9:1). Extracts were later transmethylated (24 hrs; 40 °C) with 1 ml methanolic acetyl chloride (30:1) and derivatised with 50 µl of *bis*-trimethylsilyltrifluoroacetamide (BSFTA, 1% trimethylsilylchloride; Stigma; 30 min @ 40 °C). Extracts were stored at −20 °C until analysis.

GC-MS analysis was carried out using a Varian 450 Gas Chromatographer Mass Spectrometer. Extracts were run in batches and loaded onto the column (Agilent VF-MS column: 30 m x 0.25 mm, 0.25 µm; carrier gas helium @ 1 mL min^{-1}) using a CP8400 autosampler and a CP-1177 split/splitless injector. The column was fed directly into the electron (EI) source of a Saturn 220 mass spectrometer (ionisation potential 70 eV; source temperature 220 °C; trap current 300 µA; full data acquisition mode). Chromatograms were reviewed and processed using Varian MS Workstation software (version 6.9.1). Compounds were identified by comparison of their mass spectra and relative retention times with authentic standards (Supelco TM37 FAME mix; 47085-U; 47015-U; 47033 Sigma-Aldrich) using the total ion current (TIC) chromatogram. Compound concentrations were calculated by comparison of peak areas of the internal standard with those of the compounds of interest. The relative response factors of the analytes were determined individually and/or for similar compounds. Organic contamination in procedural blanks extracted with each sample batch was subtracted from the sample values. Reproducibility of similar lipid analyses was determined to be ±15% by Kiriakoulakis et al. (2000). Concentrations were normalised to volume of water as an indicator of food

availability. The contribution of phytoplankton in each sample was calculated by the sum of $C_{14} - C_{22}$ saturated fatty alcohols (Volkman et al., 1998), straight chained fatty acids and $C_{16:1(n-7)}$ (Harwood and Russell, 1984; Conte et al., 2003) and PUFAs (e.g. Duineveld et al., 2012); see also supplementary information. Similarly, bacterial indices were calculated by the sum of $C_{18:1n7}$ and odd numbered saturated and branched fatty acids (Volkman and Johns, 1977; Duineveld et al., 2012).

## C.3. Results

### *C.3.1. Bottom trawling intensity and rugosity correlation*

Fishing occurred up to depths of around 1300 m right across the region studied (~ 7744 km$^2$), with fishing intensity clearly related to bathymetry and to large scale canyon features, such as interfluves or plateaux, up as far as the shelf break (Fig. C.2b). The combined total time spent by the fishing industry engaging in bottom trawling was 1.46 x 10$^5$ hours or just under 17 years over the 10-year period analysed. Over each VMS grid square (approximately 0.82 km$^2$) actively fished in the 10 years, the mean fishing effort was 4.8 hrs, median fishing effort was 23.4 hrs and the highest fished grid-square saw 208 hrs of bottom trawling (fishing effort from VMS having an accuracy of approximately 88% after Gerritsen and Lordan, 2011). The highest bottom fishing values were found out along the interfluves and plateaus adjacent to steeper slopes. Although concentrated on lower slopes and shallower waters, fishing effort regularly occurred on steeper inclines (> 10°) on canyon flanks around the edges of interfluves and occasionally in waters deeper than 1000 m. As of December 2016, deep-sea bottom trawling below 800 m deep is prohibited in these waters by EU law (EU 2016/2336).

In an effort to assess the most appropriate type of analysis, an initial plot of rugosity against slope was constructed with fishing points split between high and low around their median (Fig. C.4). This identified the non-linear nature of the dataset, where the relationship between slope and rugosity may be different with different levels of fishing activity. High levels of fishing only occurred on low slopes and less complex rugosity, whereas low levels of fishing occurred over the whole region considered. Further examination of the data suggested that the calculated variation in rugosity
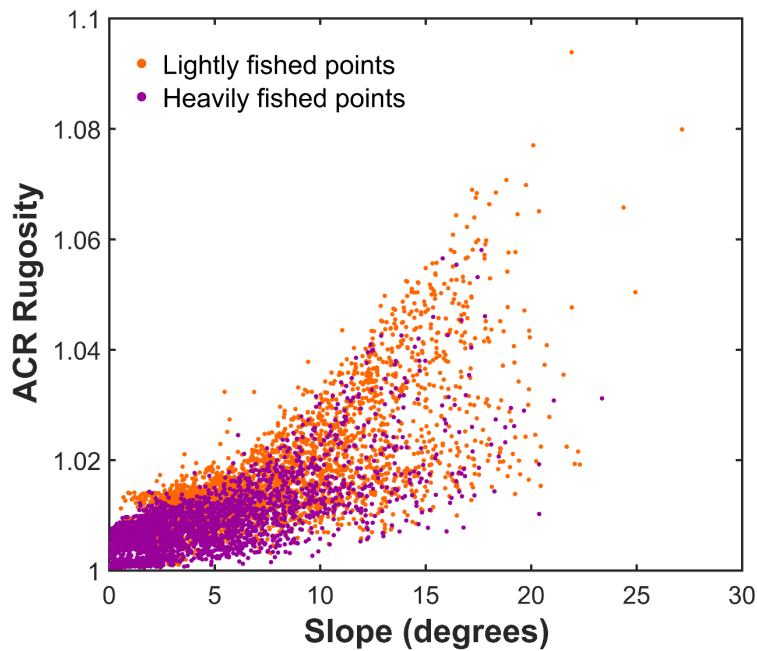
**Fig. C.4.** ACR Rugosity against slope angle for all VMS grid cells split between high (purple) and low (orange) fishing by their median.

among grid squares was lower in more heavily fished areas. This pattern changed with slope (Fig. C.5). By splitting the rugosity values into heavily and lightly fished grid squares (using median fishing effort: 23.4 hrs), standard deviation of rugosity can be summarized for each subset and viewed as a proxy for heterogeneity of seafloor roughness. For shallower slopes there was no difference between high and low fished grid squares, but at higher slopes the more heavily fished areas had less variation in rugosity (roughness) values.
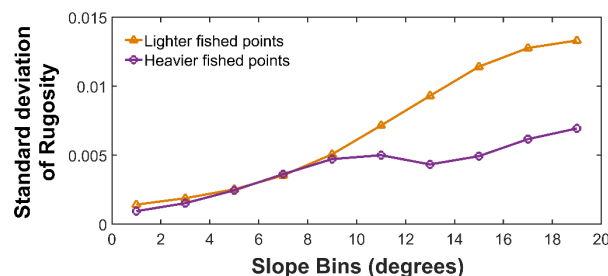


**Fig. C.5.** Canyon branch WC3: Standard deviation of rugosity among grid cells for the heavier fished (purple) and lighter fished (orange) data points. Split between 'heavy' and 'light' fishing on the basis of the median VMS fishing value.

There was statistical evidence for location, slope and fishing intensity all being related to changes in rugosity (Table C.T1). Judged by GCV scores, models with only two variables were inferior to a model that contained all four predictors (comparing models 1 – 3). Allowing all four variables to interact (model 4) did not improve predictive value compared to the model where all variables had independent effects (model 3). A model with terms where slope and fishing interacted, along with a geographic interaction (model 6), had the lowest GCV score and highest adjusted-$R^2$ of the alternative models. This can therefore be viewed as the most informative summary of the relationships between variables.

**Table C.T1**

Generalised Additive Model (GAM) fits to predict rugosity values in the full dataset, excluding cells with zero fishing (n = 6241 grid cells). Model predictors: R = Rugosity, Ln = longitude, Lt = Latitude, V = VMS fishing hours, S = slope angle. Variables in brackets have been modelled as interacting predictors. Generalised Cross Validation (GCV) scores indicate the relative performance of models, with lower values indicating better fits. Adjusted $R^2$ values are a less robust indicator of model fit, but are included as their interpretation is more intuitive as an indicator of the performance of models at fitting the data.

| Model | Terms | GCV $\times 10^{-5}$ | Adj R$^2$ % |
|---|---|---|---|
| 1 | Ln + Lt | 6.12 | 38.9 |
| 2 | S + V | 3.39 | 64.1 |
| 3 | Ln + Lt + S + V | 2.51 | 74.9 |
| 4 | (Ln × Lt × S × V) | 2.53 | 74.9 |
| 5 | (Ln × Lt) + V | 4.81 | 52.1 |
| 6 | (Ln × Lt) + (S × V) | 2.46 | 75.6 |
| 7 | (Ln × Lt) + S | 2.49 | 55.2 |

The geographic effect (Fig. C.6a) is a general decrease in rugosity with increasing latitude, with some variation in the rate of change with longitude, as is expected in this area going from deep canyon to shelf. Independent of the geographic pattern, rugosity contours show increasing roughness with steeper slopes (Fig. C.6b). The interaction with fishing intensity indicated a local increase in rugosity for low slope areas (particularly between 30 and 100 fishing hours), reflected in the deflection of the fitted contour at low slopes. For example, the average rugosity on seabed with less than 0.5 degree slope was 1.0048 (SE 0.00011) between 40 and 70 VMS hours and 1.0045 (SE 0.00011) at all other VMS values. Rugosity contours for areas with slopes steeper than 10° suggested that rugosity decreased with increased fishing. This pattern can be interpreted by comparing areas with low and high fishing effort for the same slope value. For example, at zero fishing, the predicted residual variation rugosity is above 0.005 on a 10° slope; at 50 fishing hours residual rugosity was predicted to be below 0.005 at the same slope value.
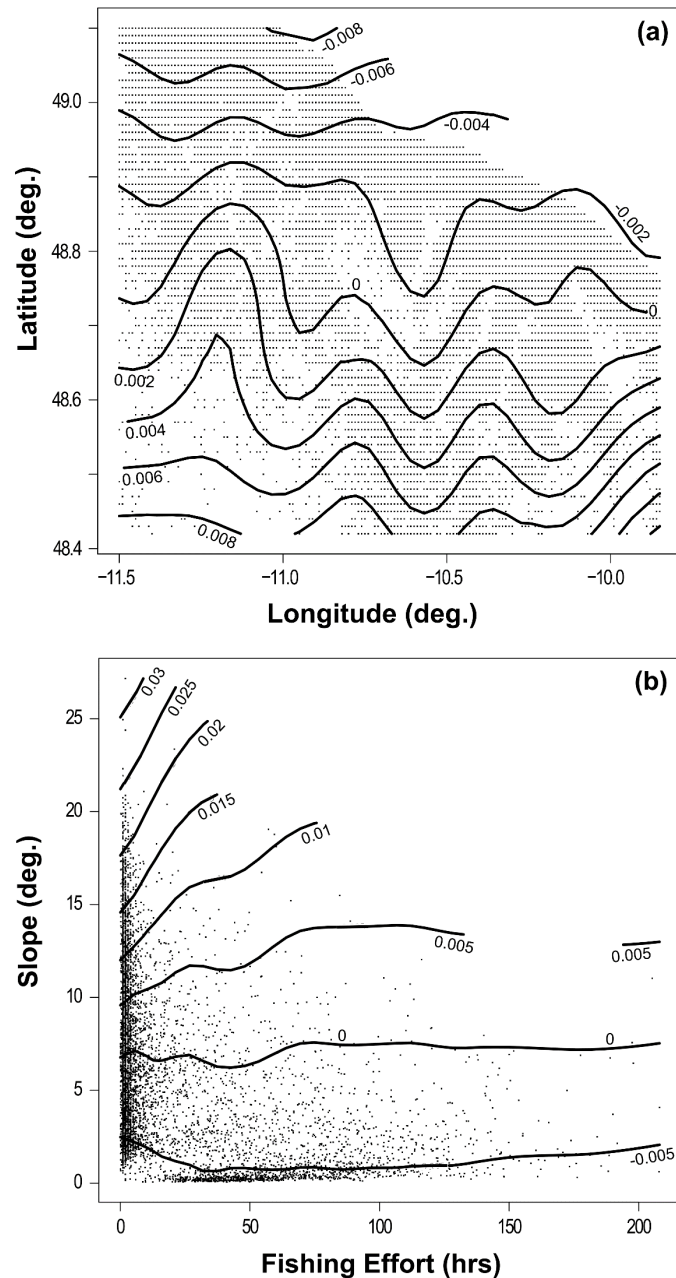
**Fig. C.4.** (a) Geographical representation of data points with contours of predicted residual variation rugosity as output by GAMs package mgcv (Wood, 2017). (b) Partial residual plot showing the combined influence of fishing effort and slope on rugosity. Contours of rugosity indicate the GAM fit to data for the whole Whittard Canyon region, controlling for the other predictors in the best model. Points indicate the distribution of observations for each predictor.

An east-west variation in fishing intensity was discovered across the four main canyon branches studied (WC1–WC4). Due to its geometry and the distribution of fishing intensity around that channel, WC4 was the largest probable contributor to down-slope sediment flux; followed by WC3 (Table C.T2). WC2 and WC1 to the west contributed least. By focussing on the interfluves flanking the WC4 canyon

branch channel, the largest fishing intensity per area (79.6 hrs km$^{-2}$ over the 10 years) was identified out of the whole region. There was very little fishing occurring on slopes greater than 20°, consequently this was chosen as a boundary between slopes fished and not fished. As with individual canyon branch results, these focused areas (Table C.T2), such as ones fished just above slopes of 20°, displayed a steady west to east increase (~ 5.3 hrs km$^{-2}$) in fishing intensity.

**Table C.T2**
Fishing intensity (hrs/km2) for each canyon branch, showing results for whole branches and also broken down into specific areas within branch.

| | Whole canyon branch | | | Shallower and higher fished interfluves | | | Areas directly above 20° slope | | |
|---|---|---|---|---|---|---|---|---|---|
| | Fishing (h) | Area (km$^2$) | Effort (h/km$^2$) | Fishing (h) | Area (km$^2$) | Effort (h/km$^2$) | Fishing (h) | Area (km$^2$) | Effort (h/km$^2$) |
| WC1 | 5755.6 | 220.4 | 26.1 | 5264.4 | 101.0 | 52.1 | 54.3 | 10.0 | 5.4 |
| WC2 | 5926.7 | 264.8 | 22.4 | 5766.4 | 92.1 | 62.6 | 133.6 | 12.0 | 11.1 |
| WC3 | 8847.2 | 214.1 | 41.3 | 8423.5 | 118.1 | 71.3 | 196.5 | 12.4 | 15.9 |
| WC4 | 11132.3 | 260.9 | 42.7 | 10779.5 | 135.5 | 79.6 | 278.6 | 13.1 | 21.3 |

*C.3.2. Sediment plumes within the canyon channels.*

Trawling, whilst modifying the seabed, also generates sources of suspended material at the shelf edge adjacent to the branches of the Whittard system. Sediment plumes had been observed in branches WC3 and WC4 during the 2013 survey (Wilson et al., 2015a). Since those reported observations, further plumes have been observed in the WC2 and WC4 branches during a subsequent survey in 2016. Both the along canyon and mid-water conditions due to trawling plume activity were apparent from vertical profiles of 10m averaged derived SPM concentrations (Fig. C.7). Under what were considered typical non-plume or background conditions, Benthic Nepheloid Layers (BNLs) of thickness 100–200 m have SPM concentrations within a canyon branch typically reached values similar to the corresponding surface plankton layers (0.15–0.4 mg l$^{-1}$, hatched shading in Fig. C.7a). The highest values occurred at bottom depths associated with boundary currents or internal wave energy enhancement (Wilson, 2015b). The immediate aftermath of what was considered a trawling plume event in WC4 resulted in an increase in benthic layer SPM concentrations, in excess of 1 mg l$^{-1}$ throughout the entire length of the canyon branch that was sampled (Fig. C.7b). Maximum BNL SPM concentration was 8 mg l$^{-1}$ in the mid-canyon section. Furthermore, values in excess of 0.3 mg l$^{-1}$, found over small spatial extents at certain depths in normal conditions, now occupied the lower 200–400 m adjacent to the seabed along the entire >45 km of the canyon branch surveyed. Overall, this section suggested a plume had recently passed through WC4.
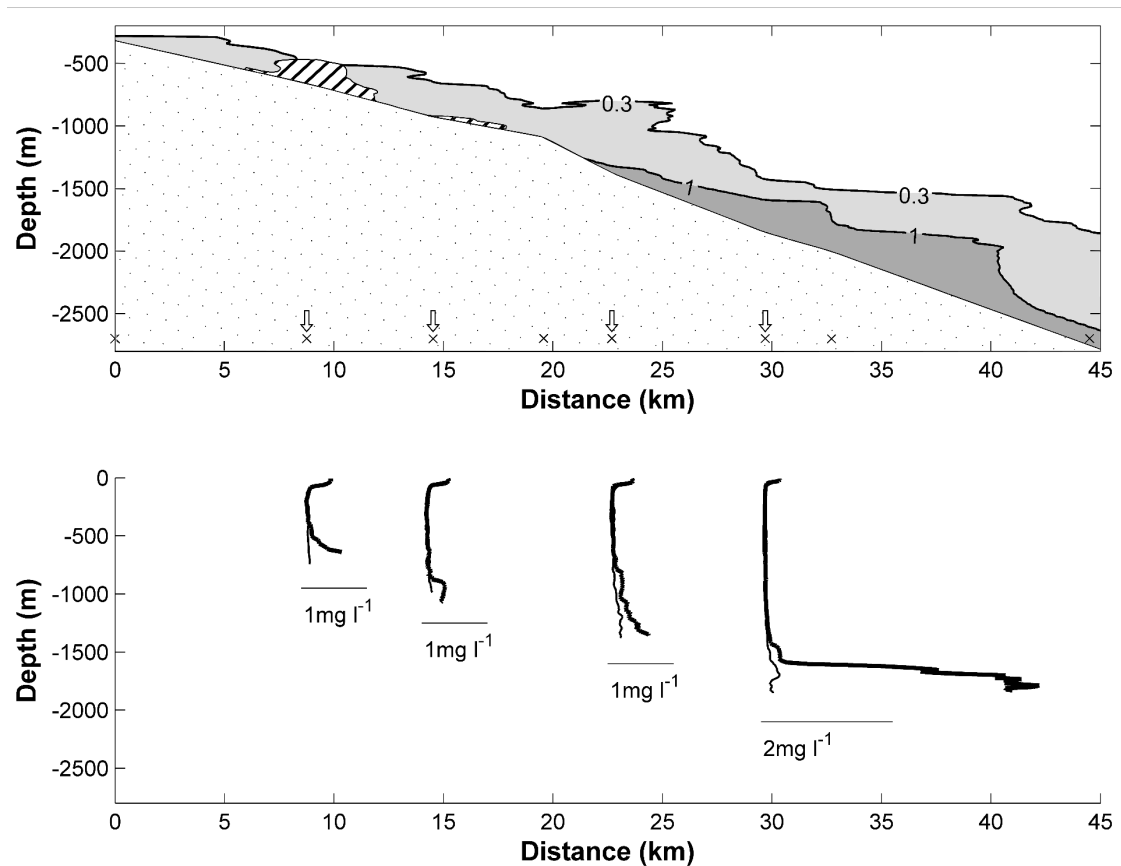
**Fig. C.7.** (a) Along channel section of SPM con- centration (mg l−1) in WC4 in the immediate aftermath of a trawling plume, showing the 0.3 and 1 mg l−1 contours only. For comparison the hatched area indicates the regions where SPM concentrations > 0.3 mg l−1 were measured in other canyon branches when no trawling plumes were evident during the survey. The station lo- cations are shown by the 'x'. In (b), selected vertical profiles of SPM for the above section are indicated in the thick line with thin line showing examples from the same depth in unaffected branches.

Under typical (i.e. non-trawling plume) conditions, vertical profiles of density and derived SPM showed a bottom boundary layer region from 1300 m to 15 mab (meters above seabed) marked by a step in the density gradient (Fig. C.8a). No well-defined bottom mixed density layer was apparent in this profile although often present in other vertical density profiles. An overall stratified layer up to 600 m depth was present above the bottom layer, typical to that associated with the depth range at, or adjacent to, the permanent thermocline (Fig. C.8a). The mid water layers contained small vertically homogeneous/near homogeneous density layers, including reversals in the density gradient, of vertical extent 1-10 m. A BNL in the lower 50 m of the water column is associated with a peak value of SPM reaching 1 mg l^{-1} (Fig. C.8b). A subsequent vertical profile made five days later at the same location indicated a much more turbid BNL with a peak value of 7.7 mg l^{-1} (the axis

scale truncates the plume) but with a significant increase in background (mid water) SPM concentrations starting at ~ 1200 m depth, or ~ 170 mab. This high concentration BNL was associated with a well-mixed bottom density layer capped by a pycnocline of density difference ~0.05 kg m$^{-3}$ (Fig. C.8f).

Associated with the typical vertical profiles of density and SPM, individual Thorpe density displacements in mid water occurred with magnitude up to 1–5 m over small vertical extents, with an increase in the magnitude of displacement packets below 1000 m (Fig. C.8c). A large overturn was highlighted between 1200–1300 m with maximum displacements peaking at 30 m immediately above the bottom boundary region. For the plume event, similar mid water characteristics in Thorpe displacements were again present with a significant increase in amplitude per overturn region below 1150 m. Increased amplitude in displacements (up to 20 m) between 1200–1300 m were associated with the upper of the two-layer BNL and maximum displacements immediately above the seabed. $L_T$ values up to 2 m were found between depths 600–1000 m, with values increasing to ~ 5 m below 1000 m



**Fig. C.8.** Vertical profiles of (a) σt, (b) SPM (mg l−1), (c) individual Thorpe displacements (m), (d) Thorpe Length Scale for overturns (m) and (e) log10 of the turbulent energy dissipation (ε, W kg−1), for the WC4 location at ~1380 water depth in 2016 (see Fig. 2a; K8). (f – j) The corresponding profiles at the same location during a plume event 31 h later. Note in (g), the SPM scale is cut off at 5 mg l−1, for clarity – the maximum value in the near bottom turbid layer was 8 mg l−1.

and a peak of 12 m associated with the upper layer of the BNL (Fig. C.8d). Corresponding values of the turbulent kinetic energy dissipation ($\varepsilon$) indicated that the small mid water overturns had values of $\varepsilon$ between $10^{-9}$–$10^{-8}$ W kg$^{-1}$ for the typical (pre-plume) scenario (Fig. C.8e). The large overturn immediately above the BBL/BNL was slightly larger (3 x $10^{-8}$ W kg$^{-1}$). For the plume event, $L_T$ values above the BNL were similar to typical values and increased significantly below 1200 m with values of O(10m) in the upper BNL and peaking at 22 m in the lower BNL layer (Fig. C.8i). Turbulent energy dissipation during the plume event was generally larger in mid water compared to typical mid water conditions with a number of values in excess of $10^{-8}$ W kg$^{-1}$ (Fig. C.8j). Values peaked between 1200–1300 m (Upper BNL, ~ $10^{-7}$ W kg$^{-1}$).

A second example of a trawling plume showed a plume that occurred at a depth above the BBL, presumably the plume reaching equilibrium density before the seabed was reached (Fig. C.9). This profile was made 30 hours after one in the same location which indicated no enhanced BNL concentration layer, and suggested a plume was captured by the CTD profile near the end of the plume event. The main plume was centred at 1200 m (water depth was 1370 m), about 100 m thick, with SPM concentration peaking at 5 mg l$^{-1}$, over an order of magnitude larger than non-plume BNL values (Fig. C.9b). Individual overturns and displacements were fewer in number than in the previous example but generally larger in scale (30–40 m in vertical extent with displacements peaking at 15–20 m (e.g. at 850–900 m and 800 m, Fig. C.9c). The upper boundary of the main plume was associated with a larger overturn between 1150–1220 m and displacements up to 30 m. Turbulent energy dissipation (Fig. C.9e) was elevated for the overturns at 800, 850–900 m and for the smaller of the two plumes at 1000–1100 m, with values close to $10^{-7}$ W kg$^{-1}$, or an order of magnitude larger than the typical mid water values associated with small overturns. The main plume overturn had an $\square$ of $10^{-6}$ W kg$^{-1}$, the maximum energy dissipation estimated from the profiles analysed and perhaps reflecting the capture, rather than the aftermath of, the plume event.
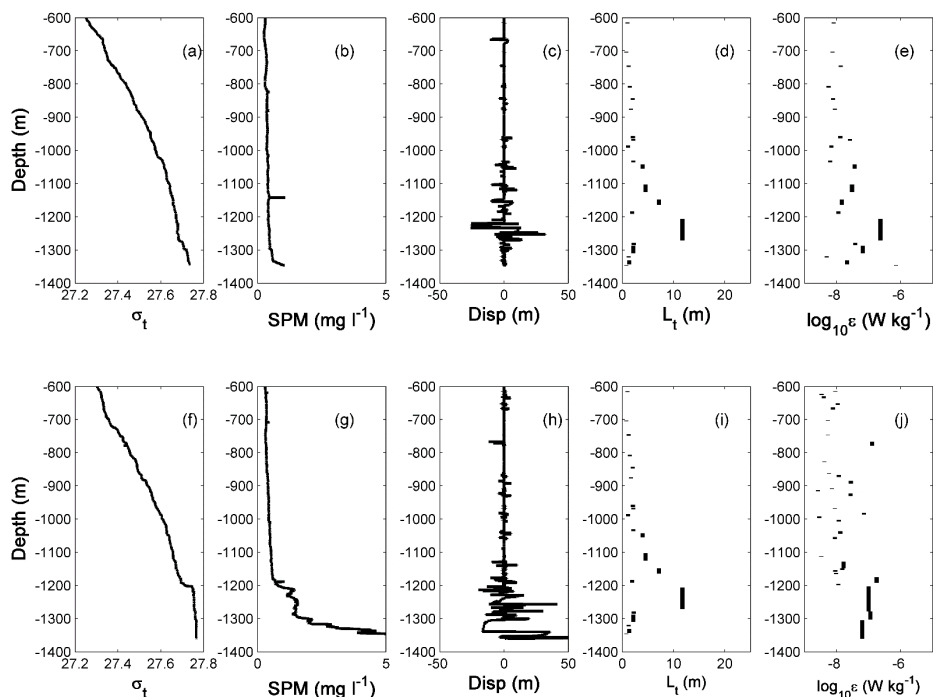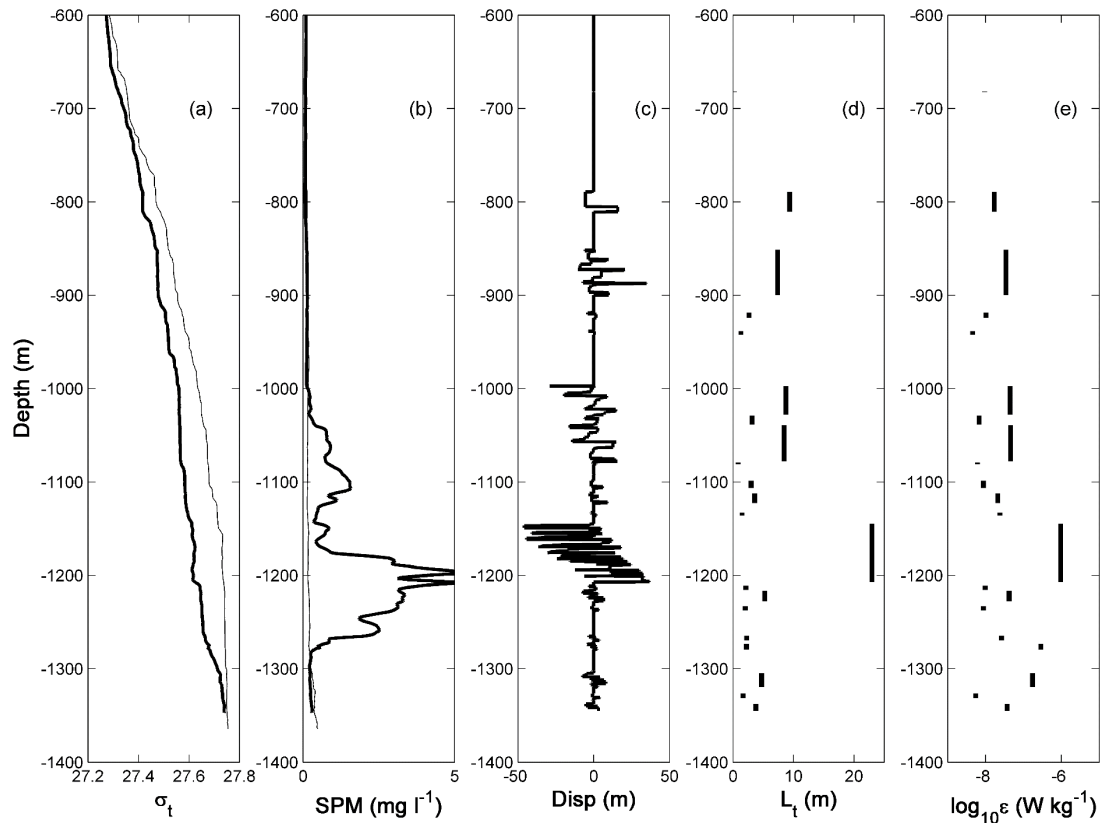
**Fig. C.9.** Vertical profiles of (a) σt, (b) SPM (mg l−1), (c) individual Thorpe displacements (m), (d) Thorpe Length Scale for overturns (m) and (e) log10 of the turbulent energy dissipation (ε, W kg−1), for the WC3 location at ~1385 water depth, 2013 (see Fig. C.2a; K9)

### C.3.3. Variation in quality and quantity of suspended particulate material

The SAPs sampled SPM concentrations in the four E/BNLs (1308–1370 m) varied across the four branches (WC1–WC4; see location in Fig. C.2a) with mean values of SPM = 1.01 ±0.86 mg l⁻¹ (Table C.T3). Highest values were detected in WC4 (2.160 mg l⁻¹) and associated with bottom trawling activity. Although sampled during the same period of trawl activity, lower SPM concentrations (0.29 mg l⁻¹) were detected in the adjacent branch (WC3). High SPM concentrations were also detected in WC1 (SPM = 1.18 mg l⁻¹) but were not previously linked to bottom trawling on the western side of the canyon system. Material from the near-surface has a molar C/N value of 6.4, typical of oceanic surface water, while C/N values from the E/BNLs at depth ranged from 8.2–22.2 across the four branches, with the lowest values in WC4 and highest in WC1.

Lipids (total fatty acids and alcohols) detected in suspended Particulate Organic Matter (sPOM) across the four branches displayed complexity and heterogeneity in both their composition and concentration (Fig. C.10 & Table C.T3). As four of the five filters were torn on recovery (a sampling artefact) and POC may have passed through onto the second filter, concentrations are normalised to volume of water filter (ng l$^{-1}$) here rather than OC content for a more reliable interpretation. The number of individual compounds identified differed greatly, with material from the east showing less complexity (16±6 V 34±17 individual compounds). Total lipid concentrations across the four branches, ranged between 181.5–1301.9 ng l$^{-1}$ (Fig. C.10), with higher values found on the eastern side of the system. As a reference point, the concentration of total lipids in the near surface was 1510.4 ng l$^{-1}$, comparable to those in the east (1092.3 ±296.4 ng l$^{-1}$), while concentrations in the west were twice as low (349.3 ±237.3 ng l$^{-1}$).

Table C.T3

Biogeochemical data for four samples (Locations S1 – 4; see Fig. 2a) and the surface sample (Ss) used in this study with mean ± standard deviation for Western and Eastern samples. SPM: suspended particulate matter; C:N: molar carbon to nitrogen ratio; MUFA: monounsaturated fatty acids; PUFA: polyunsaturated fatty acids. Individual compounds, lipid group and primary biomarkers used for indices are shown in Appendix A. * indicates torn filters.

| Variable | Unit | Surface | WEST | | | | EAST | | | |
|---|---|---|---|---|---|---|---|---|---|---|
| Branch | | * | WC1* | WC2* | | | WC3* | WC4 | | |
| Sample depth (mab) | | 12 | 1308 (12 mab) | 1335 (20 mab) | Mean | SD | 1370 (7 mab) | 1368 (15 mab) | Mean | SD |
| SPM | mg l$^{-1}$ | NA | 1.18 | 0.43 | 0.80 | 0.53 | 0.29 | 2.16 | 1.23 | 1.32 |
| C/N | Molar | 6.36 | 22.19 | 9.25 | 15.72 | 9.15 | 19.52 | 8.16 | 13.84 | 8.03 |
| Total lipids normalised to water | ng l$^{-1}$ | 1510.44 | 517.07 | 181.50 | 349.29 | 237.29 | 1301.85 | 882.74 | 1092.30 | 296.36 |
| Saturated fatty acids | ng l$^{-1}$ | 607.40 | 94.96 | 85.79 | 90.37 | 6.48 | 465.90 | 332.84 | 399.37 | 94.09 |
| MUFA | ng l$^{-1}$ | 319.84 | 309.20 | 85.66 | 197.43 | 158.07 | 174.37 | 157.16 | 165.77 | 12.17 |
| PUFA | ng l$^{-1}$ | 556.22 | 87.29 | 6.87 | 47.08 | 56.86 | | 20.72 | 20.72 | |
| Alcohol | ng l$^{-1}$ | 26.98 | 25.63 | 3.18 | 14.40 | 15.87 | 661.58 | 372.03 | 516.80 | 204.75 |
| Saturated fatty acids | % | 40.21 | 18.36 | 47.27 | 32.82 | 20.44 | 35.79 | 37.70 | 36.75 | 1.36 |
| MUFA | % | 21.18 | 59.80 | 47.19 | 53.50 | 8.91 | 13.39 | 17.80 | 15.60 | 3.12 |
| PUFA | % | 36.82 | 16.88 | 3.79 | 10.33 | 9.26 | 0.00 | 2.35 | 1.17 | 1.66 |
| Alcohol | % | 1.79 | 4.96 | 1.75 | 3.35 | 2.26 | 50.82 | 42.14 | 46.48 | 6.13 |
| Unsaturated fatty acids | % | 58.00 | 76.68 | 50.98 | 63.83 | 18.17 | 13.39 | 20.15 | 16.77 | 4.78 |
| *Indices* | | | | | | | | | | |
| Phyto | ng l$^{-1}$ | 1182.73 | 315.85 | 136.39 | 226.12 | 126.90 | 1222.93 | 820.26 | 1021.59 | 284.73 |
| | % | 78.30 | 61.09 | 75.15 | 68.12 | 9.94 | 93.94 | 92.92 | 93.43 | 0.72 |
| | ng l$^{-1}$ | 66.85 | 25.92 | 13.93 | 19.93 | 8.47 | 20.50 | 29.83 | 25.17 | 6.60 |
| Bacterial | % | 4.43 | 5.01 | 7.68 | 6.35 | 1.88 | 1.57 | 3.38 | 2.48 | 1.28 |

Variability in the principal lipid classes (saturated fatty acids, MUFAs, PUFAs and alcohols) was evident (Fig. C.10). Fatty acids ranged from C14 to C22 (see supplementary information for most commonly identified compounds). Saturated fatty acids and MUFAs were well represented across the four samples and accounted for 34.8 ±12.0% and 34.6 ±22.6%. PUFAs represented < 16.9%, except in the surface (36.8%). The greatest variance in dominant lipid class was observed in the alcohols, ranging from 1.8–50.8% with a mean of 3.4 ±2.3% in the western branches (WC1 & 2) and 46.5 ±6.1% in eastern (WC3 & 4).

Although PUFAs were rare, particularly in eastern branches, lipid biomarkers of phytoplankton origin accounted for 93.43 ±0.7% of the total lipids in WC3 and WC4. In comparison WC1 & WC2 had lower concentrations with 68.12 ±9.9% of the total lipids represented by compounds that indicated phytoplankton origin. Near-surface waters showed lower percentages of phytoplankton than any of the samples at depth (78.3%).
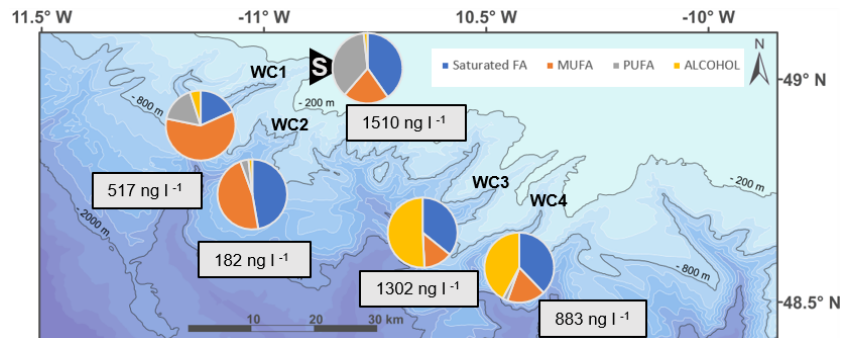


**Fig. C.10.** Map image showing concentrations of total lipids normalised to volume of water (ng l−1) detected in suspended particulate organic matter collected in four branches (WC1 – 4) and at the surface of Whittard Canyon in June 2013. Pie charts show the contribution of saturated fatty acids, monounsaturated fatty acids (MUFAs), polyunsaturated fatty acids (PUFAs) and fatty alcohols in each sample (locations: S1 – 4 and surface sample Ss; see Fig. C.2a).

All samples showed some level of bacterial reworking in the lipid signatures (4.4 ±2.6%).  Bacterial biomarkers followed the opposite pattern to the phytoplankton markers, with higher mean values in the western branches (6.4 ±1.9) and lower in the eastern (2.5 ±1.3%), further indicating that material in the eastern branches is more recently suspended and fresher.

**C.4. Discussion**

Based on a contemporary snapshot (last 10 years) of an area where fishermen have pushed out into deeper fishing grounds, fishing intensity was found to be variable across the Whittard Canyon (Fig. C.2). Highest fishing intensity was generally associated with smoother morphology, especially over steeper sloping parts of canyon interfluves (Fig. C.3).  The trawling vessels used were only limited by the physical constraints of their gear and slopes greater than 15° (> 1300 hrs in 10 years) were regularly fished, but rarely over slopes > 20° (90 hrs in 10 years).

Trawling along the continental margin immediately to the east of Whittard Canyon is seasonal, with most fishing occurring between July and March with a maximum in August (Sharples et al., 2013). Due to the considerable width of the Celtic Shelf and large distances from the nearest fishing ports, and to the size and complexity of the Whittard Canyon, the canyon does not endure the same localised fishing intensity or working weekday cycles found at other submarine canyons more connected to coastal regions, e.g. along the NW Mediterranean shelf edge (e.g. Palanques et al., 2006).

It can be estimated that grounds at Whittard are fished an average of 1.7 times per year. This is calculated by isolating the grounds most frequently fished as those above 800 m (an area of 4456 km$^2$), using a fishing effort of 1.37 x10$^4$ hrs per year, a trawl speed of 5.5 km hr$^{-1}$ (Pilskaln et al., 1998; O'Neill and Summerbell, 2011) and a typical door spread of 100 m for deep water fishing (Gerritsen et al., 2013; Payo-Payo et al., 2017). Assuming a re-suspended mass of 1.6 kg m$^{-2}$ of fished area (Oberle et al., 2016), a first order estimate of 7.13 Mt total sediment per year may be mobilised and potentially enter the Whittard system via trawling. Notwithstanding the approximations and assumptions made here, this estimate highlights the ability for anthropogenic forcing to alter natural sediment flux, especially in areas in proximity to steep slopes with potential for triggering sediment gravity flows (Palanques et al., 2006; Martín et al., 2014c). Focusing on individual branches, ground over the flanks of WC4 were found to be fished 2.6 times the regional average, affording it the greatest potential for remobilising substrate. Using fishing intensity (Table C.T2), an approximation of resuspended sediment at WC4 can be estimated (this time for 'fishing intensity', after O'Neill and Summerbell, (2011), as opposed to 'fished area') of 9.54 x 10$^5$ tonne yr$^{-1}$. Even if a large proportion of this resettles locally there remains the potential for large quantities of material to be transported down canyon to deeper waters. These rough estimates and to a lesser extent those for WC3 and WC1 & 2 further west, have implications for generation of sediment gravity flows (Martín et al., 2014a), enhanced nepheloid layers (Wilson et al., 2015b) and general sediment dynamics, as well as a changing seafloor geomorphology. Traditional studies of sediment flux across continental margins must take these anthropogenic affects into consideration, especially in canyons, such as Whittard, which are more prone to a net export flux, (natural or anthropogenic), due to large distance from riverine sources (Oberle et al., 2016).

Our results provide a statistical interpretation of the relationship between bottom trawling and seafloor roughness in the vicinity of a large terrestrially distant submarine canyon system, using a rugosity index independent of slope. Rugosity varies across many scales and in doing so moderates benthic habitat at similar scales (Wilson et al., 2007; Dunn and Halpin, 2009). As with slope angle (20°), rugosity is a physical constraint to bottom trawling but it has proven challenging to constrain a rugosity cut-off point for fishing activity. The Whittard Canyon area is likely enduring the same effects from seafloor ploughing as those found at La Fonera Canyon in the NW Mediterranean by Puig et al. (2012) albeit at a slower rate and wider geographical area. The GAMs analysis highlighted a complex association between VMS fishing effort and rugosity (Table C.T1 & Fig. C.6b). Where fishing activity occurred on steeper slopes, there were areas of less complex rugosity than would be expected in the absence of fishing. A cause and effect relationship, i.e. whether fishing vessels seek out sloping areas of lower complexity or whether the activity of fishing has reduced complexity in slope areas where active, could not be established. Results here, however, are in line with other studies (e.g. Puig et al., 2012; Payo-Payo et al., 2017). In this respect, future work is planned to focus on cause of seabed alteration in Whittard by conducting a 'before and after' analysis of previous (Irish National Seabed Survey, INSS) and new multibeam bathymetric surveys and correlating those results with VMS data.

Significant trawling induced sediment plumes are generated within the canyon channels of the Whittard system, remnants of which have been observed in light transmission profiles of up to 200 m thick adjacent to the seabed (Fig. C.7). Such anthropogenic sourced sediment plumes had been suggested to occur in Whittard Canyon previously (Wilson et al., 2015b), and there is undisputed evidence for them in a number of canyons at the NW Mediterranean continental margin (e.g. La Fonera Canyon (Martín et al., 2014b)). Trawling induced plumes are, therefore, another mechanism for creating down canyon sediment flows to add to those generated by naturally occurring processes, such as storm wave mobilisation of sediment (Xu et al., 2004), tidally generated (Lee et al., 2009), or riverine flood events (Khripounoff et al., 2009).

The sediment gravity flows observed here are energetic, with an estimated turbulent energy dissipation ($\varepsilon$) an order of magnitude greater than for benthic nepheloid layers that occur under background conditions, despite the observations being made

post event (Figs. C.8, 9). Values in $\varepsilon$ up to $10^{-6}$ W kg$^{-1}$ were estimated from Thorpe length scale analysis of density overturns in CTD profiles. The use of Thorpe length scale is a simple and indirect method to determine $\varepsilon$ (e.g. Mater et al., 2013), with additional errors in absolute values related to the small number of overturns sampled here (e.g. MacDonald et al., 2013). Furthermore, $\varepsilon$ is dependent on the variability of $L_T$ with Ozmidov length scale $L_O$, and $L_T$ probably represents the turbulent kinetic energy level more than the dissipation (Mater et al., 2015); also mean values should be treated with caution. Notwithstanding this, the dissipation values of $\varepsilon$ appear reasonable even if estimated from a few profiles. The dissipation values found here are comparable to those estimated from similar analysis, although through different forcing conditions. For example, in Gaoping Canyon a value of order $10^{-8}$ W kg$^{-1}$ (Lee et al., 2009) was found using the Thorpe displacement method, ~ 2 x $10^{-6}$ W kg$^{-1}$ with maximum Thorpe displacements of 30 m. In the head of Monterey Canyon Gregg et al. (2005), correcting previousvalues found in upper Monterey canyon using microstructure measurements (Carter and Gregg, 2002), estimated values of $\varepsilon$ ~1.97 x $10^{-7}$ W kg$^{-1}$ but attributed this to tidal mixing.

The values found, however, do suggest the fact that the plume events were associated with enhanced turbulent kinetic energy that would keep material in suspension for extended periods of time. This was observed in the aftermath of a trawl event in WC4, with enhanced SPM concentrations apparent over a large vertical range throughout the canyon section (e.g. Fig. C.8b). The increase in overturn scale and dissipation values in mid water also highlight the possibility that intermediate nepheloid layers may be generated as remobilised sediment enters the channel from the interfluves where trawling is most intense (Fig. C.2b). The elevated dynamics associated with the plumes will also allow detachment of sediment laden water from the main plumes away from the bottom boundary, such as those observed in La Fonera Canyon at a bottom depth of ~ 600 m (Martín et al., 2014c). Evidence for that in Whittard comes from the observation of a turbid layer immediately above the bottom boundary and generally elevated turbulent energy in mid water during the event highlighted in Fig. C.8. Trawl induced plumes measured in 2013 in WC3 and WC4 were found in water depths associated with the mid canyon reaches that had steepest canyon walls, which would promote gravity flows from the adjacent interfluves (Wilson et al., 2015b). The generation of thick BNLs and INLs, together with elevated turbulent energy levels within the water column, suggests that material will be kept in suspension for longer and that interpretation of BNL/INL

sources, drivers and distribution patterns are likely to be anthropogenically influenced.

The impacts of potentially introducing, even a small fraction of the 7.13 Mt sediment per year suspended by bottom trawling activities, into the canyon system cannot be overlooked.  The area of the northern Bay of Biscay has high primary productivity, in the region of 200 gC m$^{-2}$ yr$^{-1}$ (Wollast and Chou, 2001). Organic carbon burial has been estimated at 0.05 g m$^{-2}$ yr$^{-1}$ at the upper slope break of the Goban Spur and 0.11 g m$^{-2}$ yr$^{-1}$ further down slope (van Weering et al., 1998). Perhaps, the high energy density plumes induced by trawl activity can exceed the natural export of recently deposited material from the shelf and slope (Wollast, 1998). From a climate perspective, the anthropogenic enhancement of natural sediment transport off shelf to the deeper margin below the permanent thermocline, and hence out of reach from atmospheric influence, has implications for carbon sequestration (e.g. Holt et al., 2009).

Whittard canyon, like many other submarine canyons, hosts rich biodiversity (e.g. De Leo 2010; Vetter et al., 2010). Diverse communities of benthic and suspension feeding fauna (Fig. C.11) seek refuge and utilise the enhanced food input that is sustained by the canyon morphology (Huvenne et al., 2011; Johnson et al., 2013). It would seem likely that adding such volumes of material will have an influence on the natural biogeochemical status of sinking, food rich, particles in the deep-sea (Billet et al., 1983). Some studies have even suggested that anthropogenic modification by trawling can have greater effects than seasonal input of carbon (Sañé et al., 2013).

Wilson et al. (2015b) showed high concentrations of SPM within canyon branches most likely associated with trawling activities on the adjacent spurs. Furthermore, we have shown here that the area surrounding WC4 (most easterly branch) is heavily influenced by trawling. While Duineveld et al. (2001) and Amaro et al. (2015) also reported episodic events transporting substantial amounts of SPM, the cause of these events was not identified. SPM concentrations in the two eastern branches (WC3 & 4) varied dramatically (1.2 ±1.3 mg l$^{-1}$) as well as the OC content and C/N ratios (51.2 ±40.8%; 13.8 ±8). However, the lipid composition from WC3 & 4 was remarkably similar; with SFAs and alcohols dominating in both samples (SFAs: 36.8 ±1.4; Alcohols: 46.5 ±6.1) (Fig. C.10). Contrary to that found by Amaro et al., (2015),
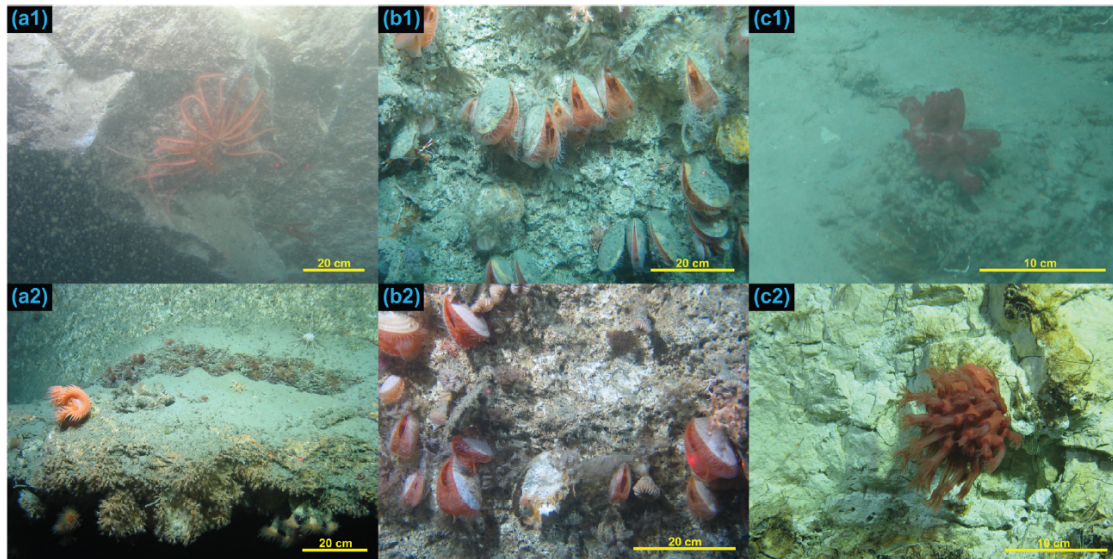
**Fig. C.11.** Photo images from Whittard Canyon 2013 – 2016, displaying contrasting sediment concentrations both in the water column and resettling on benthic fauna. (a1): Cloudy water surrounds a Brisingid starfish; WC3. (a2): Very clear water and a Flytrap anemone; WC1. (b1): Sediment laden Acesta excavata; WC3. (b2): Clean A. excavata; WC3. (c1): The soft coral Anthomastus topped with a vail of sediment; WC3. (c2): An Anthomastus perched on a canyon wall with polyps fully extended. Note that the Anthomastus (c1) with retracted polyps may have become sediment covered during earlier ROV manoeuvres adjacent to site (visibility was not sufficient to determine this from the video), but the quantity of loose sediment available for such coverage may have been introduced by trawling.

here many of the individual compounds identified have phytoplankton origins (> 90%) and are a good food source to canyon communities within the eastern branches. Furthermore, C/N values in WC4 were comparable to surface values (7.3 ±1.3) and would suggest that at least some of the material is fresh and has been rapidly transported to this depth (1370 m) within the canyon. It is likely these compounds are utilised before reaching the channel of the system (Amaro et al., 2015). The lipid composition from the western branches was notably different and had dramatically lower alcohol content (3.4 ±2.3%) and higher contributions of both MUFAs (53.5 ±8.9%) and PUFAs (10.3 ± 9.3%) (Fig. C.10). Huvenne et al. (2011) also reported differences in their lipid compositions between different branches, albeit the samples were also collected at different depths. They attributed differences in the contributions of PUFAs (in the east) and MUFAs (in the west) to variations in the contributions from phytoplankton and zooplankton from/at distinct locations and this may also be the case here. However, results presented here would suggest that anthropogenic loading should also be considered when

interpreting the biogeochemical signatures within a multi-channel system, particularly given the regional variation in fishing intensity.

Other studies have also found differences between western and eastern branches of the canyon systems in faunal community compositions and abundance (Gunton et al. (2015) and references within) and in sediment characteristics (Duros et al., 2011; 2012; Hunter et al., 2013) and have been related to physical dynamics. Recent modelling and glider observations (Amaro et al., 2016; Aslam et al., 2017) have shown that the heterogeneity of benthic dynamics within Whittard Canyon is large with highly variable energy fluxes (in direction and magnitude) across the various branches. Trawling may input more material into the system and high energy plumes may transport fresh material from shelf regions to greater depths within the canyon, but local dynamics in each branch will also influence the local material transport and spatial heterogeneity in the canyon biogeochemistry. Furthermore, the biogeochemical data presented here only show a snap shot in time. Indeed, although low concentrations of SPM were detected at the site in WC3 (Fig. C.2. Sample point: S3), the sampling date (14th June 2013) coincided with the detection of trawl induced ENLs in as defined by Wilson et al (2015b) in WC3. Given this and the high C/N values, these measurements may be from the remnants of a trawl plume. The initial particle loading and duration since the passage of a trawling plume event will determine the biogeochemical composition of the suspended organic material, which further explains the highly heterogenous C/N values measured here and in ENLs by Wilson et al., (2015b).

Compositional differences between organic material from western and eastern branches suggest that there may be a zonal trend in anthropogenically introduced sediment supply, however further work is needed. The lack of replicates and limited number of samples presented here, does not allow for robust statistical analysis of any relationship or difference. There were no statistically significant results for any of the two-sample T-tests (assuming unequal variances) preformed, but there were strong indications that there is a difference between contributions of some lipid groups, (e.g. alcohols $t = -9.3$, $p = 0.07$). Other studies have suggested that lipids are too labile to examine this question (Sañé et al., 2013), but here we have shown that lipids may be used as sensitive biomarkers and may provide greater insight into the alteration of organic material in the canyon by natural and/or trawling processes.

Alterations to the food source may have positive and negative implications depending on the species feeding mechanism/habitat (e.g. Billett et al., 1983; Ramirez-Llodra et al., 2005; Quattrini et al., 2015 and references within). Increased input into the system may favour suspension feeding fauna/fauna living on walls, while benthic organisms may be victim to a food source with less bioavailability and higher degradation at the seabed. Fig. C.11 presents a set of photo images, in order to visualise the varying conditions experienced by local fauna. Species that are accustomed to low sedimentation rates would be forced to endure any extra deposition introduced by trawl fishing. These are often slow growing and/or niche species susceptible to minor changes in their environment. Although these images cannot infer any impacts from anthropogenic events, they do portray the wide variation of sedimentary settings found.

In recent times, the adverse effects of pollution have been realised within the marine realm, for example, from offshore hydrocarbon drill cuttings on delicate cold-water coral habitats (Purser and Thomsen, 2012). Toxic compounds, such as trace metals (e.g. Palanques et al., 2008; Heimbürger et al., 2012; Sousa et al., 2012), along with general marine litter (Tubau et al., 2015), especially micro-plastics, are being increasingly discovered on continental shelves, margins and canyons. If trawling induced plumes can induce enhanced sediment flux across the margin, then equally they have the capacity to accelerate the spread of other anthropogenic processes, such as contamination, from shelf to deep ocean regions. This anthropogenic forcing can be accentuated even further by the funnelling effect of submarine canyons like those found at Whittard Canyon, even when located some distance from the coastal zone.

# Appendix D: Public Engagement

Following is a list and brief description of the main Education and Public Engagement (EPE) activities undertaken during and as part of this PhD programme:

- Engaged with the SFI STEAM Art Project in conjunction with artist Liing Heaney, culminating in a virtual exhibition for schools and the public, complete May 2021

- Conducted two local radio interviews on the trawling noise paper and ocean science, Apr. 2021

- Featured in article on ocean noise in national newspaper (Michael Viney, Irish Times), Apr. 2021

- Article published in national newspaper on trawling noise paper (Lorna Bogue, Irish Independent), Dec. 2020

- Science Twitter account, e.g., a tweet about the PhD project's paper on trawling noise reached 5392 impressions and 263 engagements, Dec. 2020

- Gave a talk to industry/public stakeholders at iCRAG2019 showcase, Dec. 2019

- Organised and carried out two half-day ocean science workshops for 5th and 6th classes, Kilcolgan Educate Together National School, Dec. 2018

- Organised and carried out an ocean science workshop for 'Girls into Geoscience' NUIG, Nov. 2018

- Public presentation on project for Galway Earth and Ocean Society, Nov. 2018

- Public talk for cleancoasts.org (An Taisce) titled: 'Polluted Pathways: A Toxic Ocean Journey', NUI Galway, Mar. 2018

- SFI workshop in communications and public engagement, Feb. 2018

- Organised and carried out two half-day ocean science workshops for 2nd class, Kilcolgan Educate Together National School, Oct. 2017

- Science blogs for offshore research surveys, Oct. and Jun. 2019; Jun. 2018

- NUI Galway open days, Digital Ocean Conference, ocean climate demonstrations, science exhibition and outreach stands, 2017 – 2019

**The PANiC Team.** Left to right: Jennifer Law (undergrad, NUIG), Kieran Adlum (P&O Glider pilot), Dr. Martin White (Chief Scientist, NUIG), Eoghan Daly (Project Lead, NUIG), Liam Strachan (undergrad, NUI Galway), Sibéal Regan (undergrad, GMIT and MMO with IWDG).

NUIG: National University of Ireland, Galway
GMIT: Galway-Mayo Institute of Technology
MMO: Marine Mammal Observer
IWDG: Irish Whale and Dolphin Group